

**ANALYSIS OF THE PHYSIOLOGICAL MECHANISMS UNDERLYING THE
BIOLOGICAL ACTIVITY OF *SARGASSUM FUSIFORME* FUCOIDAN TO
ALLEVIATE INSULIN RESISTANCE**

by

Ya Zhang

B.S., Tangshan Normal University, 2014
M.S., Wenzhou University, 2017

DISSERTATION SUBMITTED IN PARTIAL FULFILLMENT OF
THE REQUIREMENTS FOR THE DEGREE OF
DOCTOR OF PHILOSOPHY
IN
NATURAL RESOURCES AND ENVIRONMENTAL STUDIES

UNIVERSITY OF NORTHERN BRITISH COLUMBIA

September 2021

© Ya Zhang, 2021

ABSTRACT

Type 2 diabetes mellitus (T2DM) is a chronic metabolic disease characterized by hyperglycemia resulting from progressive loss of β -cell insulin secretion frequently on the background of insulin resistance. T2DM, also known as non-insulin-dependent diabetes, accounts for more than 90% of all cases of diabetes. Insulin resistance (IR) refers to the reduced sensitivity of peripheral tissues to insulin and is one of the important triggers of type 2 diabetes. *Sargassum fusiforme* polysaccharide exhibits diverse biological activities, and more and more studies have shown it has a significant effect in improving insulin resistance with almost no side effects. *Sargassum fusiforme* fucoidan (SFF) is one of the main active components with active ingredients such as antioxidants and hypoglycemic lipids. However, the ameliorative effects of SFF on high-fat diet-induced insulin resistance mice and its underlying physiological mechanisms are not clear. Hence, the polysaccharides were extracted and purified from *Sargassum fusiforme*, and fucoidan (SFF), which has good antioxidant activity, was screened using a *drosophila melanogaster* aging model. The effect of SFF on the amelioration of insulin resistance in mice was investigated with a high-fat obese insulin resistance mice model. By gut microbiota and metabolomics techniques, the effect of SFF on intestinal metabolites and its mechanism of alleviate IR were investigated. After treatment with 200 mg/kg SFF for 8 weeks, it was found that SFF could reduce body weight, fasting blood glucose and homa-IR in insulin resistance mice. SFF could effectively activate Nrf2/ARE antioxidant signaling pathway in the liver and promote Nrf2 entry into the nucleus and downstream gene transcription. Metabolomics and intestinal microecology revealed that SFF could upregulate TUDCA level and downregulate ceramide level in mice colon and serum, and this change was dependent on gut microbiota. TUDCA effectively inhibits the FXR/SHP signaling pathway activated by a

high-fat diet, thereby reducing the biosynthesis of enteric-derived ceramides. In addition, TUDCA in the liver could compete with Nrf2 to bind Keap1 to reduce the formation of the Nrf2/Keap1 complex, reduce Nrf2 ubiquitination, and thus contribute to Nrf2/ARE signaling activation. In conclusion, fucoidan from *S. fusiforme* was able to modulate gut microbiota, increased the levels of the intestinal metabolite TUDCA, reduced biosynthesis of enteric-derived ceramides and activated the Nrf2/ARE pathway, which in turn significantly improved insulin resistance induced by high-fat diet in mice. This study provides a new research idea for the study of brown algae fucoidan in metabolic diseases.

Keywords: *Sargassum fusiforme*; Fucoidan; insulin resistance; ceramide; TUDCA; Nrf2

CO-AUTHORSHIP

For all the chapters in this dissertation, I was the principal investigator, including design of the studies, acquisition of data, and analysis of data. I wrote the manuscripts and was responsible for incorporating comments and feedbacks in the revised manuscripts. Dr. Mingjiang Wu and Dr. Ron Thring supervised guided me throughout my PhD studies, both at Wenzhou University and the University of Northern British Columbia, including the experimental design and execution, data analysis, and revision of the dissertation and manuscripts. Dr. Haibin Tong also contributed to the design and implementation of experiments and helped review and improve the manuscripts, so he was included in some of my publications. Dr. Peichao Chen provided useful suggestions in animal experiment and contributed some comments on the manuscripts, so they were included in related publications.

Publication and authorships from this dissertation (Published or prepared for submission):

Zhang, Y., Xu, M., Hu, C.X., Liu, A.M., Chen, J.J., Gu, C.F., Zhang, X., You, C.P., Tong, H.B., Wu, M.J.*, Chen, P.C.* *Sargassum fusiforme* Fucoidan SP2 Extends the Lifespan of *Drosophila melanogaster* by Upregulating the Nrf2-Mediated Antioxidant Signaling Pathway. *Oxidative Medicine and Cellular Longevity*. 2019, 2019:e 8918914. (Chapter 3)

Chen, P.C.[#], Zhang, Y.[#], Xu, M., Chen, H.J., Zou, H.X., Zhang, X., Tong, H.B., You, C.P.*, Wu, M.J.* Proteomic landscape of liver tissue in old male mice that are long-term treated with polysaccharides from *Sargassum fusiforme*. *Food Funct.* 2020, 11(4):3632-3644. (Chapter 3)

Zhang, Y.[#], Zuo, J.H.[#], Yan, L.P.[#], Cheng, Y., Li, Q.J., Wu, S.Y., Chen, L., Thring, R., Yang, Y., Gao, Y.T.*, Wu, M.J.*, Tong, H.B.* *Sargassum fusiforme* fucoidan alleviates high-fat diet-induced obesity and insulin resistance associated with the improvement of hepatic oxidative stress and gut microbiota profile. *Journal of Agricultural and Food Chemistry*, 2020, 68, 10626–10638. (Chapter 4)

Zhang Y., Liu, J., Wu, S.Y., Chen, L., Thring, R., Yang, Y., Wu, M.J., Tong, H.B. (2021) *S. fusiforme* Fucoidan alleviates insulin resistance by inhibiting the FXR/SHP signaling pathway to reduce intestinal-derived ceramide biosynthesis. *Preparation*. (Chapter 5)

TABLE OF CONTENTS

| | |
|--|-----|
| ABSTRACT | III |
| CO-AUTHORSHIP | V |
| TABLE OF CONTENTS | VI |
| GLOSSARY | IX |
| ACKNOWLEDGEMENT | XII |
| Chapter 1 | 1 |
| GENERAL INTRODUCTION | 1 |
| 1.1. Background | 1 |
| 1.2. Objectives of the study | 4 |
| 1.3. Organization of the dissertation | 6 |
| 1.4. Highlights of innovation | 6 |
| Chapter 2 | 8 |
| LITERATURE REVIEW | 8 |
| 2.1. Insulin resistance | 8 |
| 2.1.1 Obesity and insulin resistance | 10 |
| 2.1.2. Oxidative stress and insulin resistance | 11 |
| 2.2. The role of Nrf2 pathway in obesity and insulin resistance | 12 |
| 2.2.1. The role of Nrf2 in obesity | 13 |
| 2.2.2. The role of Nrf2 in insulin resistance | 15 |
| 2.3. Gut microbiota | 20 |
| 2.3.1. Development and stability of the gut microbiota | 21 |
| 2.3.2. Composition of the gut microbiota | 23 |
| 2.3.3. Gut microbiota functions | 25 |
| 2.3.4. Gut microbiota and insulin resistance | 26 |
| 2.4. Fucoidan in insulin resistance | 27 |
| 2.4.1. Fucoidan | 28 |
| 2.4.2. Structure of Fucoidan | 28 |
| 2.4.3. Fucoidan and Metabolic Syndrome | 30 |
| Chapter 3 | 33 |
| SARGASSUM FUSIFORME FUCOIDAN SP2 EXTENDS THE LIFESPAN OF DROSOPHILA MELANOGASTER BY UPREGULATING THE NRF2-MEDIATED ANTIOXIDANT SIGNALING PATHWAY | 33 |
| Abstract | 33 |
| 3.1. Introduction | 35 |
| 3.2. Materials and methods | 36 |
| 3.2.1. Materials and reagents | 36 |
| 3.2.2. Extraction of Polysaccharides from <i>S. fusiforme</i> | 37 |
| 3.2.3. Stress-Induced Survival Rate Assays and Lifespan Assay | 38 |
| 3.2.4. HPLC Analysis | 39 |
| 3.2.5. Fourier Transform-Infrared (FT-IR) Spectroscopy | 40 |
| 3.2.6. Detection of Triglyceride (TG) Content | 40 |
| 3.2.7. Scavenging Activity of DPPH (1,1-Diphenyl-2- Picrylhydrazyl Radical 2,2-Diphenyl-1- (2,4,6-Trinitrophenyl) Hydrazyl) Radical | 40 |
| 3.2.8. FRAP (Ferric Ion Reducing Antioxidant Power) and ABTS (2,2'-Azino-Bis(3- Ethylbenzothiazoline-6-Sulfonic Acid)) Assays | 41 |
| 3.2.9. Measurements of the MDA Content and the Enzymatic Activities of CAT and SOD .. | 41 |
| 3.2.10. qRT-PCR Analysis | 41 |

| | |
|---|------------|
| 3.2.11. Statistical Analysis..... | 42 |
| 3.3. Results..... | 42 |
| 3.3.1. The Fucoidan SP2 Exhibits Excellent Antioxidant Activity..... | 42 |
| 3.3.2. Chemical Composition of SP2..... | 44 |
| 3.3.3. SP2 Promotes Longevity in <i>D. melanogaster</i> | 45 |
| 3.3.4. SP2 Enhances the Endogenous Antioxidant Capacity of <i>D. melanogaster</i> | 47 |
| 3.3.5. Expansion of <i>D. melanogaster</i> Lifespan by SP2 Involves the CncC/Nrf2/ARE Signaling Pathway..... | 50 |
| 3.3.6. SP2-Alleviated Heat Stress Depends on the CncC/Nrf2 Signaling Pathway..... | 53 |
| 3.3.7. SP2 Has No Significant Effect on Body Weight..... | 54 |
| 3.4. Discussion..... | 55 |
| 3.5. Summary..... | 60 |
| Chapter 4..... | 61 |
| SARGASSUM FUSIFORME FUCOIDAN ALLEVIATES HIGH-FAT DIET-INDUCED OBESITY AND INSULIN RESISTANCE ASSOCIATED WITH THE IMPROVEMENT OF HEPATIC OXIDATIVE STRESS AND GUT MICROBIOTA PROFILE..... | 61 |
| Abstract..... | 61 |
| 4.1. Introduction..... | 62 |
| 4.2. Materials and methods..... | 64 |
| 4.2.1. Materials and chemicals..... | 64 |
| 4.2.2. Extraction of <i>S. fusiforme</i> Fucoidan..... | 64 |
| 4.2.3. Experimental animals..... | 65 |
| 4.2.4. Experimental design..... | 65 |
| 4.2.5. Intraperitoneal glucose and insulin tolerance tests..... | 66 |
| 4.2.6. H&E staining..... | 67 |
| 4.2.7. Biochemical analysis..... | 67 |
| 4.2.8. Immunoblotting..... | 68 |
| 4.2.9. Quantitative RT-PCR..... | 68 |
| 4.2.10. Analysis of gut microbiota by 16S rRNA amplicon sequencing..... | 70 |
| 4.2.11. Statistical analysis..... | 70 |
| 4.3. Results..... | 71 |
| 4.3.1. SFF suppresses body weight gain and fat accumulation in HFD-fed mice..... | 71 |
| 4.3.2. SFF inhibits hyperlipidemia and liver steatosis in HFD-fed mice..... | 75 |
| 4.3.3. SFF alleviates HFD-induced insulin resistance..... | 76 |
| 4.3.4. SFF increases mRNA expression of lipolysis-related genes..... | 79 |
| 4.3.5. SFF reverses HFD-induced oxidative stress and Nrf2 repression..... | 80 |
| 4.3.6. SFF remodels the structure of gut microbiota in HFD-fed mice..... | 85 |
| 4.3.7. SFF improves intestinal integrity and inflammation..... | 91 |
| 4.4. Discussion..... | 93 |
| 4.5. Summary..... | 100 |
| Chapter 5..... | 102 |
| SARGASSUM FUSIFORME FUCOIDAN ALLEVIATES INSULIN RESISTANCE BY REDUCTION OF INTESTINAL-DERIVED CERAMIDE BIOSYNTHESIS VIA INHIBITING FXR/SHP SIGNALING PATHWAY..... | 102 |
| Abstract..... | 102 |
| 5.1. Introduction..... | 102 |
| 5.2. Materials and methods..... | 105 |
| 5.2.1. Materials and reagents..... | 105 |
| 5.2.2. Animal experiments..... | 105 |
| 5.2.3. Biochemical Analysis..... | 107 |
| 5.2.4. Determination of hepatic/serum TUDCA..... | 107 |
| 5.2.5. Quantitative RT-PCR..... | 107 |

| | |
|---|------------|
| 5.2.6. Cell culture | 109 |
| 5.2.7. Immunoblotting | 109 |
| 5.2.8. Analysis of gut microbiota by 16S rRNA amplicon sequencing..... | 110 |
| 5.2.9. Non-targeted metabolome analysis | 111 |
| 5.2.10. Statistical analysis | 113 |
| 5.3. Results | 113 |
| 5.3.1 SFF prevents obesity-driven metabolic disorder and remodels intestinal metabolites | 113 |
| 5.3.2 SFF inhibits the biosynthesis of intestine-derived ceramides. | 117 |
| 5.3.3 TUDCA reduces ceramide biosynthesis by inhibiting the FXR signaling pathway. | 120 |
| 5.3.4 Gut microbiota is a key target for SFF to alleviate insulin resistance..... | 124 |
| 5.4. Discussion | 131 |
| 5.5. Summary | 136 |
| Chapter 6..... | 137 |
| SARGASSUM FUSIFORME FUCOIDAN IMPROVES INSULIN RESISTANCE BY INCREASING | |
| HEPATIC TUDCA ACTIVATION OF NRF2/ARE SIGNALING PATHWAY..... | 137 |
| Abstract | 137 |
| 6.1. Introduction | 138 |
| 6.2. Materials and methods..... | 142 |
| 6.2.1. Materials and reagents..... | 142 |
| 6.2.2. Animal experiments | 142 |
| 6.2.3. Cell culture | 144 |
| 6.2.4. siRNA Transfection..... | 144 |
| 6.2.5. Glucose uptake assay..... | 144 |
| 6.2.6. Flow cytometry assays | 145 |
| 6.2.7. Quantitative RT-PCR | 145 |
| 6.2.8. Western blot analysis..... | 146 |
| 6.2.9. Co-immunoprecipitation | 147 |
| 6.2.10. Determination of hepatic/serum TUDCA | 147 |
| 6.2.11. Statistical analysis | 148 |
| 6.3. Results | 148 |
| 6.3.1. TUDCA improves obesity and insulin resistance in <i>ob/ob</i> mice..... | 148 |
| 6.3.2. TUDCA activates the Nrf2/ARE signaling pathway in <i>ob/ob</i> mice liver | 153 |
| 6.3.3. TUDCA improves PA-induced insulin resistance and lipid peroxidation | 154 |
| 6.3.4. Effects of fucoidan to alleviate insulin resistance are mediated by gut microbiota | 160 |
| 6.3.5. Correlation between gut microbiota abundance and mice TUDCA..... | 161 |
| 6.4. Discussion | 163 |
| 6.5. Summary | 166 |
| Chapter 7..... | 167 |
| CONCLUSION AND RECOMMENDATIONS..... | 167 |
| 7.1. Synthesis and conclusion | 167 |
| 7.2. Limitations and future research | 170 |
| References..... | 173 |
| APPENDIX A..... | 197 |
| APPENDIX B..... | 207 |
| APPENDIX C..... | 213 |

GLOSSARY

| | |
|----------------------------|--|
| 2-NBDG | 2-Deoxy-2-[(7-nitro-2,1,3-benzoxadiazol-4-yl) amino]-d-glucose |
| 4-HNE | 4-Hydroxynonenal |
| 7 α / β -HSDH | 7 α / β -hydroxysteroid dehydrogenase |
| ABTS | 2, 2'-Azino-Bis(3-Ethylbenzothiazoline-6-Sulfonic Acid) |
| ACP | Acid phosphatase |
| AKP | Alkaline phosphatase |
| Akt | Protein Kinase B |
| ALT | Alanine aminotransferase |
| AMA | American Medical Association |
| AP-1 | Activator protein 1 |
| ARE | Antioxidant response element |
| AST | Aspartate aminotransferase |
| ATRA | All-trans-retinoic-acid |
| AUC | Area under curve |
| Baat | Bile acid-CoA:amino acid N-acyltransferase |
| BAs | Bile acids |
| BG | Blood glucose |
| BMI | Body mass index |
| BSH | Bile salt hydrolase |
| CAT | Catalase |
| CncC | Cap 'n' collar isoform-C |
| Co-IP | Co-immunoprecipitation |
| Cyp7a1 | Cholesterol 7 α -hydroxylase |
| DCFA | 2'7'-dichlorofluorescein diacetate |
| D-Gal | D-galactose |
| D-GalA | D-galacturonic acid |
| D-Glc | D-glucose |
| D-GlcA | D-glucuronic acid |
| D-Man | D-mannose |
| DPPH | 1,1-Diphenyl-2-picrylhydrazyl |
| D-Xyl | D-xylose |
| ER | Endoplasmic reticulum |
| ERK | Extracellular regulated protein kinases |
| FAPROTAX | Functional annotation of prokaryotic Taxa |
| FBG | Fasting blood glucose |
| FFA | Free fatty acid |

| | |
|----------------|---|
| FGF21 | Fibroblast growth factor 21 |
| FINS | Fasting serum insulin |
| FRAR | Ferric Ion Reducing Antioxidant Power |
| GAPDH | Glyceraldehyde-3-phosphate dehydrogenase |
| Gpx4 | Glutathione peroxidase 4 |
| GSH | Reduced glutathione |
| GSSG | Oxidized glutathione |
| Gst | Glutathione S-transferase |
| HDL-c | High-density lipoprotein |
| HFD | High-fat diet |
| HIF-1 α | Hypoxia-inducible factor 1 α |
| Ho-1 | Heme oxygenase 1 |
| HOMA-IR | Homeostasis model assessment-estimated insulin resistance |
| HPLC | Liquid chromatography |
| HSP | High SP |
| Il-1 β | Interleukin-1 β |
| Il-6 | Interleukin-6 |
| IPGTT | Intraperitoneal glucose tolerance test |
| IPITT | Intraperitoneal insulin tolerance test |
| IR | Insulin resistance |
| IRS-1 | Insulin receptor substrate 1 |
| JNK | c-Jun N-terminal kinase |
| KEAP1 | Keleh-like ECH-associated protein |
| L-Ara | L-arabinose |
| LC-MS | Liquid chromatography-tandem mass spectrometry |
| LDA | Latent Dirichlet <i>allocation</i> |
| LDL-c | Low-density lipoprotein |
| LEfSe | LDA Effect Size |
| LPS | Lipopolysaccharides |
| L-Rha | L-Rhamnose |
| LSP | Low SP |
| MAPs | Marine animal-derived polysaccharides |
| MDA | Malondialdehyde |
| MetS | Metabolic syndromes |
| MPPs | Marine plant-derived polysaccharides |
| MSP | Middle SP |
| NADPH | Nicotinamide Adenine Dinucleotide Phosphate |
| NAFLD | Nonalcoholic fatty liver disease |

| | |
|----------------|--|
| NASH | Nonalcoholic steatohepatitis |
| NCD | Normal chow diet |
| NF- κ B | Nuclear factor kappa B |
| NOX | NADPH oxidases |
| Nqo1 | NAD(P)H:quinone oxidoreductase-1 |
| Nrf2 | NF-E2-related factor 2 |
| OPLS-DA | Orthogonal partial least squares discrimination analysis |
| p53 | Tumor protein p53 |
| P65 | Hypothetical protein |
| PBS | Phosphate-buffered saline |
| PCR | Polymerase Chain Reaction |
| PKC | Protein kinase C |
| PMP | 1-Phenyl-3-methyl-5-pyrazo- lone |
| PPAR- γ | Peroxisome proliferator-activated receptor γ |
| Prdx1 | Peroxiredoxin 1 |
| ROS | Reactive oxygen species |
| SCFAs | Short-chain fatty acids |
| SFF | <i>Sargassum fusiforme</i> fucoidan |
| SHC | Src homology domain- containing protein |
| Slc7a11 | Solute carrier family 7 member 11 |
| Sod | Superoxide dismutase |
| SPH | Sphingosine |
| T2DM | Type 2 diabetes mellitus |
| T-CHO | Total cholesterol |
| TG | Triacylglycerol |
| TNF- α | Tumor necrosis factor- α |
| TUDCA | Tauroursodeoxycholic acid |
| UDCA | Ursodeoxycholic acid |
| UPGMA | Unweighted pair group method with arithmetic mean |
| WT | Wild type |
| Zo-1 | Zonula occludens-1 |

ACKNOWLEDGEMENT

First of all, I would like to express my gratitude and appreciation for my supervisors Dr. Ron Thring and Dr. Mingjiang Wu whose guidance, support and encouragement have been invaluable throughout this study. Without their help and advice, I would not have been able to complete this research. Further, I would like to thank my other supervisory committee members: Dr. Jianbing Li, and Dr. Ranjana Bird for their insightful comments, guidance, and discussions.

Special thanks to Dr. Haibin Tong from Wenzhou university, for sharing his expertise and guidance. He continuously provided encouragement and was always willing to help me with my research. I would like to express my thanks to Dr. Bill McGill, Dr. David Connell, Dr. Ken Otter, and Dr. Peter Jackson as my course supervisors in my first year of PhD. They encouraged me to take a broader view of my research and this later helped me to identify my research questions.

Many thanks to Dr. Dark Qi, Yitian Gao, and Xu Zhang for their support and professional advice with sample analysis at Wenzhou Laboratory Service. I would like to extend my thanks to several UNBC and Wenzhou university faculty and staff, especially Dr. Huixi Zou who lend me their lab equipment and supplies, provided me assistance in sample preparation, or helped me in other ways.

My gratitude also extends to the graduate students at UNBC and Wenzhou university for sharing their knowledge, skills, and thoughts; they are Jingjing Shi, Yuan Tian, He Liu, Jian Liu and Yang Cheng. I would also like to extend my gratitude to all my friends in China and Canada for always being supportive, inspiring, and understanding. The friendship from my friends has helped me to gather my strength to pass through many hard times during my PhD study.

I would like to dedicate this work to my family for their unconditional supports and love. Special thanks go to my mother, who is a strong woman and my role model, and my father, who has taught me to be brave and not afraid of any challenges in my life.

Chapter 1

GENERAL INTRODUCTION

1.1. Background

Sargassum fusiforme belongs to the genus *Sargassum* in the family Sargassaceae and is a typical dual-purpose brown algae, considered one of the most important cash crops in China, Japan and Korea^{1,2}. *S. fusiforme* is farmed on a large scale in the coastal areas of China's Zhejiang, Liaoning and Fujian provinces and up to 10,000 tonnes of *S. fusiforme* are produced annually in China^{3,4}, together with *Porphyra*, *Laminaria* and *Undaria* are known as the four most valuable edible brown algae in China^{5,6}. Consumed as a health food, it is now mostly exported to other Asian countries such as Japan and Korea⁶. The nutritional value of brown algae itself drives its market demand further up, year after year⁷. At the same time, brown algae contain numerous active ingredients such as proteins, lipids, polysaccharides and esters⁸⁻¹⁰. Among these, brown algae polysaccharides are a family of highly sulphated homologous and heterologous polysaccharides widely distributed in brown algae and several marine invertebrates⁸⁻¹¹.

Metabolomics is an emerging histological technique developed after genomics and proteomics to analyse the complex metabolites of the human body. It focuses on the qualitative and quantitative analysis of molecules of less than 1000 relative molecular weight produced by cells, tissues, blood and other biological systems that receive external stimuli or disturbances. Metabolomics technology offers the possibility of prediction and early diagnosis of type 2 diabetes¹². In recent years, several studies have used metabolomics techniques to conduct comprehensive and systematic studies on the changes of metabolites in patients with type 2 diabetes, searching for bio-markers and possible metabolic pathways of

type 2 diabetes, and providing data to reveal the pathogenesis of type 2 diabetes. Numerous studies have shown that the metabolites that undergo significant changes after the onset of T2DM are mainly amino acids, esters, carbohydrates and their upstream and downstream metabolites¹³. In amino acid metabolism, diabetes causes upregulation of leucine, isoleucine, phenylalanine, methionine, taurine, valine and glutamine metabolism, and downregulation of glutamate, tryptophan, alanine, histidine, lysine, tyrosine, glycine and serine; in lipid metabolism, diabetes causes upregulation of free fatty acids, acetoacetate, acetylcarnitine, palmitic acid and cholesterol, and downregulation of phosphorylcholine and sphingomyelin. In glucose metabolism, citric and lactic acid are upregulated and pyruvate, malate, succinic acid and ferredoxin are downregulated^{14,15}. These findings not only provide a basis for early diagnosis and active treatment of diabetes, but also provide new ideas and references for the development of hypoglycaemic drugs.

Gut microbiota, composed of trillions of microorganisms, plays a number of important physiological roles involving food digestion and metabolism. Recently, accumulated evidence has demonstrated that the modulation of the gut microbiota by dietary ingredients can ameliorate obesity and its complications¹⁶. Especially, indigestible marine plant-derived polysaccharides (MPPs) and marine animal-derived polysaccharides (MAPs) can be metabolized and fermented in the gut as nutraceuticals and gut microbiota modulators affecting intestinal ecology¹⁷. Shang *et al.*¹⁸ found that dietary fucoidan from brown seaweeds can modulate the gut microbiota to the advantage of the host probably in a structure-dependent way (such as linkage mode, molecular weight and monosaccharide composition) by enriching the amount of *Lactobacillus* and *Ruminococcaceae* and decreasing the abundance of *Peptococcus*, which is a gut microbiota modulator for health promotion and treatment of intestinal dysbiosis. Another example is the attenuation of HFD-induced obesity

and inflammation by high molecular weight *Ganoderma lucidum* polysaccharide via increasing the ratio of Bacteroidetes/Firmicutes in gut microbiota and maintaining the integrity of intestinal barrier¹⁹. Gut microbiota analysis has shown that *Ophiocordyceps sinensis* polysaccharides could selectively promote the growth of *Parabacteroides goldsteinii*, a bacterium that has been shown to be negatively associated with obesity²⁰. These studies suggest that fucoidan and polysaccharides can positively regulate the gut microbiota, thereby achieving an anti-obesity effect.

Type 2 diabetes mellitus (T2DM) is a chronic metabolic disease characterized by hyperglycemia resulting from progressive loss of β -cell insulin secretion frequently on the background of insulin resistance. T2DM, also known as non-insulin-dependent diabetes, accounts for more than 90% of all cases of diabetes¹⁵. Insulin resistance (IR) refers to the reduced sensitivity of peripheral tissues to insulin and is one of the important triggers of type 2 diabetes. Insulin resistance (IR) affects nearly one-third of the world's population, and it is a key pathophysiological feature of metabolic syndrome, defined as a decrease in the response of the peripheral tissues to insulin, and inhibition of several insulin-stimulated metabolic pathways, such as glucose transport, glycogen synthesis and anti-lipolysis^{21,22}. Individuals with IR are predisposed to several serious metabolic disorders, including T2D, dyslipidemia, hypertension, atherosclerosis, and nonalcoholic fatty liver disease (NAFLD)²³. IR is generally caused by an excessive nutrient intake (e.g. massive fat intake) attributable to an energy imbalance^{24,25}. Abnormality in lipid metabolism is associated with the overproduction of reactive oxygen species (ROS), and long-term HFD aggravates the burden of anti-oxidative system²⁶. Therefore, the impairment of endogenous redox system by chronic HFD feeding is essential to the occurrence of IR in peripheral metabolic tissues.

Nrf2 (NF-E2-related factor 2) is a potent transcription factor and plays an essential role

in regulating the expression of many cytoprotective genes, such as superoxide dismutase (Sod), and catalase (Cat), NAD(P)H:quinone oxidoreductase-1 (Nqo1), heme oxygenase 1 (Ho-1), glutathione S-transferase (Gst), and glutathione peroxidase (Gpx), in response to oxidative stresses²⁷. Growing evidence shows that activation of Nrf2 and Nrf2-regulated endogenous antioxidant system improves insulin sensitivity in the peripheral tissues, and prevents the development of IR²⁸⁻³⁰. In the present study, the effects of SFF on obesity and obesity-associated IR in HFD-fed mice was conducted. In the present study, the effects of SFF on obesity-associated IR, oxidative stress markers, serum biochemical parameters and pathological changes in liver and intestine of HFD-fed mice were investigated. Also, the impact of SFF on gut microbiota and metabolite were then analyzed by 16S rRNA sequencing and metabonomics. Our study has presented new insights into the prevention of energy imbalance-induced obesity and its related metabolic diseases by *S. fusiforme* fucoidan.

1.2. Objectives of the study

Based on the evidence and data in the literature review, the aim of this study was to further investigate the effects of *Sargassum fusiforme* fucoidan on insulin resistance, intestinal microecology and metabolites in mice with high-fat diet-induced obesity, and to analyse the relationship between changes in intestinal microecology and metabolites and the level of insulin resistance, obesity, and oxidative stress in mice. The results of the study also showed the relationship between the alteration of intestinal microecology and metabolites and the level of insulin resistance, obesity and oxidative stress. This will provide new reference data for the application of *Sargassum fusiforme* fucoidan in metabolic diseases and provide further insight into the biological mechanisms. Specifically, the research in this dissertation focuses on the following areas.

1. Antioxidant effects of *Sargassum fusiforme* fucoidan on aging models

The soluble polysaccharides were extracted from *Sargassum fusiforme* by heat extraction and alcoholic precipitation to obtain alginate, aminaran and fucoidan respectively; the *in vitro* antioxidant capacity and *in vivo* anti-aging activity of the three polysaccharides were investigated, and one polysaccharide with the best antioxidant activity was selected for further study.

2. Alleviating effects of fucoidan on insulin resistance in high-fat diet-induced obese mice

The effects of fucoidan (200mg/kg) on body weight, diet, fasting blood glucose, glucose tolerance, insulin tolerance, insulin, free fatty acids, lipid levels, liver function, antioxidant enzymes, lipid peroxidation and tissue morphology were investigated in a high-fat diet-induced insulin resistance model.

3. Effects of fucoidan on intestinal microecology in mice on high-fat diet

The effects of fucoidan on the intestinal microecology of mice on a high-fat diet were determined by PCR amplification of the 16S rRNA gene and Miseq sequencing, and by analysis of the gut microbiota structure (alpha diversity analysis, beta diversity analysis and Lefse analysis, etc.) and metabolic functions. Comparative analysis of the effects of fucoidan on the structure and function of the gut microbiota of HFD mice; also, analysis of the relationship between fucoidan-altered gut microbiota and obesity parameters, etc.

4. Effects of fucoidan on intestinal metabolites in mice

Based on intestinal metabolomics analysis, the relationship between TUDCA and sphingosine/ceramide in intestinal absorption was investigated. A pseudo-germfree mouse model was constructed using a combination of antibiotic treatments to investigate whether fucoidan has been targeted by intestinal microecology for its effect on insulin resistance.

5. Effects of TUDCA on insulin resistance in *ob/ob* mice and biological mechanism of TUDCA activation of Nrf2/ARE signaling pathway.

We used the *ob/ob* mouse insulin resistance model to determine the physiological effects of TUDCA that are consistent with those of fucoidan, and combined molecular docking and Co-immunoprecipitation techniques to analyze the regulatory effects of TUDCA binding to KEAP1 to inhibit the ubiquitinated degradation of Nrf2. This will provide a theoretical basis for the elucidation of the ameliorative effect of fucoidan on insulin resistance.

1.3. Organization of the dissertation

The dissertation is structured as follows: in Chapter 2, literature works were reviewed and summarized. In Chapter 3, the *in vitro* and *in vivo* antioxidant activity of fucoidan was screened and the activation of the Nrf2/ARE signalling pathway by fucoidan was determined. In Chapter 4, the effects of fucoidan on improving insulin resistance in high-fat diet-induced obese mice and its effects on gut microbiota were determined. Chapters 5 and 6 investigated the effects of fucoidan on the absorption of TUDCA and sphingosine to alleviate IR, including TUDCA inhibits ceramide synthesis and the inhibition of ubiquitinated degradation of Nrf2 by TUDCA. Chapter 7 provides the conclusion of this research and recommendations for future research.

1.4. Highlights of innovation

(1) In this study, *Sargassum fusiforme* polysaccharides were extracted and purified, the antioxidant effects of the three extracts were compared and the polysaccharide (SFF, *Sargassum fusiforme* fucoidan) with optimal antioxidant activity was selected from them for further study.

(2) The effects of SFF on the alleviation of insulin resistance were investigated in depth to increase the evidence that seaweed polysaccharides exert hypoglycemic and hypolipidemic activity through the reduction of oxidative stress.

(3) The effects of SFF on intestinal microecology and metabolites in an obese IR mice model were analyzed through a histological approach to search for differential metabolic markers and their biological interpretation.

(4) Pseudo-germfree mouse experiments demonstrated an intermediate targeting role for gut microbiota in the exertion of insulin resistance by SFF.

(5) TUDCA is proposed to reduce the synthesis of enteric-derived ceramide through inhibition of the FXR/SHP signaling pathway, providing a new resolution of insulin resistance alleviation by SFF.

(6) TUDCA binds to KEAP1 to inhibit the ubiquitinated degradation of Nrf2, elucidating the mechanism of action of SFF in alleviating oxidative stress.

Chapter 2

LITERATURE REVIEW

2.1. Insulin resistance

Type 2 diabetes (T2D) has become a decisive medical challenge in the 21st century¹⁵. The over-consumption of relatively cheap, underfed, calorie-dense and highly palatable foods in developed and some developing countries has led to a significant increase in overweight and obesity. In the United States, the overall prevalence of pre-diabetes, diabetes and diabetic complications exceeds 50%³¹. Although not all obese individuals develop T2D (this varies from person to person), it has to be acknowledged that obesity is one of the main factors in the development of T2D and that the prevalence of T2D is positively correlated with the prevalence of obesity¹². The current definition of T2D is mainly secondary to the inadequate action of the main glucose-lowering hormone: insulin. Therefore, understanding the physiological mechanisms of insulin is one of the essential strategies for the effective treatment of T2D. The term "insulin resistance" refers to a decreased metabolic response of target cells or peripheral tissues to insulin, or an impaired lowering effect of circulating or injected insulin on blood glucose at the level of the whole organism. Insulin resistance is a pre-condition of type 2 diabetes, and obesity and sedentary behavior affect 9% of the US population susceptible to the disease. In addition, diabetes can cause serious complications, including neuropathy, retinopathy, kidney failure and cardiovascular disease, leading to ischaemic heart disease and nearly 75,000 amputations each year³².

Subjects are identified as having insulin resistance when serum levels of circulating insulin are high and the necessary conditions for a glucose-lowering response cannot be met.

Various clinical entities- diabetes mellitus, non-alcoholic fatty liver disease, malnutrition, polycystic ovary syndrome -are accompanied by elevated fasting plasma insulin concentrations²¹. The continued secretion of insulin increases the workload of the pancreas, which in turn leads to beta cell hypofunction and is one of the main mechanisms for the development of overt T2D²². Unfortunately, the importance of insulin resistance in the pathogenesis of T2D is often overlooked and research on insulin resistance as the best predictor of future T2D diagnosis is urgent. Furthermore, as insulin action has different functions in different cell types, insulin resistance has varying response criteria in various insulin target tissues^{23,33}.

Figure 2.1. briefly describes the two classical insulin signaling pathways³⁴. The insulin signaling pathway is activated when insulin binds to the insulin receptor on the cell membrane. The interaction of insulin with its receptor activates an intrinsic tyrosine protein kinase that autophosphorylates the receptor as well as downstream substrates. In the classical pathway, a family of proteins known as insulin receptor substrates (IRS) acts as downstream substrates for insulin, which activates a cascade of serine-protein kinases. Akt (protein kinase B) is a major branching point with numerous downstream substrates leading to a variety of physiological functions, including balancing energy and maintaining metabolic homeostasis. The secondary pathway ("ras/MAP-kinase") is also a serine-protein kinase cascade. However, this pathway regulates transcription, cell growth and differentiation, and protein synthesis³⁴.

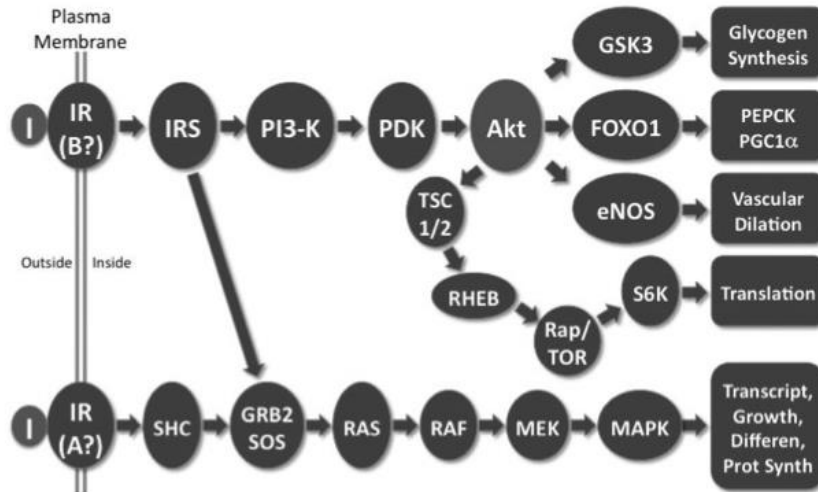


Figure 2.1 Two insulin signaling pathways mediate the numerous actions of insulin. The insulin receptor (IR) is a tetramer consisting of two alpha subunits and two beta subunits that span the plasma membrane. A gene encodes the alpha and beta subunits, which are cleaved post-translationally and held together by disulfide bonds. There are two pro-IR isoforms, a short one and a long one, produced by alternative splicing of exon 11. Thus, the alpha subunit of IR-B contains 12 additional amino acids at its C-terminus. These two isoforms are known to have different functions, encompassing cell metabolism (top) versus mitosis (bottom). In both pathways, insulin (I) binding activates an intrinsic tyrosine protein kinase that makes the receptor as well as downstream substrates including IRS (insulin receptor substrate) or SHC (Src homology domain-containing protein).

2.1.1 Obesity and insulin resistance

Obesity affects physical health and can induce a variety of metabolic diseases including insulin resistance, type 2 diabetes, cardiovascular disease and metabolic syndrome. Obesity has now become a serious problem for individuals, the health-care system and society as a whole³⁵. The American Medical Association (AMA), the largest organisation of doctors in the USA, has identified obesity as a physical disease in its own right³⁶. Although obesity can lead to a variety of metabolic diseases, it is not inevitable in the development of the disease. What has to be acknowledged is that obesity is positively correlated with the development of metabolic disease and identifying obese individuals at higher risk of obesity-related disease is

crucial as it will allow limited resources to be used more effectively for intensive therapeutic approaches^{37,38}. In recent years, several studies have demonstrated that insulin resistance, as a pre-diabetic condition, is likely to be a sign of early release and that insulin resistance may even be considered a major causative factor in diabetes, cardiovascular disease, metabolic syndrome, etc³⁹.

2.1.2. Oxidative stress and insulin resistance

The complex relationship between oxidative stress and inflammation and insulin resistance is now beginning to be explored in a number of studies⁴⁰. The production and accumulation of ROS in cells or tissues activates the organism's own detoxification system, and when the antioxidant capacity is not in balance with the ROS produced, oxidative stress is induced. Low concentrations of ROS are beneficial to the signaling cascade between cells, but above a certain level ROS can trigger discomfort in the body. Low concentrations of ROS help the body's own cell proliferation and metastasis, while high concentrations of ROS accumulate to induce apoptosis⁴¹. Therefore, may give rise to a different cancer treatment method focused on enhancing ROS production in cancer cells⁴². A growing evidence suggests a close relationship between oxidative stress and insulin resistance. Firstly, overweight or obesity-induced insulin resistance in the body occurs through specific molecular signaling pathways such as oxidative phosphorylation, superoxide production by oxidase (NOX), aldehyde auto-oxidation, and polyol and hexosamine pathways. Dysregulation of these specific molecular signaling pathways can lead to systemic oxidative stress^{43,44}.

A variety of deleterious conditions can produce oxidative stress, such as hyperleptinemia, hyperglycemia, endothelial dysfunction, elevated lipid levels, impaired mitochondrial function, and vitamin and mineral deficiencies, all of which can lead to insulin

resistance⁴⁵. Oxidative stress plays a key role in the pathogenesis and development of complications of insulin resistance⁴³. It has recently been shown that by activating adipocyte differentiation, preadipocyte oxidative stress triggers obesity and metabolic disorders by activating adipocyte differentiation, preadipocyte proliferation and increasing the size of mature adipocytes⁴⁶. In addition, oxidative stress can also influence hypothalamic neurons that control satiety and hunger behavior to increase food intake in the daily diet⁴⁷. In addition to the role of oxidative stress in the pathogenesis of obesity, chronic inflammation also plays a non-negligible pathogenic role. Multiple studies have shown that oxidative stress plays an equally pathogenic role in chronic inflammatory diseases⁴⁸. Pro-inflammatory cytokines, such as IL-1 β , IL-6 and TNF- α , have been suggested to contribute to oxidative stress-induced inflammation. Sustained oxidative stress/inflammation may contribute to diabetes, cardiovascular, cancer and neurological diseases⁴⁴. Oxidative stress in the body can activate a variety of transcription factors, including activator protein 1 (AP-1), NF- κ B, tumour protein p53 (p53), peroxisome proliferator-activated receptor γ (PPAR- γ), hypoxia-inducible factor 1 α (HIF-1 α), β catenin/Wnt and Nrf2, which are transcription factors that will further induce the production of inflammation and metabolic disorders⁴⁸.

2.2. The role of Nrf2 pathway in obesity and insulin resistance

As a classical antioxidant signaling pathway, the Nrf2 pathway plays a central role in metabolic homeostasis as an antioxidant and anti-inflammatory. A number of studies now suggest that the Nrf2 pathway may be a key target for improving insulin resistance and obesity. Studies targeting Nrf2 have mostly been conducted in animal models, and the regulation of Nrf2 has been investigated by two different approaches: genetic manipulation such as Nrf2 Knockout (KO) or Keap1 Knockdown (KD) mice and administration of Nrf2 pharmacological activators^{49,50}. The Nrf2 KO mouse model was constructed so that a

constitutive lack of Nrf2 expression, mainly manifested by the inability of cells to produce antioxidant enzyme genes in response to oxidative stress. In contrast to Nrf2 KO mice, Keap1 KD mice were genetically engineered to study the effects of constitutive over-expression of Nrf2. Based on these two different modification methods and animal models, some conflicting experimental data were derived. In the following, we provide a discussion of the role of Nrf2 in obesity and insulin resistance in the context of recent current research.

2.2.1. The role of Nrf2 in obesity

Chartoumpakis DV *et al.* investigated the role of Nrf2 in a 6-month-long high-fat diet-induced obesity mouse model⁴⁹. It was shown that Nrf2-KO mice could protect against partial obesity damage induced in a high-fat diet. Transcript levels of fibroblast growth factor 21 (FGF21) were significantly increased in plasma, liver and white adipose tissue of Nrf2-deficient mice compared to wild-type mice. In another study of high-fat diet (containing 60% fat) induced obese mice, Shin S. *et al.* found that Nrf2-deficient mice gained less weight compared to wild-type mice⁵⁰. Combining these experimental data, it was found that a high-fat diet induced obese mice, whereas when Nrf2 expression was reduced the body weight of the mice was reduced. It has also been shown that targeted knockdown of Nrf2 in mouse adipose tissue reduces adipose tissue mass and inhibits weight gain in mice on a high-fat diet (40 kcal% fat)⁵¹. Interestingly, keap1-hypo mice showed similar results to Nrf2 KO mice under a high-fat diet, with both showing a decrease in body weight. Slocum *et al.* concluded that the keap1-hypo mouse model suppressed high-fat diet-induced (60 kcal% fat) insulin resistance and obesity under sustained activation of the Nrf2 pathway, reduced accumulation of cholesterol and lipids in the liver⁵². In addition, Xu J. *et al.* found that obesity and lipid accumulation in white adipose tissue were reduced in Keap1-knockdown mice with sustained activation of the Nrf2 pathway under high-fat diet induction⁵³.

Gene editing of Nrf2 or Keap1 revealed a significant effect of the Nrf2 pathway on body weight in mice fed a high-fat diet. In contrast to this finding, some studies concluded that after eight weeks of high-fat diet treatment, there was instead a tendency for a slight increase in body weight in Nrf2-deficient mice compared to wild-type mice. In another study, Zhang *et al.* investigated the effects of the Nrf2 antioxidant pathway on high-fat diet-induced obesity in Nrf2-deficient mice⁵⁴, wild-type mice and Keap1 knockout mice. The results showed that genetic alterations in Nrf2 did not prevent diet-induced weight gain and obesity in mice. In summary, most studies using Nrf2-deficient or increased Nrf2 activity mice showed a decrease in body weight under high-fat diet conditions compared to wild-type mice. However, there are still studies that have concluded that there is no significant change in body weight using a high-fat diet with a relatively low fat content, either in Nrf2-deficient mice or normal wild-type mice^{54,55}. This also suggests that the fat content of the high-fat diet is critical to the effect of body weight in mice, which may be one of the reasons for the conflicting experimental results.

With increasing evidence that Nrf2 plays a key role in the regulation of energy metabolism and lipid metabolism, various Nrf2 pharmacological activators and natural antioxidants targeting Nrf2 have been tested in animal models of high-fat diet-induced obesity to identify novel agents for the treatment of metabolic disorders. As a potent agonist of Nrf2, Oltipraz prevented high-fat diet-induced weight gain and fat accumulation⁵⁶. In addition, Shin S.⁵⁰ and his colleagues found that treatment of high-fat diet-induced obese mice with CDDO imidazolide, another potent agonist of Nrf2, prevented high-fat diet-induced obesity by increasing energy expenditure and oxygen consumption and reducing high-fat food intake in mice⁵⁷. The treatment of high-fat diet-induced obese mice with CDDO imidazolide prevented diet-induced weight gain, adipose tissue and liver lipid accumulation

by increasing energy expenditure and oxygen consumption and reducing high-fat food intake. However, these functions were absent in Nrf2-deficient mice, suggesting that activation of the Nrf2 pathway could prevent obesity and metabolic disorders. Finally, under high-fat diet conditions, some of the active small molecules (phenolactone, epigallocatechin 3-gallate, etc.) can alleviate insulin resistance and insulin resistance-induced inflammatory responses through Nrf2/Keap1 signalling^{58,59}.

2.2.2. The role of Nrf2 in insulin resistance

Due to the critical antioxidant, cytoprotective and anti-inflammatory roles played by the Nrf2 pathway, many scientists have conducted numerous studies to investigate the effects of the Nrf2 pathway on insulin resistance and potential therapeutic mechanisms. With the current development of gene editing technology, the use of transgenic mouse models after knocking down Nrf2 and Keap1 to investigate the strong link between the Nrf2 pathway in obesity and insulin resistance is promising⁶⁰.

In the Nrf2-deficient mouse model, the lack of Nrf2-induced antioxidant enzymes and cytoprotection is hypothesized to exacerbate insulin resistance and obesity under high-fat dietary conditions (containing 60% fat). In another study, Nrf2-KO mice were found to induce insulin resistance and lipid accumulation in the mouse liver through activation of the NF- κ B signaling pathway under high-fat diet-feeding conditions. In addition, Nrf2-deficient mice showed an increase in the associated oxidative stress indicators 4-HNE and malondialdehyde, and a decrease in SOD and glutathione levels⁵⁹. This suggests that Nrf2 deficiency has a positive effect on insulin resistance and glucose homeostasis in a high-fat diet-induced obese mouse model, but experimental results that are inconsistent with this remain. Under high-fat diet feeding, Nrf2-KO improved insulin resistance in the liver compared to wild-type mice⁵⁴, and, Nrf2 KO mice showed better insulin sensitivity than WT

mice under high-fat diet feeding⁶¹. Finally, both *in vitro* and *in vivo* settings, Meher A.K. *et al.* demonstrated that Nrf2 deficiency protects mice from insulin resistance in chronic high-fat diet feeding by reducing adipose tissue inflammation⁵⁹. It is interesting to note these studies showed a positive effect of Nrf2 deficiency on insulin resistance, provided that systemic Nrf2-deficient mice were used, rather than tissue-specific deletion mice⁶². A recent study used a targeted specific knockout Nrf2 mouse model to further investigate the specific effects of Nrf2 on different metabolic organs⁶³. The results of this study showed that cell-specific deletion of Nrf2 in mouse adipocytes induced insulin resistance and continued to worsen under high-fat diet feeding conditions. In contrast, insulin sensitivity was significantly improved in the hepatocytes of Nrf2-deficient mice⁶⁴. Similarly, a study using leptin-deficient *ob/ob* mice showed that specific knockout of the Nrf2 gene in adipocytes resulted in reduced white adipose tissue mass, but not improved insulin resistance, and even led to a more severe metabolic syndrome. This study revealed that activation of the Nrf2 pathway in adipocytes upregulates the expression of antioxidant genes, which in turn reduces the accumulation of cellular ROS and plays a novel role in improving insulin sensitivity⁶⁵. Thus, it can be concluded from all the studies discussed above that the complexity of the Nrf2 pathway gives rise to inconsistent results regarding its effects on obesity and insulin resistance (**Table 2.1**).

Table 2.1. The role of Nrf2 pathway in obesity and IR.

| Model | Obesity | IR | Year | Authors |
|--|-----------|-----------|------|------------------------------------|
| Nrf2 inactivation | | | | |
| 12 weeks HFD (41 Kcal% fat) in Nrf2-KO mice | Decreased | Decreased | 2010 | Pi, J. <i>et al.</i> |
| 180 days HFD (60 kcal% fat) Nrf2 KO mice | Decreased | Decreased | 2011 | Chartoumpekis, D.V. <i>et al.</i> |
| 10 weeks HFD(60 kcal% fat) in Nrf2 KO mice | Decreased | Decreased | 2012 | Meher A.K. <i>et al.</i> |
| adipocyte-specific Nrf2 KO in Ob/Ob mice | Decreased | Increased | 2013 | Xue, P. <i>et al.</i> |
| 20 weeks HFD (45 kcal% fat) Nrf2 KO mice | Decreased | Decreased | 2014 | Meakin, P.J. <i>et al.</i> |
| 8 weeks HFD (22 kcal% fat) Nrf2 KO mice | Increase | Increased | 2016 | Liu Z. <i>et al.</i> |
| 170 days HFD(60 kcal% fat) in adipocyte-specific Nrf2 KO mice | No change | Increased | 2018 | Chartoumpekis, D.V. <i>et al.</i> |
| 170 days HFD(60 kcal% fat) in hepatocyte-specific Nrf2 KO mice | No change | Decreased | 2018 | Chartoumpekis, D.V. <i>et al.</i> |
| 12 weeks HFD (70 kcal% fat) in Nrf2 KO mice | Increased | Increased | 2019 | SamPATH, C. <i>et al.</i> |
| Ovariectomy Nrf2 KO in C57BL/6J mice | Increased | Increased | 2020 | Wu, X.W. <i>et al.</i> |
| Nrf2 activation | | | | |
| 28 weeks HFD (45 Kcal% fat) in mice treated with Nrf2 activator oltipraz | Decreased | Decreased | 2011 | Yu, Z. <i>et al.</i> |
| 36 days HFD(60 kcal% fat)Lep(ob/ob) Keap1 knockdown (KD) mice | Decreased | Increased | 2012 | Xu J. <i>et al.</i> |
| 12 weeks HFD (39.7 kcal% fat) Keap1 KD mice | No change | N/A | 2012 | Zhang, Y.K. <i>et al.</i> |
| 90 days HFD (60 kcal% fat) in Keap1 hypo mice | Decreased | N/A | 2016 | Slocum, S.L. <i>et al.</i> |
| skeletal muscle-specific Keap1 KO mice | Decreased | Decreased | 2016 | Urano, A. <i>et al.</i> |
| 17 weeks HFD (45 kcal% fat)in mice with epigallocatechin 3-gallate | Decreased | N/A | 2017 | SamPATH, C. <i>et al.</i> |
| Keap1 KD in lipodystrophic mice | N/A | Decreased | 2018 | Chartoumpekis, D. V. <i>et al.</i> |
| 5 months HFD (60 kcal% fat) in Nrf2+/+ mice | N/A | Decreased | 2018 | Tarantini, S. <i>et al.</i> |
| 12 weeks HFD (70 kcal% fat) in Nrf2+/+ mice | Decreased | Decreased | 2019 | SamPATH, C. <i>et al.</i> |
| 12 weeks HFD (45 kcal% fat) in mice treated with liraglutide | Decreased | Decreased | 2020 | Han X. <i>et al.</i> |

In accordance with previous findings, the sustained activation of the Nrf2 pathway prompted in Keap1-deficient mice may provide a novel therapeutic strategy to investigate the role of Nrf2 in various metabolic diseases. It was shown that insulin signaling in the liver of Keap1-KD leptin-deficient *ob/ob* mice was inhibited and insulin resistance was not improved under short-term high-fat feeding⁵⁴. In contrast, Uruno A. *et al.* demonstrated increased activation of Nrf2 in skeletal muscle by generating a skeletal muscle-specific Keap1 knockout lean mouse model. This sustained activation of Nrf2 increased the expression of glycogen branching enzymes and the phosphorylase b kinase alpha subunit protein, which in turn improved insulin resistance and increased glucose uptake⁶⁶. Constitutive enhancement of Nrf2 signaling induced by knockout of Keap1 prevented impaired metabolism and insulin resistance in lipodystrophic mice by inhibiting lipid synthase in the liver⁶⁷.

The physiological mechanisms underlying the role of Nrf2 in insulin resistance have not been fully elucidated. Studies using the Nrf2 KO and Keap1 KD mouse models have yielded inconsistent results on the role of the Nrf2 pathway in insulin resistance. This suggests that deletion or activation of Nrf2 in different specific tissues (liver, muscle, adipose tissue) may lead to different effects on insulin resistance (**Table 2.2**)⁶⁰. In addition, the variability of the mice themselves, the fat content of the high-fat diet and the duration of feeding, the degree of variability in mouse strains, and differences in the genetic background of the animals may also have an effect on insulin resistance. What is certain is that, in addition to studies on systemic deficient Nrf2, more attention needs to be paid in the future to the specific targeting of Nrf2 to tissue deletion or activation.

Table 2.2. The role of Nrf2 pathway in IR: systemic vs. tissue-specific KO of Nrf2.

| Model | KO type | Obesity | IR | Year | Authors |
|--|-----------------|-----------|-----------|------|-----------------------------------|
| Insulin resistance decreased | | | | | |
| Nrf2 inactivation | | | | | |
| 12 weeks HFD (41 Kcal% fat) in Nrf2-KO mice | systemic | Decreased | Decreased | 2010 | Pi, J. <i>et al.</i> |
| 180 days HFD (60 kcal% fat) Nrf2 KO mice | systemic | Decreased | Decreased | 2011 | Chartoumpekis, D.V. <i>et al.</i> |
| 10 weeks HFD(60 kcal% fat) in Nrf2 KO mice | systemic | Decreased | Decreased | 2012 | Meher A.K. <i>et al.</i> |
| 170 days HFD(60 kcal% fat) in hepatocyte-specific Nrf2 KO mice | Hepatocyte | No change | Decreased | 2018 | Chartoumpekis, D.V. <i>et al.</i> |
| KO mice | | | | | |
| 20 weeks HFD (45 kcal% fat) Nrf2 KO mice | systemic | Decreased | Decreased | 2014 | Meakin, P.J. <i>et al.</i> |
| Nrf2 activation | | | | | |
| 28 weeks HFD (45 Kcal% fat) in mice treated with oltipraz | systemic | Decreased | Decreased | 2011 | Yu, Z. <i>et al.</i> |
| Keap1 KD in lipodystrophic mice | systemic | N/A | Decreased | 2018 | Chartoumpekis, D.V. <i>et al.</i> |
| skeletal muscle-specific Keap1 KO mice | skeletal muscle | Decreased | Decreased | 2016 | Uruno, A. <i>et al.</i> |
| Ovariectomy Nrf2 KO in C57BL6/J mice | systemic | Increased | Increased | 2020 | Wu, X.W. <i>et al.</i> |
| Insulin resistance increased | | | | | |
| Nrf2 inactivation | | | | | |
| adipocyte-specific Nrf2 KO in Ob/Ob mice | adipocyte | Decreased | Increased | 2013 | Xue, P. <i>et al.</i> |
| 170 days HFD(60 kcal% fat) in hepatocyte-specific Nrf2 KO mice | adipocyte | No change | Decreased | 2018 | Chartoumpekis, D.V. <i>et al.</i> |
| KO mice | | | | | |
| 8 weeks HFD (22 kcal% fat) Nrf2 KO mice | systemic | Increase | Increased | 2016 | Liu Z. <i>et al.</i> |
| Nrf2 activation | | | | | |
| 36 days HFD(60 kcal% fat)Lep(ob/ob) Keap1 knockdown mice | systemic | Decreased | Increased | 2012 | Xu J. <i>et al.</i> |

Studies have shown that the decreased antioxidant capacity caused by obesity may lead to insulin resistance and even type 2 diabetes⁶⁸. Other studies have also shown that compared with healthy individuals, the activity of antioxidant enzymes (such as SOD, CAT, GPX, etc.) in obese patients is significantly reduced⁶⁹. In addition, another mouse study found that compared with the normal group, the activity of antioxidant enzymes in obese rats was inhibited by a high-fat diet⁷⁰. Therefore, as a potential drug for improving metabolic diseases, it is urgent to develop the medicinal value of Nrf2 activators. The Nrf2 pathway is expected to improve insulin resistance by counteracting oxidative stress and inflammation caused by obesity to maintain the body's redox homeostasis. Studies have shown that resveratrol (an Nrf2 agonist) can activate Nrf2 by activating the ERK pathway instead of the p38 or JNK pathway, thereby alleviating the insulin resistance of HepG2 cells induced by methylglyoxal and increasing HO-1 and glyoxalase expression level⁷¹. In addition, other effective Nrf2 agonists, such as oltipraz, curcumin and notoginsenoside R1, etc., have been pharmacologically studied in obese mice. The study by Yu Z. *et al.* proved that oltipraz treatment of obese mice induced by a high-fat diet can upregulate Nrf2 target antioxidant enzymes in the mouse liver, such as CAT and SOD, and reduce endoplasmic reticulum stress and inflammation⁶¹. Another group of studies extracted natural plant compound curcumin for research and found that curcumin can also significantly reverse the increase in malondialdehyde and ROS caused by high-fat diet, and increase the expression of antioxidant enzyme HO-1 in skeletal muscle, thereby improving obesity-induced insulin resistance⁷². Finally, the latest research shows that one of the main components of notoginseng saponins, notoginsenoside R1, can significantly improve dyslipidemia and insulin resistance in diabetic mice⁷³.

2.3. Gut microbiota

At present, obesity has become a global health challenge. In both developed and developing countries, the proportion of obese people is increasing sharply⁷⁴. Today, there are more than 500 million obese people in the world, which will not only increase a lot of economic costs but also pose a threat to public health⁷⁵. Obesity is not only an increase in weight, it also makes individuals prone to obesity. Obesity can cause many diseases, including cardiovascular disease, diabetes, non-alcoholic fatty liver, cancer and some aging-related diseases. Several key genes are involved in the determination of obesity, but this genetic susceptibility may only explain a small part of the disease mechanism in obese people, but cannot explain the increase in this pathological incidence. Obesity stems from the relationship between complex genetic interactions and environmental factors (such as diet, food composition, and/or lifestyle). In general, it is caused by the long-term imbalance between energy intake and expenditure and the excessive accumulation of body fat⁷⁶. Currently, the complex pathways leading to the development of overweight and obesity have not been fully studied. Recent studies have shown that intestinal flora (the trillions of bacteria that usually exist in the human gastrointestinal tract) is likely to also be involved in the regulation of obesity⁷⁷. The body is a complex whole, and more and more evidences show that the gut microbiota and its bacterial genome may directly affect the acquisition of lipids and participate in the physiological processes of energy regulation and fat storage⁷⁸. In general, these findings increase the possibility that the gut microbiota plays a role in regulating the host's energy metabolism, and provide a new treatment strategy for the study of obesity and related metabolic diseases.

2.3.1. Development and stability of the gut microbiota

It is currently believed that the placenta is not interfered by bacteria in the mother's body, although a small amount of bacteria will enter the placenta through the circulation of

body fluids during the entire gestation process to form tiny microflora⁷⁹. After the baby is born, bacteria from the mother and the surrounding environment will quickly invade the baby's intestines and colonize to form a stable microbial community. The composition of this microbiota depends on various factors, including the method of birth (cesarean section or vaginal delivery), breastfeeding or formula feeding, antibiotic treatment or environmental hygiene⁸⁰. Because of the continuous changes in the environment, the community composition of babies will still change in the first few years of the formation of the microbiota. Influencing factors include developmental changes in the intestinal environment, host genotypes and the introduction of solid foods, etc. Basically, a more complex and stable community close to the adult gut microbiota is established in the intestines of infants when they are about 3 years old⁸¹. In the adult population, if the surrounding environment and diet of the settlers remain unchanged, the gut microbiota remains basically stable. Then, when the digestive physiology and diet of the elderly change, the gut microbiota will be greatly changed⁸². In the adult population, dietary factors or antibiotic treatment can cause changes in the gut microbiota, but this change is short-lived. For example, in adults with a single oral antibiotic for short-term treatment, the gut microbiota will change its original structure for up to 4 weeks, and then the gut microbiota tends to return to its original composition after 4 weeks⁸³.

Of course, some antibiotics may have super effects, and some bacteria may not recover after several months of treatment. Repeated contact with antibiotics may cause the diversity of the flora to decrease⁸⁴. Similarly, changes in diet can also lead to changes in the composition of the gut microbiota. Food provides nutrients to the host and microbiota, and their bacterial species may be favorably or adversely affected by the dietary species. A current study believes that genetic mutations cause no more than 12% of the changes in the structure of the gut

microbiota, and changes in the diet structure of mice can explain 57% of the total structural variation of the gut microbiota⁸⁵. In humans, the gut microbiota in babies and their mothers has been identified, and the two are extremely similar. The gut microbiota is affected by both genotype and environmental exposure. The results show that family members have more similar microbiota than unrelated individuals, but the degree of variation between identical twins is similar, indicating that early environmental exposure is a key determinant of adult intestinal bacterial communities⁸⁶. In addition, this study also shows that if the bacterial composition of each microbial group is different (all 154 individuals have no shared bacterial species), there are a variety of shared microbial genes called "core microbiomes", reflecting the evolutionary convergence of unrelated bacterial species. Since the genotype and environmental exposure of each individual is different, the final composition of the microbiota is unique and specific to each individual⁸⁷. A recent study believes that due to the uniqueness of the gut microbiota, individuals can be uniquely identified based on the microbiota alone⁸⁸. Nevertheless, the intestinal flora is still a controversial issue, and further in-depth research needs to be carried out.

2.3.2. Composition of the gut microbiota

In humans, the gut microbiota accounts for about 1 kilogram of our body weight. It is a complex and dynamic ecosystem. Current studies have shown that it co-evolves with the host⁸⁹. It is now recognized that the microbial community in our intestines is regarded as a new organ that affects the health of the body by regulating human metabolism, immunity and endocrine⁹⁰. However, there are still a large part of intestinal bacteria that cannot be cultivated due to the special growth environment, so our understanding of the gut microbiota is still very one-sided⁹¹. For a long time, the cultivation of microbiota has been restricted by technical problems. As early as the 1980s, it introduced a new culture-independent method to identify

bacteria based on 16S rRNA gene sequencing. Now, more and more molecular technology developments make it possible to reliably assess the gut microbiota. Although archaea and eukaryotes also exist in the intestines, bacteria clearly dominate. A total of nine families of bacteria and at least one family of archaea colonize the adult human intestine⁹². This is only a small part of the more than 70 bacterial families and 13 archaea families known in the biosphere. In addition, three bacterial families, namely Firmicutes (Gram-positive), Bacteroidetes (Gram-negative) and Actinobacteria (Gram-positive) dominate the intestinal flora of adults, accounting for more than 90% of all bacteria. *Methanobrevibacter smithii* hydrogen-consuming methanogens dominate the archaeal domain⁹³. The above data are obtained from stool samples corresponding to colonic populations. But this part of the data only comes from the colon. It is reported that the proportion and types of bacteria in the gastrointestinal tract are affected by changes in the intestinal environment, such as oxygen, pH, and nutrient utilization. Therefore, the bacterial concentration in the lower part of the gastrointestinal tract is higher, that is, close to the hind-gut. Assuming that this intestinal segment is mainly composed of anaerobic bacteria, aerobic bacteria dominate in the proximal intestine. However, the results of molecular analysis show that the same bacteria are present in different areas of the intestine, but the proportions of different species are different⁹⁴.

With the advancement of science and technology, the human microbiome project has entered a new era. The improvement of sequencing and bioinformatics capabilities not only enables people to understand the types of bacteria that exist, but also their gene content⁹⁵⁻⁹⁷. It is estimated that using these technologies, there are about 1014 types of microorganisms in the human gastrointestinal tract (ten times more cells than the entire human body), and each intestinal flora is composed of 500–1000 different bacteria⁹⁸. At present, the MetaHit Alliance has released a bacterial catalog, which contains nearly 10 million non-redundant

genes. The results obtained by sequencing the stool samples of 1267 individuals indicate that the human microbiome contains at least 100 times that of the human genome⁹⁹⁻¹⁰¹.

The human body has an average of 500-600,000 bacterial genes, about half of which are shared by most individuals (functional core). The intestinal flora has many functions in humans, and may greatly promote the diversity of metabolism in the human population, but not all individuals have this function. In addition, according to the composition of the intestinal flora, humans divide it into three different bacterial groups¹⁰². This intestinal type concept is based on the co-occurrence of bacterial species. The intestinal type is dominated by Bacteroides, Prevotella, and Luminococcus. Although differences in bowel types were found to be independent of geographic location, age, gender, or body mass index, these bowel types were associated with differences in long-term eating patterns^{103,104}. Although the concept of intestinal type is still controversial, it is crucial to establish a relationship between intestinal flora and health and define what constitutes healthy and undesirable bacterial communities.

2.3.3. Gut microbiota functions

The intestinal flora is in a symbiotic relationship with the human body, and it can perform basic functions that the human body cannot perform. Therefore, the intestinal microbiota is essential for maintaining normal gastrointestinal and digestive functions as well as immune function^{105,106}. Studies have found that the microbiota in the intestine can ferment food components that cannot be digested by human digestive juices, and synthesize vitamins and other essential micronutrients. In addition, the intestinal flora can also metabolize toxins and carcinogens in the diet, convert cholesterol and bile acids to ensure the maturity of the immune system. The intestinal flora also has the function of affecting the growth and differentiation of intestinal epithelial cells, and prevents intestinal pathogens by regulating

intestinal angiogenesis¹⁰⁷. In the past few decades, a close relationship has been established between the gut microbiota and human health. Studies have reported that the imbalance of the intestinal flora can induce many diseases, including immune dysfunction and viral infections. Studies have shown that the intestinal microbiota is also related to several non-intestinal diseases, including diabetes, cardiovascular disease, obesity, liver and even brain diseases, etc.¹⁰⁸.

2.3.4. Gut microbiota and insulin resistance

There is growing evidence that the gut flora is one of the key factors regulating host-environment interactions, particularly the absorption and digestive response to food intake¹⁰⁹. It is now widely accepted that the gut flora can influence the body's differential metabolic and energy balance regulatory responses to nutrient intake, which may be related to microbiota structure. Consistent with specific bacterial flora being detrimental to metabolic homeostasis in metabolic regulation, it is hypothesized that organisms without gut bacteria may be protected from diet-induced obesity¹¹⁰. On the other hand, the high heterogeneity of human gut bacteria has been found to be protective of the organism and has the potential to reduce the risk of obesity and its complications¹¹¹. The risk of obesity and its complications may be reduced by the heterogeneity of human intestinal bacteria. Interestingly, genetic clustering analysis indicated that dietary restriction was also able to modulate the gut microbiota¹¹². The results of this analysis suggest that this process involves an increase in the proliferation of certain bacteria, and that this flora may reverse certain diseases when recovered¹¹³. Notably, it has been reported that in experimental models, diet-induced metabolic disturbances may be directly associated with the development of insulin resistance, and not with obesity. This may be mediated by direct regulation of flora or at least partial regulation of metabolism by gut bacteria¹¹⁴. There is conclusive evidence that

excessive consumption of saturated fat-rich diets can increase bacterial production of pro-inflammatory lipopolysaccharides and can increase intestinal permeability and enhance systemic inflammation. The concept of metabolic endotoxaemia has now emerged as representing a potential key dietary modifier of diet-related obesity-related metabolic disorders, including insulin resistance¹¹⁴. From a mechanism of action perspective, the level of short-chain fatty acids (SCFA) produced by bacterial fermentation plays an important role in nutrient intake, which is tied to the occupancy and function of the gut microbiota itself¹¹⁵.

2.4. Fucoidan in insulin resistance

The marine environment provides humans with a wealth of chemical and biological supplies. The unique compounds of marine plants and algae are considered to be an important source of cosmetics, dietary supplements, agrochemicals and pharmaceuticals¹¹⁶. Seaweeds, classified as green algae, red algae and brown algae, among others, are capable of producing a variety of biologically active metabolites¹¹⁷. Currently, research has been conducted on several components of marine seaweeds with nutritional health and pharmaceutical activities^{118,119}. In about 2000 For about 2000 years, brown algae (e.g. *Sargassum spp.*) have been used as a Traditional Chinese Medicine (TCM) to treat a variety of diseases¹²⁰. Traditionally, brown algae have been used to treat tumours, kidney disease, eczema, oedema, testicular pain, swelling, cardiovascular disease, atherosclerosis, ulcers, frostbite, psoriasis and asthma, among other conditions¹²¹. The therapeutic effects of brown algae are now scientifically approved. Brown algae contain several components that can be explained by their pharmacological effects *in vivo* and *in vitro*. Brown algae metabolites have several biological activities as anti-cancer, anti-inflammatory, anti-bacterial, anti-viral, neuroprotective and anti-HIV. Fucoidan polysulphate is one of the active ingredients in brown algae and several studies and reviews have previously been carried out on its

biological activity, for example by producing antioxidant, antitumour, immunomodulatory, antiviral and anticoagulant activities for the treatment of several metabolic diseases¹²².

2.4.1. Fucoidan

The first extraction process for fucoidan was carried out in 1913 from a brown algae such as *Fingerling kelp*, *fucus vesiculosus* and *Nocosum nodosum*¹²³. Fucoidan is a negatively charged and highly hygroscopic complex polysaccharide¹²⁴. Fucoidan is found in high concentrations in brown algae, mainly in *Fingerling kelp*, *Nodosum nodosum*, *Aspergillus macrosporidian* and chlorella leaves. Fucoidan is soluble in water and acid solutions. Since its first publication in 1913, the number of studies on fucoidan has increased significantly, especially in the last few years. The reason for this increase in research is that fucoidan may have antitumour, anticoagulant and antioxidant effects, as well as an important role in the regulation of glucose and cholesterol metabolism¹²⁵. In addition, fucoidan is of considerable interest as a component of fucoidan polysaccharides. It has also been reported that fucoidan may provide protection against liver damage and urinary failure. Clearly, these studies are gradually flourishing as the biological activity of fucoidan is carried out. As the research continues to accumulate, the biological activity and health-related benefits of fucoidan are becoming increasingly available.

2.4.2. Structure of Fucoidan

Fucoidan is known as a polysaccharide rich in fucose and sulphate groups and is mainly derived from the extracellular matrix of brown algae. Fucose is composed of L-fucose, a sulphate group and one or more small proportions of glucose, xylose, mannose, rhamnose, arabinose, galactose, glucuronide and acetyl groups and is present in a variety of brown algae¹²⁶⁻¹²⁸. The researchers also used galacto-humulose to represent a type of rock algae etiolated glycan. Galacto-humicans are referred to as monosaccharides and the

monosaccharides are composed of galactose and fucose, similar to rhamnase fucoglycans (rhamnase and fucose) and rhamnagalacto-humicans (rhamnase, galactose and fucose). In addition to the structure of fucose, there are differences between the different types of algae. However, rockweed dependans usually have two types of homogamellose (**Figure 2.2**). One type (I) contains repeating (1→3)-L-furanoglucan and the other type (II) contains alternating and repeating (1→3)- and (1→4)-L-furanoglucan¹²⁹.

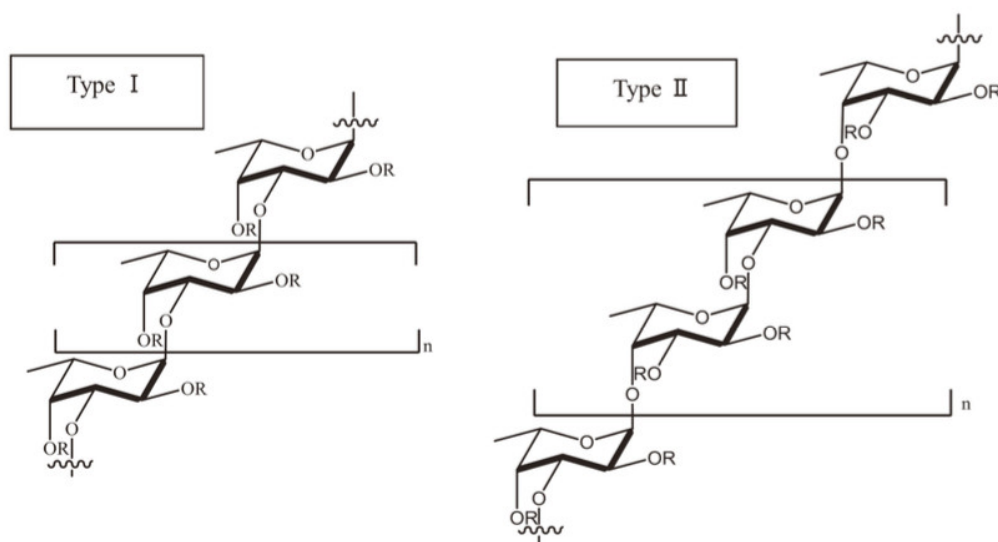


Figure 2.2 Type I and type II of common backbone chains in brown seaweed fucoidan. R can be fucopyranose, glucuronic acid and sulfate groups, while the location of galactose, mannose, xylose, rhamnase, arabinose and glucose in several kinds of seaweed species remains unknown.

Reports based on the fucoidan structure have led to further structural refinement of fucoidan sulfates. Studies have reported that most fucoidan-derived rockweed species have alternating bonds of (1→3)- α -L-fucose and (1→4)- α -L-fucose^{130,131}. The structures nodule algae rockweed and fucoidan resemble each other, differing significantly only according to the sulphate pattern and the presence of glucuronic acid¹³². There are many species of fucoidan, such as *Fusarium fuciformis*, *Fusarium distichulate* and *Pelvetia canaliculate*, for

example, *Fucus serratus*, *Fucus distichus* and *Pelvetia canaliculate*¹³³. Exceptions do exist, from *Bifurcaria bifurcata* and *Himanthalia* elongated rockweed dependans do not follow or are attributed to this structural feature¹³⁴. Identifying the structure of rockweed dependans according to the species to which they belong presents a challenge.

Another important fact worth noting is that the structure of the rockweed etiolated glycans is also highly dependent on the harvesting season. This is based on the fact that *Undaria pinnatifida*, a rockweed dependant glycan, shows unique properties and biological activity, especially when harvested in different seasons^{135,136}. In addition, it should be noted that purification methods also play a crucial role in the structure of rockweed dependant glycans. To some extent, new purification methods have revealed that the structure of rockweed etiolated glycans consists of multiple components¹³⁷. One investigation reported that the structure of crude rockweed etiolated glycans derived from *Aspergillus nodosus* revealed the predominance of $[\rightarrow(3)\text{-}\alpha\text{-L-Fuc}(2\text{SO}_3\text{-})\text{-}(1\rightarrow4)\text{-}\alpha\text{-Fuc}(2,3\text{diSO}_3\text{-})\text{-}(1)]_n$ ¹³⁸. However, from the same species, the rockweed glycosyl residues, consisting mainly of $\alpha\text{-}(1\rightarrow3)$ with sparsely attached $\alpha\text{-}(1\rightarrow4)$, are highly branched¹³⁹. Thus, the use of various extraction methods can lead to different structures. For example, one report indicated that one species yielded two different structures of rockweed etiolated glycans, in particular galactan and ureidoalkaloids¹⁴⁰. It should therefore be emphasised that the purification technique is one of the determinants of the structure and associated biological activity.

2.4.3. Fucoidan and Metabolic Syndrome

In recent years, fucoidan has received a lot of attention as a treatment for diabetes and other types of metabolic syndrome (MetS). Fucose derived from *Fusarium verticillioides* has been suggested as an alpha-glucosidase inhibitor for the treatment of diabetes¹⁴¹. In other studies, fucose has been cited as having the ability to attenuate diabetic retinopathy by

inhibiting VEGF signaling¹⁴². Low molecular weight fucose has been found to provide protection against diabetes-related symptoms in Goto-Kakizaki rats¹⁴³. Fucose can also provide protection against diabetes-related symptoms by modulating AMPK signaling and GLUT4 activity. Fuc-Pg can also improve glucose tolerance by modulating AMPK signaling and GLUT4 activity¹⁴⁴. Some studies have mentioned that Fuc-Pg with 310 kDa Mw can be used as a functional food for the treatment of MetS¹⁴⁵. Fuc-Pg reduces body weight in mice fed a high-fat diet and also reduces hyperlipidaemia and protects the liver from steatosis¹⁴⁶. degeneration. At the same time, Fuc-Pg reduced serum inflammatory cytokines and reduced infiltration of the macrophages into the adipose tissue. Furthermore, since it was identified as a tetrasaccharide repeat unit with a $[\rightarrow 3\text{Fuc}(2\text{S},4\text{S})\alpha 1 \rightarrow 3\text{Fuc}\alpha 1 \rightarrow$ backbone, the therapeutic effect on MetS was declared to be mainly related to the 4-O sulphated structure of the rockweed etiolated glycan.

With the rapid development of gut microbial research, fucodian is considered in some cases to be a prebiotic that regulates the gut ecosystem or microbiome. It promotes the growth of beneficial bacteria, which is the mechanism that inhibits MetS development¹⁴⁷. Parnell *et al.* showed that prebiotics containing rockweed etiolated glycans can stimulate the growth of probiotic organisms by providing a favourable environment for to regulate blood glucose and metabolism¹⁴⁸. Cheng *et al.* also demonstrated that *Clostridium perfringens rockweedii glycan* (SFF) could alter intestinal flora during the attenuation of streptozotocin-induced hyperglycaemia in mice¹⁴⁹. SFF had a yield of 6.02%, a sulphate content of up to 14.55% and a mean Mw of 205.8 kDa. This study was conducted on diabetic mice After 6 weeks of administration, SFF significantly reduced fasting blood glucose, diet and water intake. In additional, SFF reduced pathological changes in heart and liver tissue, thus improving liver function. Similarly, SFF inhibited oxidative stress in STZ-induced diabetic

mice, a manifestation associated with MetS. Also, SFF significantly altered the intestinal flora of diabetic mice, notably SFF reduced the relative abnormalities of intestinal bacteria associated with diabetes, which may be a potential mechanism for alleviating diabetic symptoms.

Even though the results shown in this section seem to have important implications for the reversal of diabetes and MetS, it should be noted that related research is still being conducted globally. The reason for this is based on the fact that scientists are still searching for the mechanism that gives fucoidan the ability to reverse diabetes or MetS. Other factors to consider are short-chain fatty acids (SCFA), which are well known to provide a beneficial environment in the gut after oral administration of oral fucoidan, as fucoidan cannot be digested by gastrointestinal enzymes, although their fermentation is thought to be possible. They are ideal for SCFA production by intestinal flora. Therefore, depending on interest, others may study fucoidan through the physiology or pathophysiology of the gut, and some may explore the liver and/or pancreas as they play an integral role in digestion, particularly in the gut, and some may study the microbiological background alongside the exact mechanism of fucoidan dependency. The reality is that research, which is still in its early stages, needs to be completed before fucoidan can be considered as a drug or future therapy for MetS and diabetes. A solid future program and/or direction may need to be well established when using a particular type of fucoidan.

Chapter 3

SARGASSUM FUSIFORME FUCOIDAN SP2 EXTENDS THE LIFESPAN OF DROSOPHILA MELANOGASTER BY UPREGULATING THE NRF2-MEDIATED ANTIOXIDANT SIGNALING PATHWAY^{1,2}

Abstract

Damage accumulated in the genome and macromolecules is largely attributed to increased oxidative damage and a lack of damage repair in a cell, and this can eventually trigger the process of aging. Alleviating the extent of oxidative damage is therefore considered as a potential way to promote longevity. SFPS, a heteropolysaccharide extracted from the brown alga *Sargassum fusiforme*, has previously been shown to alleviate oxidative damage during the aging process in mice, but whether SFPS could extend the lifespan of an organism was not demonstrated. Furthermore, the precise component within SFPS that is responsible for the antioxidant activity and the underlying mechanism of such activity was also not resolved. In this study, SFF, a fucoidan derived from SFPS, was shown to exhibit strong antioxidant activity as measured by *in vitro* radical-scavenging assays. SFF also improved the survival rate of *D. melanogaster* subjected to oxidative stress. The flies that were fed with a diet containing SFF from the time of eclosion displayed significant enhancement in lifespan and reduced accumulation of triglyceride at the old-age stage. In addition, SFF markedly improved the activities of the antioxidant enzymes, superoxide dismutase (SOD), catalase (CAT), and

¹ This work has been published as Ya Zhang, Man Xu, Chenxi Hu, Amei Liu, Junjie Chen, Chenfei Gu, Xu Zhang, Cuiping You, Haibin Tong, Mingjiang Wu, Peichao Chen. *Sargassum fusiforme* Fucoidan SP2 Extends the Lifespan of *Drosophila melanogaster* by Upregulating the Nrf2-Mediated Antioxidant Signaling Pathway. *Oxid Med Cell Longev.* 2019,14:8918914. DOI: 10.1155/2019/8918914.

² This work has been published as Peichao Chen, Ya Zhang, Man Xu, Huixi Zou, Haibin Tong, Cuiping You, and Mingjiang Wu. Proteomic landscape of liver tissue in old male mice that are long-term treated with Polysaccharides from *S. fusiforme*. *Food Funct.*, 2020, 11(4):3632-3644. DOI: 10.1039/D0FO00187B.

glutathione peroxidase (GSH-Px) and reduced the contents of the malondialdehyde (MDA) and oxidized glutathione (GSSG) in old flies. Furthermore, SFF also upregulated the expression levels of the nuclear factor-erythroid-2-like 2 (nfe2l2 or nrf2) and its downstream target genes, accompanied by a dramatic reduction in the expression of kelch-like ECH-associated protein 1 (keap1, a canonical inhibitor of the Nrf2) in old flies. Additional support linking the crucial role of the Nrf2/ARE pathway to the antioxidant effect of SFF was the relatively high survival rate under heat stress for *D. melanogaster* individuals receiving SFF supplement, an effect that was abolished by the inclusion of inhibitors specific for the Nrf2/ARE pathway. Collectively, the results indicated that SFF, a *S. fusiforme* fucoidan, could promote longevity in *D. melanogaster* by enhancing the Nrf2-mediated antioxidant signaling pathway during the aging process.

Keywords: *S. fusiforme*; SFF; Nrf2/ARE; oxidative stress; aging

3.1. Introduction

Aging is a time-dependent and gradual decline in the physiological function of an organism, which ultimately results in diseases and death. It is now well accepted that the cause of aging and the factors that promote aging are related to genes, oxidative stress, signaling pathways, and energy metabolism¹⁵⁰⁻¹⁵². Although the exact cause of aging is still a controversy, it is well acknowledged that these factors are interconnected and they also interact with each other. The concept that oxidative damage can promote aging is well recognized^{153,154}. Cumulative genomic and cellular damages might induce the time-dependent loss of function in living organisms, and this is predominantly a result of oxidative damage¹⁵⁵. However, the anti-aging effect conferred by antioxidants remains inconclusive, since the extension of lifespan achieved by long-term consumption of antioxidants such as vitamin E, vitamin A, beta-carotene, and glutathione (GSH) is not consistent among different organisms, and in human, an increase in the mortality has even been observed¹⁵⁶⁻¹⁵⁸. Therefore, the strategy of using antioxidant to promote longevity should be optimized.

Free radicals such as reactive oxygen species (ROS) and reactive nitrogen species (RNS) are considered as the major drivers of oxidative damage. These free radicals and the onset of oxidative damage can be neutralized or alleviated by detoxifying and antioxidant enzymes such as SOD, CAT, and GSH-Px, which are transcriptionally regulated by the Nrf2/ARE signaling pathway¹⁵⁹. Nrf2 is a transcriptional factor that plays an indispensable role in the detoxification and antioxidant systems, and *nfe2l2*, the gene encoding Nrf2, has even been proposed to act as a longevity gene^{160,161}. Unsurprisingly, knocking out the *nfe2l2* gene in mice has been shown to dramatically reduce the capacity of stress resistance and cellular protection, thus accelerating the aging process^{162,163}. Additionally, Nrf2 is highly expressed in young mice and naked mole rats^{164,165}. There have been numerous studies showing that

activation of the Nrf2/ARE signaling pathway can slow down the aging process or ameliorate aging-related diseases^{166,167}. However, more substantial evidence is still needed to confirm the antiaging effect conferred by the activation of the Nrf2/ARE signaling.

Sargassum fusiforme is a seaweed that has earned its reputation as a longevity-promoting vegetable in Northeastern Asia since it can modulate metabolism, strengthen immune response, and maintain redox homeostasis¹⁶⁸. Many studies have shown that polysaccharides extracted from *S. fusiforme* possess antioxidant, antitumor, and immunomodulatory activities¹⁶⁹. Our previous studies have revealed that SFPS, a heteropolysaccharide extracted from *S. fusiforme*, can significantly improve the antioxidant defense in aging mice by promoting Nrf2-dependent stress resistance and cellular protection¹⁷⁰. However, whether SFPS might also extend the lifespans of organisms, in general, remains undetermined.

In this study, we screened several fractions of polysaccharides derived from SFPS. The screening procedure combined *in vitro* cell-free antioxidant assay with *in vivo* oxidative-resistant test. The results suggested that long-term SFF supplement could significantly prolong the lifespan of *D. melanogaster* and enhance its antioxidant capacity. Subsequent experiment further showed that the SFF could significantly activate the CncC/Nrf2-mediated antioxidant signaling pathway, thus enhancing the stress resistance and antiaging capacity of *D. melanogaster*. Collectively, the data suggested that SFF might promote longevity in *D. melanogaster* through activating the Nrf2/ARE signaling pathway.

3.2. Materials and methods

3.2.1. Materials and reagents

Sargassum fusiforme was harvested from the coast of Wenzhou, Zhejiang Province, China. L-Rhamnose (L-Rha), D-galacturonic acid (D-GalA), D-mannose (D-Man), and D-

xylose (D-Xyl) were purchased from China National Institute for the Control of Pharmaceutical and Biological Products. Luteolin, all-trans-retinoic-acid (ATRA), D-glucuronic acid (D-GlcA), D-glucose (D-Glc), D-galactose (D-Gal), and L-arabinose (L-Ara) were purchased from Sigma-Aldrich. 1-Phenyl-3-methyl-5-pyrazolone (PMP) was purchased from Major Chemicals Co. Ltd. (Hangzhou, China). Acetonitrile (HPLC-grade) was obtained from Merck (E. Merck, Darmstadt, Germany). Other utilized chemicals used were of analytical reagent grade.

3.2.2. Extraction of Polysaccharides from *S. fusiforme*.

Fresh *S. fusiforme* was dried to a constant weight and then pulverized to powder, which was then used for polysaccharide extraction as described previously. In brief, the powder was initially defatted in 95% ethanol, and then the heteropolysaccharide SFPS was isolated from the residual fraction by hot-water extraction and ethanol precipitation. Subsequently, fractionation of SFPS, which involved CaCl₂ precipitation to separate the fucoidan from the alginate, yielded three fractions, designated as SP1, SP2, and SP3 (**Figure 3.1**).

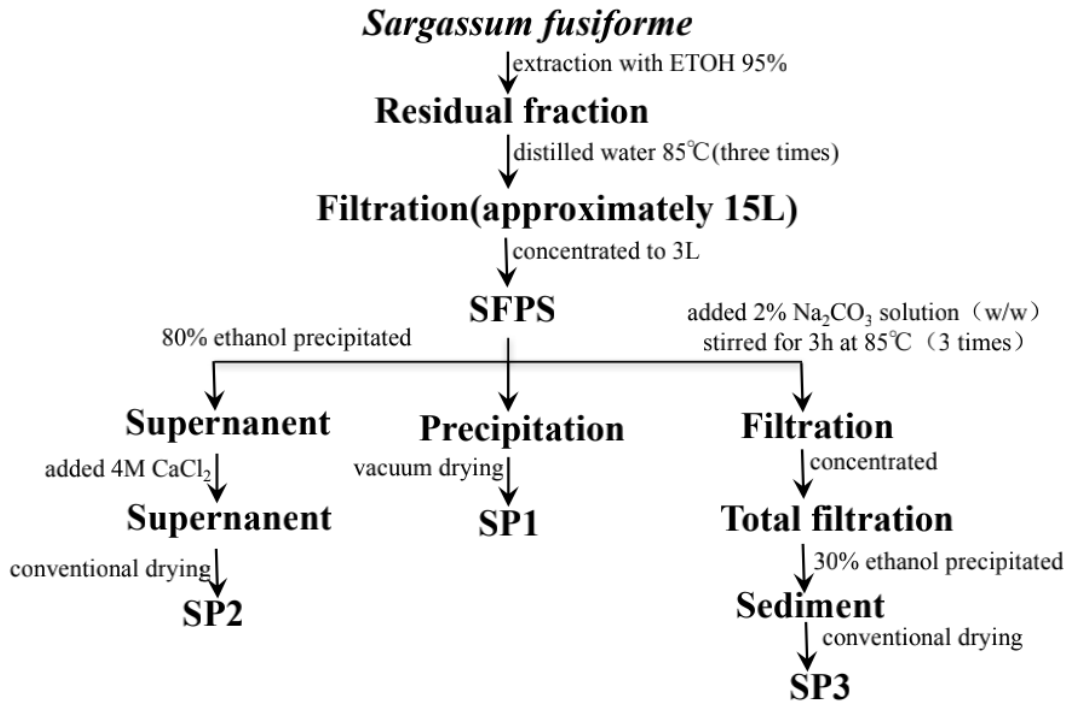


Figure 3.1. The extract technological process of the polysaccharides from *S. fusiforme*.

3.2.3. Stress-Induced Survival Rate Assays and Lifespan Assay.

Drosophila melanogaster individuals (male and female) were maintained at 25°C and 60% relative humidity and under a 12 h light : 12 h dark cycle. According to the gender, the virgin flies were separated within 8h after eclosion. They were reared on basal medium (10.5% cornmeal (w/v), 10.5% sucrose (w/v), 2.1% yeast (w/v), 1.3% agar (w/v), and 0.4% propionic acid (v/v)) without or with polysaccharide. Male flies were randomly divided into four groups, with at least 100 flies per group. One group was reared on basal medium only (Con group) while the remaining groups were each reared on basal medium plus 1.6g/L SP1, SP2, or SP3 for 10 days. After that, the flies were transferred to a medium containing 5 mmol/L paraquat, and the number of dead flies from each group was recorded every 10 h. Lifespan assay: the lifespan assay was carried out from the time of eclosion to death. The flies were reared on basal medium without or with different concentrations of SP2 (0.4 g/L: low

concentration of SP2, LSP; 0.8g/L: median concentration of SP2, MSP; and 1.6g/L: high concentration of SP2, HSP). The number of dead flies from each group was recorded every day until all the flies were dead. Heat stress-induced survival rate assay with/without inhibition of the Nrf2/ARE signaling pathway: to block the Nrf2/ARE signaling, flies were reared on basal medium containing, in addition to SP2, the chemical inhibitor of the Nrf2/ARE pathway, luteolin or all-trans-retinoic acid (ATRA). The flies were divided into five groups: C or control group (no inhibitor), L1 group (15 μ mol/L luteolin), L2 group (30 μ mol/L luteolin), A1 group (0.125 g/L ATRA), and A2 group (0.25 g/L ATRA). The concentration of SP2 used was the concentration that yielded the best antiaging effect for each sex, as determined from the result of the life-span experiment. The flies were reared in a 30°C incubator to provide heat stress, and the number of dead flies from each group was recorded every day until all the flies were dead. In addition, another lot of flies were prepared in the same way; but after 10 days, 15 flies per sample and 3 samples per group were taken for RNA extraction, whereas 25 flies per sample and 3 samples per group were used taken for protein extraction at a specific time. The RNA and protein samples were used for subsequent qRT-PCR and antioxidant activity assays, respectively.

3.2.4. HPLC Analysis.

The molecular weight of SP2 was determined by high-performance gel-permeation chromatography (HPGPC) using a Waters HPLC apparatus equipped with a TSK-gel G-5000PWXL column (Φ 7 8 mm \times 300 mm ID, TOSOH, Japan) and a Waters 2414 refractive index detector. The SP2 sample (20 μ L of 5 mg/mL preparation) was injected into the column and eluted with 0.2M NaCl at a flow rate of 0.6mL/min and a column temperature of 45°C. The molecular weights were estimated by reference to the calibration curve obtained from the elution of Dextran T-series standards of known molecular weights. HPLC was performed with

a Hypersil ODS-3 column (4.6 mm × 250 mm) using a mobile phase consisting of 83.0% (v/v) phosphate-buffered saline (PBS, 0.1 mol/L, pH6.9) and 17% acetonitrile (v/v). The flow rate was set at 0.8mL/min, and the eluent was monitored by absorbance at 254nm. D-Glc, D-Gal, L-Ara, L-Rha, D-Xyl, D- Man, L-Fuc, D-GalA, and D-GlcA were used as reference monosaccharides.

3.2.5. Fourier Transform-Infrared (FT-IR) Spectroscopy.

The FT-IR spectrum of the SP2 was obtained with a Tensor 27 spectrophotometer (Bruker Daltonics, Ettlingen, Germany). The SP2 sample was mixed with KBr powder and then pressed into a 1mm thick disk, which was then used to obtain the spectrum, recorded in the frequency range of 4000-400cm⁻¹.

3.2.6. Detection of Triglyceride (TG) Content.

Twenty-five flies from each experimental group were randomly taken at a specific time point to determine the content of triglyceride. Triglyceride content was determined by measuring the concentration of soluble triglyceride. The flies were first combined and homogenized in normal saline. The homogenate was centrifuged at 3000 × g, and the concentration of TG in the supernatant was measured using a Genzyme Triglyceride Kit purchased from Nanjing Jiancheng Incorporation (Nanjing, China).

3.2.7. Scavenging Activity of DPPH (1,1-Diphenyl-2- Picrylhydrazyl Radical 2,2-Diphenyl-1-(2,4,6-Trinitrophenyl) Hydrazyl) Radical.

The effect of SP2 on free radical- scavenging activity was evaluated by measuring the level of DPPH-scavenging activity using a DPPH-scavenging assay kit purchased from Nanjing Jiancheng Incorporation (Nanjing, China). Polysaccharide solution was prepared by dissolving the polysaccharide powder in distilled water as previously described¹⁶⁹. Next, the

polysaccharide solution was added to DPPH reagent (in 95% ethanol) to yield a final concentration of 0.4, 0.8, or 1.6g/L, and the reaction mixture was thoroughly mixed by shaking and then incubated in the dark for 30 min at room temperature. After that, the absorbance of the resulting solution was read at 517 nm against a blank. DPPH radical-scavenging activity was calculated using the equation: DPPH – scavenging rate(%) = $1 - \frac{A1-A2}{A0} \times 100\%$, where A0 is the absorbance of the DPPH alone, A1 is the absorbance of DPPH+polysaccharide, and A2 is the absorbance of the polysaccharide only.

3.2.8. FRAP (Ferric Ion Reducing Antioxidant Power) and ABTS (2,2'-Azino-Bis(3-Ethylbenzothiazoline-6-Sulfonic Acid)) Assays.

FRAP and ABTS assays were performed using assay kits purchased from Nanjing Jiancheng Incorporation (Nanjing, China) but with an additional control consisting of the sample only to account for the absorbance due entirely to the polysaccharide¹⁷⁰. FRAP reagent was prepared by mixing 300 mmol/L acetate buffer (pH 3.6) with 10 mmol/L 2,4,6-tripyridyl-s-triazine (TPTZ) and 20 mmol/L FeCl₃ in a volume ratio of 10:1:1, while ABTS radical was prepared by mixing the ABTS solution (7mmol/L) with potassium persulfate (2.45 mmol/L).

3.2.9. Measurements of the MDA Content and the Enzymatic Activities of CAT and SOD.

Twenty-five flies from each group were randomly collected at a specific time and then homogenized as one sample. After centrifugation at 3000 × g, the supernatant was used for MDA, CAT, and SOD assays performed with assay kits purchased from Nanjing Jiancheng Incorporation (Nanjing, China). The principles of the assay kits were based on previously described methods.

3.2.10. qRT-PCR Analysis.

Total RNA was extracted from whole flies using the TRIzol reagent. Fifteen flies per

sample and three samples per group were taken for total RNA extraction. The total RNA extracted from each sample was then subjected to qRT-PCR analysis using the AffinityScript qPCR cDNA synthesis kit. The primers for the target genes were designed based on the sequences retrieved from FlyBase (<http://flybase.org>). The sequences of the primers are listed in Table 1. Quantitative RT-PCR assay was performed in a Roche LightCycler 480 platform using the SYBR Green II method. The transcript level of each gene was calculated by the $\Delta\Delta C_t$ method with reference to that of the Rp49 gene and then normalized to the corresponding control group (**Table 3.1**).

Table 3.1. The sequence and use of primers

| Gene | FlyBase no. | Forward primers (5'-3') | Reverse primers (5'-3') |
|-------|-------------|-------------------------|-------------------------|
| cncC | FBgn0262975 | GTCGCCACTAAAACCGCATC | TTGTTCTTTCCACGCCGACG |
| Keap1 | FBgn0038475 | TACGAAGATAGTGACGCCCC | GTGAAAGACGCTGGTGGAGT |
| ho-1 | FBgn0037933 | ATGACGAGGAGCAGCAGAAG | ACAAAGATTAGTGCGAGGGC |
| gclc | FBgn0040319 | GAGCCATTAGTGCCGTTAGT | GTCTTTCGTCTTCGTCTTGG |
| Rp49 | FBgn0002626 | CCCTCTTCCAGCCATCGTTC | CCACCGATCCAGACGGAGTA |

3.2.11. Statistical Analysis.

The data were expressed as mean \pm SD of, at least, three separate experiments. Statistical analyses were carried out by two-way ANOVA and Fisher's LSD multiple comparison tests by SPSS 17.0. Differences among groups were considered statistically significant at the $P < 0.05$ level.

3.3. Results

3.3.1. The Fucoidan SP2 Exhibits Excellent Antioxidant Activity.

It is well acknowledged that oxidative damage contributes to aging, and therefore, factors that enhance resistance to oxidative stress are considered to have anti-aging effects. We have previously reported that the SFPS, an *S. fusiforme* heteropolysaccharide, possesses antioxidant activity and shown that it can significantly alleviate aging-related stresses. However, the active component of SFPS responsible for the antiaging effect was not further evaluated. To address this issue, SFPS was fractionated into three fractions, which were designated as SP1, SP2, and SP3 (**Figure 3.1**). SP1 and SP2 were both fucoidan whereas SP3 was alginate. In order to select the most promising candidate, the antioxidant capacities of SP1, SP2, and SP3 were determined by both *in vitro* and *in vivo* methods. SP2 displayed the highest antioxidant activity as shown by radical- and ion-scavenging activities, in particular, the ABTS clearance rate of SP2 was twice the rate of SP1 (**Figure 3.2**). All three polysaccharides significantly enhanced the average survival time of *D. melanogaster* individuals that were treated with 5 mmol/L paraquat to induce oxidative stress. The flies that did not receive polysaccharide supplement died within 48 h of paraquat treatment. Twenty-four hours after paraquat treatment, the survival rate of the flies that had been given SP2 was 70%, whereas those of flies that had been given SP1 and SP3 were 55.4% and 57.2%, respectively, while flies that did not receive polysaccharide had a survival rate of just 39.5% (**Figure 3.2**). The results suggested that SP2 might be an effective antioxidant, and therefore, it was chosen for further antiaging assessment.

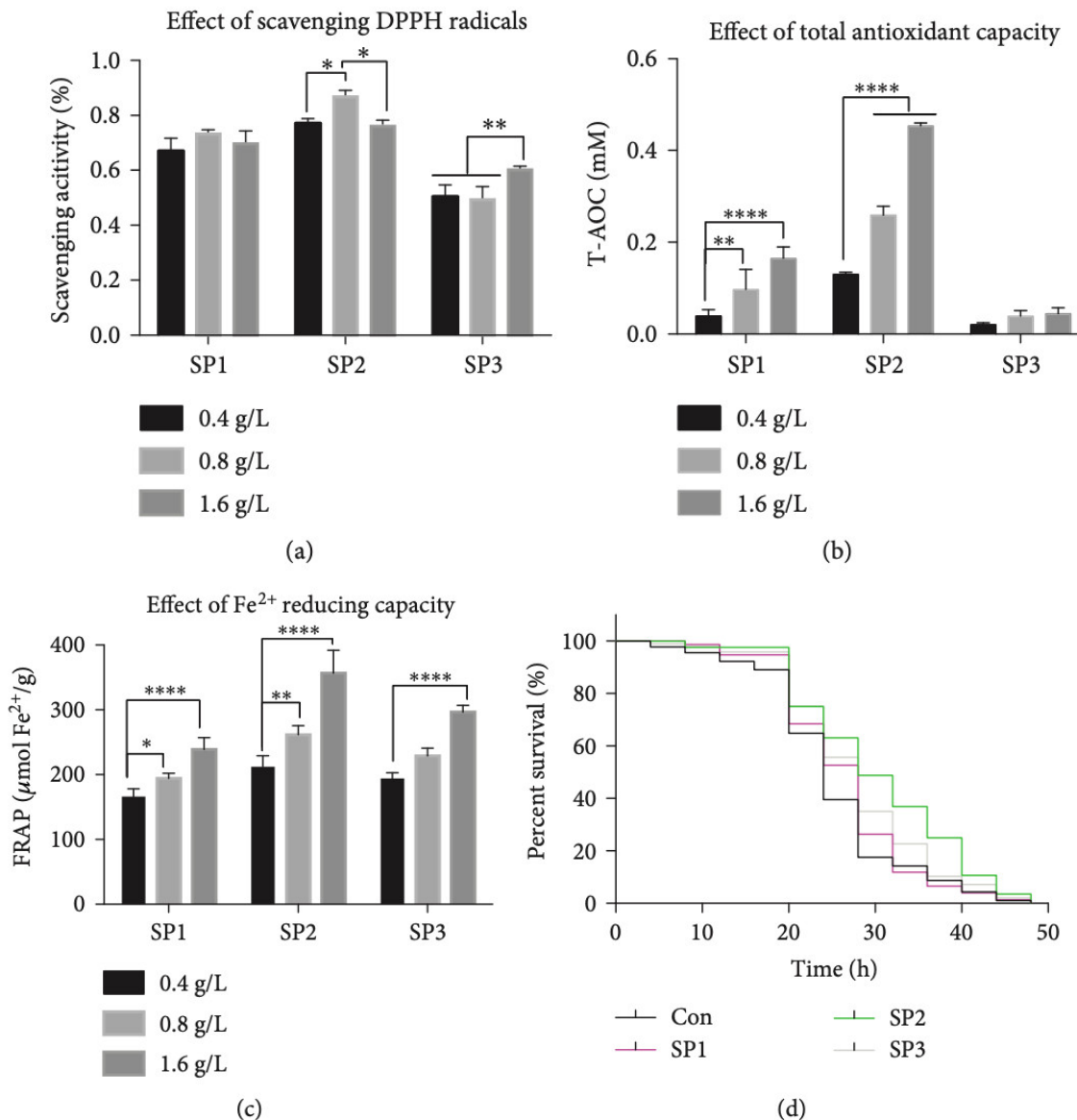


Figure 3.2. Antioxidant capacity of the different polysaccharides fractionated from SFPS. Antioxidant activity of the polysaccharides was assayed in three different cell-free systems. (a) DPPH-scavenging activity, (b) ABTS-scavenging activity, and (c) radical-scavenging activities and Fe²⁺ reducing. Data are shown as mean±SD from three determinations. (d) Fruit flies were randomly collected (100 flies/group) and reared on basal medium without (control group) or with 1.6 g/L of SP1, SP2, or SP3 for 10 days. Subsequently, the *in vivo* oxidative resistant capacity was evaluated by determining the survival rate of the flies following exposure to oxidative stress induced by 5 mmol/L paraquat, given as a diet.

3.3.2. Chemical Composition of SP2.

The bioactivity of a compound is closely related to its chemical composition and structure. Therefore, it is vital to explore the structure-activity relationship of SP2. SP2 was determined to be a fucoidan with fucose being the major monosaccharide (52.89%), while sulfate radical, which is a unique modification of fucoidan, accounted for about 15.3%. SP2 also contained a relatively high content of Xyl (12.1%), Gal (11.51%), and Glc (11.33%) (**Table 3.2**).

Table 3.2. Chemical composition of SP2

| Molecular weight (kDa) | Sulfate content (%) | Monosaccharide composition (%) | | | | | | | | |
|------------------------|---------------------|--------------------------------|------|-------|------|-------|-------|-------|-----|-------|
| | | Man | Rha | Glc A | GalA | Glc | Gal | Xyl | Ara | Fuc |
| 2.4×10 ⁵ | 15.3 | 3.50 | 1.77 | 1.11 | 2.61 | 11.33 | 11.51 | 12.10 | -- | 52.89 |

Notes: Man: D-mannose; Rha: L-rhamnose; GlcA: D-glucuronic acid; GalA: D-galacturonic acid; Glc: D-glucose; Gal: D-galactose; Xyl: D-xylose; Ara: L- arabinose; Fuc: L-fucose.

3.3.3. SP2 Promotes Longevity in *D. melanogaster*.

The *in vitro* antioxidant activity assay and the *in vivo* oxidative stress resistance assay both demonstrated the remarkable antioxidant capacity of SP2. However, the question as to whether SP2 could promote longevity under normal condition needed to be addressed. First, the flies were reared, from the time of eclosion, on media supplemented with different concentrations of SP2. The result revealed a significant increase in lifespan for the flies receiving SP2 supplement (**Figure 3.2, Table 3.3**). Interestingly, the effect of SP2 on the lifespan of the flies varied with gender. At a concentration of 1.6 g/L in the medium, SP2 extended the mean lifespan by about 22%, but it extended the male lifespan by a maximum of 10%. At 0.8 g/L, SP2 extended the mean lifespan by about 24% and the female lifespan by a maximum of 10% (**Table 3.3**). Further- more, SP2 also slowed down the accumulation of

triglyceride (TG) in the aging flies (**Figure 3.4**). Old flies are known to accumulate high levels of TG because of a significant decline in their metabolism, and thus, the accumulation of TG has been considered as an aging index. Our data was therefore consistent with SP2 having an antiaging effect, which was clearly demonstrated by its ability to increase the lifespan of *D. melanogaster*.

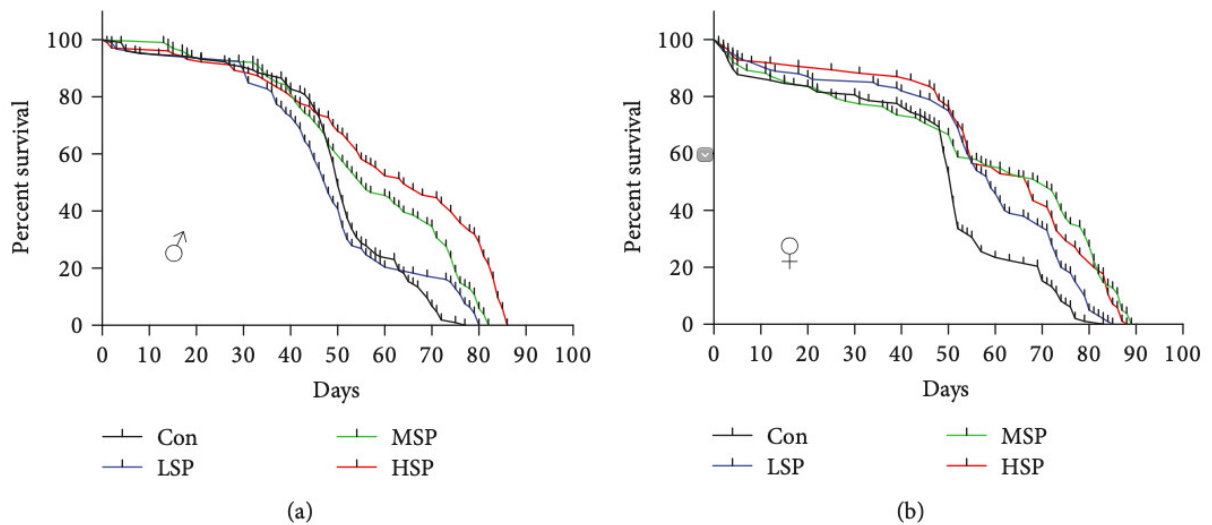


Figure 3.3. SP2 extends the lifespan of *D. melanogaster*. Male (a) and female (b) fruit flies were reared on medium containing no SP2 (Con) or different concentrations of SP2 (0.4 g/L (LSP), 0.8 g/L (MSP), and 1.6 g/L (HSP)); the number of dead flies from each group was counted daily; n > 250 flies.

Table 3.3. Effect of the SP2 to the lifespan of *D. melanogaster*.

| | Female | | | | Male | | | |
|---------------|----------|-----------|-----------|-----------|----------|----------|----------|-----------|
| | Con | LSP | MSP | HSP | Con | LSP | MSP | HSP |
| N | 270 | 288 | 281 | 288 | 291 | 283 | 272 | 275 |
| Max. lifespan | 83.0±1.7 | 85.1±1.0 | 91.5±1.1* | 87.1±2.3 | 80.2±1.2 | 84.3±3.6 | 84.5±2.2 | 88.4±1.9* |
| Mean lifespan | 59.7±1.3 | 66.9±1.3* | 74.1±0.9* | 70.4±0.8* | 58.2±2.5 | 56.0±3.6 | 65.3±1.9 | 71.1±3.0* |

Notes: mean ± SD, * P < 0.05.

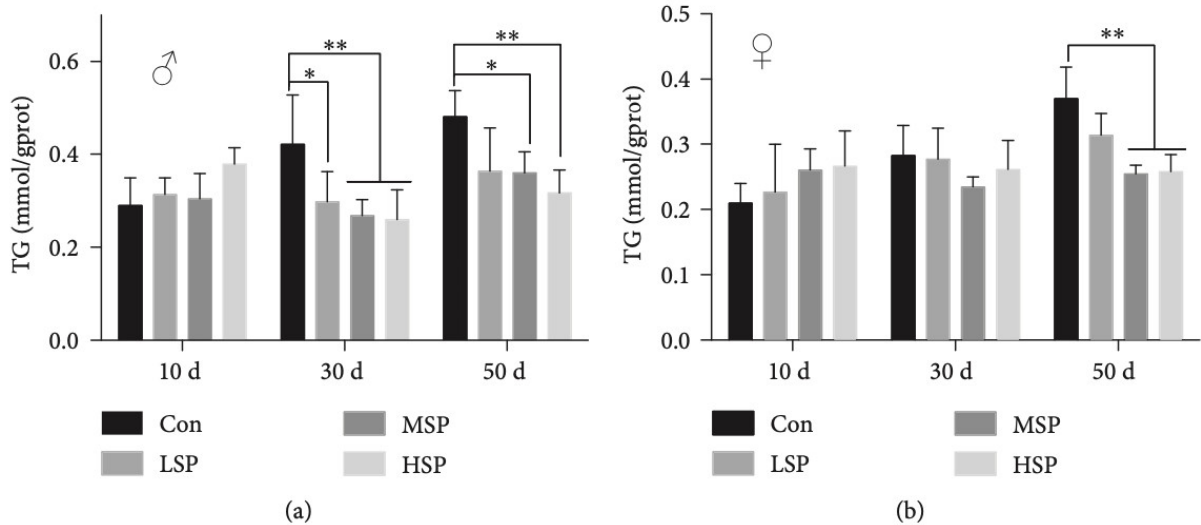
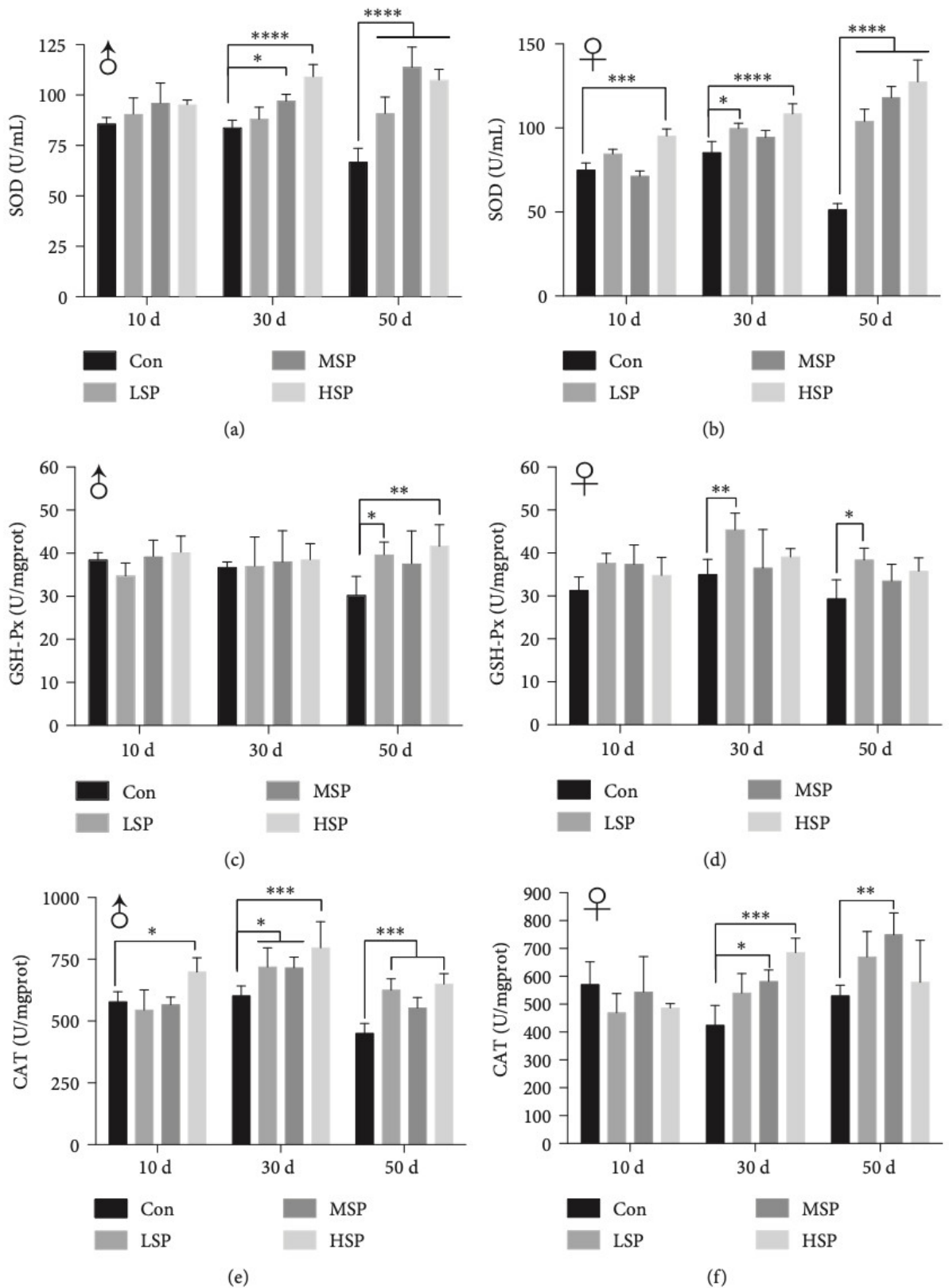


Figure 3.4. SP2 decreases the accumulation of triglyceride (TG) in *D. melanogaster* during the aging process. The flies were supplemented with varied concentrations of SP2 (0 (Con), 0.4 g/L (LSP), 0.8 g/L (MSP), and 1.6 g/L (HSP), and the contents of soluble TG in the male (a) and female (b) flies of different ages were then measured. Data are shown as the mean \pm SD from three determinations, each used the extract obtained from 25 flies. * and ** indicate a significant difference at the $P < 0.05$ and $P < 0.01$ levels, respectively.

3.3.4. SP2 Enhances the Endogenous Antioxidant Capacity of *D. melanogaster*.

Endogenous antioxidant activity is an important indicator for determining the aging status of an organism. For example, significant declines in peroxidase and superoxide dismutase activities have been observed in aging organisms, from yeast to human. Analysis of the antioxidant capacity of *D. melanogaster* over time revealed an overall decrease in 50-day-old individuals (**Figures 3.5 and 3.6**). Furthermore, the content of MDA in these individuals also increased during the aging process, and the ratio of GSH/GSSG, commonly used as an oxidant index, was reduced. In contrast, 50-day-old flies that had been given SP2 supplement exhibited significant increases in the levels of SOD, CAT, and GSH-Px activities. SP2 supplement also reduced the content of MDA in these individuals by as much as 50% and increased the GSH/GSSG ratio by about two folds (**Figures 3.5**). Taken together, these results suggested that SP2 supplement could slow the decline in antioxidant defense of *D.*

melanogaster during the aging process.



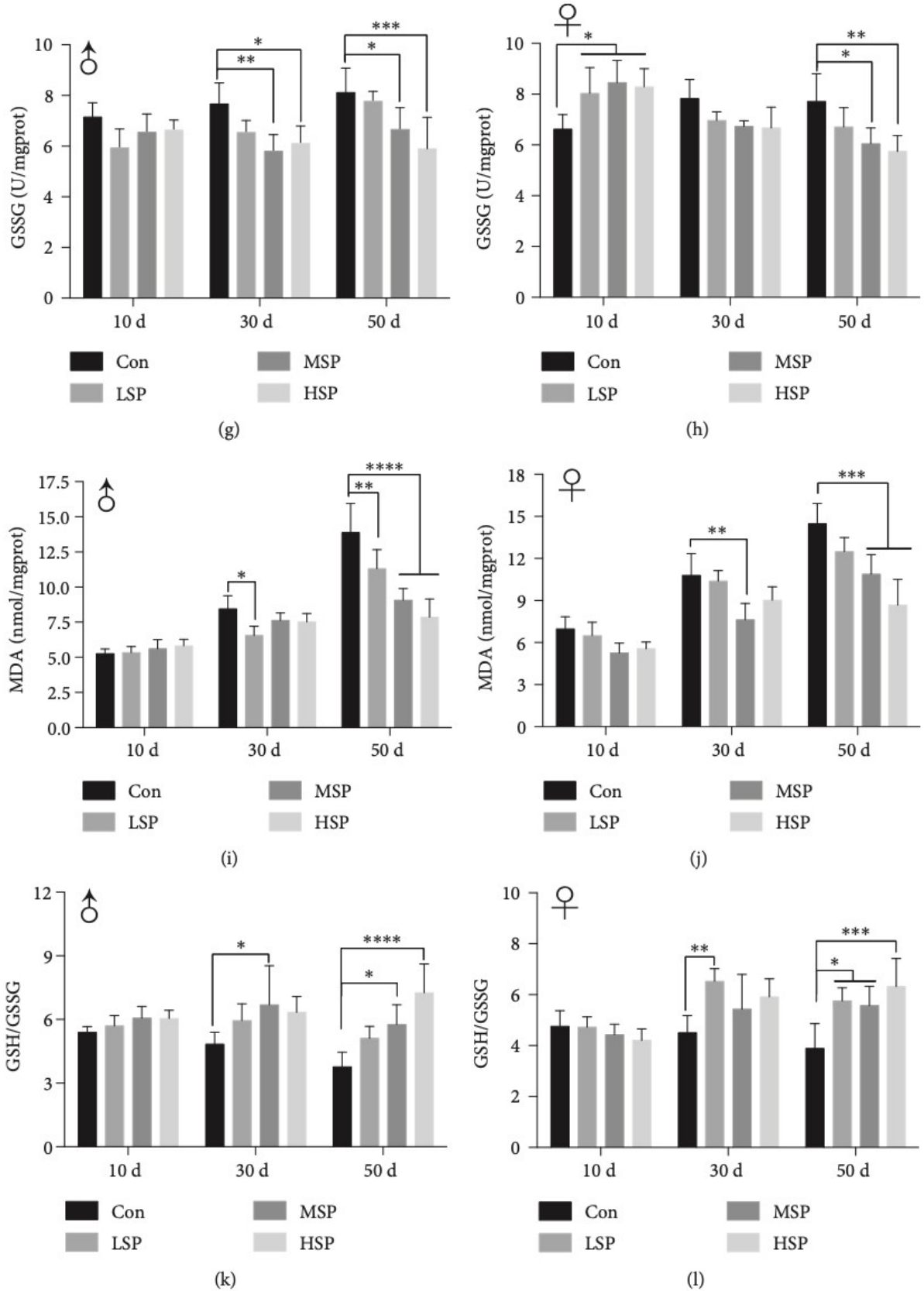


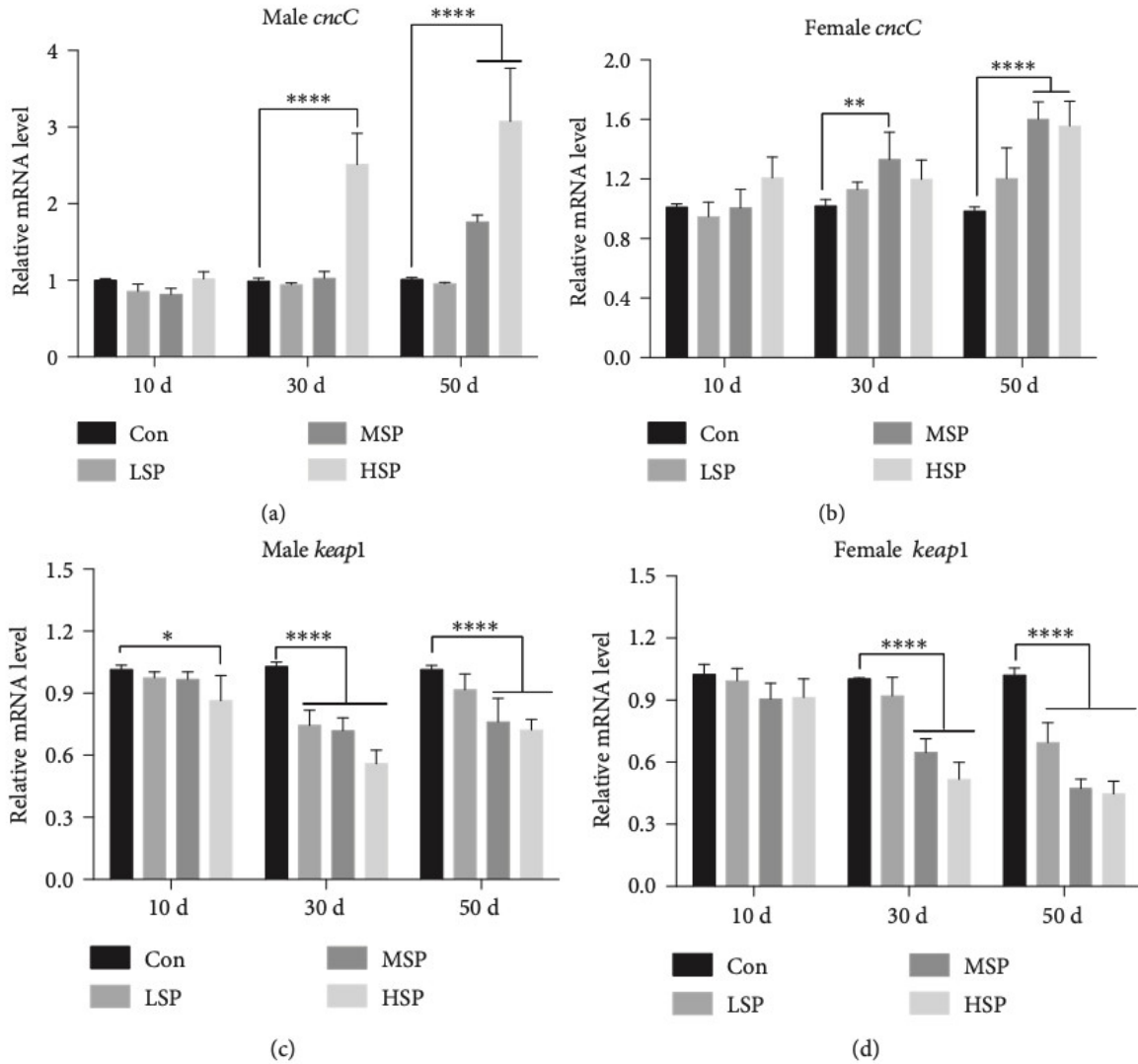
Figure 3.5. SP2-supplemented diet slows down the decline in the antioxidant capacity of *D.*

***melanogaster* during the aging process.** The fruit flies were reared on a medium containing no SP2 (Con) or different concentrations of SP2 (0.4 g/L (LSP), 0.8 g/L (MSP), and 1.6 g/L (HSP)), and their antioxidant capacity was analyzed at different ages. SOD activity (a, b); GSH-Px level (c, d); CAT activity (e, f); CSSG content (g, h); MDA content (i, j), and GSH/GSSG (k, l). The antioxidant capacity was determined for both male flies (a, d, e, g, i, and k) and female flies (b, d, f, h, j, and l). Data are shown as mean \pm SD from three determinations, each used the extract obtained from 25 flies. *, ** and *** indicate a significant difference at the $P < 0.05$, $P < 0.01$, and $P < 0.001$ levels, respectively.

3.3.5. Expansion of *D. melanogaster* Lifespan by SP2 Involves the CncC/Nrf2/ARE Signaling Pathway.

Nuclear factor erythroid 2-related factor 2/antioxidant responsive element (Nrf2/ARE) is one of the most important antioxidant pathways that counteract oxidative stress and damage. Nrf2 is conserved in metazoan, and in *D. melanogaster*, it is called CncC. Previous studies have shown that SFPS can upregulate the Nrf2/ARE signaling pathway to alleviate aging stress in mice^{169,170}. Whether SP2 might stimulate the Nrf2/ARE signaling pathway to enhance the lifespan of *D. melanogaster* was the focus of this study. First, the mRNA levels of *CncC* (*nrf2*) and its classical inhibitor *keap1* in the flies of different ages were measured. The results revealed a remarkable upregulation of the *CncC*, and dramatic downregulation of *keap1* mRNA levels in the old flies that had been given moderate (MSP) and high (HSP) concentrations of SP2 supplement (**Figures 3.6.a-d**). The transcriptional activity of Nrf2 was further determined by measuring the mRNA levels of its representative downstream target genes: *Ho-1* and *Gclc*. As expected, the mRNA levels of these downstream antioxidant genes were markedly upregulated at the 30-day-old and 50-day-old old stages in both sexes (**Figures 3.6.e-h**). Collectively, the results suggested that the Keap1/Nrf2/ARE signaling pathway might be significantly activated by SP2 during the aging process, thereby enhancing the

antioxidant capacity of *D. melanogaster* individuals that had been given SP2 supplement, with the consequence of extending their lifespans.



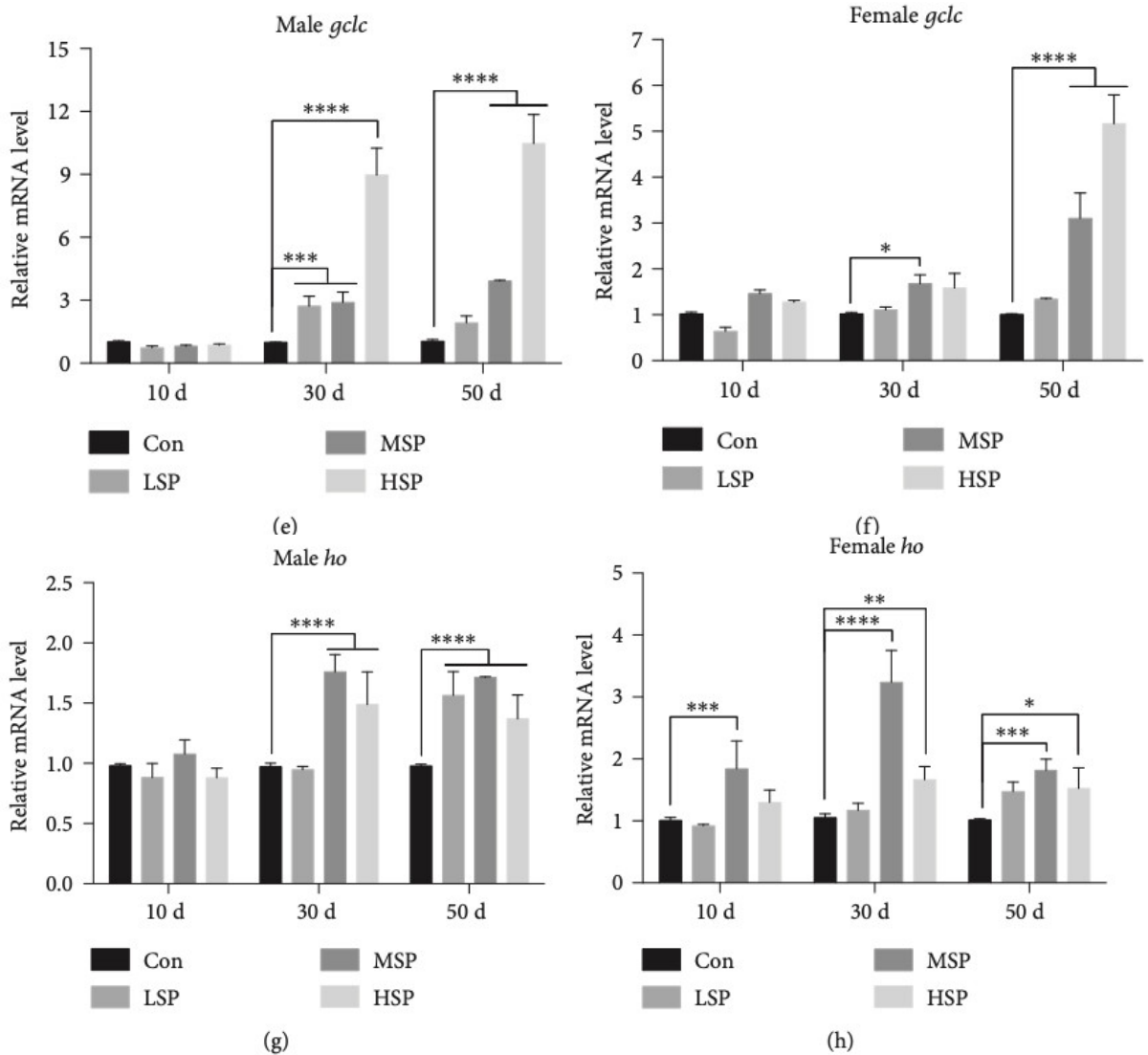
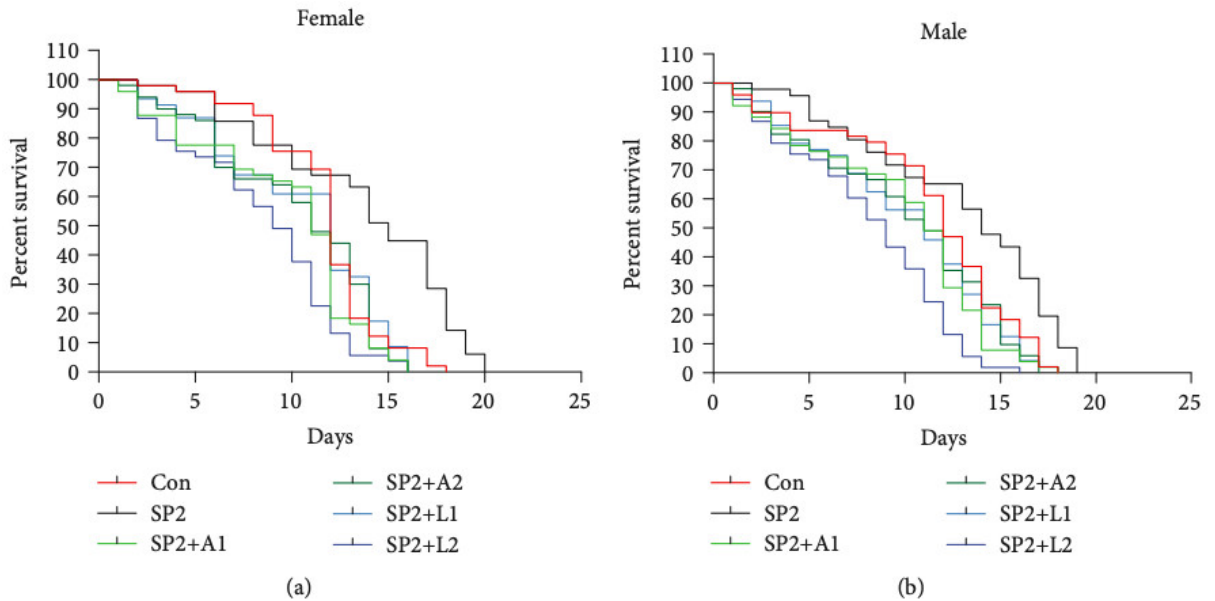


Figure 3.6. SP2 supplement upregulates the Keap1/CncC/ARE signaling pathway in aging flies. Fruit flies were reared on basal medium containing no SP2 (Con) or different concentrations of SP2 (0.4 g/L (LSP), 0.8 g/L (MSP), and 1.6 g/L (HSP)) over 50 days. The flies were taken at different time intervals, and the mRNA levels of the representative genes (*cncC*, *keap1*, *gclc*, and *ho*) of the Keap1/CncC/ARE signaling pathway were measured by qRT-PCR using the *rp49* gene as the reference gene. (a, b) *cncC*, (c, d) *keap1*, (e, f) *gclc*, and (g, h) *ho*. The expression levels of the genes were evaluated by the $\Delta\Delta C_t$ method and normalized to those of the corresponding control. Data are shown as mean \pm SD from three determinations, each used the RNA extracted from 15 flies. *, ** and *** indicate a significant difference at the $P < 0.05$, $P < 0.01$, and $P < 0.001$ levels, respectively.

3.3.6. SP2-Alleviated Heat Stress Depends on the CncC/Nrf2 Signaling Pathway.

To validate that SP2 might exhibit anti-stress effect via the Nrf2-mediated signaling pathway, the Nrf2/ARE signaling was blocked by the chemical inhibitor, luteolin or ATRA. In order to accelerate the aging process, the flies were subjected to heat stress at 30°C. SP2 supplement significantly extended the lifespan of the flies under heat stress, but this effect was neutralized when the flies also received luteolin or ATRA in the medium (**Figures 3.7A and B**). Furthermore, the mRNA levels of the *cncC* gene and its representative downstream target genes, *ho*, *cat*, and *gclc*, in flies that were given just SP2 supplement were significantly upregulated compared with the control (no SP2 supplement) but declined relative to the control when the flies received both SP2 plus luteolin or ATRA (**Figures 3.7C and F**). The effect of SP2 on stress resistance, therefore, appeared to be largely dependent on the CncC/Nrf2/ARE signaling pathway.



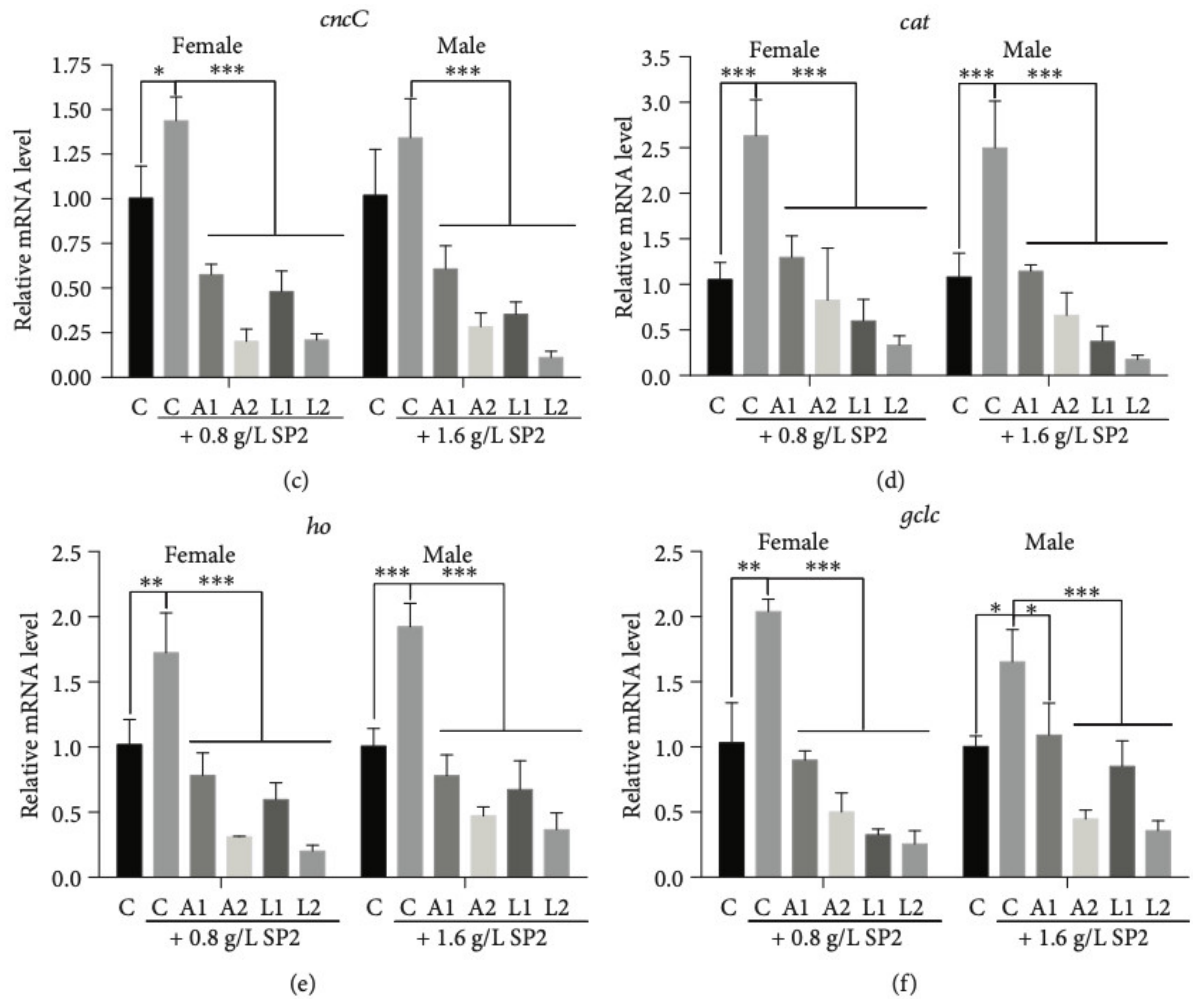


Figure 3.7. SP2-mediated stress-resistant effect in fruit flies is dependent on the CncC/Nrf2/ARE signaling. Fruit flies were reared on medium containing no SP2 (Con) or different concentrations of SP2 (0.4 g/L (LSP), 0.8 g/L (MSP), and 1.6 g/L (HSP)) without and with all-trans-retinoic-acid (A1, 0.125 g/L; A2, 0.25 g/L) or luteolin (L1, 15 μ mol/L; L2, 30 μ mol/L), and the survival rates of the flies were determined. (a) Survival rate of male flies; (b) survival rate of female flies. In addition, samples of the flies were also taken after 10 days of treatment, and the transcript levels of *cncC* (c), *cat* (d), *ho* (e), and *gclc* (f) were then measured by qRT-PCR using the *rp49* gene as a reference gene. The expression levels of the genes were evaluated by the $\Delta\Delta C_t$ method, and then normalized to those of the corresponding control. Data are shown as mean \pm SD from three determinations, each used the RNA extracted from 15 flies. *, ** and *** indicate a significant difference at the $P < 0.05$, $P < 0.01$, and $P < 0.001$ levels, respectively.

3.3.7. SP2 Has No Significant Effect on Body Weight.

To investigate whether SP2 might affect food intake or trigger calorie restriction in fruit flies, the body weights of the flies given SP2 supplement were compared with those not receiving SP2. SP2 appeared to increase the body weights of the flies as measured at 10, 30, and 50 days, but the increases were not significant for both male or female groups (**Figure 3.8**). This suggested that SP2 did not restrict the food intake in *D. melanogaster*.

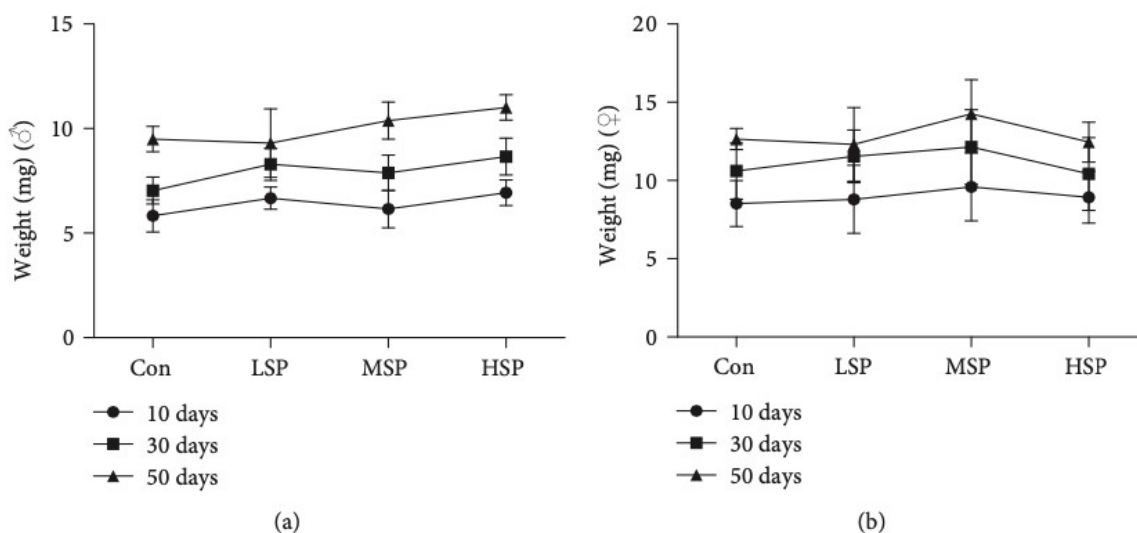


Figure 3.8. Effect of SP2 on *D. melanogaster* body weight. Body weights of male and female flies at different ages and reared on medium without (Con) or with different concentrations of SP2: LSP (0.4 g/L), MSP (0.8 g/L), and HSP (1.6 g/L). Data are shown as mean \pm SD from three determinations, each based on 10 flies.

3.4. Discussion

The use of *Sargassum fusiforme* by Traditional Chinese Medicine to treat thyroid diseases and as a health maintenance agent was first recorded in the ancient pharmaceutical book Shennong Bencaojing, but information concerning the effective components and the related mechanisms is still lacking. *S. fusiforme* has even been regarded as a longevity-

promoting vegetable because it helps to modulate metabolism, strengthen immune response, and maintain redox homeostasis¹⁶³. However, the claim that it promotes longevity has not been supported by any direct evidence, despite numerous studies demonstrating that extracts prepared from *S. fusiforme*, which contain predominantly polysaccharides, have different biological activities, such as antitumor and antioxidant activities^{167,168}. We have previously reported that the heteropolysaccharide SFPS extracted from *S. fusiforme* can enhance resistance to oxidative stress and even ameliorate the aging process in mice^{169,170}. However, there was no evidence to prove that *S. fusiforme* can extend the lifespan of an organism. In this study, we showed that the fucoidan SP2 (SFF), which was extracted from SFPS, could markedly prolong the lifespan of *D. melanogaster*, and to the best of our knowledge, this could be the first direct evidence to support the claim that *S. fusiforme* is a longevity-promoting vegetable.

We have integrated *in vitro* and *in vivo* antioxidant assays to screen for a promising antiaging candidate from among the different fractions extracted from SFPS. Initial tests revealed SFF to be a promising candidate, as it exhibited the best antioxidant activity and gave the highest survival rate when fed to the flies (**Figure 3.2**). SFF was therefore chosen for further study to examine its longevity-promoting effect. Indeed, SFF could increase the lifespan of the flies, further supporting its role as a longevity-promoting polysaccharide (**Figures 3.3 and 3.4**). Although the integrated screening method described in this study was robust, the extent of its validity and practicality may require further study, as the *in vitro* antioxidant assay may simply depend on a redox reaction, while the *in vivo* antioxidant assay depends on both nonenzymatic antioxidant and enzymatic systems. Previous studies that attempted to evaluate the antiaging effect of some antioxidants such as vitamin C, vitamin E, and β -carotene did not produce conclusive. Good consistency in antioxidant capacity between

in vivo and *in vitro* assays was obtained for SFF (**Figure 3.2**). Therefore, regardless of the extent of application for this anti-aging screening, the data gathered for SFF alone indicated that at least, our integrated method might provide a feasible and effective screening approach for other polysaccharides derived from brown alga, which might have the ability to slow down aging caused by oxidative damages.

It is worth noting that we merely provided one evidence of a promising anti-aging compound based on its strong antioxidant activity. However, aging is a complex process that also correlates with the down-regulation of metabolism and protection of cellular components against internal or external inflicted damage¹⁷¹. A decrease in antioxidant capacity and an accumulation of TG have been suggested as the hallmarks of aging.¹⁷² The content of TG decreased significantly in 50-day-old flies but increased slightly in 10-day-old flies when the flies were given SFF supplement (**Figure 3.4**). This suggested that SFF significantly promoted metabolism during the aging process and yet exerted no negative impact on development in young flies. The activities of SOD, GSH-Px, and CAT and the contents of MDA and GSH are usually used to provide a comprehensive assessment of the antioxidant capacity of an organism. SFF supplement significantly up-regulated the levels of SOD, CAT, and GSH-Px activities in the aging flies but down-regulated the content of MDA and the ratio of GSSG/GSH in these flies (**Figure 3.5**). Intriguingly, SFF did not interfere with the redox balance in 10-day-old flies but comprehensively slowed down both the decline in antioxidant capacity and the increase in oxidative stress in 30-day-old and 50-day-old flies (**Figure 3.5**). In addition, the lack of statistical significance in body weight increase for the flies given SFF supplement compared with their control counterparts suggested that long-term SFF supplement could significantly restore the loss of antioxidant capacity in *D. melanogaster* during the aging process without having any significant effect on growth (**Table 3.3**), and this

applied to both male and female flies.

Aging is also a process of time-dependent decline in function, with cumulative damage in biomacromolecules and down-regulation of cellular defense and damage repair. This is reminiscent of the expression pattern of Nrf2, a crucial stress regulator in the aging process, which is down-regulated in aging organisms¹⁷³, although the expression starts to decrease from the middle-age stage¹⁶⁹. Defect in Nrf2 can result in a decline of stress resistance and hence a shortened lifespan. Thus, it is of great importance to show whether reversing the decline of the Nrf2 expression would slow down the aging process. It has been validated that upregulation of the Nrf2 expression, either by genetic manipulation or by pharmacological interference, can significantly ameliorate the extent of aging-related diseases and/or retard the aging process¹⁷⁴⁻¹⁷⁶. In flies given SFF supplement, significant upregulation in the expression of cncC and its downstream target genes (*gclc*, *cat*, and *ho*) occurred, which further promoted stress resistance and longevity (**Figures 3.3–3.6**). Conversely, the stress-resistant effect of SFF was dramatically repressed by inhibitors of the CncC/Nrf2/ARE signaling, such as trans-retinoic-acid and luteolin (**Figure 3.7**). Although our data have clearly demonstrated the involvement of CncC/Nrf2/ARE signaling in enhancing lifespan, other anti-stress-related signaling pathways should not be excluded, since these inhibitors might also act on other genes or their products. Nevertheless, the data did indicate that the Nrf2/ARE signaling pathway plays pivotal roles in anti-aging, and targeting this pathway would be a promising approach for the screening of anti-aging compounds^{177,178}.

However, it must be stressed that the ectopic expression of Nrf2 in an organism can adversely affect its development¹⁷⁹. For example, constitutive activation of the Nrf2 gene induces hyperkeratosis in the esophagus and forestomach, leading to postnatal lethality¹⁸⁰. It is also fatal to overexpress Nrf2 during embryonic development, as Nrf2 also modulates

decisions concerned with the fate of the cell¹⁸¹. Therefore, spatiotemporal manipulation of Nrf2 should also be considered. Intriguingly, under normal condition, SFF did not seem to influence the overall antioxidant capacity and CncC/Nrf2/ARE signaling pathway at the young-age stage of the flies (**Figures 3.5 and 3.6**), suggesting that it might have no adverse effects on postnatal development and growth. Though the underlying mechanism requires further study, this could be an important property of SFF when carrying out future anti-aging development.

An increasing number of studies suggest that polysaccharides from other sources such as mushroom, hemp seed, and okra can also up-regulate the Nrf2/ARE signaling thus ameliorating oxidative damages, aging, diabetes, and other aging-related diseases¹⁸². In addition to *S. fusiform* fucoidan, the fucoidans from other algae have also been shown to enhance the Nrf2/ARE signaling, which can ameliorate liver injury and neurodegenerative diseases^{183,184}. However, the underlying mechanism by which polysaccharides upregulate the Nrf2/ARE signaling pathway remains unclear. It is possible that the bioactivities of polysaccharides may be intensively related to their molecular structures, which are determined by the molecular weight, chemical modification, monosaccharide composition, linkage types, and chain conformation of the polysaccharides. Fucoidans consist of a group of certain fucose-containing sulfated polysaccharides, which have been reported to possess many biological activities, including immunomodulatory, anti-inflammatory, antitumor, antioxidation, antiviral, and anti-coagulant activities^{185,186}. However, the precise structure-activity relationships (SAR) for these polysaccharides remain largely undetermined. A fucoidan usually has a backbone of (1 → 3)-linked or (1 → 3)- and (1 → 4)-linked α -L-fucopyranosyl but also contains sulfated galactofucans, glucuronic acid, glucose, or xylose at different locations and to different extents¹⁸⁷. Relatively high contents of xylose (12.10%),

galactofucans (11.51%), and glucose substitutions (11.33%) were found in SFF (**Table 3.2**), and this might be crucial for its antioxidant and antiaging functions. Thus, future study should focus on the relationship between monosaccharides and their bioactivity in oxidative aging. Polysaccharides administered via diets would not be directly absorbed by the small intestine¹⁸⁹, and thus, their biological effects in the organisms are thought to be associated with their roles in modulating gut environment. For this reason, we speculated that SFF might modulate the gut environment of *D. melanogaster*, but confirmation of this aspect, including the elucidation of the relationship between microbiota composition and the structure of the SFF, will be a subject of further investigation.

3.5. Summary

We have optimized an effective method for screening the antiaging property of polysaccharides by integrating *in vitro* antioxidant screening and *in vivo* antioxidant resistance assay. Based on this method, SFF, a fucoidan extracted from the *S. fusiforme* heteropolysaccharide SFPS, was shown to have longevity-promoting activity. SFF significantly activated the Nrf2/ARE signaling pathway, hence slowing down the decline in antioxidant defense capacity of *D. melanogaster* and increased its lifespan. This study has provided direct evidence of a longevity-promoting polysaccharide and revealed the worthiness of further research into SFF as a health supplement.

Chapter 4

SARGASSUM FUSIFORME FUCOIDAN ALLEVIATES HIGH-FAT DIET-INDUCED OBESITY AND INSULIN RESISTANCE ASSOCIATED WITH THE IMPROVEMENT OF HEPATIC OXIDATIVE STRESS AND GUT MICROBIOTA PROFILE³

Abstract

Sargassum fusiforme fucoidan (SFF) exhibits diverse biological activities. Insulin resistance (IR) implicated in type 2 diabetes (T2D) has become an epidemic health issue worldwide. In this study, we investigated whether SFF can improve insulin sensitivity in high-fat diet (HFD)-fed mice. Our present data showed that SFF significantly reduced fasting blood glucose and IR index along with improved glucose tolerance. Impaired phosphorylation of Akt was also restored by SFF. Furthermore, SFF decreased the levels of MDA and 4-HNE-modified protein and increased GSH/GSSG ratio as well as elevated antioxidant enzymes and activated Nrf2 signaling. SFF also increased the abundance and diversity of gut microbiota in the obese mice, as well as improved intestinal integrity and inflammation. Our findings suggested that SFF ameliorated HFD-induced IR through activating the Nrf2 pathway, remodeling gut microbiota, and reducing intestinal inflammation, thus providing a novel perspective into the treatment strategy on metabolic disease.

Keywords: *Sargassum fusiforme*, fucoidan, insulin resistance, Nrf2, gut microbiota

³ This work has been published as Zhang, Ya; Zuo, Jihui; Yan, Liping; Cheng, Yang; Li, Qiaojuan; Wu, Siya; Chen, Ling; Thring, Ron; Yang, Yue; Gao, Yitian; Wu, ming; Tong, Haibin. *Sargassum fusiforme* fucoidan alleviates high-fat diet-induced obesity and insulin resistance associated with the improvement of hepatic oxidative stress and gut microbiota profile. J Agric Food Chem. DOI: 10.1021/acs.jafc.0c02555.

4.1. Introduction

Sargassum fusiforme is one of the most popular brown algae that are used as food in China, Japan, and South Korea^{1,2}. As *S. fusiforme* is considered as an alga with great economic importance, it is cultured on a vast scale in the coastal zone of Zhejiang and Fujian Provinces, China, with as much as 10 000 tons of the dried seaweed produced per year in China, making this seaweed one of the four most valuable cultivated edible seaweeds (along with Porphyra, Laminaria and Undaria) in China, and most of which is exported to Japan and South Korea, where it is consumed as health food³⁻⁵. The market demand for *S. fusiforme* has greatly increased because of its nutritional values. Among the many active components of *S. fusiforme* is fucoidan, a family of highly sulfated homo- and hetero-polysaccharides extensively distributed in the brown algae and several marine invertebrates^{6,7}. Fucoidan is considered as one of the most important bioactive macromolecules in *S. fusiforme*, and *S. fusiforme* fucoidan has been reported to possess multiple bioactivities, such as hypolipidemic, immunomodulatory and anti-tumor, and antioxidant activity⁸⁻¹¹.

Gut microbiota, composed of trillions of microorganisms, plays a number of important physiological roles involving food digestion and metabolism. Recently, accumulated evidence has demonstrated that the modulation of the gut microbiota by dietary ingredients can ameliorate obesity and its complications¹⁶. Especially, indigestible marine plant-derived polysaccharides (MPPs) and marine animal-derived polysaccharides (MAPs) can be metabolized and fermented in the gut as nutraceuticals and gut microbiota modulators affecting intestinal ecology¹⁷. Shang *et al.*¹⁸ found that dietary fucoidan from brown seaweeds can modulate the gut microbiota to the advantage of the host probably in a structure-dependent way (such as linkage mode, molecular weight and monosaccharide composition) by enriching the amount of *Lactobacillus* and *Ruminococcaceae* and decreasing the abundance of *Peptococcus*,

which is a gut microbiota modulator for health promotion and treatment of intestinal dysbiosis. Another example is the attenuation of HFD-induced obesity and inflammation by high molecular weight *Ganoderma lucidum* polysaccharide via increasing the ratio of Bacteroidetes/Firmicutes in gut microbiota and maintaining the integrity of intestinal barrier.¹⁹ Gut microbiota analysis has shown that *Ophiocordyceps sinensis* polysaccharides can selectively promote the growth of *Parabacteroides goldsteinii*, a bacterium that has been shown to be negatively associated with obesity²⁰. These studies suggest that fucoidan and polysaccharides can positively regulate the gut microbiota, thereby achieving an anti-obesity effect.

Insulin resistance (IR) affects nearly one-third of the world's population, and it is a key pathophysiological feature of metabolic syndrome, defined as a decrease in the response of the peripheral tissues to insulin, and inhibition of several insulin-stimulated metabolic pathways, such as glucose transport, glycogen synthesis and antilipolysis^{21,22}. Individuals with IR are predisposed to several serious metabolic disorders, including T2D, dyslipidemia, hypertension, atherosclerosis, and nonalcoholic fatty liver disease (NAFLD)²³. IR is generally caused by an excessive nutrient intake (e.g. massive fat intake) attributable to an energy imbalance.^{24,25} Abnormality in lipid metabolism is associated with the overproduction of reactive oxygen species (ROS), and long-term HFD aggravates the burden of anti-oxidative system.²⁶ Therefore, the impairment of endogenous redox system by chronic HFD feeding is essential to the occurrence of IR in peripheral metabolic tissues.

Nrf2 (NF-E2-related factor 2) is a potent transcription factor and plays an essential role in regulating the expression of many cytoprotective genes, such as superoxide dismutase (*Sod*), and catalase (*Cat*), NAD(P)H:quinone oxidoreductase-1 (*Nqo1*), heme oxygenase 1 (*Ho-1*), glutathione S-transferase (*Gst*), and glutathione peroxidase (*Gpx*), in response to oxidative

stresses²⁷. Growing evidence shows that activation of Nrf2 and Nrf2-regulated endogenous antioxidant system improves insulin sensitivity in the peripheral tissues, and prevents the development of IR²⁸⁻³⁰. In the present study, the effects of SFF on obesity and obesity-associated IR in HFD-fed mice was conducted. In the present study, the effects of SFF on obesity-associated IR, oxidative stress markers, serum biochemical parameters and pathological changes in liver and intestine of HFD-fed mice were investigated. Also, the impact of SFF on gut microbiota was then analyzed by 16S rRNA sequencing. Our study has presented new insights into the prevention of energy imbalance-induced obesity and its related metabolic diseases by *S. fusiforme* fucoidan SFF.

4.2. Materials and methods

4.2.1. Materials and chemicals

Normal chow diet (NCD, containing 10% fat by energy) and high-fat diet (HFD, containing 60% fat by energy) were purchased from Beijing HFK Bio-Technology Co., Ltd. (Beijing, China). HFD was stored at -20 °C throughout the study to maintain freshness and prevent degradation of fat. Insulin from bovine pancreas was provided by Sigma–Aldrich (St. Louis, MO, USA). Radioimmunoprecipitation assay (RIPA) buffer was purchased from Beyotime (Shanghai, China). Anti-Nrf2 and anti-4-HNE antibodies were purchased from Abcam (Cambridge, UK). Antibodies against Akt, phospho-Akt (Ser473), AMPK α , phospho-AMPK α (Thr172), I κ B, phospho-I κ B (Ser32), p65, phospho-p65 (Ser536), GAPDH, β -tubulin and Lamin B were purchased from Cell Signaling Technology (Beverly, MA, USA). All other chemical reagents used were analytical grade.

4.2.2. Extraction of *S. fusiforme* Fucoidan

Sargassum fusiforme fucoidan (SFF) was prepared and characterized as previously reported²⁷, the brief steps are as follows. After drying and milling, the *S. fusiforme* was defatted

in 80% ethanol for 12 h. The fucoidan from defatted algal powder was extracted by soaking 0.01 M HCl (1:20, w / v), stirred for 6 h and filter through a mesh nylon sieve. Then, add 4M CaCl₂ to remove impurities such as alginate. Supernatant was dialyzed (MWCO 1000 Da) against deionized water for 48 h. The sample was then concentrated and precipitated with four volumes of 95% ethanol, kept at 4 °C for 12 h. The precipitate was collected by centrifugation and further deproteinated by a freeze–thaw process and Sevag method.²⁸ Briefly, Sevag reagent (chloroform:*n*-butanol = 4:1, v/v) was added to sample aqueous solution in the ratio of 1:5 (v/v), and then the mixed solution is violently shaken for 1 h. Denatured proteins jelly will appear in the interface between aqueous phase and solvent phase, and removed via centrifugation. Then, the sample was collected, dialyzed, and lyophilized to yield *S. fusiforme* fucoidan (SFF). Through physical and chemical analysis, SFF contained 81.33% carbohydrate, 12.53% uronic acid, and 17.36% sulfate. SFF was composed of 8 kinds of monosaccharides, including mannose, rhamnose, glucose, glucuronic acid, galacturonic acid, galactose, xylose and fucose with molar ratios of 10.89: 3.29: 4.32: 4.53: 14.02 : 18.33: 3.57: 41.05 respectively.

4.2.3. Experimental animals

Male ICR mice (32 ± 2 g) were purchased from Laboratory Animal Center at Wenzhou Medical University (Certificate no. SYXK Z2015-0009). The mice were kept at 22-24 °C and 50 ± 5% humidity, with a 12 h light/dark cycle. They were given access to diet and water at adlibitum and were allowed to acclimatize for one week before the start of the experiment. The NCD group was fed NCD whereas the other groups were fed HFD throughout the study. All animal experiments were approved by the Wenzhou University Animal Care and Use Committee.

4.2.4. Experimental design

A total of 30 mice were initially divided into NCD group (n = 10), whereas the other 20 mice were fed HFD. After 8 weeks of HFD feeding, the 20 mice were randomly divided into two groups HFD group (n = 10) and HFD+SFF group (n =10). NCD group and HFD group received physiological saline, while HFD+SFF group received physiological saline with SFF at 200 mg/kg. Treatments were administered intragastrically once per day for 6 weeks. **Figure 4.1** shows a schematic diagram for the design of the experiment. After the test for glucose and insulin tolerance, the blood samples were obtained from the mice fasted overnight by eyeball extirpating and centrifuged to collect serum, and stored at -80 °C for further assay. Subsequently, the mice were sacrificed, the livers were harvested, weighed and snap-frozen in liquid nitrogen, and then stored at -80 °C. The abdominal fat, colon and ileum were peeled off and weighed, fixed in 10% formalin for haematoxylineosin (H&E) staining. Abdominal fat was calculated by the following formula:

$$\text{Subcutaneous fat index} = \text{wet weight of adipose tissue/bw} * 100\%$$

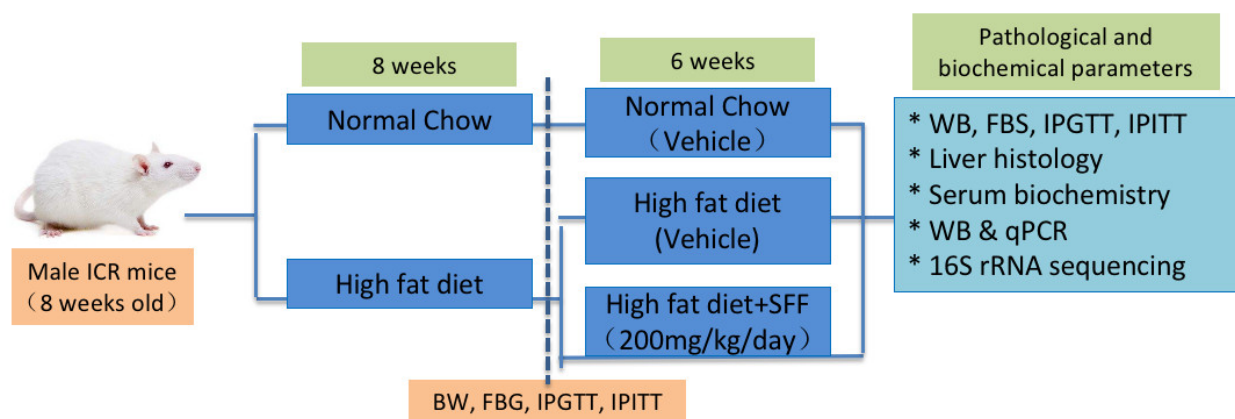


Figure 4.1. Schematic overview for the animal experimental design

4.2.5. Intraperitoneal glucose and insulin tolerance tests

Intraperitoneal glucose tolerance test (IPGTT) and intraperitoneal insulin tolerance test (IPITT) were performed as previously described³⁰. Briefly, mice were fasted overnight and

intraperitoneally injected with glucose (2 g/kg·bw in saline) or fasted for 4 h and then intraperitoneally injected with insulin (0.75 U/kg·bw in saline) for IPGTT and IPITT, respectively. Blood glucose (BG) level was measured at the tip of tail by using Accu-Chek glucometer (Abbott, USA) at 0, 15, 30, 60, and 120 min after glucose administration. A BG concentration-time plot showed the changes in glucose levels with time. Changes in glucose levels with time were determined from a blood glucose concentration versus time plot, by calculating the AUC (area under curve) from IPGTT and IPITT results.

4.2.6. H&E staining

Freshly isolated subcutaneous adipose tissues and colon from each group of mice were rapidly fixed in 10% formalin at room temperature for 24 h, followed by dehydration and embedding in paraffin. The specimens were then serially sliced into 5- μ m thick slices. The slices were then subjected to H&E staining to examine the sizes of the adipocytes and colon morphology. Five random fields from each section were examined, and the numbers of adipocyte was measured using the Image-Pro Plus (Version 6.0, Media Cybernetics) software.

4.2.7. Biochemical analysis

Total cholesterol (T-CHO), triacylglycerol (TG), free fatty acid (FFA), high-density lipoprotein (HDL-c), low-density lipoprotein (LDL-c), fasting blood glucose (FBG), fasting serum insulin (FINS), catalase (CAT), malondialdehyde (MDA), aspartate aminotransferase (AST), alanine aminotransferase (ALT), acid phosphatase (ACP) and alkaline phosphatase (AKP) were determined using biochemical kits purchased from Jiancheng Bioengineering Institute (Nanjing, China). The ratio of reduced glutathione (GSH) to oxidized glutathione (GSSG) was determined by a GSH:GSSG kit (Jiancheng Bioengineering Institute, Nanjing, China). Homeostasis model assessment-estimated insulin resistance (HOMA-IR) was calculated by the following formula:

HOMA-IR = serum glucose (mmol/L) × serum insulin (mU) /22.5

4.2.8. Immunoblotting

Liver tissues were homogenized with ice-cold RIPA lysis buffer containing protease and phosphatase inhibitors (Beyotime, Shanghai, China). The homogenates were centrifuged at $10\,000 \times g$ for 20 min at 4 °C to remove the insoluble precipitate. The protein concentration in the supernatant was determined using a BCA protein assay kit (Beyotime, Shanghai, China) according to the manufacturer's protocol. The protein concentration for each sample was adjusted to an equal amount and denatured in boiling water for 5 min. Equal aliquots (40 µg) of protein samples were subjected to 10% SDS-PAGE and transferred to PVDF membranes (Millipore, Bedford, MA, USA). After blocking with 5% nonfat milk (dissolved in TBST) for 1 h, the membranes were incubated with the indicated antibodies at 4 °C overnight, followed by incubation with the appropriate HRP-conjugated second antibodies for 1 h at room temperature. Chemiluminescent detection was performed using the ECL Plus Western blotting reagent (TransStart, Beijing, China). The semi-quantitative analysis for the densitometry of each band was performed using ImageJ software.

4.2.9. Quantitative RT-PCR

The samples were extracted by a TRIzol reagent (Invitrogen, Carlsbad, CA, USA). The cDNA was synthesized from RNA using a reverse transcription kit (Takara, Dalian, China) in accordance with the manufacturer's protocol. SYBR Green PCR Master Mix (Applied Biosystems, Foster City, CA, USA) was used for real-time PCR. The sequences of the specific primers are shown in **Table 4.1**. A LightCycler480 *q*RT-PCR system (Roche, Mannheim, Germany) was used for the amplification under the following reactions: 95 °C for 15 min, followed by 40 cycles at 95 °C for 10 s, 60 °C for 20 s, and 72 °C for 20 s. The level of the transcripts, expressed as fold change, was calculated according to formula $2^{-\Delta\Delta ct}$ method.

Table 4.1. Designed primer sets for qRT-PCR

| <i>Gene</i> | Primer | 5'-3' | Size (bp) |
|-------------------------------|-----------|-------------------------|-----------|
| <i>Nrf2</i> | sense | AAGAATAAAGTCGCCGCCCA | 326 |
| | antisense | GAAAAGGCTCCATCCTCCCG | |
| <i>Cat</i> | sense | GCAGATACCTGTGAACTGTC | 229 |
| | antisense | GTAGAATGTCCGCACCTGAG | |
| <i>Sod2</i> | sense | GCACATTAACGCGCAGATCA | 241 |
| | antisense | AGCCTCCAGCAACTCTCCTT | |
| <i>Slc7a11</i> | sense | GCCAGCGAAGGCTGAAACAC | 101 |
| | antisense | CTGTTCGGTCGTGACTTCCC | |
| <i>Gpx2</i> | sense | CATCCTGTCTTCGCCTACCT | 97 |
| | antisense | TTGATGGTTGGGAAGGTGCG | |
| <i>Gpx4</i> | sense | GCCTCGCAATGAGGCCAAAAC | 124 |
| | antisense | GGGAAGGCCAGGATTCGTAA | |
| <i>Txnrd1</i> | sense | ATTCTGGCTGGTATCGGCT | 95 |
| | antisense | ATGGTCTCCTCGCTGTTTGT | |
| <i>Tnfa</i> | sense | ACCCTCACACTCACAAACCA | 212 |
| | antisense | ATAGCAAATCGGCTGACGGT | |
| <i>Il-1β</i> | sense | TGCCACCTTTTGACAGTGATG | 220 |
| | antisense | AAGGTCCACGGGAAAGACAC | |
| <i>Il-6</i> | sense | CCCCAATTTCCAATGCTCTCC | 141 |
| | antisense | CGCACTAGGTTTGCCGAGTA | |
| <i>Zo-1</i> | sense | ACTATGACCATCGCCTACGG | 114 |
| | antisense | GGGGATGCTGATTCTCAAAA | |
| <i>Occludin-1</i> | sense | CGGTACAGCAGCATTGGTAA | 123 |
| | antisense | CTCCCCACCTGTCGTGTAGT | |
| <i>G6pd2</i> | sense | AGGCTGGCGTATCTTCACAC | 163 |
| | antisense | CTCAGTGCTTGTGAGTACCCT | |
| <i>Prdx1</i> | sense | GGGACCCATGAACATTCCCTT | 159 |
| | antisense | CCAACGGGAAGATCGTTTATTGT | |
| <i>Ho-1</i> | sense | CACGCATATACCCGCTACCT | 175 |
| | antisense | CCAGAGTGTTCAATTCGAGCA | |
| <i>Nqo1</i> | sense | TCACCTGGGCAAGTCCATTC | 241 |
| | antisense | TGCCCTGAGGCTCCTAATCT | |
| <i>Keap1</i> | sense | TACACAGCGGGCGGTTACT | 244 |
| | antisense | TCATAGAGGCACAGGGCGA | |
| β -actin | sense | CGTGGGCCGCCCTAGGCACCA | 214 |
| | antisense | TTGGCCTTAGGGTTCAGGGGGG | |

4.2.10. Analysis of gut microbiota by 16S rRNA amplicon sequencing

Total fecal DNA was extracted using CTAB/SDS method. The V4 region of the 16S rRNA was amplified using the universal primers 515F and 806R. All PCR reactions were carried out with Phusion® High-Fidelity PCR Master Mix (New England Biolabs). Then, the mixture PCR products were purified with GeneJET™ Gel Extraction Kit (Thermo Scientific). Sequencing libraries were generated using Ion Plus Fragment Library Kit 48 rxns (Thermo Scientific) following manufacturer's recommendations. The library quality was assessed on the Qubit® 2.0 Fluorometer (Thermo Scientific). At last, the library was sequenced on an Ion S5™ XL platform (Thermo Scientific) and 400 bp/600 bp single-end reads were generated.

Paired-end reads were merged using FLASH (V1.2.7), and the raw fastq files were processed by QIIME (version 1.7.0). Sequence analysis was performed by Uparse software (v7.0.1001), and Sequences with $\geq 97\%$ identity were assigned to the same Operational Taxonomic Units (OTUs). Pair-group method with arithmetic means (UPGMA) clustering was generated using the average linkage and conducted by QIIME software (V1.7.0). Linear discriminant analysis (LDA) was carried out to determine the highly dimensional gut microbes and characteristics associated with NCD mice, HFD mice and HFD+SFF mice. The Spearman's rho nonparametric correlations between the gut microbiota and obesity-related indexes were determined using R packages (V2.15.3), and the indexes of α diversity, including FBG, weight, BMI, FFA, T-CHO, TG, LDL-c, liver weight, adipocytes weight, HOMA-IR, and HDL-c were displayed.

4.2.11. Statistical analysis

Statistical analysis for bacterial diversity with a small sample size was conducted using the Mann–Whitney U test (SPSS, Chicago, USA). Statistical comparisons among experimental groups were analyzed by one-way ANOVA and Duncan's multiple-comparison test using the

SPSS software program (Version 21; SPSS). Data are represented as mean \pm SD. A $P < 0.05$ was considered statistically significant.

4.3. Results

4.3.1. SFF suppresses body weight gain and fat accumulation in HFD-fed mice.

After eight weeks of HFD-feeding, the mice in HFD group developed various metabolic disorders reminiscent of diabetes, such as overweight, hyperglycemia, and glucose intolerance (**Figures 4.2 and 4.3**). HFD-fed mice that received SFF treatment exhibited reduced body weight gain and the significant differences in body weight began to appear from the fourth week. After feeding SFF for 6 weeks, HFD feeding had significantly increased body weight and weight gain compare with NCD group, however, SFF treatment led to a significant decrease in body weight (52.4 ± 1.45 g) compared to that of HFD group (57.6 ± 1.93 g) (**Figures 4.4a and 2b**). In addition, BMI was significantly reduced in the HFD+SFF group compared with the HFD group (**Figure 4.4c**). It is worth noting that the amounts of food intake (**Figure 4.4d**) for the HFD+SFF and HFD groups were roughly the same, but water consumption by the HFD+SFF group was slightly reduced compared with the HFD group (**Figure 4.4e**). Abdominal fat (**Figure 4.4f**) was significant reduced in the HFD+SFF group compared with the HFD group. H&E staining revealed much larger adipocytes in the HFD-fed mice than in the NCD-fed mice. The adipocytes in the mice from the HFD+SFF group were significantly reduced compared with mice from the HFD group but were still larger than those of the NCD group. While the dietary supplementation with SFF significantly reduced the adipose size of HFD group (**Figure 4.4g**). Furthermore, the number of adipocytes in the HFD group was also much less than that of the HFD+SFF group. These results showed that SFF could suppress body weight gain and fat accumulation caused by HFD feeding.

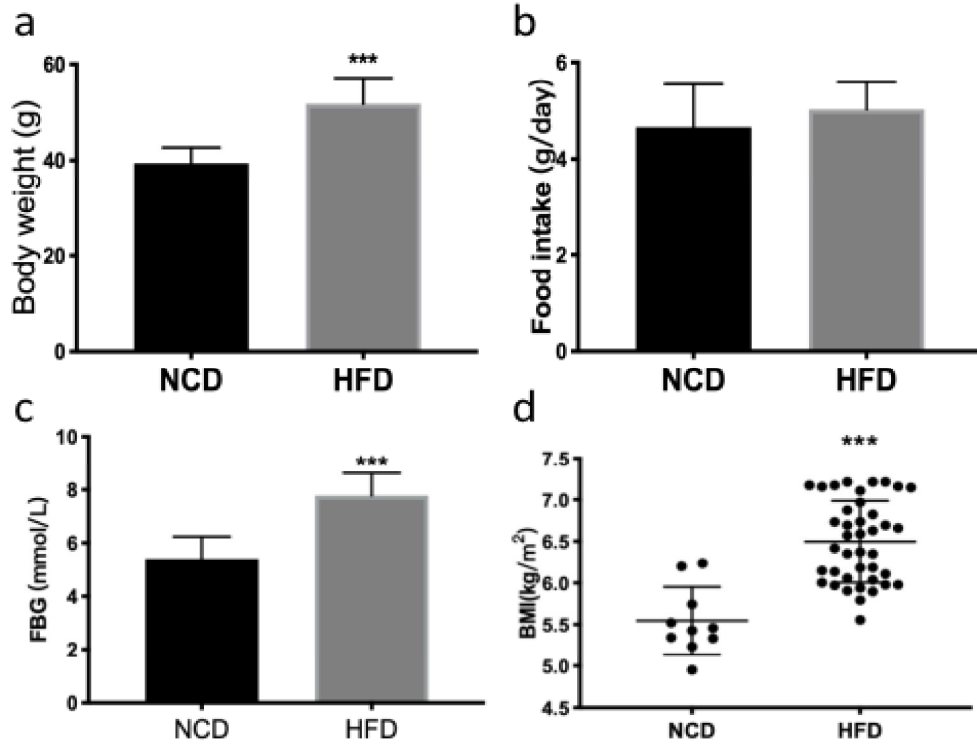


Figure 4.2. HFD-induced metabolic disorder in a mouse model. ICR male mice were fed NCD or HFD for 8 weeks. (a) Body weight; (b) food intake; (c) FBG; (d) BMI are shown. Data are represented as mean \pm SD. * $P < 0.05$, ** $P < 0.01$ and *** $P < 0.001$.

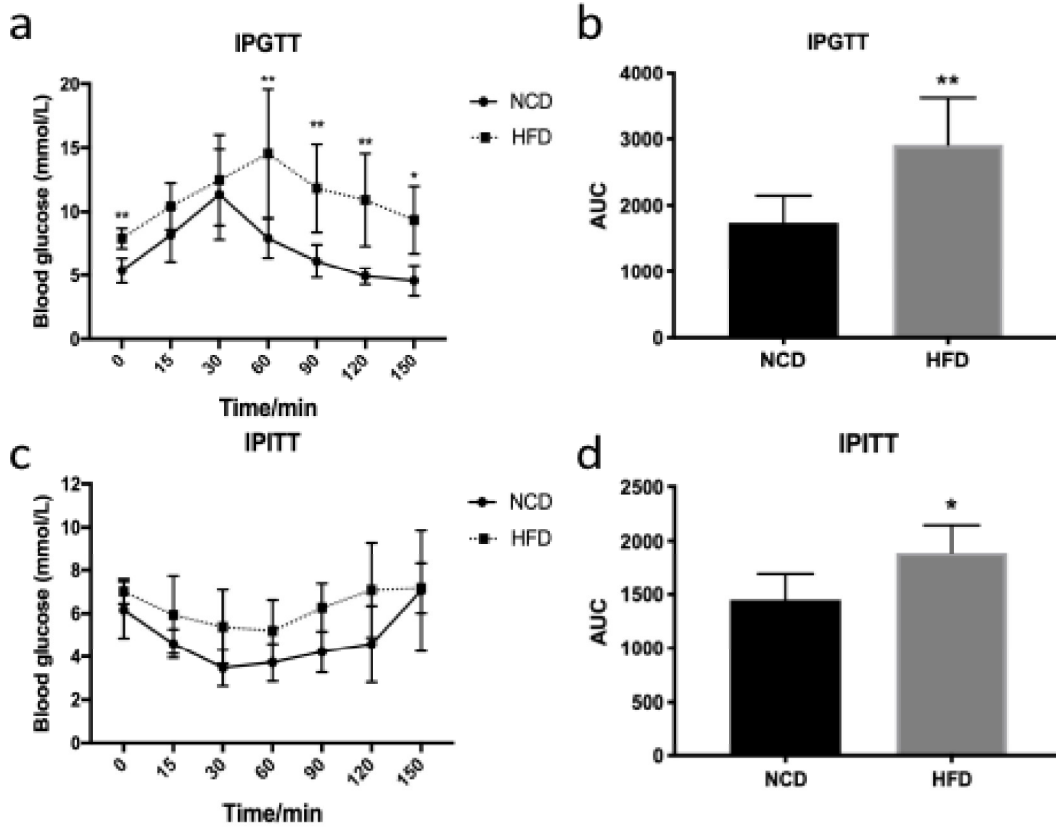
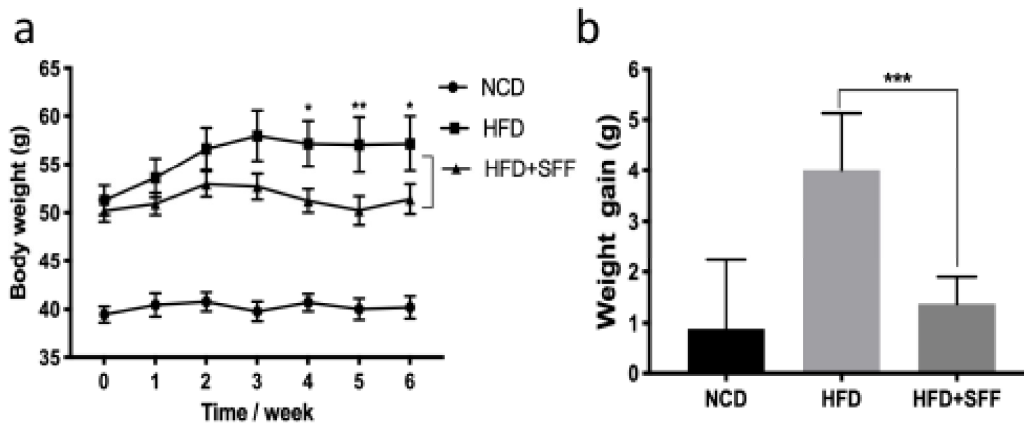


Figure 4.3. HFD-induced insulin resistance in a mouse model. ICR male mice were fed NCD or HFD for 8 weeks. (a) IPGTT; (b) AUC of IPGTT; (c) IPITT; (d) AUC of IPITT. Data are represented as mean \pm SD. * $P < 0.05$, ** $P < 0.01$ and *** $P < 0.001$.



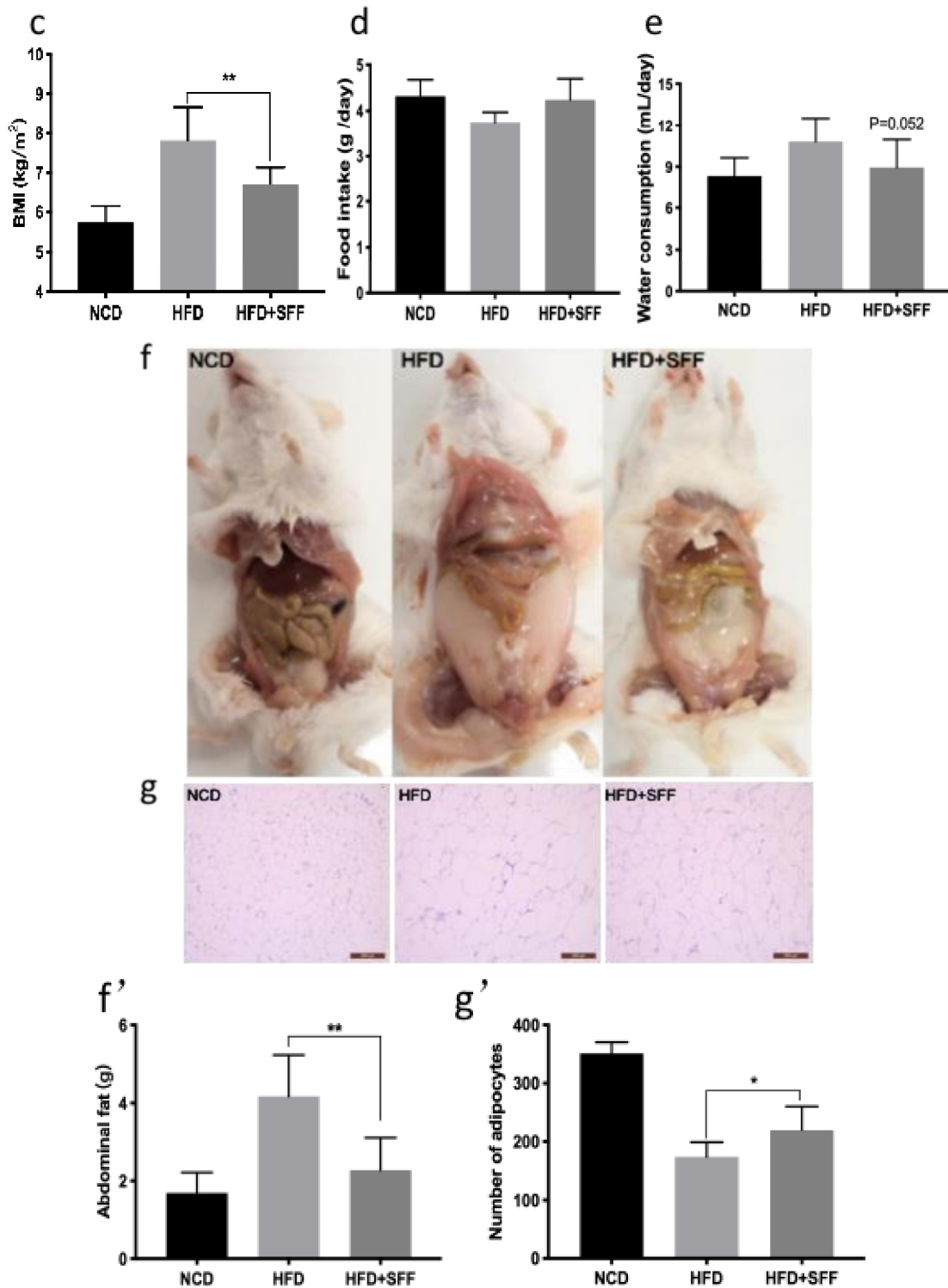


Figure 4.4. *S. fusiforme* fucoidan reduces fat accumulation in HFD-fed mice. (a) body weight; (b) weight gain; (c) BMI; (d) food intake; (e) water consumption; (f) abdominal fat and (f') abdominal fat weight; (g) H&E staining of epididymal adipose tissue (400×, scale bar = 200 μm) and (g') number of adipocytes. Data are represented as mean ± SD. *P < 0.05, **P < 0.01, and ***P < 0.001.

Table 4.2. The Effect of *S. fusiforme* Fucoidan on Serum/Liver Lipid Levels in HFD-fed Mice

| | NCD | HFD | HFD+SFF |
|--------------------|----------------|-------------|---------------|
| Serum | | | |
| T-CHO (mmol/L) | 3.97±0.76*** | 10.29±1.24 | 8.49±1.15* |
| TG (mmol/L) | 2.141±0.20 | 2.743±0.34 | 1.76±0.43*** |
| HDL-c (mmol/L) | 0.31±0.067*** | 0.211±0.043 | 0.273±0.073 |
| LDL-c (mmol/L) | 1.44±0.38*** | 3.532±0.44 | 2.835±0.50* |
| FFA (mmol/L) | 1.828±0.221** | 2.518±0.242 | 2.05±0.341* |
| Liver | | | |
| T-CHO (mmol/gprot) | 0.085±0.010*** | 0.123±0.022 | 0.094±0.015* |
| TG (mmol/gprot) | 0.090±0.013 | 0.140±0.033 | 0.094±0.019** |

Data are expressed as mean ± SD.

* Indicates significantly different from the HFD group at the * $P < 0.05$, ** $P < 0.01$, and *** $P < 0.001$ level.

4.3.2. SFF inhibits hyperlipidemia and liver steatosis in HFD-fed mice

As shown in the **Table 4.2**, the HFD-fed mice had higher serum levels of T-CHO, TG, and LDL-c than the NCD group ($P < 0.05$), indicating the abnormal lipid metabolism caused by chronic HFD feeding. SFF intervention significantly decreased the serum levels of T-CHO, TG, and LDL-c ($P < 0.05$, compared with the HFD group). In addition, the serum of the HFD group contained a higher concentration of FFA, which was 27.3% higher than that of the NCD group, while the concentration of FFA decreased significantly of the HFD+SFF group relative to HFD group. Compared with the HFD group, the levels of T-CHO and TG in the liver of the HFD+SFF group were significantly reduced, suggesting that SFF treatment probably prevented the onset of diet-induced hepatic dyslipidemia and steatosis. As for the physiological functions of the liver (**Table 4.3**), ALT and AST levels in the serum of the HFD group increased by 1.35- and 1.49-fold, respectively, compared with those of the NCD group. ALT and AST levels in the

HFD+SFF group decreased by 13.4% and 32.2%, respectively, compared with HFD group. Similar trends were observed for serum AKP and ACP levels. These data indicated that SFF-treatment could alleviate the damage in liver function caused by HFD diet.

Table 4.3. The Effect of *S. fusiforme* Fucoïdan on Liver Function in HFD-fed Mice.

| Group | ALT (U/L) | AST (U/L) | ACP (U/L) | AKP (U/L) |
|---------|------------|------------|--------------|-------------|
| NCD | 50.0±8.9** | 35.6±3.8** | 0.57±0.113** | 0.83±0.179* |
| HFD | 71.7±10.3 | 51.5±5.6 | 0.81±0.153 | 1.21±0.237 |
| HFD+SFF | 56.8±6.3* | 37.8±6.9** | 0.54±0.135* | 0.89±0.103* |

Data are expressed as mean ± SD.

* Indicates significantly different from the HFD group at the * $P < 0.05$ and ** $P < 0.01$ level.

4.3.3. SFF alleviates HFD-induced insulin resistance

After six weeks of SFF-treatment, the overnight-fasted mice were subjected to IPGTT assay. Oral administration of glucose increased BG level within 30 min in the HFD group, and it remained at a high level over the next 90 min (**Figure 4.5a**). In the case of the NCD group, the level of BG reached the peak within 30 min of glucose administration, but was restored to almost the initial level after 120 min. SFF-treatment significantly inhibited the rise of BG level in HFD-fed mice after oral administration of glucose. The AUC of HFD+SFF group was significantly decreased compared with that of the HFD group (**Figure 4.5b**, $P < 0.05$), suggesting that SFF improved the insulin sensitivity of the HFD-fed mice. The improvement of insulin resistance (IR) was also supported by the results from IPITT. All mice fasted for 4 h were evaluated on the basis of IPITT. After the mice were intraperitoneally injected with insulin at a dose of 0.75 U/kg, the BG levels measured at 0, 15, 30, 60, and 120 min revealed that the mice in NCD group took more advantage of insulin than the HFD-fed mice (**Figure 4.5c**). Significant ($P < 0.01$) difference in AUC (**Figure 4.5d**) between the HFD group and

HFD+SFF group suggested that SFF increased the utilization of insulin and improved insulin sensitivity in the HFD-fed mice.

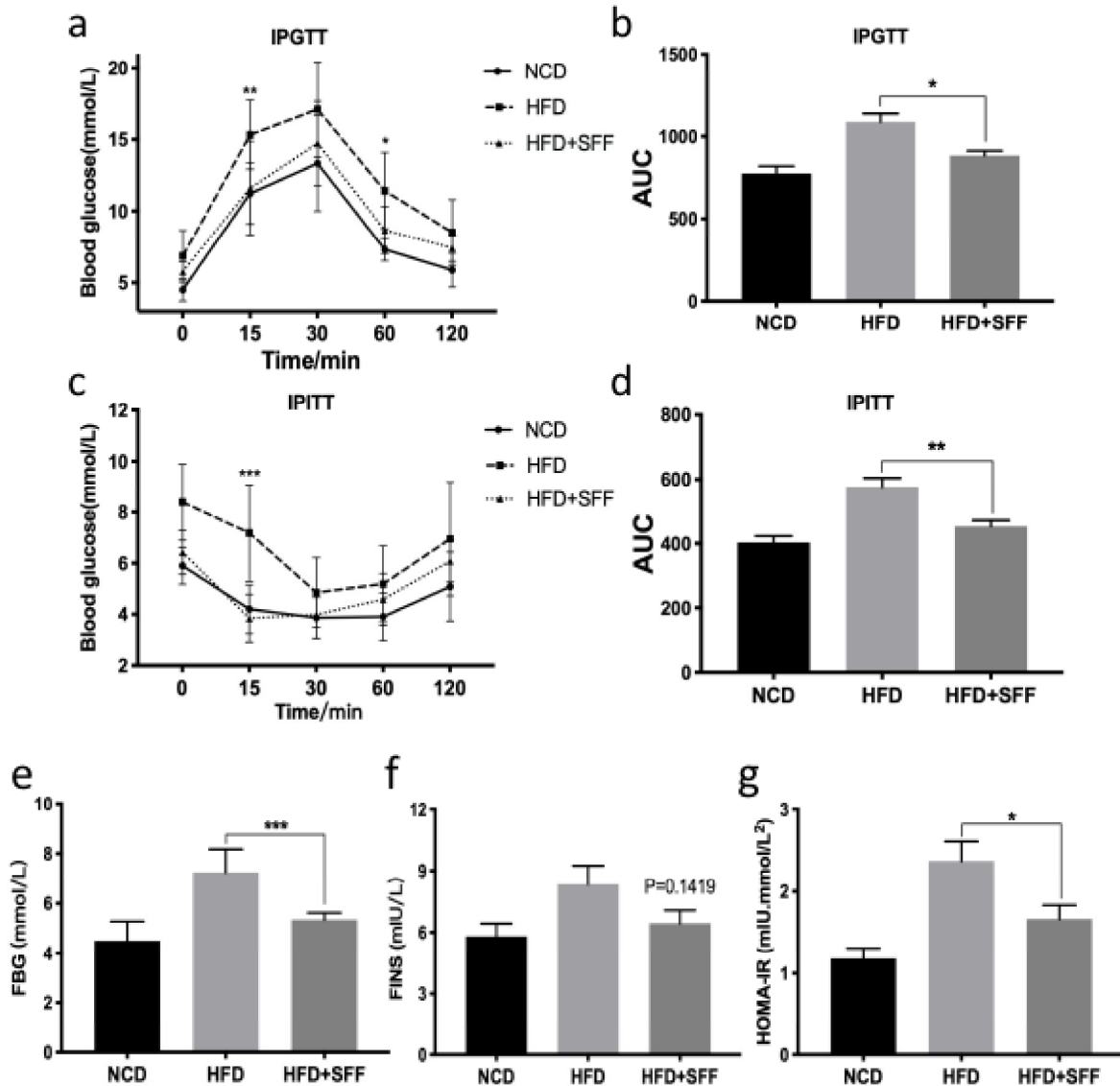


Figure 4.5. SFF improves insulin sensitivity in diet-induced obese mice. At week 19, mice were fasted overnight (12 h) and submitted to intraperitoneal glucose tolerance tests (a) and its area under curve (b). At week 18, mice were fasted for 4h and insulin tolerance tests (c), its area under curve (d) were carried out after intraperitoneal insulin injections (ipITT, 0.75 IU/kg). Blood was collected and used to assess fasting glucose (e), insulin (f), and HOMA-IR (g). One-way repeated measures ANOVA with a Student-Newman-Keuls post hoc test was used to assign significance to the differences groups. *P < 0.05, **P < 0.01 and ***P < 0.001. Data are expressed as the mean ± SEM.

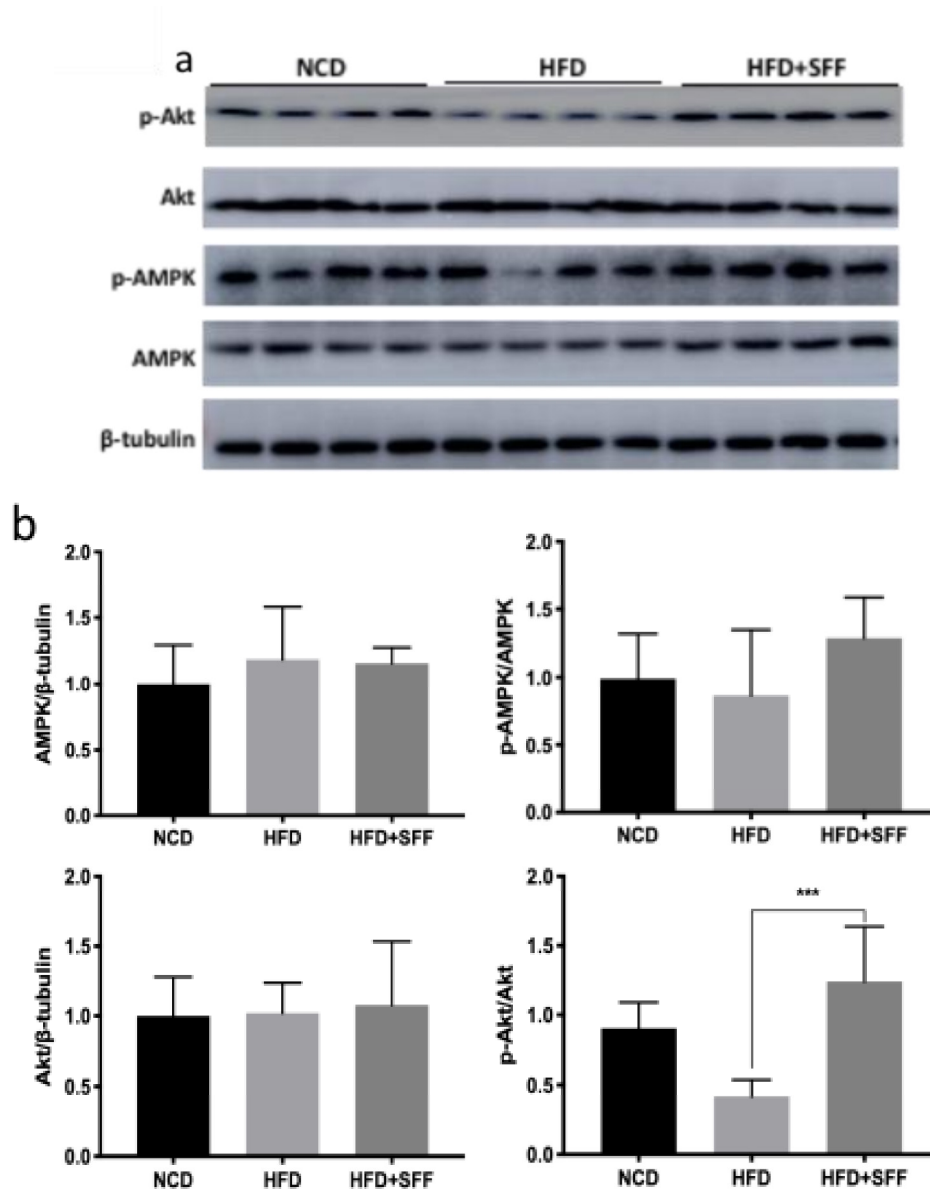


Figure 4.6. SFF improves hepatic insulin signaling. Protein levels of p-Akt (Ser473), total Akt, p-AMPK (Thr172) and total AMPK were analyzed by western blotting (a). The ratio of phosphorylated Akt/total Akt and phosphorylated AMPK/total AMPK was quantified by densitometry using ImageJ software (b). Data are represented as mean \pm SD. Statistical significance considered as * $P < 0.05$, ** $P < 0.01$ and *** $P < 0.001$.

Mice in the HFD group had significantly higher FBG level than mice in the NCD group (Figure 4.5e). When these mice were also given SFF, the level of FBG decreased, resulting in as much as 25% reduction, but remained higher than that of the NCD group. FINS stayed at a

high level in HFD group (**Figure 4.5f**), whereas decreased in HFD+SFF group, but there was no significant difference in FINS level between HFD group and HFD+SFF group ($P = 0.1419$). While HOMA-IR was significantly decreased in HFD+SFF group compared with that of the HFD group ($P < 0.05$), indicating that SFF could lead to a reduction in HFD-induced IR (**Figure 4.5g**). The phosphorylation of liver Akt (at Ser473) in the HFD group was decreased compared with the NCD group (**Figures 4.6**), indicating that insulin signaling was impaired by HFD feeding. In contrast, the phosphorylation of liver Akt in the HFD+SFF group was significantly ($P < 0.05$) enhanced compared with the HFD group, suggesting that SFF could enhance insulin sensitivity in the HFD-fed mice.

4.3.4. SFF increases mRNA expression of lipolysis-related genes

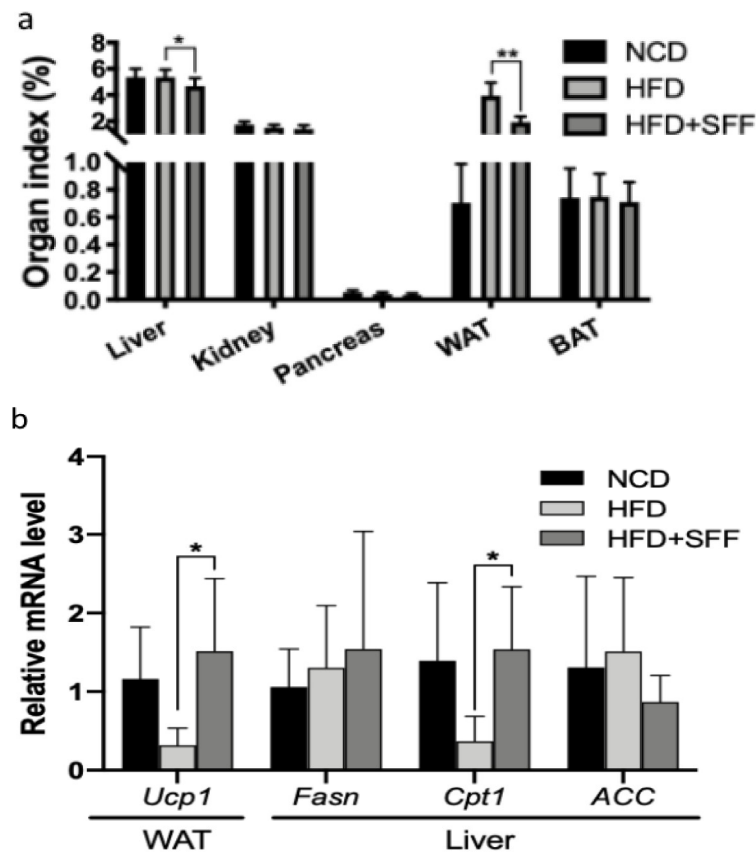


Figure 4.7. SFF increases mRNA expression of lipolysis-related genes. (a) organ index and (d) the relative mRNA levels of Fasn, Cpt1, Acc in liver and Ucp1 in WAT were shown. Data are represented

as mean \pm SD. * $P < 0.05$, ** $P < 0.01$, and *** $P < 0.001$.

After 16 weeks of HFD feeding, multiple organ weights were analysed in mice. White adipose tissue weight and liver weight were significantly higher in HFD mice compared to NCD (**Figure 4.7a**). This suggests that the main cause of weight gain in mice is from an increase in liver and white adipose tissue. The mRNA expression of genes related to lipid metabolism in WAT and liver was analysed. The mRNA levels of fatty acid synthase (FASN), acetyl CoA hydroxylase (ACC), carnitine palmitoyltransferase (CPT1) and uncoupling protein-1 (UCP1) showed differences in white adipose tissue and liver of mice. The mRNA expression of *Ucp1* was greatly lower in white adipose tissue of mice in the HFD group than in the NCD group; however, this gene was significantly upregulated in the HFD+SFF group ($P < 0.05$). Similarly, mRNA expression of *Cpt1* in the liver of mice in the HFD group was significantly lower than that in the NCD group, while it was dramatically increased in the HFD+SFF group (**Figure 4.7b**). These data suggest that SFF promotes lipolysis in mice liver and white adipose tissue by upregulating lipolytic gene expression.

4.3.5. SFF reverses HFD-induced oxidative stress and Nrf2 repression

To investigate the effects of oxidative stress during alleviating HFD-induced IR by SFF, we further measured the MDA level in the plasma and liver (**Figure 4.8b**), a product of lipid peroxidation. The liver MDA level was significantly higher in the HFD group (11.34 nmol/mg of protein) than that in the NCD group (9.10 nmol/mg protein). This suggests SFF exhibited a well protective effect against lipid peroxidation, the increase of MDA level both in plasma and liver can be significantly ($P < 0.05$) inhibited by SFF. CAT activity in the HFD group strongly decreased due to the increased oxidative stress compared to the NCD group. In contrast, SFF significantly inhibited the decrease of CAT activity both in plasma and liver induced by HFD feeding (**Figures 4.8**). In addition, the GSH:GSSG ratio is also an essential index of redox

status, was determined. HFD feeding was found to reduce the GSH:GSSG ratio by approximately 75%, while SFF administration strongly prevented the reduction (**Figure 4.9**). 4-HNE is one of the most studied cytotoxic products of lipid peroxidation. HFD feeding significantly increased the amount of 4-HNE-modified proteins, while SFF administration clearly reduced this protein modification (**Figures 4.9**).

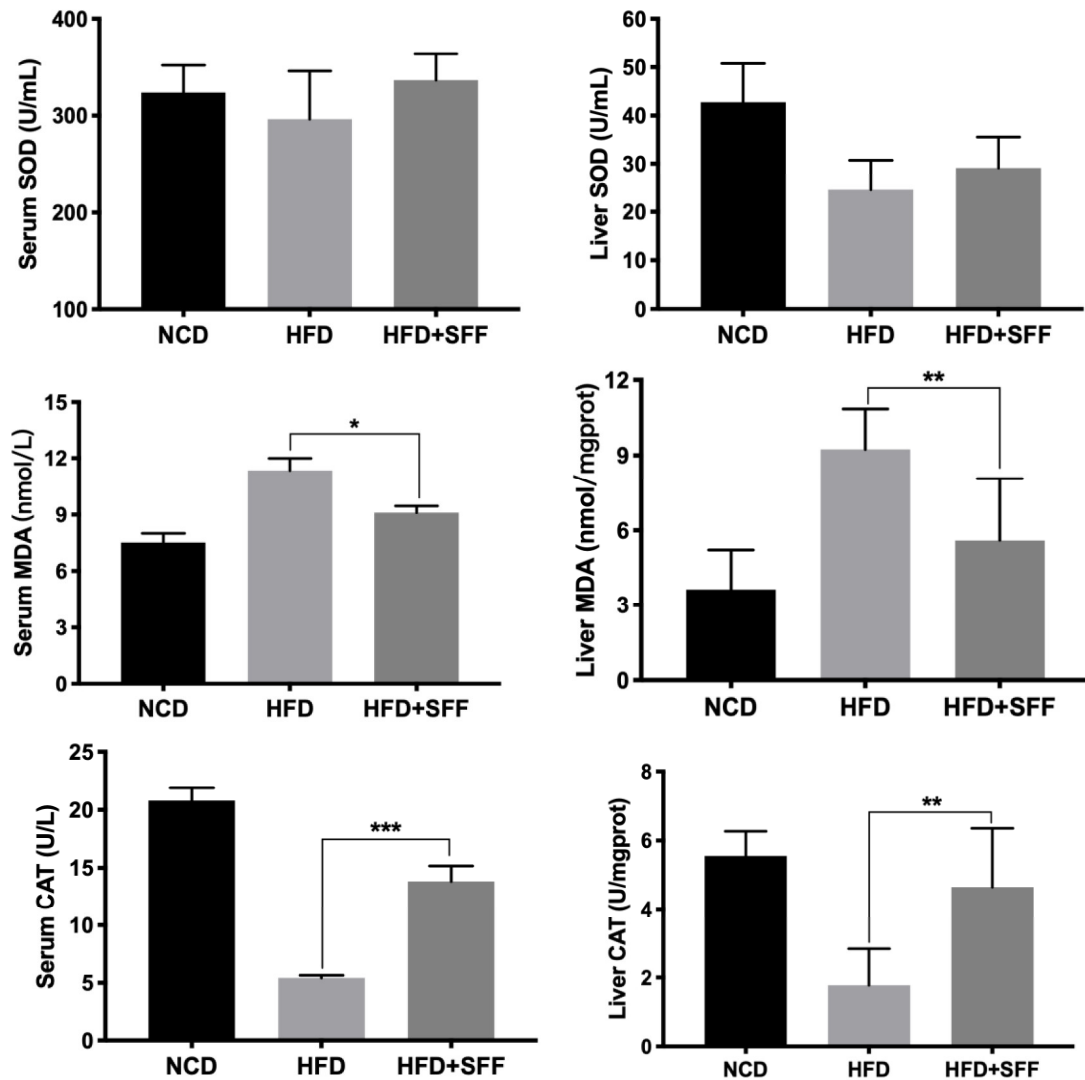


Figure 4.8. *S. fusiforme* fucoidan increased the activity of antioxidant enzymes in the liver and serum of mice on a high-fat diet. Serum/liver CAT, SOD, and MDA are shown. Data are represented as mean \pm SD. *P < 0.05, **P < 0.01, and ***P < 0.001.

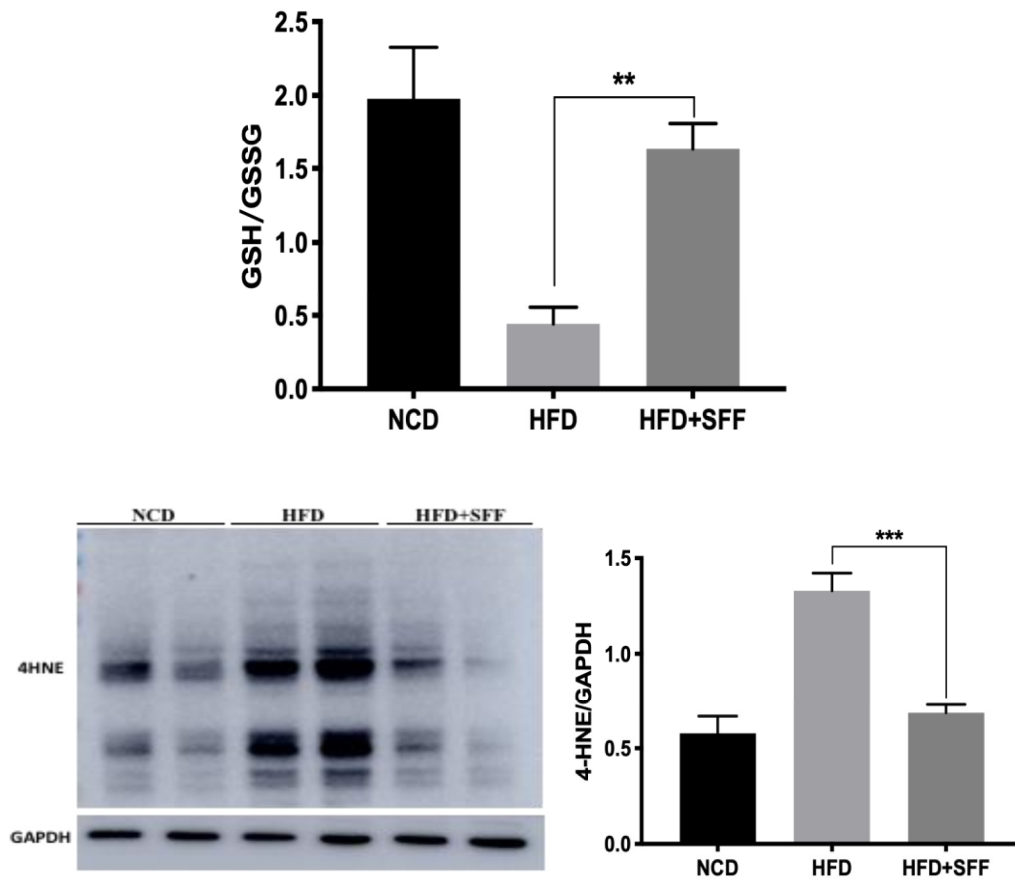
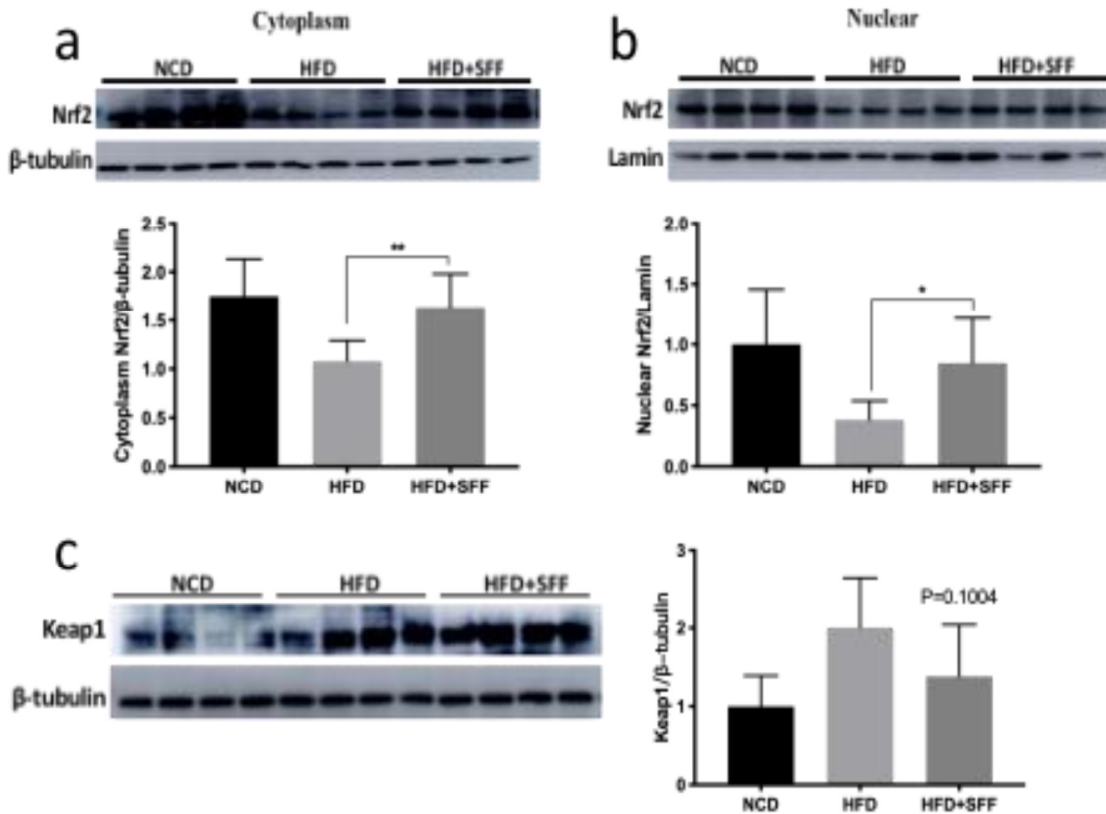


Figure 4.9. *S. fusiforme* fucoidan ameliorates HFD-induced oxidative stress. (a) GSH:GSSG ratio in the liver; (b) Western blot and quantification of 4-HNE-modified proteins in the liver. Data are represented as mean \pm SD. * $P < 0.05$, ** $P < 0.01$, and *** $P < 0.001$.

Furthermore, both of the expression levels of Nrf2 and KEAP1, as well as their transcriptional levels of *Nrf2* and *Keap1* were evaluated by immunoblotting and quantitative RT-PCR, respectively. Compared with the HFD group, the Nrf2 expression in the liver cytoplasm was significantly up-regulated in the HFD+SFF group (**Figures 4.10a and b**). In addition, SFF can promote more Nrf2 to enter or remain in the nucleus, and continuously stimulate the activation of Nrf2/ARE signaling and initiate the expression of downstream genes. KEAP1 binds to Nrf2 and promotes rapid ubiquitination and degradation of Nrf2. HFD

accelerates the degradation of Nrf2, and after administration of SFF, the expression of KEAP1 in the liver was decreased (Figure 4.10c). These changes are consistent with increased mRNA level of *Nrf2* by SFF administration (Figure 4.10d). Nrf2 regulates the expression of a variety of detoxification and antioxidant enzymes, SFF significantly up-regulated the mRNA levels of *Cat*, *Sod2*, *Slc7a11*, *G6pd2*, *Prdx1*, *Gpx2* and *Gpx4*, these genes are essential for the balance of oxidative stress in the body. Meanwhile the activation of NF- κ B signaling was weakened by SFF treatment, evidenced by the lower levels of p-p65 and p-I κ B in SFF-treated versus HFD-fed mice (Figures 4.11). Overall, SFF reverses the hepatic oxidative stress and Nrf2 repression, as well as inflammation induced by HFD feeding.



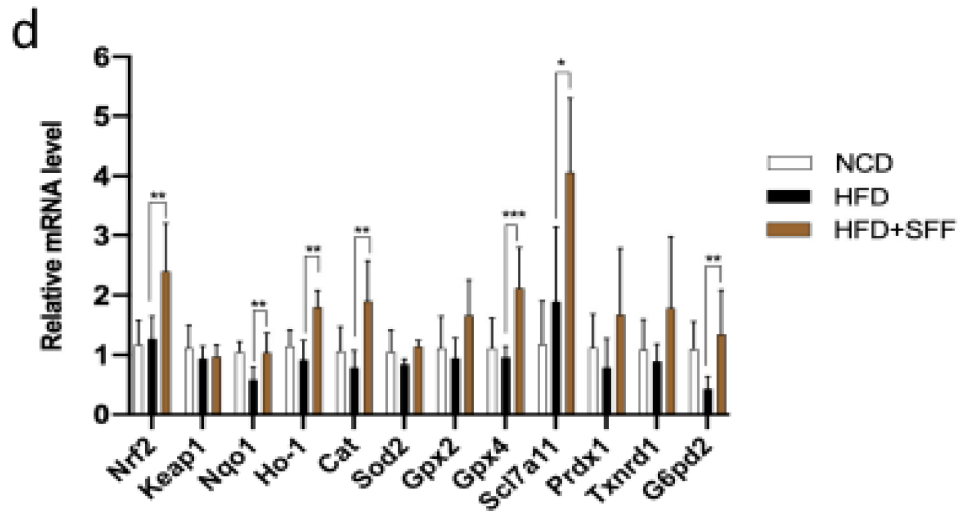


Figure 4.10. *S. fusiforme* fucoidan reverses HFD-induced Nrf2 repression and improves the expression of detoxification and antioxidant enzymes. Western blot of phosphorylated Nrf2 in nuclear (a) and plasma (b) and quantitative analysis for the densitometry of phosphorylated Nrf2 in protein level performed using ImageJ software; (c) Western blot and quantitative analysis of KEAP1; (d) relative mRNA levels of Nrf 2 and representative downstream genes: *Cat*, *Sod2*, *Slc7a11*, *Txnrd1*, *G6pd2*, *Prdx1*, *Gpx2*, and *Gpx4*. Data are represented as mean \pm SD. *P < 0.05, **P < 0.01, and ***P < 0.001.

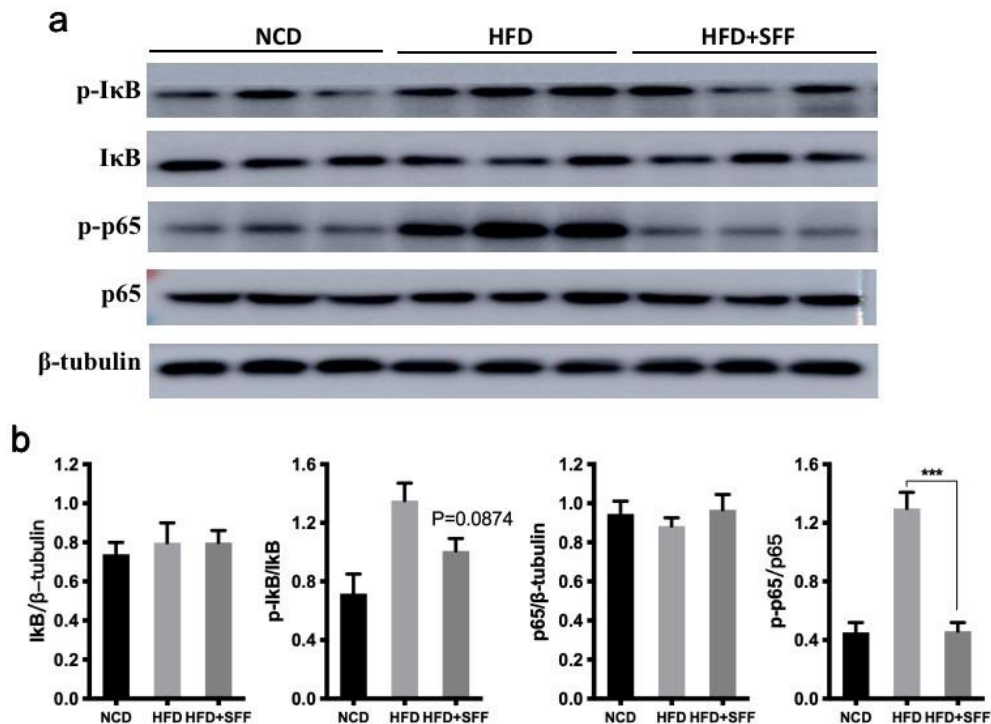


Figure 4.11. SFF relieves liver inflammation in HFD feeding mice. (a) Western blot of p65/I κ B and phosphorylated p65/I κ B in liver; (b) quantitative analysis for the densitometry in protein level using ImageJ software. Data are represented as mean \pm SD. ***P < 0.001.

4.3.6. SFF remodels the structure of gut microbiota in HFD-fed mice

Gut microbiota is closely related to the development of metabolic syndrome. We further assessed the effects of SFF treatment for 6 weeks on gut microbiota in the HFD-fed obese mice by performing the V4 hypervariable regions of 16S rRNA-based amplicon sequencing of fecal samples. Following all quality trimming and checking, a dataset consisting of 80004 highly qualified reads was collected for subsequent analysis. To profile the specific changes in the gut microbiota, we analyzed the UPGMA clustering and the relative abundance of the predominant taxa identified from sequencing in the three groups. Comparing with the HFD group, the microbiota structure in the HFD+SFF group had higher similarity with the NCD group (**Figure 4.12a**). Furthermore, a detailed overview of the intestinal bacteria composition of each group was illustrated at the phylum level, and the dominant phyla including Firmicutes, Bacteroidete, Proteobacteria and Deferribacteres showed significant differences among all the groups. Firmicutes was the most abundant phylum in all samples, accounting for 41.1% in the NCD group, 61.7% in the HFD group and 54.3% in the SFF group of the microbiota composition (**Figure 4.12b**), indicating that SFF significantly decreased the abundance of Firmicutes. The relative abundance of Bacteroidetes showed a sharp decrease in the HFD group when compared to the NCD group. The gut microbiota of the HFD group was characterized by an increased Firmicutes/Bacteroidetes ratio (**Figure 4.12c**). A detailed overview of the gut microbiota composition was illustrated at the genus level (**Figure 4.12d**), the HFD group showed a decrease in the bacteria proportion of *Bacteroides*, *Lactobacillus* and *Alistipes* compared with the NCD group, whereas SFF treatment reshaped the structure of gut microbiota and improved

those bacteria. In addition, compared with the HFD group, the proportion of *Helicobacter* in the SFF group was significantly reduced.

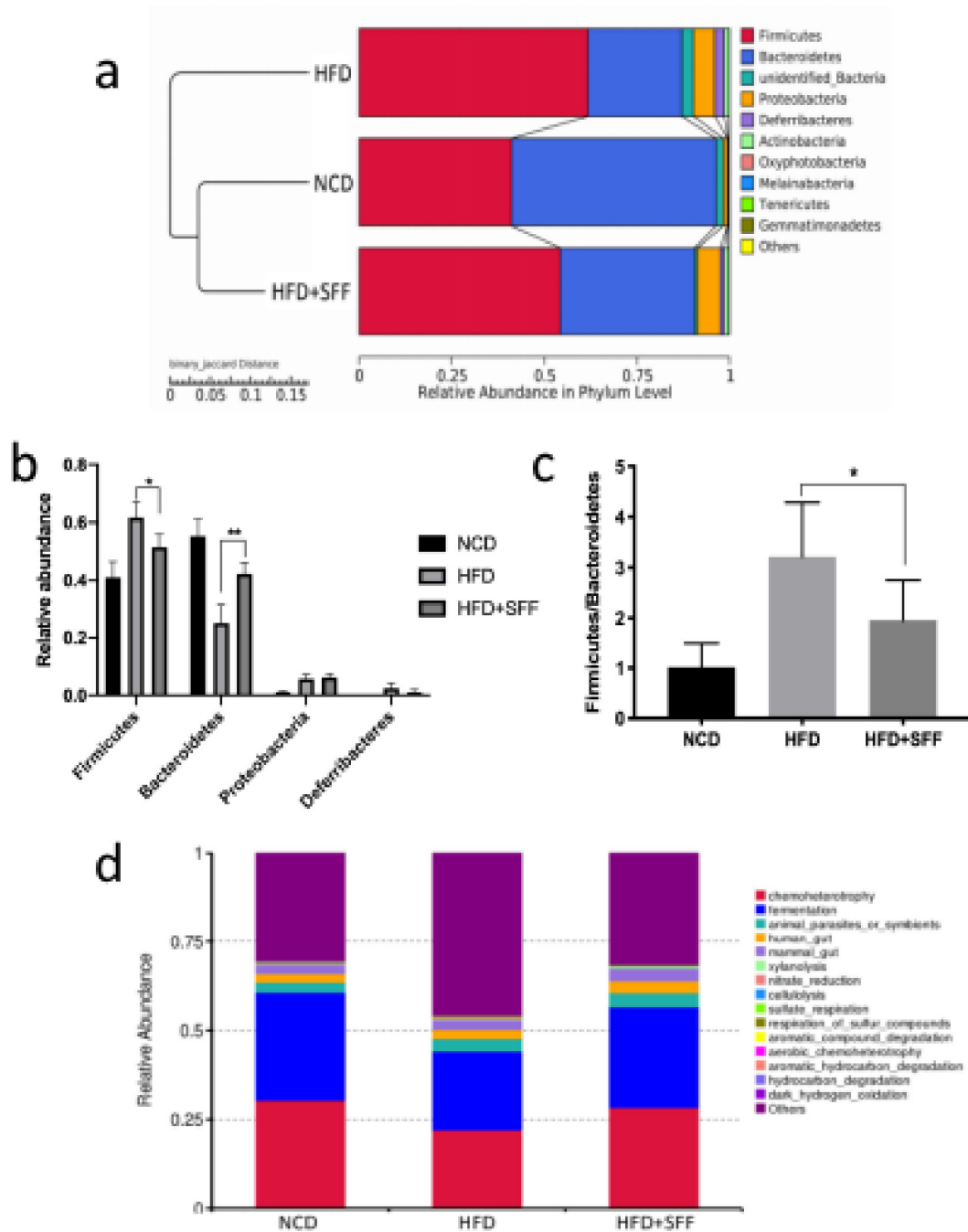


Figure 4.12. *S. fusiforme* fucoïdan remodels the structure of gut microbiota in HFD-fed mice. (a) composition of gut microbiota at the phylum level; (b) relative abundance of the main phylum; (c) ratio

of Bacteroidetes to Firmicutes; (d) composition of gut microbiota at genus level. Data are represented as mean \pm SD. *P < 0.05 and **P < 0.01.

To identify the specific bacterial taxa in each group, the composition of the microbiota from NCD, HFD and HFD+SFF groups were compared by linear discriminant analysis (LDA). The LDA scores (**Figure 4.13**) were higher than 3 indicating a higher relative community abundance in the corresponding group than in the other two groups. The composition of gut microbiota among the three groups showed distinct variations. HFD+SFF showed selective enrichment in 9 communities including: p_Bacteroidetes, o_Bacteroidales, g_Alistipes, s_Alistipes_shahii, g_Parabacteroides, s_Parabacteroides_goldsteinii, g_dubosiella, s_Faecalibacterium_prausnitzii, and s_Clostridium_sp_A5F502. *Erysipelotrichia*, *Romboutsia*, *Peptostreptococcaceae*, *Turicibacter*, *Desulfovibrionaceae*, etc., which were enriched due to HFD feeding, appeared in the HFD group. To determine the potential association between the gut microbiota and obesity-related physiological parameters, including body weight, weight gain and BMI, HOMA-IR; FBG, weights of liver and adipose tissue; serum levels of T-CHO, TG, LDL-c HDL-c and FFA, Spearman correlation analysis was performed. Heatmaps revealed that *Rikenella*, *Candidatus_Saccharimonas*, *Anaerotruncus*, *Odoribacter*, *Parasutterella*, *Bifidobacterium*, *Roseburia*, *Turicibacter*, *Alistipes*, *Faecalibaculum*, *Romboutsia*, and *Bacteroides* are closely associated with obesity-related physiological parameters (**Figure 4.14 and 4.15**). Of these bacteria, *Faecalibaculum*, *Turicibacter*, and *Romboutsia* enriched in the HFD group were strongly positively correlated with obesity-related physiological parameters, such as body weight, HOMA-IR, BMI, T-CHO, LDL-c and adipose tissue index. However, *Alistipes* and *Bacteroides*, which were negatively correlated with obesity-related physiological parameters, were significantly up-regulated in the HFD+SFF group. The data suggest that SFF

may play a role in improving insulin resistance by remodeling the structure of the gut microbiota.

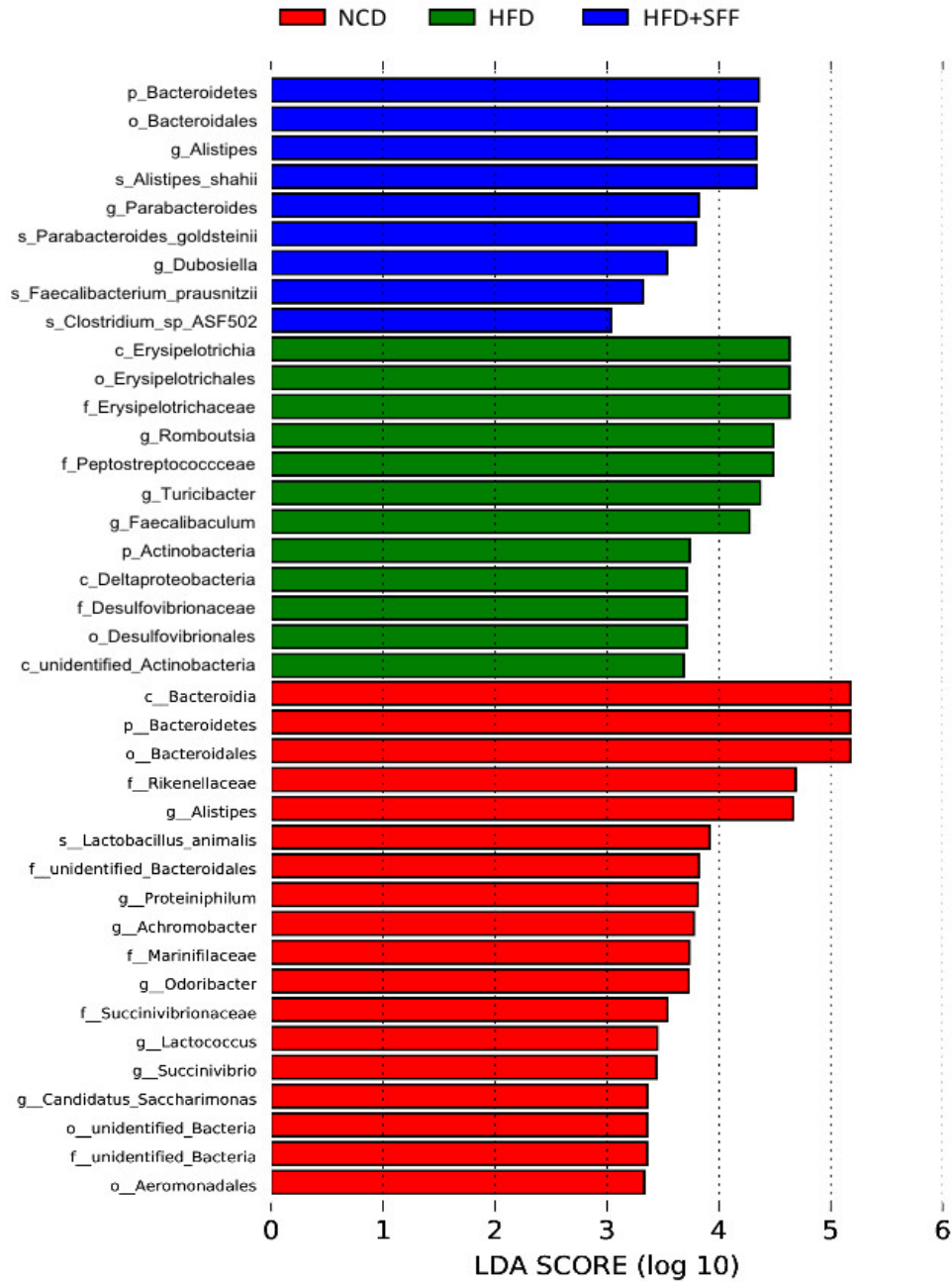


Figure 4.13. Linear discriminant analysis (LDA) score for taxa differing between treatment groups. LDA scores threshold > 3 were listed.

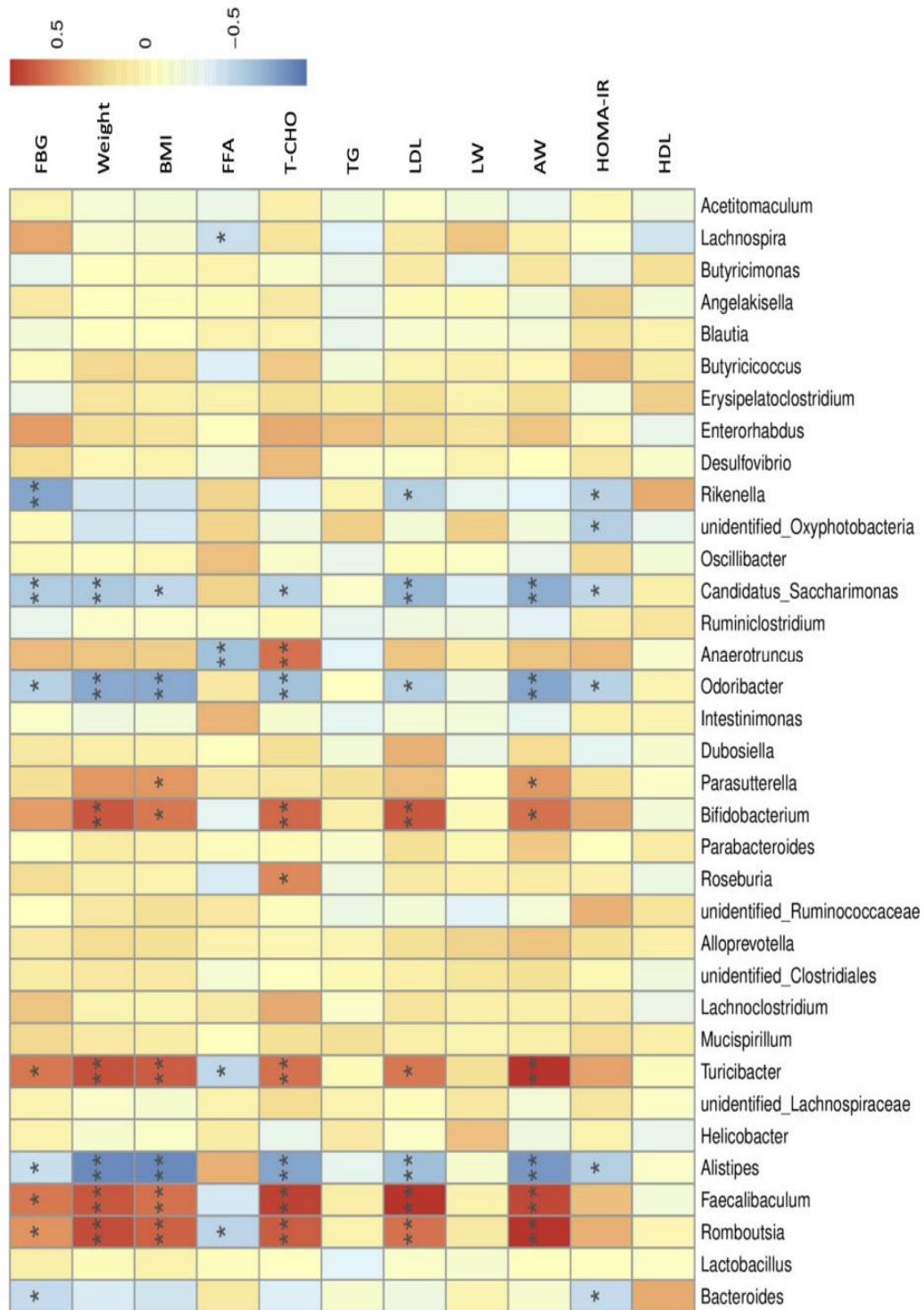


Figure 4.14. Spearman's correlation between gut microbiota and obesity-related indexes (Genus). Good's coverage and the genus with significant correlations are shown. Good's coverage and the specie with significant correlations are shown. The colors range from blue (negative correlation) to red (positive correlation). Significant correlations are marked by * $p < 0.05$ and ** $p < 0.01$.

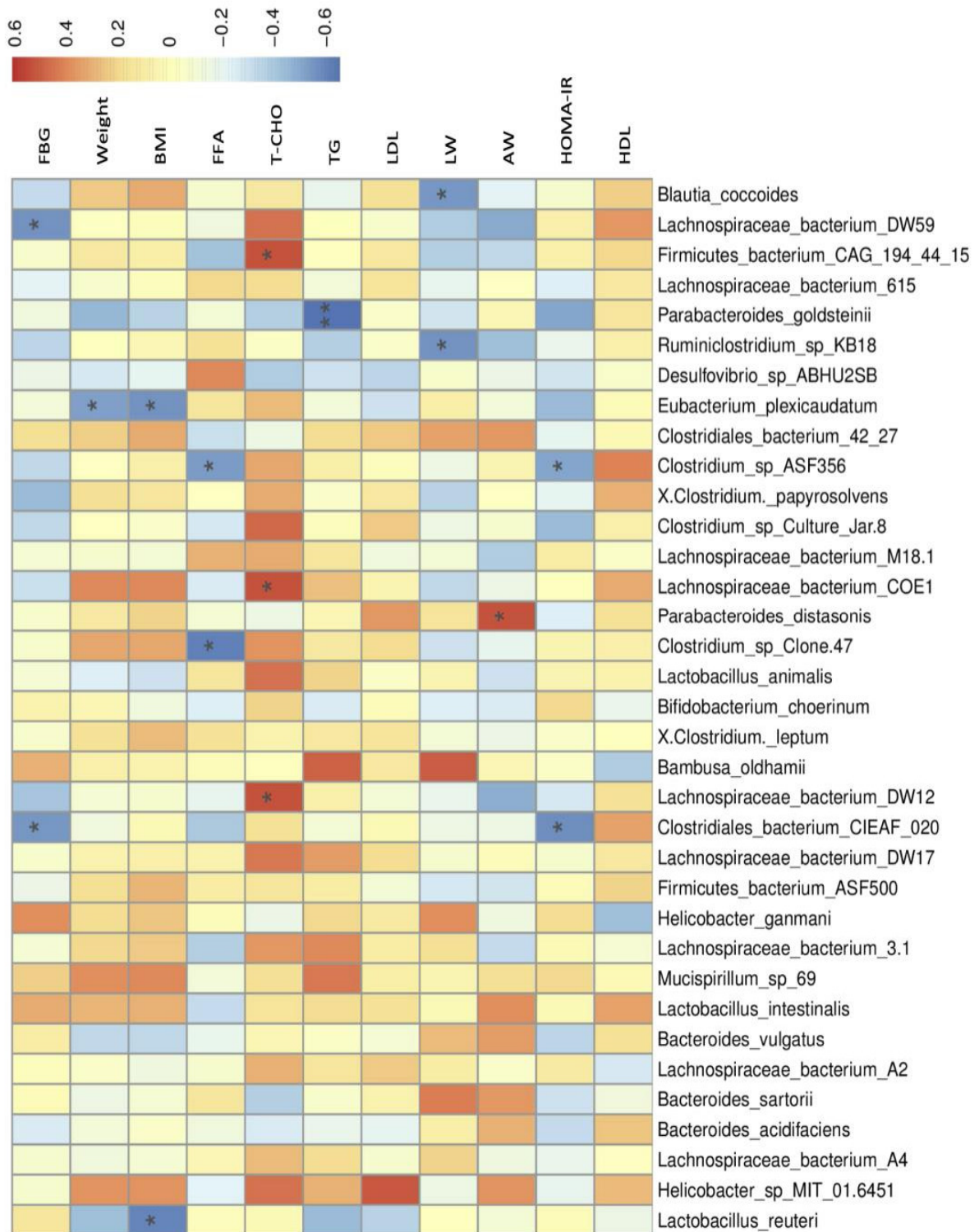


Figure 4.15. Heatmap of Spearman's correlation between the gut microbiota and obesity-related indexes (species). Good's coverage and the specie with significant correlations are shown. The colors range from blue (negative correlation) to red (positive correlation). Significant correlations are marked by * $p < 0.05$ and ** $p < 0.01$.

4.3.7. SFF improves intestinal integrity and inflammation

Increasing the proportion of pernicious bacteria in the intestine will secrete a large amount of endotoxin, increase intestinal permeability; excessive endotoxin can enter the blood to cause systemic inflammation and IR. Because of the presence of *Bacteroides* in the gut microbiota, they have been linked in improving the intestinal barrier and the integrity of mucus layer. Therefore, the up-regulation of *Bacteroides* by SFF treatment may alleviate intestinal inflammation due to HFD and improve the intestinal mucosal barrier. To evaluate the effects of SFF on the, we examined the gene expression of encoding inflammatory cytokines (*Il-6*, *Tnf- α* , and *Il-1 β*) and tight junction proteins (*Zo-1* and *Occludin-1*). The mRNA levels of *Il-6*, *Tnf- α* , and *Il-1 β* were found to be higher in the HFD group than in the NCD group; however, these mRNAs were downregulated in the HFD+SFF group ($P < 0.05$) when compared with those in the HFD group (**Figure 4.16a**). The mRNA levels of *Zo-1* and *Occludin-1* were increased in the HFD+SFF group ($P < 0.01$ and $P < 0.05$, respectively) compared with those in the HFD group (**Figure 4.16b**). In addition, the LPS content in the serum of the HFD+SFF group was slightly lower than that of the HFD group (**Figure 4.16c**). H&E staining showed normal histomorphology of the small intestine without epithelial disruption in the NCD group (**Figure 4.16d**). The pathological changes occurring in the HFD group were characterized by extensive destruction of the villi, multiple erosions and necrosis of the intestinal wall. SFF treatment significantly improved the histological structure of the intestinal wall impaired by HFD. The above data demonstrates that SFF treatment can maintain intestinal integrity and reduce intestinal inflammation, which may be associated with altered gut microbiota.

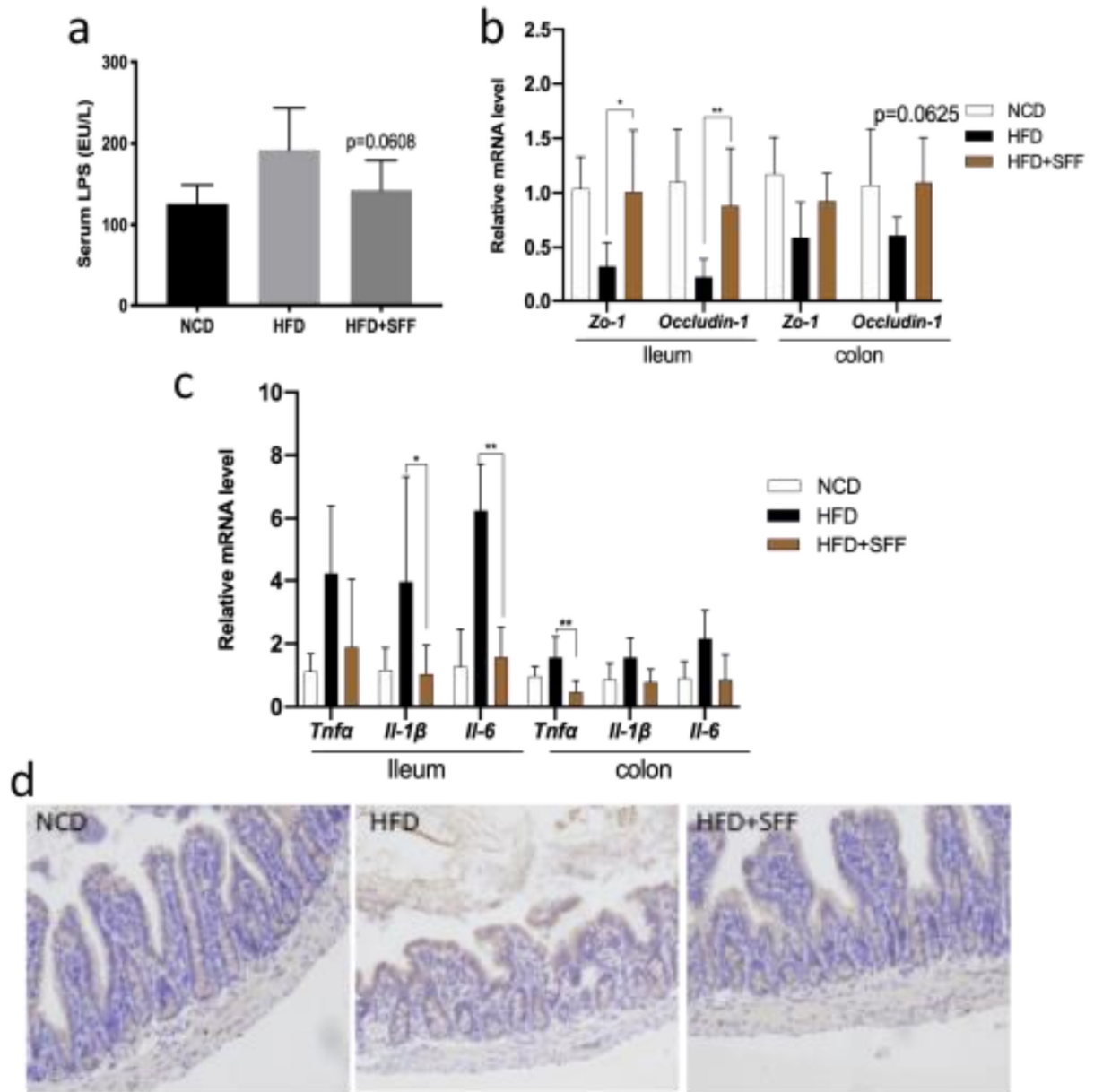


Figure 4.16. *S. fusiforme* fucoidan relieves intestinal inflammation and maintains intestinal wall integrity. (a) the relative mRNA levels of Zo1, Occludin and (b) pro-inflammatory cytokines in the ileum and colon; (c) serum LPS; (d) H&E staining of ileum (200×, scale bar = 200 μm). Data are represented as mean ± SD. * $P < 0.05$ and ** $P < 0.01$.

4.4. Discussion

Insulin resistance (IR) is as a major risk factor for developing T2D, and it is present in about 90-95% of the diabetic patients worldwide¹⁷. The consequence of IR is the restriction of glucose transport into the adipose tissue, liver or skeletal muscle, causing many metabolic syndromes, such as hyperinsulinemia, obesity and diabetes. As the mostly studied algal sulfated glycans from brown algal, fucoidan has been reported to be able to alleviate the development of metabolic disorders^{9,190}. For example, Heeba and Morsy reported that fucoidan can ameliorate the development of HFD-induced NAFLD, an effect that could be related to its hypolipidemic, insulin sensitizing, antioxidant and anti-inflammatory capacity¹⁹¹. Another research by Shang *et al.*¹⁹² shows that that fucoidans from *Laminaria japonica* and *Ascophyllum nodosum* can profoundly attenuate body weight gain, improve glucose homeostasis, and reduce chronic low-grade inflammation in diabetic mice. The hypoglycemic effect of fucoidan might be linked to its stimulation of pancreatic release of insulin and/or by reduction of insulin metabolism¹⁹³. A highly sulfated fucoidan derived from *Undaria Pinnatifida* showed strongly suppression of blood glucose and improvement of insulin sensitivity in diabetic mice¹⁹⁴. Consistent with previous studies, our findings demonstrate that the insulin sensitivity of HFD+SFF group was significantly improved as compared with that of HFD group. Therefore, the application of natural fucoidan for the treatment of metabolic syndrome with insulin resistance as the main cause has been considered as a promising strategy.

Growing evidence has shown that insulin signaling can be impaired by redox imbalance. Although the precise relationship between oxidative stress and impaired insulin signaling is not fully understood, several mechanisms have been proposed, and these include the abnormal serine/threonine phosphorylation of insulin receptor (IR) and the family of IR substrate (IRS) proteins, which can subsequently disturb the cellular redistribution and recruitment of insulin

signaling components, with the ultimate effect of the translocation of GLUT4 to the cell membrane and alteration of mitochondrial activity¹⁹⁵⁻¹⁹⁷. It is widely accepted that FFA is the essential link between ROS and IR¹⁹⁶. Oxidative stress has been proven to be caused by increased intake of HFD. Long-term HFD can elevate the levels of circulating FFA, leading to numerous adverse effects on mitochondrial function, such as the uncoupling of oxidative phosphorylation and the generation of ROS^{198,199}. The situation of redox imbalance is exacerbated by the ability of FFA to induce oxidative stress and to impair the endogenous antioxidant defenses through decreasing the concentration of intracellular glutathione^{200,201}.

According to our data, mice subjected to chronic HFD feeding developed increased oxidative stress, as judged by a decline in reduced/oxidized glutathione ratio, increased malondialdehyde level, and enhanced 4-HNE protein modification, concomitantly with higher FBG, FINS, and HOMA-IR. GSH and GSSG are acting as the main redox buffer of the cell, and they are found throughout all cellular compartments. GSH is one of the most important protective antioxidants and scavengers of ROS, and the ratio change between total GSH and GSSG is a biological index to assess oxidative damage²⁰². MDA is a toxic metabolite of lipid peroxidation, and it is widely used as a biomarker of oxidative stress during the onset of numerous metabolic diseases²⁰³. 4-HNE is a highly reactive end product of lipid peroxidation and it can react with a large number of macromolecules, such as proteins that principally contain histidine, cysteine and lysine residues. The modification of proteins, called HNE-protein adduction, would impair their activities and contribute to protein cross-linking, eventually inducing a carbonyl stress^{204,205}. When the constituents of antioxidant system are reduced, numerous free radicals are not sufficiently scavenged, causing redox imbalance, which further induce the occurrence and development of IR. A recent report has shown that fucoidan exhibits remarkable neuroprotective effect against transient global cerebral ischemia in HFD-

induced obese gerbils through the reduction of oxidative stress indicators (dihydroethidium, 8-hydroxyguanine and 4-hydroxy-2-nonenal) and the enhancement of endogenous antioxidant enzymes (SOD1 and SOD2)²⁰⁶. The decreased levels of MDA and 4-HNE protein modification, and the increased GSH/GSSG ratio and CAT activity that we observed in HFD-fed mice that received SFF treatment were also consistent with the neuroprotective effect of fucoidan.

Nrf2 plays a central role in the expression of over 250 genes, including those encoding antioxidant and detoxification enzymes, such as *Sod*, *Cat*, *Gst*, *Gpx4*, *Nqo1* and *Ho-1*²⁰⁷. The dysfunction of Nrf2/KEAP1/ARE pathway is associated with the development of IR and a wide range of metabolic disorders because of the intimate relationship between oxidative damage and IR²⁰⁸. Uruno and colleagues reported the Nrf2 overexpression in murine models via both genetic KEAP1 knockdown and pharmacological induction suggests that Nrf2 activation can improve insulin secretion and insulin sensitivity, markedly alter antioxidant-, energy consumption-, and gluconeogenesis-related gene expression in metabolic tissues, and eventually suppress the onset of diabetes in high-calorie-diet feeding mice²⁰⁹. Furthermore, Nrf2 activation can suppress HFD-induced weight gain and increase skeletal muscle oxygen consumption, mitochondrial redox homeostasis, and ATP production, as well as augment cellular glucose uptake²¹⁰. Growing evidence indicate that dietary polysaccharides are potential activators of Nrf2 signaling. Yang *et al.*²¹¹ reported that the administration of *Lycium barbarum* polysaccharide (LBP) increased the expression of antioxidant enzymes and reduced ROS levels via PI3K/Akt/Nrf2 axis, accompanied by the alleviation of HFD-induced IR in C57BL/6J mice. Moreover, fucoidan from *Laminaria japonica* possesses the neuroprotective effect in a rotenone-induced rat model of Parkinson's disease through the reduction of oxidative products by reserving mitochondrial function involving the PGC-1 α /Nrf2 pathway^{212,213}. A recent study also found fucoidan could alleviate acetaminophen-induced hepatotoxicity, and the mechanism

might be related to Nrf2-mediated anti-oxidation pathway²¹⁴. Our study provides further evidence indicating that SFF can activate Nrf2 signaling pathway and enhance the expression of SOD2 and CAT to scavenge for ROS, while the enhanced expression of *Slc7a11* and *Txnrd1* can increase intracellular glutathione levels to eliminate the lipid peroxidation products, such as MDA and 4-HNE modified proteins. Interestingly, SFF could also increase the mRNA level of *G6pd2*, which has been known as a NADPH-generating enzyme that supplies reducing power. Overall, SFF can enhance the expression of many detoxification and antioxidant enzymes to inhibit oxidative stress and, thereby attenuating IR.

Thermogenesis in the adipose tissue plays an essential role in the whole-body energy homeostasis, thereby being considered for a new therapeutic target for obesity treatment. In this phenomenon, UCP1 acts as a vital element as it converts the idling of the mitochondrial electron transport chain. This results in the release of protons and thus leads to generation of heat instead of synthesis of adenosine triphosphate (ATP)²⁰¹. The brown/beige adipocytes are known as the UCP1-positive adipocytes which possess thermogenic capacity in response to cold exposure or β 3 AR activation. The factor hydrolyze triacylglycerol (TG) into FFAs via the activation of intracellular lipases including adipose triglyceride lipase (ATGL), hormone-sensitive lipase (HSL), and monoacylglycerol lipase (MGL) and eventually induce mitochondrial biogenesis and activation²⁰³. The released FFAs serve as fuel of adaptive thermogenesis. The present study confirmed that SFF treatment decreased lipid droplet size in WAT and also promoted browning by increasing the expressions of UCP1 (**Figure 4.7**). Furthermore, we determined that SFF increased the mRNA expressions and of Cpt1 in liver. The process of lipid depletion begins with the activation of fatty acids to produce lipid acyl-CoA, which then enters the mitochondria for fatty acid β -oxidation, and CPT1 is the rate-limiting enzyme for fatty acid β -oxidation, which can promote lipid depletion. Based on our

findings, it is believed that SFF can promote beige induction in WAT of mice and facilitate lipid depletion.

Oxidative stress is a key factor in the pathogenesis of obesity²⁰⁰. Studies have shown that a high sugar and high fat diet induces liver inflammation and lipid deposition, which may be caused by upregulation of ROS to interfere with lipid metabolism-related proteins. In the rat liver and HepG2 cells induced by high fat and high sugar, the Nrf2 antioxidant pathway was inactivated, ROS-driven thioredoxin (TXNIP) was overexpressed, inflammasome activation and peroxisome activation receptor alpha (PPAR- α), carnitine palmitoyltransferase-1 (CPT-1), and peroxisome activation receptor alpha (PPAR- α) were induced. element binding protein 1 (SREBP-1) and stearoyl-CoA desaturase-1 (SCD-1) were dysregulated²⁰⁴. UCP1 transgenic mice exhibit a healthy aging phenotype, such as decreased atherosclerosis and obesity and prolonged life span. UCP1-Tg mice show a decrease in skeletal muscle mass, particularly in fast/glycolytic muscles, compared to slow/oxidative muscles, which is accompanied by an increase in food intake, oxygen consumption and glucose uptake in skeletal muscle. UCP1 overexpression also increases catalase and SOD activity as well as glutathione content in skeletal muscle. UCP1-Tg mice exhibit an increase in respiration leak consistent with UCP1 function, which is not affected by Nrf2 ablation. In contrast, Nrf2 deficiency lowers the maximum coupled respiration in wild-type and Tg mice but does not alter the expression of respiratory chain complexes, probably due to impaired substrate availability, as reported previously²⁰². Interestingly, PGC1 α expression is elevated in UCP1-Tg mice and is partially suppressed in Nrf2-knockout mice. Nrf2 activation might induce PGC1 α expression, although PGC1 α activation by AMPK and Sirt1 rather than transcriptional induction has been reported in another study²⁰⁵. Taken together, these results identified both Nrf2-dependent and/or Nrf2-independent pathways in response to CPT1 and UCP1 overexpression in the HFD+SFF mice;

however, their activation mechanisms and biological impact on MetS remain to be understood in future studies.

Gut microbiota is closely related to the energy metabolism and the occurrence of IR, obesity and T2D²⁰. With an increasing understanding of the complicated interaction between the gut microbiota and host, it is still unclear how polysaccharides exert insulin sensitization by remodeling the gut microbiota. Dietary polysaccharides generally escape digestion in the stomach and the small intestine, reaching the colon, where they are available for fermentation and thereby enhance the growth of probiotics and improve microbial diversity²¹⁵. Furthermore, diverse dietary polysaccharides from seaweed can alleviate metabolic syndrome (e.g., obesity, hyperlipidemia, and inflammation) by modulating the gut microbiota¹²⁻¹⁴. Here, SFF significantly influenced the relative abundances of Firmicutes and Bacteroides in the HFD-fed mice, consistent with our previous findings that SFF can increase the species richness, dramatically increase the relative abundance of Bacteroides and decrease Firmicutes in diabetic mice³⁰. Bacteroidetes is one of the major bacterial phyla responsible for the fermentation of complex indigestible polysaccharides such as fucoidan, inulin, pectin, arabinoxylan oligosaccharides, and arabinogalactan²¹⁶. Growing evidence indicate that dietary fucoidans can increase the abundance of Bacteroidetes, fucoidan has been shown to promote the ratio of Bacteroidetes/Firmicutes and increased the expression of *Zo-1* and *Occludin-1*^{15,217}. A fucoidan derived from brown marine algae significantly up-regulated the expression of BSH in the intestine of HFD-fed mice to alleviated obesity, and increase the ratio of Bacteroidetes/Firmicutes by up-regulating the relative abundance of Bacteroidetes²¹⁸. In addition, the declined ratio of the Bacteroidetes/Firmicutes is an indicator of microbial imbalance, associated with the development of metabolic syndrome³⁰. Therefore, increasing the ratio of Bacteroidetes/Firmicutes is of great importance for the intervention of metabolic

disorders. Our present data demonstrate that SFF can effectively increase Bacteroidetes and decrease Firmicutes, raise the ratio of Bacteroidetes/Firmicutes, improve the diversity and remodel the structure of gut microbiota. This effect of SFF might be responsible for reducing the extent of HFD-diet-induced IR in the mice.

It is widely accepted that the changes in bacterial abundance are closely correlated with the obesity-related physiological parameters. Spearman's correlation analysis revealed 14 key bacteria that were significantly associated with at least one obesity-related physiological parameter. *Rikenella*, *Candidatus_Saccharimonas*, *Odoribacter*, *Bacteroides* and *Alistipes* were negatively correlated with multiple obesity-related physiological parameters. LDA analysis revealed two dominant bacteria, *Bacteroides* and *Alistipes*, in both the NCD and HFD+SFF groups. These two bacteria have been are markedly reduced in obese individual, a condition that may be related to the disorder of glutamate metabolism²¹⁹. Liu *et al.*²²⁰ reported that increasing the abundance of *Alisipes* and *Rikenella* in the gut microbiota could improve the glucose tolerance, induce the production of SCFAs and inhibit the production of endotoxin LPS. In contrast, *Turicibacter* and *Romboutsia*, positively correlated with fat metabolism and enriched in the HFD group, can effectively promote fat decomposition and absorption^{221, 222}. *Turicibacter* was found in high abundance in the intestinal model of NAFLD mice, and Jung *et al.*²²³ reported that Kombucha can reduce the abundance of the bacteria and increase the fermentation function of bacteria to improve liver metabolic disorders. In the analysis of flora function, we also found that the supplementation of SFF could increase the bacteria proportion of the fermentation function, and the SCFA and bile acids of the secondary metabolites produced by fermentation may effectively relieve insulin resistance induced by high-fat diet²²⁴. In Spearman's correlation analysis at species level (**Figure 4.15**), a negative correlation between *Parabacteroides_goldsteinii* and TG content was found. *Cordyceps sinensis*

polysaccharides can increase the abundance of *P. goldsteinii* and reduce the weight gain and the release of inflammatory cytokines caused by HFD feeding²²⁵. In addition, *P. goldsteinii* can also produce a large amount of succinic acid, and activate intestinal FXR signaling pathway to improve the disorder of lipid and glucose metabolism, repair intestinal integrity, activate intestinal gluconeogenesis, and promote liver glycogen synthesis. Therefore, the reduction of intestinal inflammation by SFF treatment in HFD-induced obese mice might be due to the increased abundance of *P. goldsteinii*, and it was also positively correlated with the decrease in serum TG.

4.5. Summary

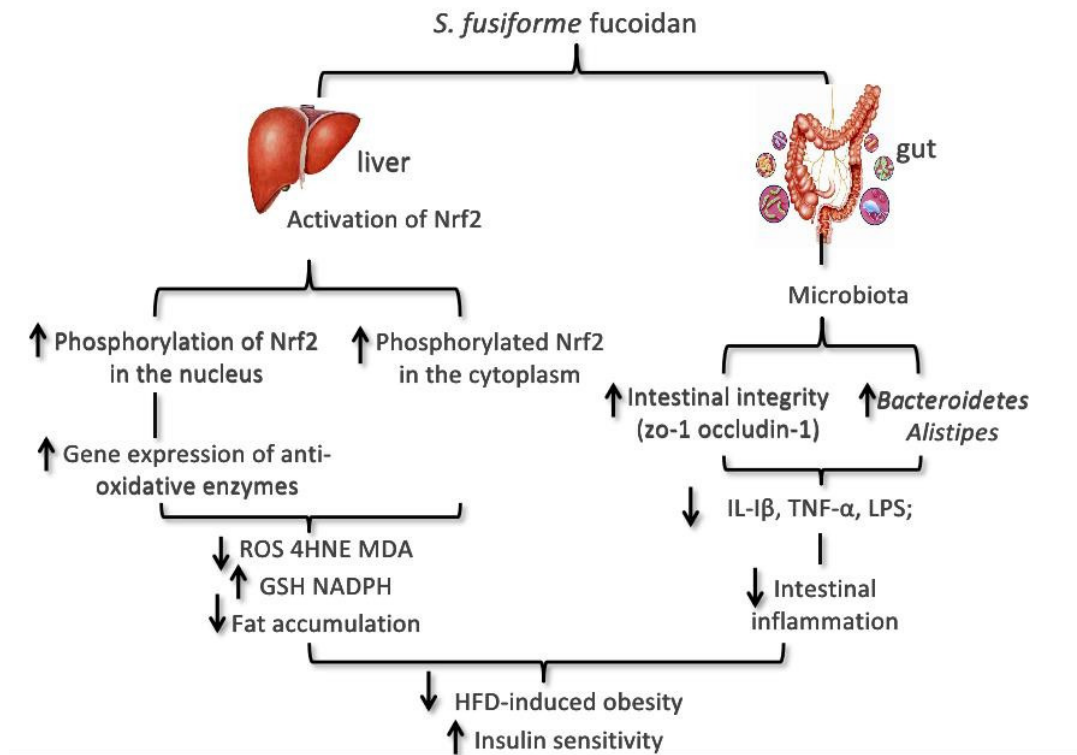


Figure 4.16. Therapeutic mechanism of *S. fusiforme* fucoidan on HFD-induced obesity.

With regard to IR or metabolic diseases, knowledge of the pivotal role of oxidative

stress in the pathogenesis and progression of these diseases originally precipitated investigation into natural antioxidants, such as vitamin C, vitamin E, anthocyanin and coenzyme Q²⁵. Although a very logical approach, antioxidant therapy may take more than simple dosing with an antioxidant. The results of antioxidant therapy have generally been disappointing, and human clinical trials have not shown any benefit of natural antioxidants as adjunct therapies in preventing or treating metabolic diseases²¹⁷. In the liver, SFF can activate the Nrf2/ARE signaling pathway, increase the expression of Nrf2 and promote its nuclear translocation, increase the expression of its downstream antioxidant enzymes and reduce the accumulation of lipid peroxides, alleviating the tissue damage caused by HFD-induced oxidative stress. On the other hand, SFF can increase the diversity and improve the structure of gut microbiota, maintain the integrity of intestinal wall, and reduce systemic inflammation. In summary, *S. fusiforme* fucoidan SFF alleviates HFD-induced insulin resistance in peripheral tissues via the Nrf2/ARE signaling pathway and gut microbiota remodeling, providing a novel potential treatment strategy for metabolic diseases.

Chapter 5

SARGASSUM FUSIFORME FUCOIDAN ALLEVIATES INSULIN RESISTANCE BY REDUCTION OF INTESTINAL-DERIVED CERAMIDE BIOSYNTHESIS VIA INHIBITING FXR/SHP SIGNALING PATHWAY

Abstract

Sargassum fusiforme fucoidan (SFF) is a highly sulfated heteropolysaccharide with various biological activities. As one of the causative factors of type 2 diabetes mellitus (T2DM), insulin resistance has become a global health issue. In this study, we investigated the potential pharmacological mechanisms by which SFF ameliorates insulin resistance in chronic high-fat diet (HFD)-fed mice. Our finding suggested that SFF significantly enhanced tauroursodeoxycholic acid (TUDCA, a conjugated bile acid) level and inhibited FXR signaling pathway in the colon. Compared to the HFD group, SFF reduced ceramide levels both in serum and colon as well as the gene expression of *SPT* and *CerS*, two crucial enzymes involved in the biosynthesis of ceramides regulated by FXR signaling. Pearson's analysis showed that the TUDCA level was positively correlated with the intestinal bacteria *Clostridium*, which was further validated in pseudo-germfree mice. Taken together, the present data suggest that SFF increased TUDCA level in the bile acid pool by remodeling the gut microbiota, then TUDCA as a natural FXR antagonist significantly inhibited the FXR/SHP signaling pathway to reduce intestinal-derived biosynthesis of ceramide and thereby improved insulin resistance in diet-induced obese (DIO) mice. This study provides new insights into the therapeutic potential of *S. fusiforme* fucoidan in metabolic disease.

Keywords : *S. fusiforme* fucoidan, insulin resistance, gut microbiota, ceramides, TUDCA

5.1. Introduction

Diabetes mellitus (DM) affect about 383 million adults, accounting for 8.3% of adult population worldwide²²⁶⁻²²⁸. For developing complications including cardiovascular diseases, mental and nervous system disorders, cancer, infections and liver disease, DM, in particular type 2 diabetes mellitus (T2DM), has grown up to be a global public health problem²⁻⁴. Most of these diseases are characterized by one distinct defect: insulin resistance (IR)². IR is defined as a diminished ability of some kinds of cells, such as adipocytes, skeletal muscle cells, and hepatocytes, to respond to the action of insulin, which plays a central role in the development of several metabolic abnormalities and diseases, such as obesity, type 2 diabetes, and metabolic syndrome²²⁸⁻²³⁰. Due to the increasing number of insulin resistant patients and the limited number of anti-diabetic medicines available, the search for new compounds, especially from marine sources, is a hot concern in the field of pharmaceutical research and development. Fucoidan is a family of highly sulphated homo- and heterogeneous polysaccharides, considered to be one of the most important bioactive macromolecules in brown algae, and has been found to improve disorders of glucolipid metabolism²³¹⁻²³⁴. He *et al.* found that fucoidan isolated from brown alga has a preventive effect on hyperglycemia in mice, presumably by activating the AMPK pathway to slow down the development of diabetes²³⁵. Sung Yi Sim found that Fucoidan from *Undaria pinnatifida* has anti-diabetic effects by stimulation of glucose uptake and reduction of basal lipolysis in 3T3-L1 adipocytes²³⁶. However, due to its complex chemical structure and difficult absorption properties, the physiological mechanisms underlying its anti-diabetic effects remain to be investigated in depth.

Metabolomics is an emerging histological technique developed after genomics and proteomics to analyse the complex metabolites of the body. It focuses on the qualitative and quantitative analysis of molecules of less than 1000 relative molecular weight produced by cells, tissues, blood and other biological systems that receive external stimuli or disturbances²³⁷⁻

²³⁹. Gut microbiota, composed of trillions of microorganisms, plays a number of important physiological roles involving food digestion and metabolism²³⁹⁻²⁴¹. Recently, accumulated evidence has demonstrated that the modulation of the gut microbiota by dietary ingredients can ameliorate obesity and its complications²⁴². Especially, indigestible marine plant-derived polysaccharides (MPPs) and marine animal-derived polysaccharides (MAPs) can be metabolized and fermented in the gut as nutraceuticals and gut microbiota modulators affecting intestinal ecology²⁴³. Combined multi-omics techniques offer the possibility of prediction and early diagnosis of type 2 diabetes²⁴⁴. In recent years, several studies have used Combined multi-omics techniques to conduct comprehensive and systematic studies on the changes of metabolites in patients with type 2 diabetes, searching for biomarkers and possible metabolic pathways of type 2 diabetes, and providing data to reveal the pathogenesis of type 2 diabetes^{245,246}.

As marine brown algae with great economic importance, *Sargassum fusiforme* is cultured on a vast scale in the coastal zone of Zhejiang, Liaoning and Fujian Provinces, China, and most of which is exported to Japan and South Korea, where it is consumed as health food²⁴⁷⁻²⁴⁹. *S. fusiforme* fucoidan (SFF) has been reported to possess multiple bioactivities, such as hypolipidemic, immunomodulatory and anti-tumor, and antioxidant activity²⁵⁰⁻²⁵². In our previous studies²⁵³⁻²⁵⁵, SFF was found to alleviate insulin resistance in diet-induced obese (DIO) mice and other metabolic disorders, such as hyperglycemia and hyperlipidemia. However, SFF is a structurally complex macromolecule that is difficult to be digested and directly absorbed by the body, and its pharmacological mechanisms of alleviation in insulin resistance remain an unsolved puzzle. Therefore, in the present study, metabolomic and 16S rRNA analysis were performed to determine the differences in intestinal metabolites and gut microbiota in DIO mice after SFF treatment. The effect of TUDCA on transcript levels of ceramide biosynthetic

enzymes was explored by *in vitro* and *in vivo* experiments. Construction of pseudo-germfree mice to determine the criticality of gut microbiota on fucoidan in alleviating insulin resistance. The results suggest that SFF is able to increase the content of TUDCA by remodeling the gut microbiota, and TUDCA alleviates insulin resistance by inhibiting the FXR signaling pathway to reduce intestinal-derived ceramide biosynthesis. Accordingly, this study provides insight into the biological mechanisms by which *S. fusiforme* fucoidan effectively ameliorates insulin resistance, offering a new strategy for the therapeutic mechanisms of marine natural medicines.

5.2. Materials and methods

5.2.1. Materials and reagents

Sargassum fusiforme fucoidan (SFF) was prepared and characterized as previously reported^{28,29}. Normal chow diet (NCD, containing 10% fat by energy) and high-fat diet (HFD, containing 60% fat by energy) were purchased from Beijing HFK Bio-Technology Co., Ltd. (Beijing, China). HFD was stored at -20°C throughout the study to maintain freshness and prevent degradation of fat. Insulin from bovine pancreas was provided by Sigma–Aldrich (St. Louis, MO, USA). Sphingosine (SPH, purity ≥ 98%), chenodeoxycholine acid (CDCA, purity ≥ 99%) and tauroursodeoxycholic acid (TUDCA, purity ≥ 99%) were purchased from Selleck (Houston, Texas, USA). Lincosib and verapamil hydrochloride were purchased from MedChemExpress (Monmouth Junction, NJ, USA). The cocktail of antibiotics used consisted of 0.5 g/L vancomycin (Sigma-Aldrich, UK) and 1 g/L neomycin, metronidazole and ampicillin (Sigma-Aldrich, UK). Radioimmunoprecipitation assay (RIPA) buffer was purchased from Beyotime (Shanghai, China). Antibodies against Akt and phospho-Akt (Ser473) were purchased from Cell Signaling Technology (Beverly, MA, USA). All other chemical reagents used were analytical grade.

5.2.2. Animal experiments

All male mice (ICR mice, 7 weeks old, body weight 25 ± 2 g) were housed in ventilated cages (three animals per cage) at the SPF facility of Wenzhou University under controlled environmental conditions (temperature $22 \pm 2^\circ\text{C}$; relative humidity 60–70%) with free access to standard laboratory chow and tap water. The mice were maintained on a regular 12/12 h light/dark cycle. All animal care and experimental procedures were approved by the Animal Care Ministry of Health and were performed in accordance with the guide for the Care and Use of Experimental Animals of Wenzhou University.

The animals were randomly assigned to groups by a colleague blinded to the experimental protocol according to the needs of the experiment, which consisted of three animal experiments. As for the pharmacological activity of SFF, one group of ICR mice was fed with NCD and the other two groups were fed with HFD. After 12 weeks of HFD feeding, one group of HFD-fed mice was administered SFF (200 mg/kg body weight), once daily (HFD+SFF group, n=8) for 8 weeks, whereas the NCD-fed mice (NCD group, n=8) and other group of HFD-fed mice (HFD group, n=8) were treated with an equal volume of saline for 8 weeks. As for the pharmacological activity of TUDCA and SFF, One group of ICR mice was fed with NCD; three groups of mice were fed with HFD, one group was fed with TUDCA (300 mg/kg body weight), one group was fed with SFF (200 mg/kg body weight) and one group was treated with an equal volume of saline as control. As for the pharmacological activity of gut microbiota, three groups of animals were fed with HFD. One group of mice was administered SFF (200 mg/kg body weight), one group of mice was administered SFF and water-feed the antibiotic mixture every three days for 24 h, and one group of mice was treated with an equal volume of saline.

During experiment, the body weight, water consumption and food intake were measured every week. At week 18, intraperitoneal glucose tolerance test (IPGTT) and intraperitoneal

insulin tolerance test (IPITT) were performed as described³⁰. Fresh feces were collected and stored immediately at -80°C for subsequent analysis. At the end of the trial, after overnight fasting for 12 h, blood samples were collected, and serum was isolated by centrifugation at $1000 \times g$ for 15 min at 4°C, and stored at -80°C for further assay. Tissues, including liver, subcutaneous fat, kidney, pancreas, colon and ileum, were weighed.

5.2.3. Biochemical Analysis

Total cholesterol (TC), triacylglycerol (TG), fasting blood glucose (FBG) and fasting serum insulin (FINS) were determined by biochemical kits purchased from Jiancheng Bioengineering Institute (Nanjing, China). Sphingosine (SPH), Ceramides (Cer) and Sphingosine-1P (S1P) were determined by biochemical kits purchased from Jingkang Bioengineering Institute (Shanghai, China). Homeostasis model assessment-estimated insulin resistance (HOMA-IR) was calculated using the following formula:

$$\text{HOMA-IR} = \text{FBG (mmol/L)} \times \text{FINS (mU)} / 22.5$$

5.2.4. Determination of hepatic/serum TUDCA

The contents of TUDCA in tissues were determined by high-performance liquid chromatography (HPLC). Briefly, 200 mg of frozen tissue was homogenized with a Qiagen TissueLyserII (Germantown, MD, USA) in 1 mL of PBS to prepare the tissue homogenates. The impurities were removed through a 0.22 μm filter, then the filtrate was precipitated by methanol and 10 μL of supernatant was analyzed using an Agilent 1290 HPLC system (Santa Clara, CA) equipped with a Hypersil ODS-2 column (5 μm , 4.6 \times 250 mm; Waters, USA). The supernatant was detected at the wavelength of 210 nm, eluted with the mobile phase of 0.03 M phosphate buffer solution (pH 4.4) and methanol (32:68, v/v) at a flow rate of 1.0 mL/min.

5.2.5. Quantitative RT-PCR

The samples were extracted by a TRIzol reagent (Invitrogen, Carlsbad, CA, USA). The cDNA was synthesized from RNA using a reverse transcription kit (Takara, Dalian, China) in accordance with the manufacturer's protocol. SYBR Green PCR Master Mix (Applied Biosystems, Foster City, CA, USA) was used for real-time PCR. The sequences of the specific primers are shown in **Table 5.1**. A LightCycler480 qRT-PCR system (Roche, Mannheim, Germany) was used for the amplification under the following reactions: 95°C for 15 min, followed by 40 cycles at 95°C for 10 s, 60°C for 20 s, and 72°C for 20 s. The level of the transcripts, expressed as fold change, was calculated according to formula $2^{-\Delta\Delta ct}$ method.

Table 5.1. Designed Primer Sets for qRT-PCR

| Gene | Primer | 5'-3' | Size (bp) |
|--------------------|-----------|------------------------|-----------|
| <i>Mus-Fxr</i> | sense | TGGGCTAGGCAAAAGATGTGA | 160 |
| | antisense | ACTGCTGCTTCTTGAGTGCT | |
| <i>Mus-Shp</i> | sense | CCAGTAGAGTGGTAGCCCG | 360 |
| | antisense | CTCCCCTCCGTACAGGTCAT | |
| <i>Mus-Fgf15</i> | sense | AGTACCTGTACTCCGCTGGT | 148 |
| | antisense | ACGTCCTTGATGGCAATCGT | |
| <i>Mus-Spt1</i> | sense | CACCGAGCACTATGGGATCA | 303 |
| | antisense | AGGGACTCTCCCACCACTTT | |
| <i>Mus-Spt2</i> | sense | TCACCTCCATGAAGTGCATC | 109 |
| | antisense | CAGGCGTCTCCTGAAATACC | |
| <i>Mus-Spt3</i> | sense | ACACAATCCTAAGACCCAGCA | 141 |
| | antisense | AGACTGGCTTATCCTCAGCATA | |
| <i>Mus-Cer2</i> | sense | AAGTGGGAAACGGAGTAGCG | 131 |
| | antisense | ACAGGCAGCCATAGTCGTTC | |
| <i>Mus-Cer4</i> | sense | GGATTAGCTGATCTCCGCAC | 197 |
| | antisense | CCAGTATGTCTCCTGCCACA | |
| <i>Mus-Cer5</i> | sense | CTTCTCCGTGAGGATGCTGT | 113 |
| | antisense | GTGTCATTGGGTTCCACCTT | |
| <i>Mus-Smpd1</i> | sense | GTTACCAGCTGATGCCCTTC | 158 |
| | antisense | AGCAGGATCTGTGGAGTTG | |
| <i>Mus-Smpd2</i> | sense | AGCAGGATCTGTGGAGTTG | 163 |
| | antisense | CTCCAGCCATGAAGCTCAAC | |
| <i>Mus-Smpd3</i> | sense | CCTGACCAGTGCCATTCTTT | 159 |
| | antisense | AGAAACCCGGTCCTCGTACT | |
| <i>Mus-β-actin</i> | sense | GTCCCTCACCCCTCCAAAAG | 266 |
| | antisense | GCTGCCTCAACACCTCAACCC | |
| <i>Homo-Fxr</i> | sense | AACCATACTCGCAATACAGCAA | 185 |
| | antisense | ACAGCTCATCCCCTTTGATCC | |
| <i>Homo-Shp</i> | sense | CCCCAAGGAATATGCCTGCC | 104 |
| | antisense | TAGGGCGAAAGAAGAGGTCCC | |
| <i>Homo-Fgf15</i> | sense | CCAGAAGACAGGCAGTAGT | 135 |

| | | | |
|---------------------|-----------|-------------------------|-----|
| <i>Homo-Spt1</i> | antisense | CTGGAGGGATTTGGGAAGG | |
| | sense | CTCCTCCCAGAGGAAGAAGTGG | 163 |
| <i>Homo-Spt2</i> | antisense | TTGCTCTCTTTCAGGCCACT | |
| | sense | TCACCTCCTGTAGTGGAGCA | 138 |
| <i>Homo-Spt3</i> | antisense | GCCCATCTCTTTCAGGCGTC | |
| | sense | GGAGTTGGAGGACCTTGTGG | 152 |
| <i>Homo-Cer2</i> | antisense | GCACAAGCGATGTGTGGTTT | |
| | sense | TCTTGATGCCCTCCCCTTTG | 110 |
| <i>Homo-Cer4</i> | antisense | TCTAGATCGGCCAGGTCAA | |
| | sense | TGCAGCTGCTCCGGGTA | 253 |
| <i>Homo-Cer5</i> | antisense | TGGACAGCATTCTCTGCTGG | |
| | sense | TGATTTTGCAAGTCTGAGATGGG | 323 |
| <i>Homo-Smpd1</i> | antisense | ACAGGTCACCTTTCCTGA | |
| | sense | TCGGCCTTAATCCTGTCAGC | 314 |
| <i>Homo-Smpd2</i> | antisense | CACAGCAGCATTGCGCTTT | |
| | sense | AACTTTGCGCCTGTTGCTG | 71 |
| <i>Homo-Smpd3</i> | antisense | TTTTCTCCAAGCTCGTCCC | |
| | sense | CGACTGGAAGCTGCCTCTTA | 124 |
| <i>Homo-β-actin</i> | antisense | TACCCGACGATTCTTTGGTCC | |
| | sense | CTCCATCCTGGCCTCGCTGT | 268 |
| | antisense | GCTGTACCTTCACCGTTCC | |

5.2.6. Cell culture

Human colon cancer (Caco-2) cells were cultured in MEM (Sigma, St. Louis, MO, USA) supplemented with 10% FBS (Gibco, South American), non-essential amino acids, pyruvate, glutamine, penicillin and streptomycin, maintained in 5% CO₂ at 37°C.

5.2.7. Immunoblotting

Sample were homogenized with ice-cold RIPA lysis buffer containing protease and phosphatase inhibitors (Beyotime, Shanghai, China). The homogenates were centrifuged at 10 000 × g for 20 min at 4 °C to remove the insoluble precipitate. The protein concentration in the supernatant was determined using a BCA protein assay kit (Beyotime, Shanghai, China) according to the manufacturer's protocol. The protein concentration for each sample was adjusted to an equal amount and denatured in boiling water for 5 min. Equal aliquots (40 µg) of protein samples were subjected to 10% SDS-PAGE and transferred to PVDF membranes (Millipore, Bedford, MA, USA). After blocking with 5% nonfat milk (dissolved in TBST) for 1

h, the membranes were incubated with the indicated antibodies at 4 °C overnight, followed by incubation with the appropriate HRP-conjugated second antibodies for 1 h at room temperature. Chemiluminescent detection was performed using the ECL Plus Western blotting reagent (TransStart, Beijing, China). The semi-quantitative analysis for the densitometry of each band was performed using ImageJ software.

5.2.8. Analysis of gut microbiota by 16S rRNA amplicon sequencing

As described previously, total bacterial DNA was extracted from the collected feces using CTAB/SDS method. Illumina MiSeq (Novogene Bioinformatics Technology Co., Ltd.) was used to analyze the 16S rRNA genes in the DNA sample to determine the composition and diversity of bacteria.

Sample preparation: Faecal samples were freshly collected at week 16 and immediately stored at -80°C. Total fecal DNA was extracted using CTAB/SDS method. The V4 region of the 16S rRNA was amplified using the universal primers 515F and 806R. All PCR reactions were carried out with Phusion[®] High-Fidelity PCR Master Mix (New England Biolabs), and the mixture PCR products were purified with GeneJET Gel Extraction Kit (Thermo Scientific). Sequencing libraries were generated using Ion Plus Fragment Library Kit (Thermo Scientific) following manufacturer's recommendations. The library quality was assessed on the Qubit 2.0 Fluorometer (Thermo Scientific). At last, the library was sequenced on an Ion S5[™] XL platform (Thermo Scientific) and 400 bp/600 bp single end reads were generated.

Data acquisition: Paired-end reads were merged using FLASH (V1.2.7), and the Raw fastq files were processed by QIIME (version 1.7.0). Sequence analysis was performed by Uparse software (v7.0.1001), and Sequences with $\geq 97\%$ identity were assigned to the same Operational Taxonomic Units (OTUs).

Data analysis: To compare the compositional OTUs of the gut microbiota in each group,

a Venn diagram was constructed using R packages (version 3.1.0) as previously documented. Mothur software packages (version V.1.30.1) were used to calculate the value of Chao1, Ace, Simpson index and Shannon index for evaluation of the community richness and community diversity. Pair-group method with arithmetic means (UPGMA) clustering was generated using the average linkage and conducted by QIIME software (V1.7.0). Linear discriminant analysis (LDA) was carried out to determine the highly dimensional gut microbes and characteristics associated with NCD mice, HFD mice and HFD+Met mice.

5.2.9. Non-targeted metabolome analysis

A non-targeted metabolome analysis of the colon contents was performed with a liquid chromatography-tandem mass spectrometry (LC-MS) method (Waters ACQUITY UPLC (Waters, America) coupled to a Thermo LTQ Orbitrap XL system (Thermo, America)). Metabolites extraction from colon contents: Colon contents were added ddH₂O (4°C) and mixed. 100 mg of sample was extracted with 1000 µL of pre-cooled methanol (-20°C). After centrifugation, the supernatant was evaporated and finally dissolved in 400 µL methanol aqueous solution (1:1, 4°C). For the quality control (QC) samples, 20 µL of extract was taken from each sample and mixed. These QC samples were used to monitor deviations of the analytical results from these pool mixtures and compare them to the errors caused by the analytical instrument itself. And the rest of the samples were used for LC-MS detection.

UPLC Conditions: Chromatographic separation was accomplished in an Acquity UPLC system equipped with an ACQUITY UPLC[®] HSS T3 (150 × 2.1 mm, 1.8 µm, Waters) column maintained at 4°C. The temperature of the auto sampler was 4°C. Gradient elution of analytes was carried out with 0.1% formic acid in water (A) and 0.1% formic acid in acetonitrile (B) at a flow rate of 0.25 mL/min. Injection of 5 µL of each sample was done after equilibration. An increasing linear gradient of solvent B (v/v) was used as follows: 0~1 min, 2% B; 1~9.5 min,

2%~50% B; 9.5~14 min, 50%~98% B; 14~15 min, 98% B; 15~15.5 min, 98%~2% B; 15.5~17 min, 2%.

Mass spectrometry conditions: The ESI-MSⁿ experiments were executed on the Thermo LTQ Orbitrap XL mass spectrometer with the spray voltage of 4.8 kV and -4.5 kV in positive and negative modes, respectively. Sheath gas and auxiliary gas were set at 45 and 15 arbitrary units, respectively. The capillary temperature was 325°C. The voltages of capillary and tube were 35 V and 50 V, -15 V and -50 V in positive and negative modes, respectively. The Orbitrap analyzer scanned over a mass range of *m/z* 89-1000 for full scan at a mass resolution of 60000. Data dependent acquisition (DDA) MS/MS experiments were performed with CID scan. The normalized collision energy was 30 eV. Dynamic exclusion was implemented with a repeat count of 2, and exclusion duration of 15 s.

Data processing: UPLC-QTOF-MS raw data were analyzed with MarkerLynx Application Manager 4.1 (Waters Corp.). The matrix from UPLC-QTOF-MS was introduced into SIMCA-P 11.0 software (Umetrics) and standardized to a mean of 0 and variance of 1, according to the formula $[X - \text{mean}(X)] / \text{std}(X)$, for multivariate statistical analysis. The *t* test with false discovery rate correction was used to measure the significance of each metabolite. Partial least-squared discriminant analysis (PLS-DA) and orthogonal partial least-squared discriminant analysis (OPLS-DA) were conducted to identify the metabolite discrimination between the two group samples. Differential metabolites were defined with variable importance in the projection (VIP) > 1.0 obtained from OPLS-DA and *P* values less than 0.05 obtained from *t* test. Differential metabolites were tentatively identified by database matching, i.e., Human Metabolome Database (HMDB) (<http://www.hmdb.ca>), Metlin (<http://metlin.scripps.edu>), massbank (<http://www.massbank.jp/>), LipidMaps (<http://www.lipidmaps.org>), mzcloud (<https://www.mzcloud.org>). Heatmaps of differential

metabolites among all groups were obtained based on spearman correlation and cluster analyses.

5.2.10. Statistical analysis

Statistical analysis for bacterial diversity with a small sample size was conducted using the Mann–Whitney U test (SPSS, Chicago, USA). Statistical comparisons among experimental groups were analyzed by one-way ANOVA and Duncan’s multiple-comparison test using the SPSS software program (Version 21; SPSS). Environmental factor correlation coefficients were analysed using the Novogene platform (<https://magic.novogene.com/>) and the sperman algorithm was used to correlate obesity parameters with gut microbiota and physiological indicators. Statistically significance was considered at the $P < 0.05$ level.

5.3. Results

5.3.1 SFF prevents obesity-driven metabolic disorder and remodels instestinal metabolites

As shown in **Figure 5.1a**, after 16 weeks of HFD feeding, mice developed various metabolic disturbances reminiscent of diabetes, such as overweight, hyperglycaemia and glucose intolerance (**Table 5.2**). Mice treated with SFF exhibited reduced body weight, BMI, organ indexes, TG, TC and improved hyperglycemia, hyperinsulinism and insulin resistance compared to the HFD group. In addition, SFF significantly increased the expression of phosphorylated Akt in both muscle and adipose tissues, suggesting that SFF can reduce the inhibition of insulin signalling by a high-fat diet (**Figure 5.2**). The intestinal metabolite profiles were further measured using lipid chromatography and mass spectrometry (LC-MS). SFF caused significantly differential changes of intestinal metabolites in HFD-fed mice evidenced by the scatter plots of OPLS-DA. Compared to HFD group, SFF treatment up-regulated 80 of intestinal metabolites and down-regulated 24 metabolites (**Figure 5.3**). A total of 13 significantly differential metabolites between HFD and HFD+SFF groups were shown in

Figure 5.1b. SFF effectively increased the content of sphingosine, 3-dehydrosphinganine, tauroursodeoxycholic acid, 1,2-dioleoyl PC, l-proline and 7-dehydrocholesterol; while decreased the content of spermidine, l-lysine, l-valine and l-ornithine in the intestine compared with the HFD group. Collectively, SFF alleviates the metabolic disorders in DIO mice and reshapes intestinal metabolites.

Table 5.2. SFF alleviates metabolic disorders caused by high-fat diet

| Parameters | | NCD | HFD | HFD+SFF |
|-----------------|---------------------------|-------------------------------|---------------|--------------|
| Body | Weight (g) | 39.4±2.50 | 59.8±6.41*** | 49.5±4.57* |
| | Weight gain (g) | 0.89±0.536 | 4.00±0.516*** | 1.38±0.563 |
| | BMI | 5.74±0.285 | 7.816±0.277* | 6.71±0.285 |
| | Food intake (g/day) | 4.32±0.174 | 3.75±0.164 | 4.24±0.174 |
| | Water consumption(mL/day) | 8.33±0.760 | 10.82±0.620* | 8.95±0.743 |
| | GTT AUC | 775±60.6 | 1086±61.4* | 882±62.6 |
| | ITT AUC | 403±32.9 | 574±31.4* | 453±34.0 |
| | Serum | Fasting blood glucose(mmol/L) | 4.50±0.375 | 7.24±0.843** |
| Insulin (mIU/L) | | 5.82±1.014 | 8.35±1.533** | 6.44±1.909 |
| HOMA-IR | | 1.18±0.251 | 2.37±0.241** | 1.66±0.258 |
| TC(mmol/L) | | 3.97±0.76 | 10.29±1.24*** | 8.49±1.15** |
| TG (mmol/L) | | 2.141±0.20 | 2.743±0.34* | 1.76±0.43** |
| FFA (mmol/L) | | 1.828±0.221 | 2.518±0.242** | 2.05±0.341 |
| HDL-c (mmol/L) | | 0.31±0.067 | 0.271±0.043 | 0.273±0.073 |
| LDL-c (mmol/L) | | 1.44±0.38 | 3.532±0.44** | 2.835±0.50* |
| Liver | Weight (g) | 2.13±0.218 | 2.92±0.361* | 2.5±0.351 |
| | Organ index | 5.14±0.271 | 5.54±0.245 | 4.88±0.572 |
| | TC(mmol/L/gprot) | 0.085±0.038 | 0.123±0.001* | 0.094±0.028 |
| | TG(mmol/L/gprot) | 0.090±0.013 | 0.141±0.012* | 0.094±0.013 |
| | ALT (U/L) | 50.0±4.45 | 71.71±4.30** | 56.87±4.45 |
| | AST (U/L) | 35.6±3.22 | 51.5±3.06*** | 37.8±3.33 |
| | ACP (U/100ml) | 0.566±0.065 | 0.813±0.061* | 0.545±0.063 |
| | AKP (U/100ml) | 0.827±0.092 | 1.211±0.089* | 0.885±0.092 |
| WAT | Weight (g) | 0.42±0.053 | 1.67±0.232*** | 1.12±0.42** |
| | Organ index | 0.67±0.127 | 3.39±0.262*** | 2.24±0.238** |
| Kidney | Weight (g) | 0.36±0.034 | 0.42±0.036 | 0.37±0.043 |
| | Organ index | 1.76±0.127 | 1.50±0.097 | 1.41±0.123 |
| Pancreas | Weight (g) | 0.193±0.032 | 0.224±0.035 | 0.185±0.043 |
| | Organ index | 0.049±0.006 | 0.041±0.008 | 0.041±0.011 |

Data are expressed as means ± SEM (n = 10).

* Indicates significantly different from the NCD group at the * $P < 0.05$, ** $P < 0.01$ and *** $P < 0.001$ level.

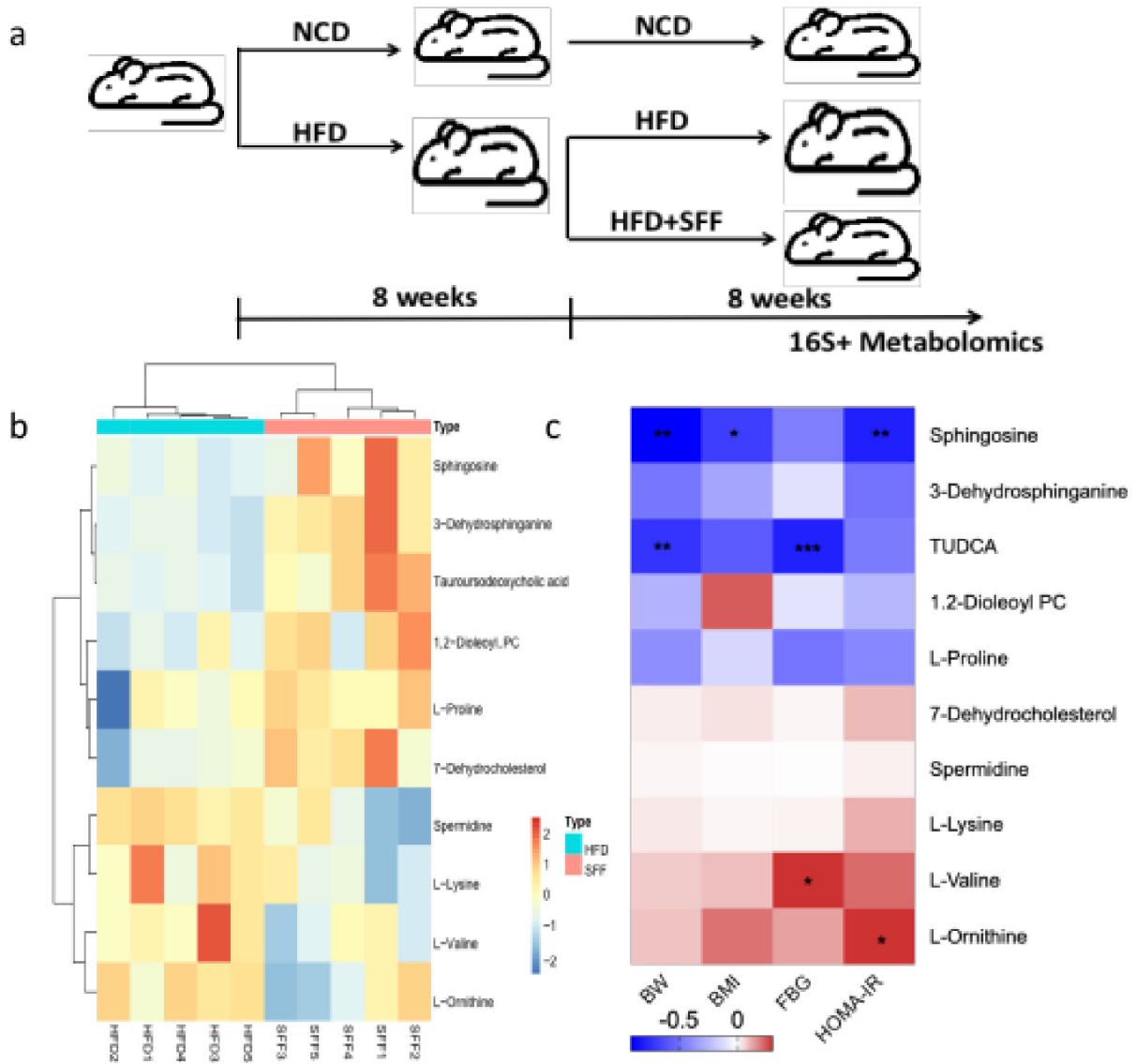


Figure 5.1. Intestinal metabolites and metabolite clustering heat map in the mode of HFD and HFD+SFF. Schematic of HFD-induced insulin resistance mice experiment (a). Metabolite clustering heat map (b) and plot of correlation coefficients between differential metabolites and metabolic disorder parameters (c).

In order to verify whether differential metabolites are closely associated with insulin resistance (IR) and obesity, linear profiles of differential metabolites in the mice intestine were plotted against parameters related to metabolic disorders. Body weight, BMI, FBG, and HOMA-IR were selected for linear analysis with differential metabolites. Sphingosine was

negatively correlated with body weight and HOMA-IR, with correlation coefficients of 0.7953 and 0.7989, respectively. Similarly, TUDCA was negatively correlated with body weight and fasting glucose, with correlation coefficients of 0.7292 and 0.9126 respectively (**Figure 5.3c**). These data suggest that SFF alleviates insulin resistance and metabolic disturbances in which bile acid TUDCA and sphingolipid metabolism may play an important role.

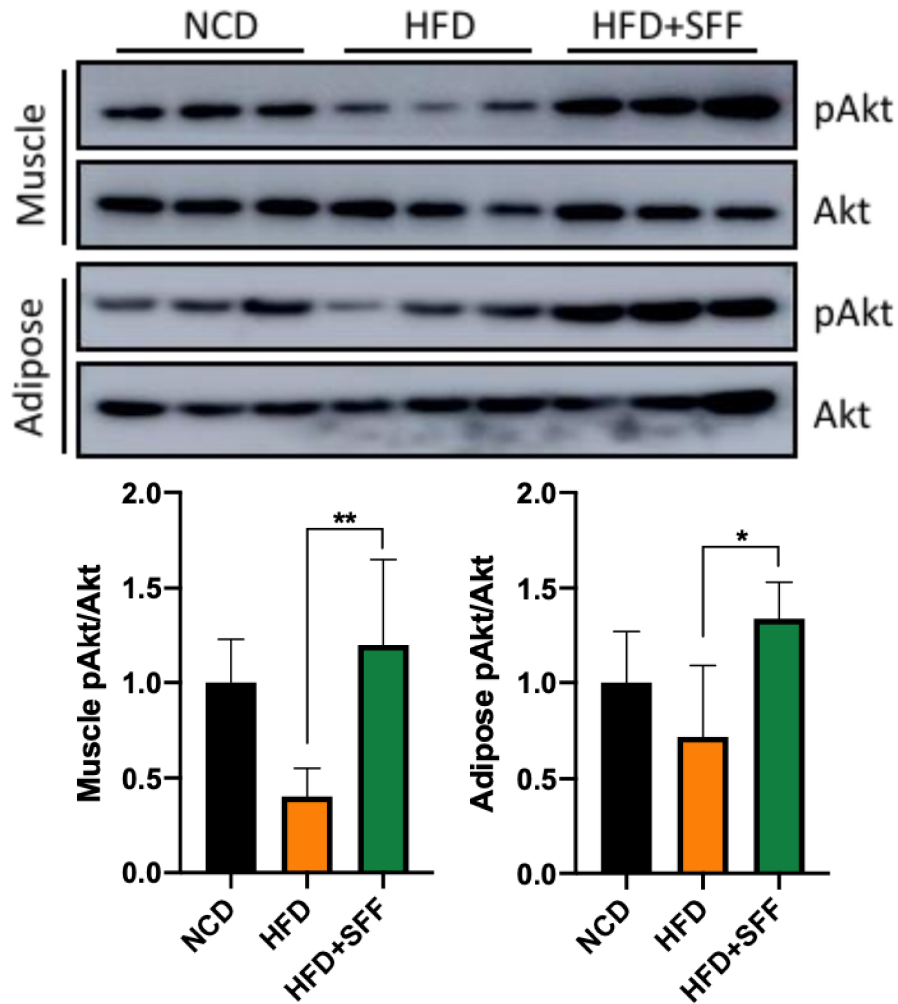


Figure 5.2. SFF alleviates the inhibition of insulin signaling in peripheral tissues by a high-fat diet. Western blot of Akt and phosphorylated Akt in muscle and adipose tissue; quantitative analysis for the densitometry in protein level was performed using ImageJ software. Data are expressed as mean \pm SD. * $P < 0.05$, ** $P < 0.01$ and *** $P < 0.001$.

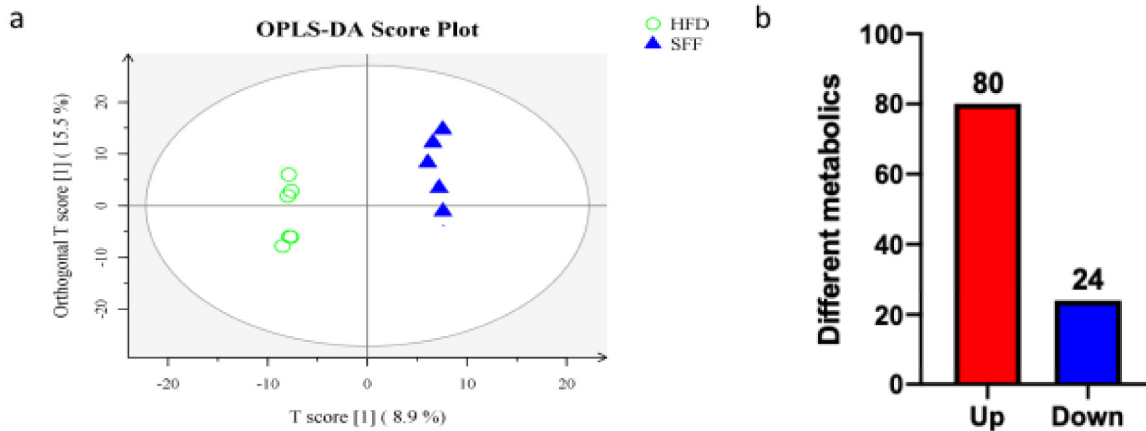
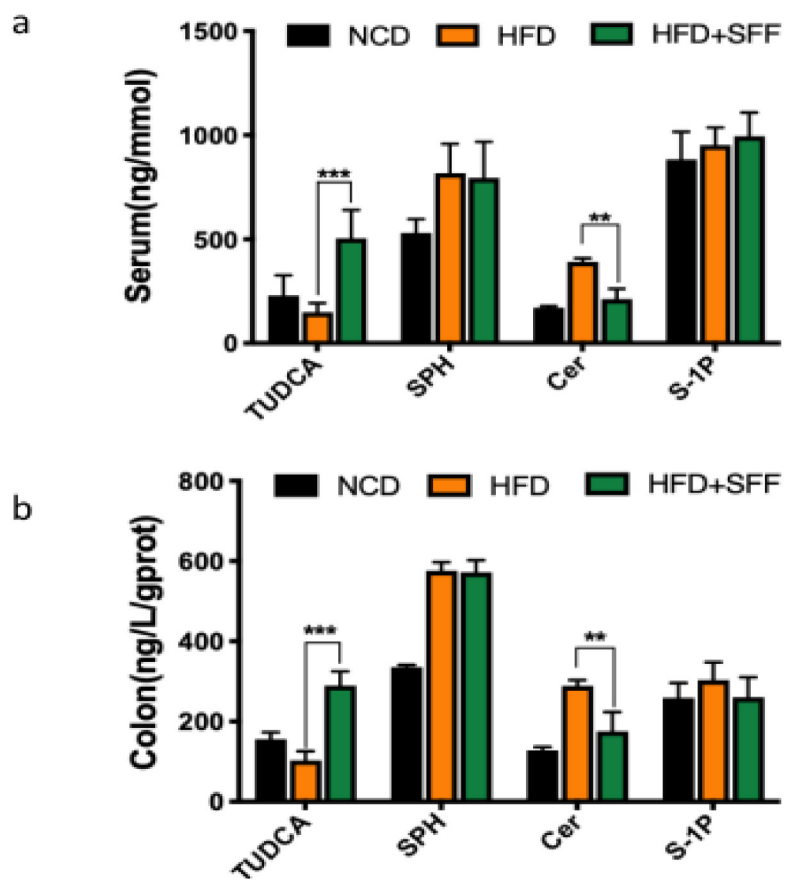


Figure 5.3. OPLS-DA score plot of the HFD and HFD+Met groups. (a) In the OPLS-DA score plot, each data point represents one mouse sample, and the distance between points in the plot indicates the similarity between samples. The number of up/down regulated metabolites (b).

5.3.2 SFF inhibits the biosynthesis of intestine-derived ceramides.



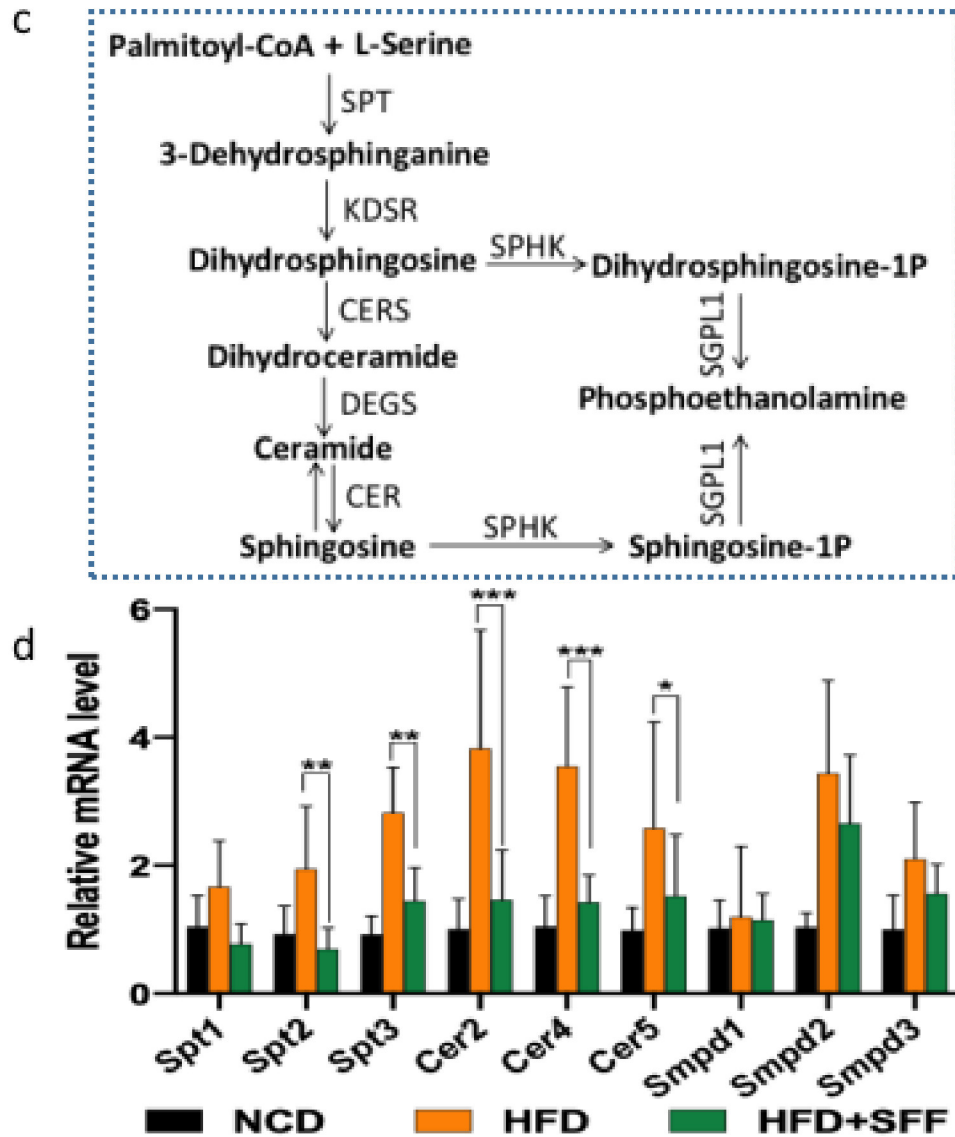


Figure 5.4. SFF inhibits the biosynthesis of intestine-derived ceramides. The levels of TUDCA, sphingosine, ceramide and S1P in serum (a) and colon (b) were determined by HPLC and ELISA. Sphingolipids de novo synthesis pathway (c). The relative mRNA levels of ceramide synthesis and degradation enzymes (*Spt1*, *Spt2*, *Spt3*, *Cer2*, *Cer4*, *Cer5*, *Smpd1*, *Smpd2*, *Smpd3*) were determined by qPCR (d). SPT (serine palmitoyltransferase), KDSR (3-keto-dihydroshinganine reductase), CERS (ceramide synthase), DEGS (desaturase), SPHK (sphingosine kinase), SGPL1 (Sphingosine-1-phosphate lyase 1), SMPD (Sphingomyelin phosphodiesterase). Data are expressed as mean \pm SD. * $P < 0.05$, ** $P < 0.01$ and *** $P < 0.001$.

IR is an important pathological feature of the metabolic syndrome, in which sphingolipid metabolism plays an important role in the development and progression of insulin resistance. It is hypothesized that the inhibition of intestinal-derived ceramide biosynthesis by TUDCA is one of the key biological mechanisms by which fucoidan alleviates insulin resistance. To further analyze whether the changes in the serum and colon metabolites were consistent with the intestinal contents, TUDCA, sphingosine and its derivatives ceramide and Sphingosine-1-phosphate (S1P) were measured by HPLC or ELISA assay. As shown in **Figure 5.4a and b**, TUDCA varied consistently in the intestine, serum and colon, and all showed an increasing trend after SFF treatment. *in vivo*, sphingosine is a prerequisite for ceramide synthesis, and it was found that serum and colon ceramide levels were significantly elevated in HFD diet mice, while SFF treatment mitigating the increase. Suppressed ceramide biosynthesis promotes insulin signaling and facilitates the alleviation of insulin resistance. Next, we analyzed key gene expressions involved in ceramide synthesis and degradation (**Figure 5.4c**) and studied the changes of the ceramide metabolism pathway under SFF intervention. mRNA expressions of enzymes involved in ceramide synthesis were significantly suppressed by SFF supplementation in HFD-fed mice, characterized by a significantly reduced level of *Spt1*, *Spt2*, *Spt3*, *Cer2* and *Cer4* compared to HFD group (**Figure 5.4d**). Inhibited conversion of sphingosine to ceramide was supposed to be the predominant way for SFF in ceramide accumulation, revealed by the significantly lower expression of the *CerS* gene compared to HFD group. Furthermore, in a linear analysis of ceramide and metabolic disorder parameters, it was found that fasting blood glucose and HOMA-IR increased with ceramide in the body under a high-fat diet (**Figure 5.5**). We speculated the suppressed ceramide synthesis predominantly contributed to the reversed insulin resistance status under the management of SFF.

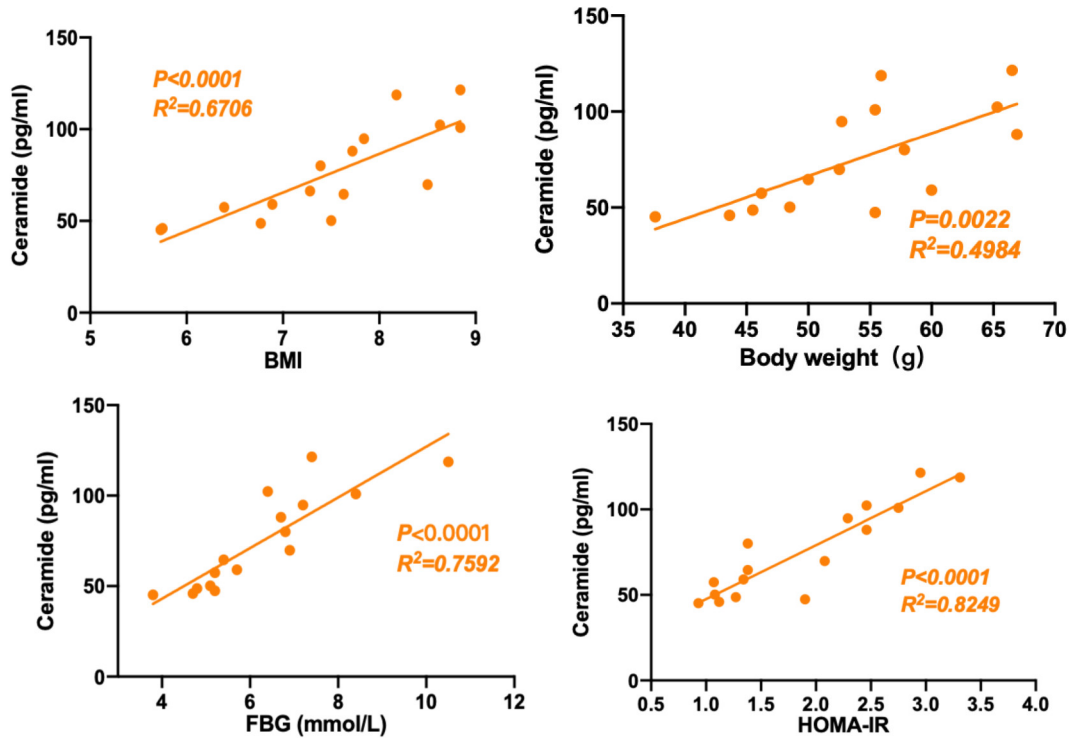


Figure 5.5. ceramide positively correlated with metabolic disorders in high-fat diet. Linear relationship between body weight, BMI, fasting glucose and HOMA-IR and ceramide.

5.3.3 TUDCA reduces ceramide biosynthesis by inhibiting the FXR signaling pathway.

Intestine-specific FXR inhibitor had an inhibitory effect on lipid absorption from the HFD. In contrast to the primary bile acids, CDCA is the most effective agonist for FXR, while conjugated bile acids, such as T α MCA, T β MCA and GUDCA, are antagonists of FXR. Caco2 cells were used to mimic the intestinal epithelial state to verify the inhibitory effect of TUDCA on FXR activation and ceramide synthesis. Cells were pretreated with CDCA to activate the FXR signaling pathway, on the basis of which it was found that the presence of SPH provided the substrate for ceramide synthesis and ceramide levels were significantly elevated; however, ceramide biosynthesis was inhibited when TUDCA was present (**Figure 5.6a and b**). Similarly, TUDCA significantly inhibited the activation of FXR signaling and reduced the expression of downstream genes *Shp* and *Fgf19* at transcript levels (**Figure 5.6c**). In addition, the expression

of genes involved in ceramide biosynthesis enzymes was also inhibited by TUDCA (**Figure 5.6d**). Linerixibat (GSK2330672) is a potent, non-absorbable and orally active inhibitor of apical sodium-dependent bile acid transporter (ASBT) that effectively reduces TUDCA uptake by Caco2 cells. Sphingosine and ceramide levels were elevated in cells pretreated with linerixibat, and the expression of *Shp* and *Fgf19* as well as *Spts* and *CerS* was increased (**Figure 5.7a-d**). Those data showed that linerixibat inhibited TUDCA uptake, prevented TUDCA from inhibiting the FXR signaling pathway and increased ceramide biosynthesis.

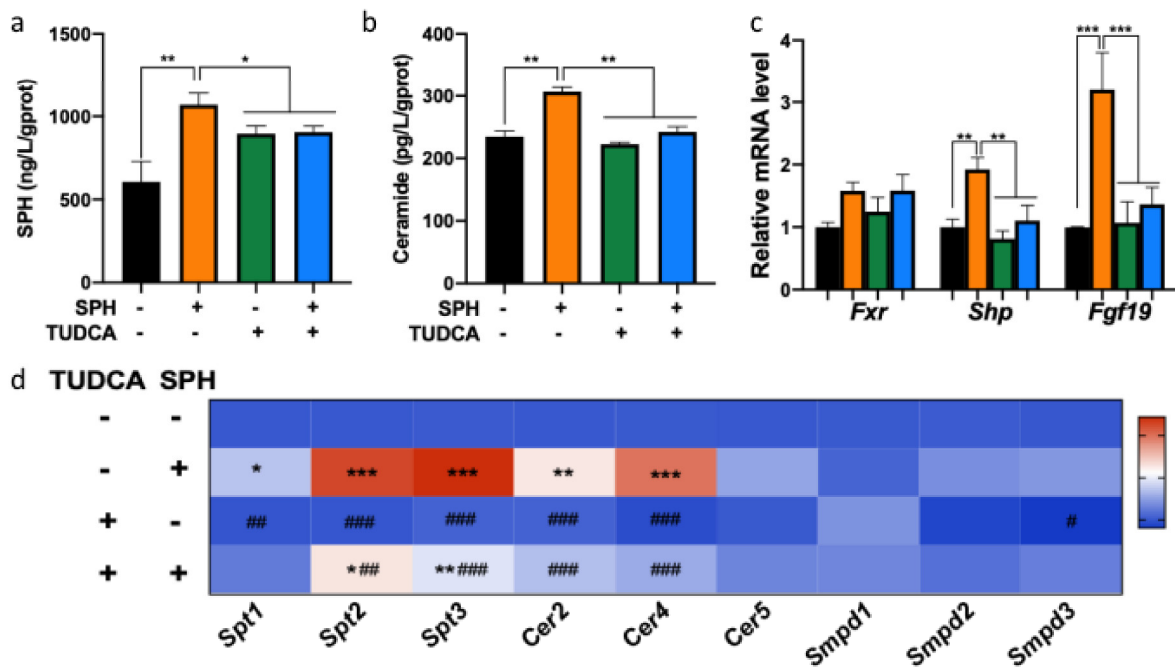


Figure 5.6 TUDCA reduces ceramide biosynthesis by inhibiting the FXR signaling pathway. After pretreatment with 100uM CDCA for 6h, Caco2 cells were treated with 50uM TUDCA for 12h. sphingosine (a) and ceramide (b) were measured in cells by ELISA. The relative mRNA levels of FXR signaling (c , *Fxr*, *Shp*, *Fgf19*) ceramide synthesis enzymes (d, *Spt1*, *Spt2*, *Spt3*, *Cer2*, *Cer4*, *Cer5*, *Smpd1*, *Smpd2*, *Smpd3*) were determined by qPCR. Data are expressed as mean \pm SD. * $P < 0.05$, ** $P < 0.01$ and *** $P < 0.001$.

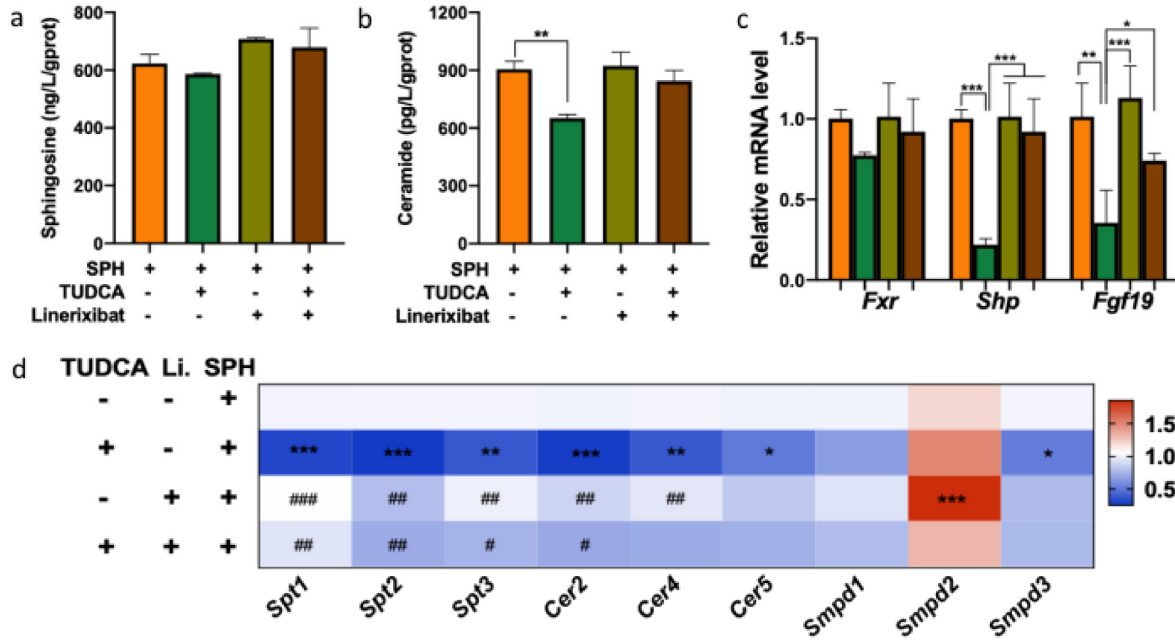
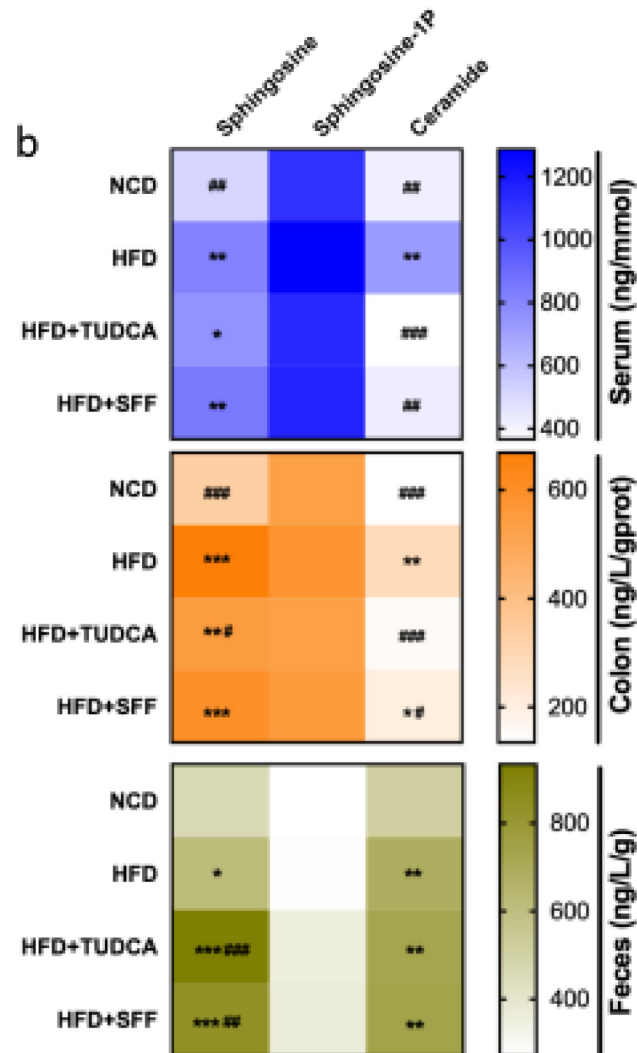
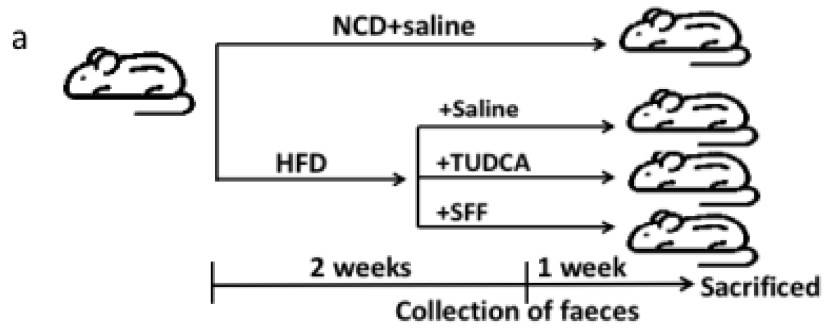


Figure 5.7 Linerixibat induces failure of the inhibitory effect of TUDCA on FXR. After pretreatment with 100 μ M CDCA for 6 h, Caco2 cells were treated with 50 μ M TUDCA and 50 nM Linerixibat for 12 h. The levels of sphingosine (a) and ceramide (b) in the cells were determined by ELISA. The relative mRNA levels of FXR signaling (c, *Fxr*, *Shp*, *Fgf19*) ceramide synthesis enzymes (d, *Spt1*, *Spt2*, *Spt3*, *Cer2*, *Cer4*, *Cer5*, *Smpd1*, *Smpd2*, *Smpd3*) were determined by qPCR. Data are expressed as mean \pm SD. * P < 0.05, ** P < 0.01 and *** P < 0.001.

To verify that SFF and TUDCA can inhibit the intestinal FXR signaling pathway, short-term *in vivo* experiments were designed (**Figure 5.8a**). It was found that sphingosine originates from intestinal absorption under high-fat feeding, while overloaded sphingosine and ceramide are excreted in the faeces (**Figure 5.8b**). Both TUDCA and SFF significantly reduced serum and intracolonic ceramide levels under a high-fat diet. Similarly, TUDCA and SFF can effectively inhibit the FXR signalling pathway (**Figure 5.8c**) and reduce the expression of ceramide biosynthesis-related enzymes (**Figure 5.8d**). These data suggest that SFF causes upregulation of TUDCA in the intestine and that TUDCA is taken up by intestinal epithelial cells to inhibit the FXR signaling pathway in order to reduce the biosynthesis of intestine-derived ceramide.



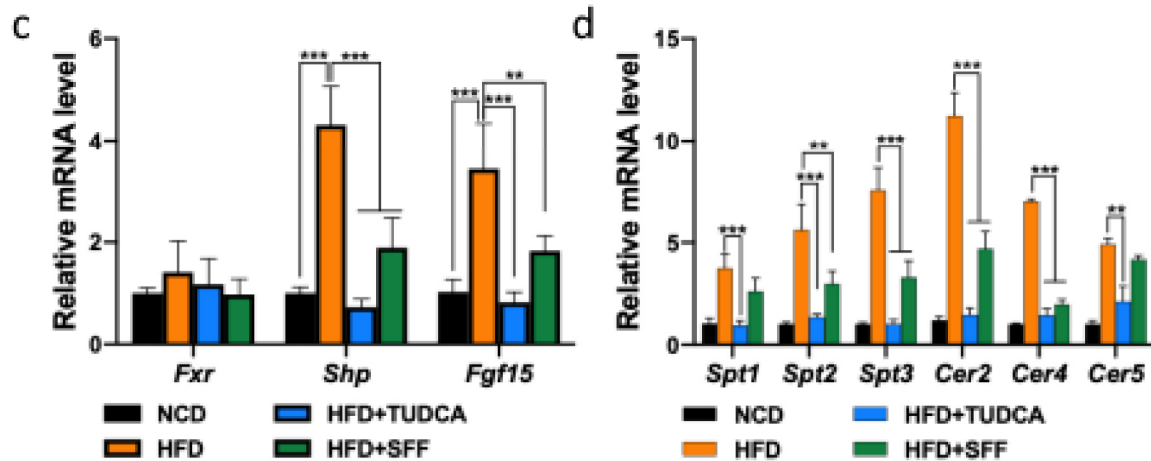
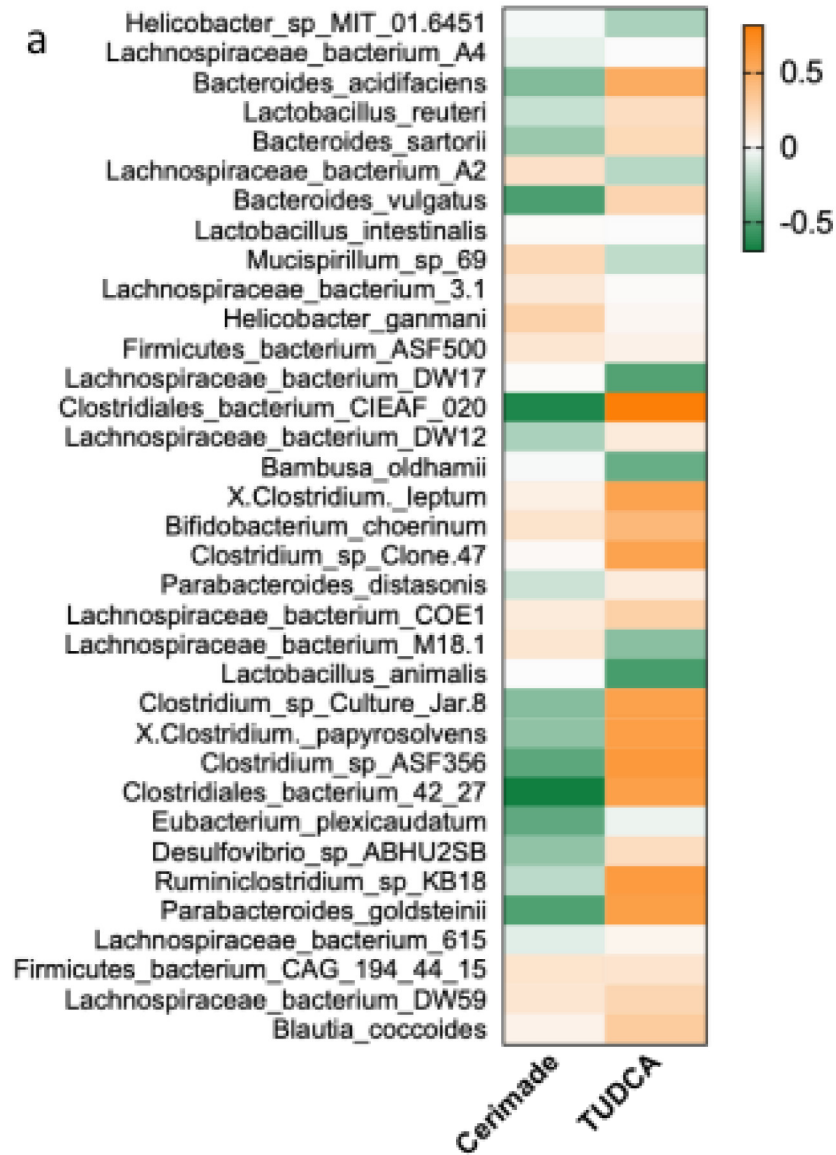


Figure. 5.8 SFF reduces intestinal-derived ceramide biosynthesis. Schematic of short-term SFF or TUDCA-treated mice experiment (a). The levels of sphingosine, ceramide and S1P in serum, colon and feces were determined by ELISA (b). The relative mRNA levels of FXR signaling (c, *Fxr*, *Shp*, *Fgf15*) ceramide synthesis enzymes (d, *Spt1*, *Spt2*, *Spt3*, *Cer2*, *Cer4*, *Cer5*) were determined by qPCR. Data are expressed as mean \pm SD. * $P < 0.05$, ** $P < 0.01$ and *** $P < 0.001$.

5.3.4 Gut microbiota is a key target for SFF to alleviated insulin resistance.

In our previous studies^{29,30}, we have found that SFF can reduce intestinal inflammation by reshaping the structure of gut microbiota. At the same time, gut microbiota can influence the composition of BA pool by producing a variety of enzymes related to bile acid metabolism, such as bile salt hydrolase and 7 α dehydroxylase. Heat maps drawn by sperman analysis found ceramide and TUDCA to be closely related to a variety of gut microbiota. As shown in **Figure 5.9**, ceramide was positively correlated with *Helicobacter*, *Lactobacillus*, *Bifidobacterium* and *Lachnospiraceae*, while ceramide was negatively correlated with *Bacillus*, *Eubacterium*, *Parabacter* and *Clostridium*. Conversely, TUDCA was positively correlated with *Bacteroides*, *Clostridium*, *Ruminiclostridium* and *Parabacteroides*, and TUDCA was negatively correlated with *Helicobacter*, *Lachnospiraceae* and *Bambusa*. Notably, several strains of *Lachnospiraceae* and *Clostridium* were associated with ceramide and TUDCA, and that the proportions of

Lachnospiraceae and Clostridium in the gut microbiota are clearly reversed. These data suggest that SFF is likely to up-regulated TUDCA levels *in vivo* by remodeling the gut microbiota Lachnospiraceae and Clostridium.



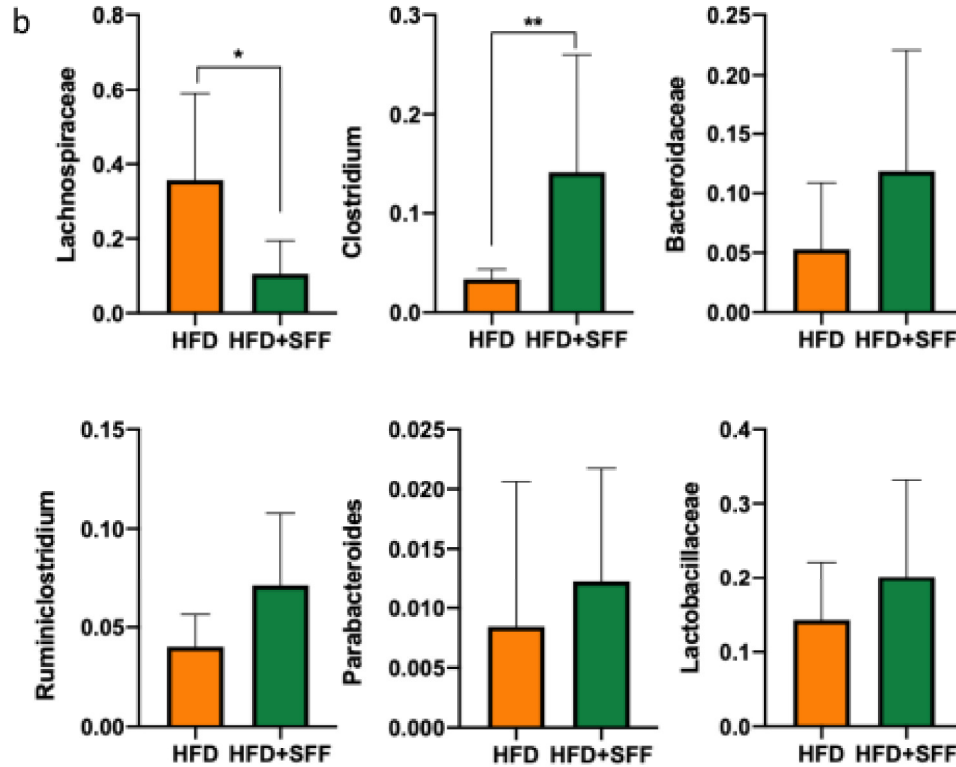
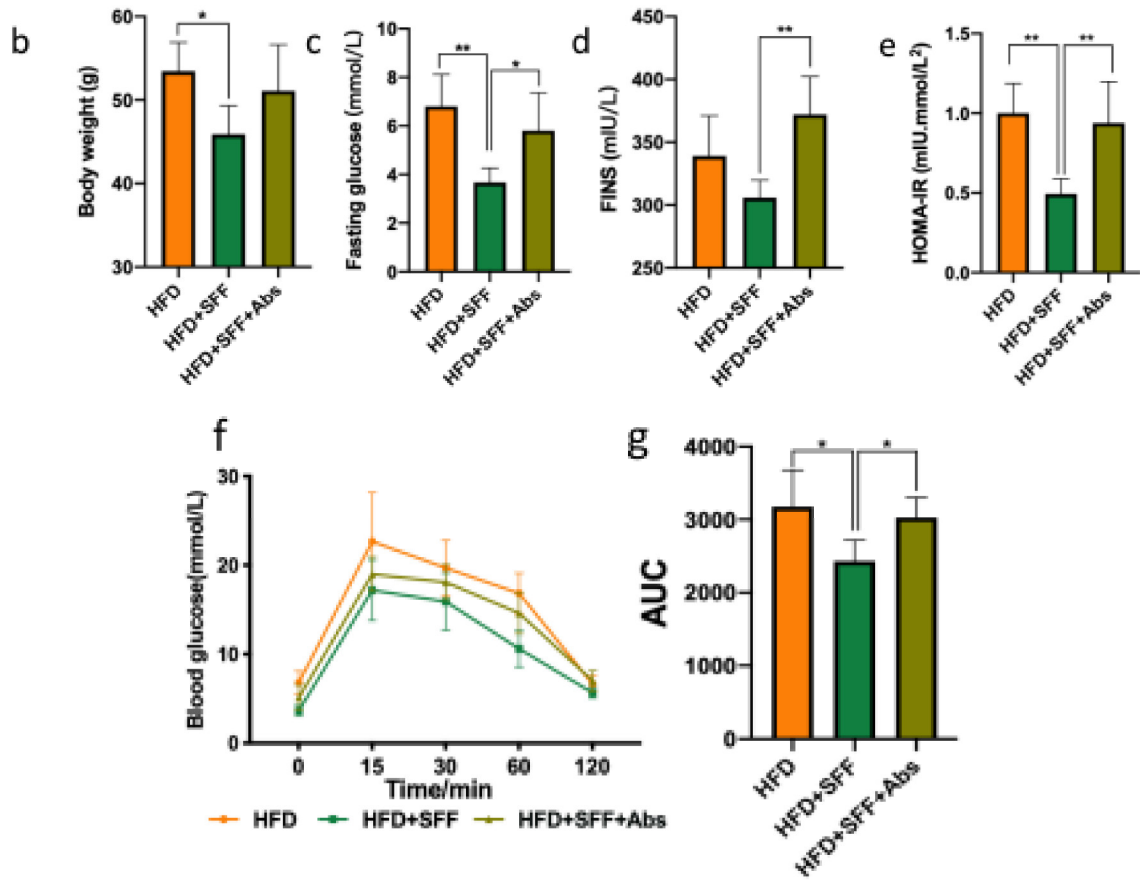
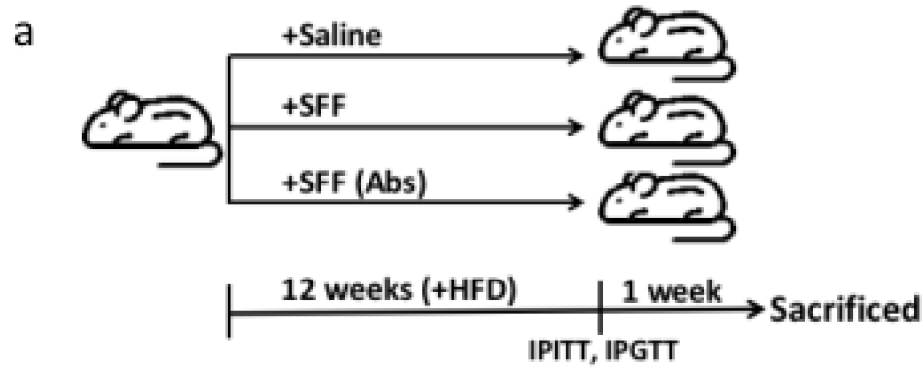


Figure 5.9. A correlation between gut microbiota and TUDCA and ceramide. Heatmap of Spearman's correlation between the gut microbiota and TUDCA/ceramide (a). Good's coverage and the specie with significant correlations are shown. The colors range from green (negative correlation) to orange (positive correlation). The relative abundance of gut microbiota between HFD and HFD+SFF (b).

Construction of pseudo-germfree mice using mixture antibiotics to verify that gut microbiota plays a key role in the alleviation of insulin resistance by SFF. The experimental procedure is shown in **Figure 5.10a**. After 12 weeks, HFD+SFF+Abs group were found to have a significant increase in fasting glucose, insulin and HOMA-IR induced by the high-fat diet compared to the HFD+SFF group (**Figure 5.10b-e**). Also, SFF was unable to reduce the triglycerides and cholesterol both in serum and liver in pseudo-germfree DIO mice (**Figure 5.11**). The amelioration of glucose metabolism and insulin sensitivity by SFF was almost abolished in pseudo-germfree DIO mice, evidenced by GTT and ITT. The fasting blood

glucose and AUC in the HFD+SFF+Abs group were significantly higher than those in the HFD+SFF group but slightly lower than those in the HFD group during the 15-60 min of glucose injection (**Figure 5.10f and g**). After the intraperitoneal injection of 0.75 U/kg insulin, the blood glucose in the HFD+SFF+Abs group was found to be significantly higher and slightly higher than that in the HFD+SFF group at the 15th and 30th min; at the 60th and 120th min, although the blood glucose in the HFD+SFF+Abs group was lower than that in the HFD group, it was still higher than that in the HFD+SFF group (**Figure 5.10h and i**).



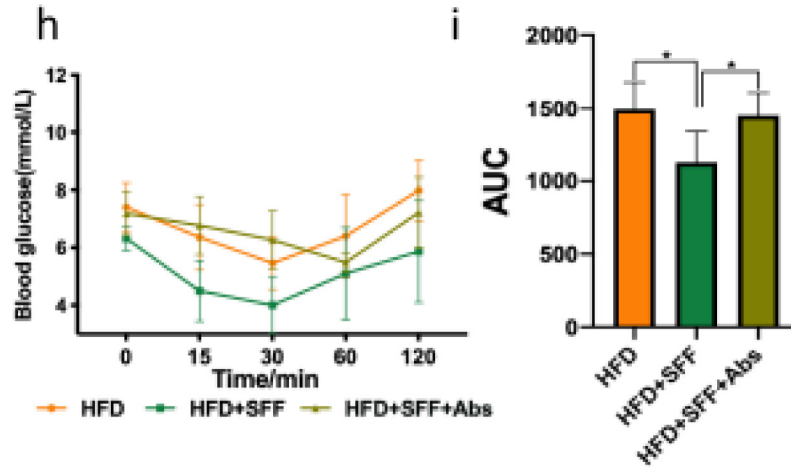


Figure 5.10. Gut microbiota is a key target for SFF to alleviated insulin resistance. Schematic of the pseudo-sterile mice experiment (a). Boy weight (b). Serum was prepared to assess FBG (c), FINS (d), and HOMA-IR (e). IPGTT (f); AUC of IPGTT (g); IPITT (h); AUC of IPITT (i) were measured at the 16th week of the experimental period. Data are expressed as mean \pm SD. Data are expressed as mean \pm SD.

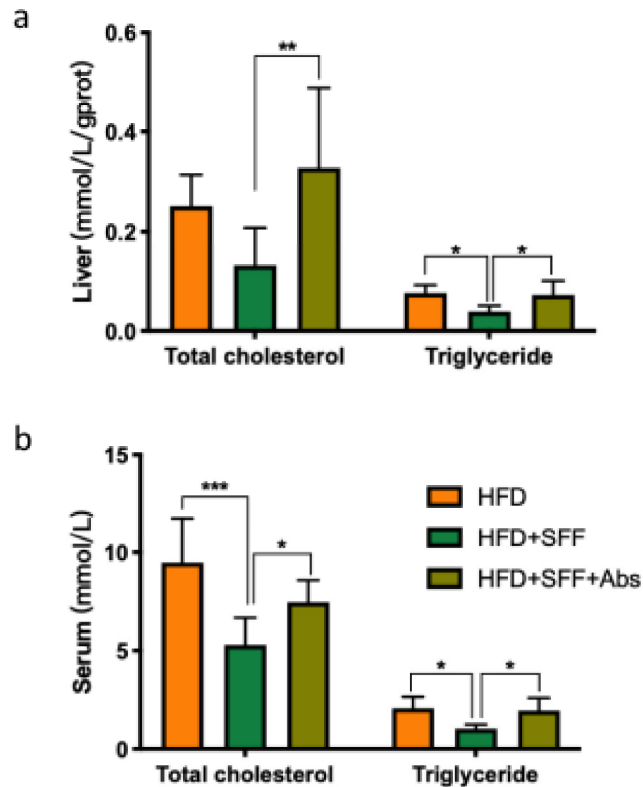
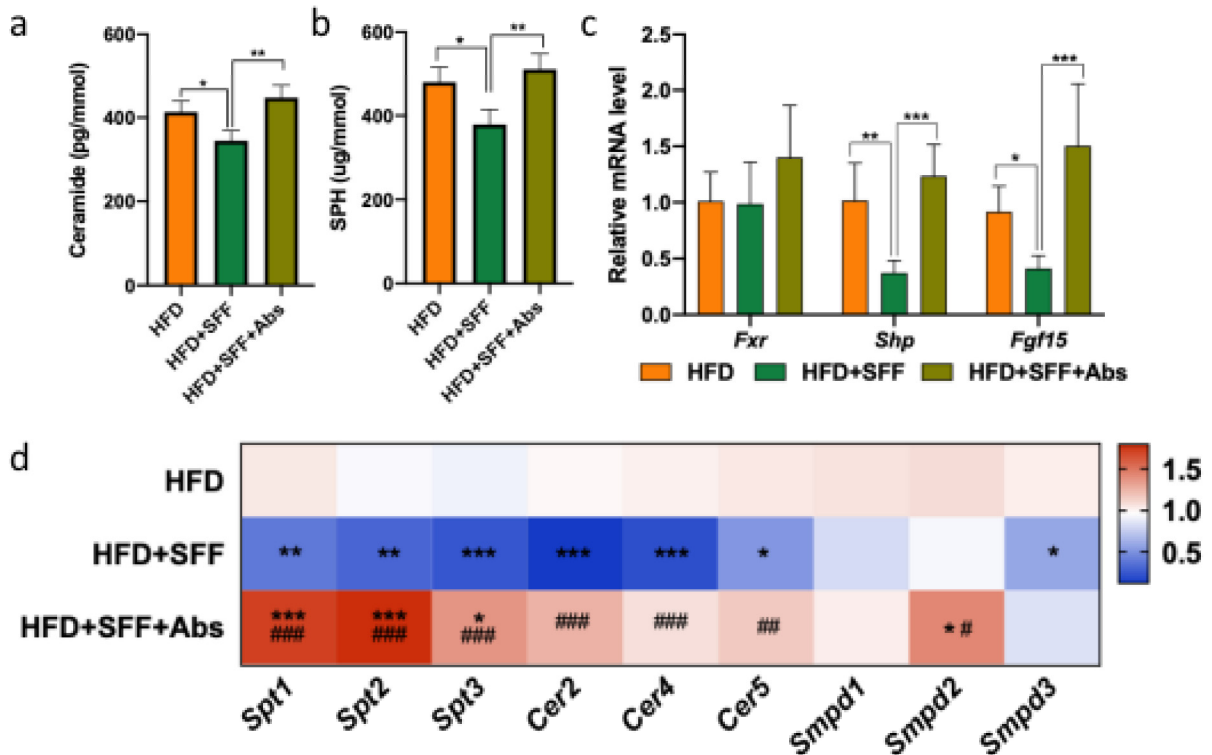


Figure 5.11. In a pseudo-sterile mice model, the effect of SFF in alleviating hyperlipidaemia disappeared. Total-CHO and TG in serum (a) and liver (b) are shown. Data are represented as mean \pm SD. Statistical significance considered as *P < 0.05, **P < 0.01 and ***P < 0.001.

In addition, the HFD+SFF+Abs group of mice failed to effectively reduce ceramide levels in the colon and serum (Figure 5.12a and b). In the absence of gut microbiota, gene expression of FXR signaling downstream of *Shp* and *Fgf15* and ceramide biosynthesis-related enzymes *Spt1*, *Spt2*, *Spt3*, *Cer2*, and *Cer4* was elevated in the colon and the inhibitory effect of SFF was almost negligible (Figure 5.12c and d). Phosphorylated Akt expression was not significantly elevated in muscle and adipose tissue of mice in the HFD+SFF+Abs group, suggesting that the effect of SFF in reducing the inhibition of insulin signalling by a high-fat diet was lost (Figure 5.12e). These data suggest that SFF alleviates insulin resistance by upregulating TUDCA to inhibit the FXR signaling pathway and ceramide synthesis, and that gut microbiota plays a key role in this process.



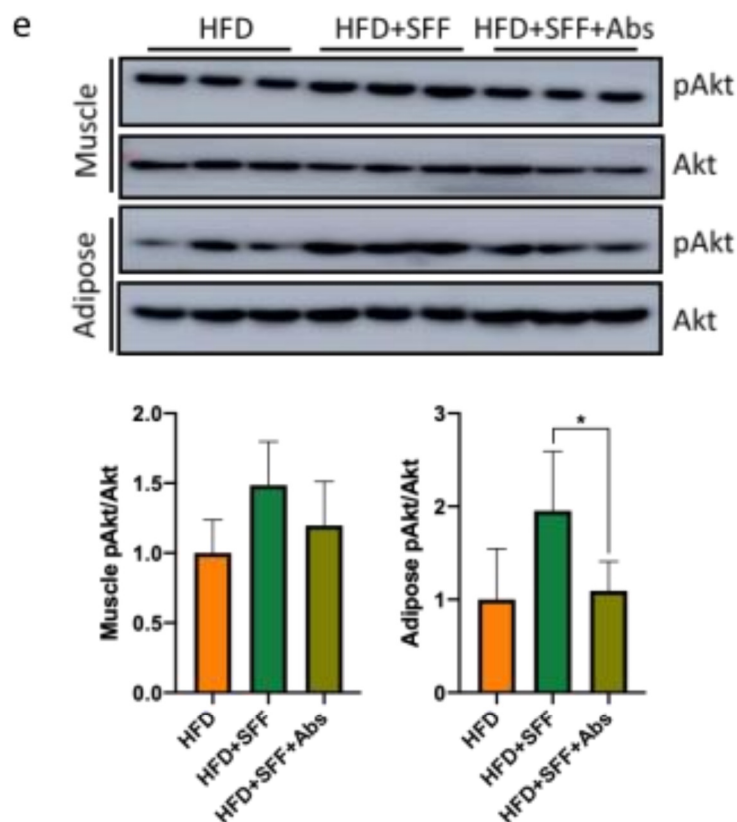


Figure 5.12 In a pseudo-sterile mice model, SFF was unable to inhibit ceramide synthesis and insulin resistance. Sphingosine (a) and ceramide (b) were measured in serum by ELISA. the relative mRNA levels of FXR signaling (c , *Fxr*, *Shp*, *Fgf15*) ceramide synthesis enzymes (d, *Spt1*, *Spt2*, *Spt3*, *Cer2*, *Cer4*, *Cer5*, *Smpd1*, *Smpd2*, *Smpd3*) were determined by qPCR. Western blot of Akt and phosphorylated Akt in muscle and adipose tissue; quantitative analysis for the densitometry in protein level was performed using ImageJ software (e). Data are expressed as mean \pm SD. * $P < 0.05$, ** $P < 0.01$ and *** $P < 0.001$.

5.4. Discussion

Insulin resistance (IR) implicated in type 2 diabetes (T2D) has become an epidemic health issue worldwide. The consequence of IR is the restriction of glucose transport into the adipose tissue, liver or skeletal muscle, causing metabolic syndromes, such as hyperinsulinemia, obesity and diabetes²²⁶⁻²²⁸. As the mostly studied sulfated glycans from brown algal, there is accumulating evidence that the intake of fucoidan is associated with improved glucose

homeostasis and insulin sensitivity in humans and animals^{256,257}. Heeba *et al*²⁵⁸. reported that fucoidan can ameliorate the development of HFD-induced NAFLD, an effect that could be related to its hypolipidemic, insulin sensitizing, antioxidant and anti-inflammatory capacity. Another example is the work reported by Shang *et al*²⁵⁹., which showed that fucoidans from *Laminaria japonica* and *Ascophyllum nodosum* can profoundly attenuate body weight gain, improve glucose homeostasis, and reduce chronic low-grade inflammation in diabetic mice. In recent years, gut microbiota has also emerged as one of the key mechanisms to explain the alleviation of insulin resistance by fucoidan. A polysaccharide extracted from *Hirsutella sinensis* is thought to selectively promote the growth of *Parabacteroides goldsteinii*, which enhanced gut integrity, reduced intestinal and systemic inflammation and improved insulin sensitivity and lipid metabolism²⁶⁰. Rimbach *et al*²⁶¹. suggest that fucoidan extracted from *Saccorhiza* balances intestinal bile acid metabolism by reshaping gut microbiota to activate the intestinal hormone GLP-1 and increase systemic insulin sensitivity. Consistent with previous studies, our results suggest that SFF treatment improves insulin resistance in high-fat diet-induced obese mice by reducing body weight and fasting glucose and increasing insulin sensitivity. Furthermore, we found that the gut microbiota-BAs-intestinal FXR axis plays a crucial role in the beneficial effects of fucoidan on glucose homeostasis. TUDCA, an FXR antagonist, may alleviate insulin resistance by inhibiting the intestinal FXR signaling pathway, leading to a reduction in intestine-derived ceramide biosynthesis. In summary, our study clarifies the mechanism by which SFF modulates the gut microbiota-BAs-intestinal FXR axis to improve glucose homeostasis in IR mice, which may be a potential therapeutic strategy for metabolic syndromes.

The "dialogue" between the gut microbiota and the organism mainly depends on microbial metabolites²³⁵. By producing various enzymes for biochemical metabolic pathways of the

intestinal microbes, gut microbiota can perform diverse metabolic activities such as the metabolism of amino acids, carbohydrates and BAs, as well as the formation of a co-metabolic relationship with the host. Modification of bile acids by gut microbiota are essential in the regulation of glucolipid metabolism and energy balance²⁶². Metabolomic data showed a significant increase in TUDCA in the intestine of the HFD+SFF group (**Figure 5.1**). Previous studies^{263,264} have shown that the reserve of TUDCA in the gut involves two main pathways: first, conjugated bile acids degradation, a process whereby bile salt hydrolases (BSH) secreted by intestinal bacteria such as Bifidobacterium and Lactobacillus convert conjugated bile acid (TUDCA) to non-conjugated bile acid (UDCA) and taurine (or glycine), which in turn change the composition of the bile acid pool and play an important role in host lipid metabolism and energy harvesting. Second, conjugated bile acids are interconverted, for example, TCDCA can be converted to TUDCA by $7\alpha/\beta$ -hydroxysteroid dehydrogenase ($7\alpha/\beta$ -HSDH), and $7\alpha/\beta$ -HSDH-producing bacteria include Eubacterium and Clostridium^{265,266}. Spearman correlation analysis showed that upregulation of TUDCA was positively correlated with the abundance of multiple Clostridium and negatively correlated with the abundance of multiple Lactobacilli bacteria (**Figure 5.9A**). It is hypothesized that the remodeling of gut microbiota Clostridium and Lachnospiraceae bacteria abundance by SFF influenced the amount and activity of BSH and $7\alpha/\beta$ -HSDH, which in turn increased TUDCA both in the intestine and serum. Similarly, Liu *et al*²⁶⁷ found that polysaccharide extracted from *Citrus aurantium L.* could balance bile acids pool and increase the levels of TUDCA and GUDCA to inhibit FXR signaling. Extracts from *Saccharhiza polyschides* also improve systemic glucose metabolism and promote insulin sensitivity by altering intestinal bile acid homeostasis, and this mechanism is closely linked to gut microbiota²⁶⁴.

BAs are natural ligand receptors and studies have shown that accumulation of conjugated bile acids inhibits the FXR signaling pathway²⁶²⁻²⁶⁴. In the present study, we found that CDCA as an agonist of FXR activates the FXR/SHP/FGF15 signaling pathway, which is inhibited when TUDCA exists. It is speculated that the ratio of agonist/antagonist ligands of FXR is altered, which is likely to affect intestinal FXR signaling. Thus, the inhibition of intestinal FXR/SHP/FGF15 signaling in mice is likely to occur as a result of alterations in the bile acid profile, and the role of conjugated bile acids, which make up a relatively small proportion of the bile acid profile, is likely to be underestimated. It was shown that FXR signaling in the gut is associated with glucose uptake, an effect that was abolished in FXR-deficient mice²³⁷, and that blocking FXR in the gut was found to reduce ceramide levels and inhibit hepatic gluconeogenesis by reducing hepatic mitochondrial acetyl-CoA and pyruvate carboxylase activity^{268,269}. These results suggest that treatment with FXR antagonists may improve glucose tolerance, insulin sensitivity and fatty liver disease partly by reducing intestinal and total ceramide levels. Thus, modifying bile acid TUDCA metabolism by remodeling gut microbiota to regulate BSH and 7 α / β -HSDH activity may be a promising therapeutic strategy for insulin resistance, T2DM and other metabolic syndromes.

Excess lipids may be delivered to nonadipose tissues that are not suited for fat storage (i.e., skeletal muscle and the liver), thus leading to the formation of specific metabolites that directly antagonize insulin action^{270,271}. The metabolic factors that induce insulin resistance almost invariably generate the sphingolipid ceramide, which is a ubiquitous regulator of cellular stress⁶. Moreover, studies in insulin-responsive cell types suggest that ceramide and/or its derivatives (e.g., ganglioside GM3 and sphingosine) antagonize insulin signaling, induce oxidative stress, and inhibit glucose uptake and storage, and thus may initiate many of the molecular defects that underlie insulin resistance^{272,273}. An exciting theory that emerges from

these observations is that the inhibition of ceramide synthesis could combat several underlying causes of insulin resistance and thus improve insulin sensitivity in tissues exposed to multiple different pathogenic factors associated with obesity^{271,272}. In the de novo pathway, ceramide synthesis begins with the condensation of serine and palmitoyl-CoA to produce 3-dehydrosphinganine under the catalysis of serine palmitoyltransferase (SPT, EC 2.3.1.50). 3-Dehydrosphinganine was then subject to a reduction process, followed by the catalysis of ceramide synthetase (CerS, EC 2.3.1.24). Ceramides finally formed via sphingolipid 4-desaturase (DEGS, EC 1.14.19.17) action on dihydroceramide²⁷³⁻²⁷⁵. The undesirable sphingolipid status triggered by a HFD was alleviated by SFF supplementation, which performed more efficiently in the inhibition of ceramides via suppressing ceramide de novo synthesis. This assertion is based on the downregulated expressions of genes encoding SPT (Spt1,2,3) and CerS (Cer2, Cer4, Cer5) (**Figure 5.3a-d**). Several ceramide species in plasma correlated with glucose tolerance and insulin secretion in mice, which were metabolically challenged by a high-fat and high-sucrose diet, including ceramides C18:0, C20:0, and C22:0^{274,276}. A HFD induced serum accumulation of ceramides, further inhibiting insulin receptor substrates and blocking the activation of Akt/PKB, respectively.

5.5. Summary

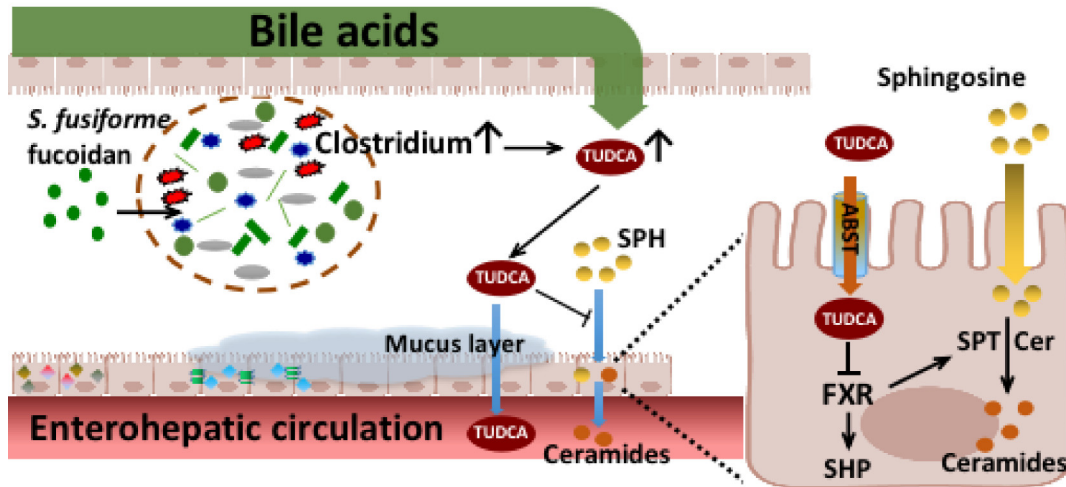


Figure 5.13. Mechanisms of ceramide biosynthesis reduction by fucoidan.

As shown in **Figure 5.13**, dietary supplementation with *S. fusiforme* fucoidan SFF prevented insulin resistance and lipid metabolic dysfunction. Remarkably, SFF remodeled the abundance of Clostridium and Lachnospiraceae and further enhanced the level of TUDCA in the colon. TUDCA acts as an antagonist of FXR to inhibit the biosynthesis of intestinal-derived ceramide, which contributes to the normalisation of insulin signaling. The findings proposed dietary therapeutic approaches for preventing or reducing hyperlipidemia and hyperinsulinism. While the explicit cellular and biochemical pathways for the inhibition of SFF on the biosynthesis of ceramides are still needed to clarify the pharmacological mechanisms involved in the alleviation of insulin resistance by SFF.

Chapter 6

SARGASSUM FUSIFORME FUCOIDAN IMPROVES INSULIN RESISTANCE BY INCREASING HEPATIC TUDCA ACTIVATION OF NRF2/ARE SIGNALING PATHWAY

Abstract

In recent years, fucoidan has received some intense interest as an agent for treating insulin resistance and other types of metabolic syndromes (MetS). In our preliminary data, we found that fucoidan could improve insulin resistance in obese mice fed a high-fat diet by altering the intestinal absorption of the metabolites sphingosine and TUDCA through remodeling of the flora. To elucidate this hypothesis, we investigated whether TUDCA could be used as a substitute for fucoidan to alleviate insulin resistance in ob/ob genetically deficient obese mice and pseudo-germfree mice. It was found that TUDCA reduced weight gain, hyperglycaemia, lipid accumulation and improved insulin sensitivity in ob/ob mice. In a HepG2 insulin resistance cell model, TUDCA was found to alleviate the insulin signaling pathway mediated through the Nrf2/ARE signaling pathway and TUDCA was further antagonized with KEAP1 to prevent Nrf2 from degradation and activate Nrf2/ARE pathway, thereby reducing intracellular ROS and improving insulin signaling. The increase in TUDCA was found to be positively correlated with *Clostridium* by sperman analysis, and These findings reveal that fucoidan remodels the gut microbiota, reduces oxidative stress and enhances This provides a novel mechanism by which fucoidan alleviates This provides a novel mechanism by which fucoidan alleviates diet-induced IR and improves metabolism.

Keywords: Fucoidan, insulin resistance, TUDCA, Nrf2/ARE, gut microbiota

6.1. Introduction

Sargassum fusiforme, an edible brown alga that belongs to the Sargassaceae family, is extensively distributed in eastern Asian countries, particularly China, Japan, and South Korea¹. *S. fusiforme* is a popular functional seaweed which can prolong life, also has been developed as a traditional Chinese medicine for thousands of years to treat patients with scrofula, oedema, indigestion, and stagnation of Qi^{2,3}. Polysaccharides, which account to 40 to 80% of dry defatted seaweed biomass, have been considered as one of the most important bioactive macromolecules in *S. fusiforme*⁴. Modern pharmacological studies have demonstrated that *S. fusiforme* polysaccharides possess multiple medicinally effects, such as anti-tumor, anti-hyperlipidemia, and immunomodulatory, and antioxidant activity⁵⁻⁷.

The polysaccharides in brown seaweeds mainly contain alginate, laminaran and fucoidan⁸. However, present studies on *S. fusiforme* polysaccharides reported the bio-activities using a mixture of polysaccharides without separating those compounds³. Recently, fucoidan has been extensively studied because of their diverse beneficial functions to human health^{106,107}. Fucoidan is a family of sulfated homo- and heteropolysaccharides, extensively distributed in the brown algae and several marine invertebrates^{106,108}. Fucoidan usually contains a high percentage of fucose and galactose residues, as well as variable levels of a range of other neutral and acidic monosaccharides, including mannose, glucose, xylose, and glucuronic and galacuronicacids¹¹¹. Fucoidan from brown seaweeds may have $-(1 \rightarrow 3)$ -backbones or repeating disaccharide units of $-(1 \rightarrow 3)$ - and $-(1 \rightarrow 4)$ -linked fucose residues with O-2 branches depending on brown algal species¹²¹⁻¹²³. Due to the structure of the main chain, fucoidan can be sulfonated at O-4, O-2, or at both positions of the fucose units¹²³.

The newest global estimate from the International Diabetes Federation is that in 221 countries there were 425 million people with diabetes mellitus (1 in 11 adults) in 2017; and it

was predicted that the number of diabetes patients aged 20–79 years will increase to 629 million or to 693 million among 18–99 years by 2045⁵⁶. With the escalating incidence, pharmacotherapy involving synthetic insulin and anti-diabetic agents is clinically administered for diabetic therapy, but these are deficient in having multiple dosage regimens, side effects, toxicity, and high costs. Therefore, it is essential to screen novel and effective medicines for the management of diabetes mellitus. Recent studies have demonstrated that the modulation of the gut microbiota may be one of the potential mechanisms contributing to the anti-diabetic effects of natural polysaccharides from seaweeds^{127,128}. Fucoidan, as macromolecular carbohydrate, is indigestible and fermentative in the colon. Fortunately, it has been widely reported that fucoidan possesses anti-diabetic activities through distinct mechanisms, such as inhibiting α -glucosidase activity, improving β -cell dysfunction, ameliorating glucose metabolism in liver and muscle tissues, enhancing insulin sensitivity¹³⁵⁻¹³⁹. However, fucoidan is an orally administered drug that reaches high concentrations in the intestine with much lower serum concentrations¹⁰, thus, the possibility that its metabolic therapeutic mechanism might be due in part to actions in the intestine cannot be ignored. Accumulated evidence shows that a high-fat diet (HFD) reduces the abundance of Lactobacilli in the small intestine. However, this can be counteracted by fucoidan, which increases the proportion of probiotics, thus, relieving the symptoms of HFD-induced diabetes¹⁴¹. Although fucoidan may play a hypoglycemic effect by improving the gut microbiota, oral administration of antibiotics to diabetic mice impairs the hypoglycemic ability of fucoidan. In addition, while fucoidan can increase the abundance of *Escherichia coli*, it can as well reduce the abundance of Intestinibacter. This can further influence diverse biological processes such as the synthesis of branched-chain amino acid and the secretion of GLP-1, thereby improving glucose tolerance and alleviating insulin resistance

(IR)¹⁴⁵⁻¹⁴⁸. These findings suggest that modulation of gut microbiota is involved in the hypoglycemic mechanism of fucoidan.

Bile acids (BAs), which are produced in the liver and serve as important ingredients of the digestive fluid in the intestine, enter the small intestine through the biliary system and participate in fat digestion and absorption^{272,273}. Gathered evidence demonstrates that BAs could improve the intestinal homeostasis by modulating the gut microbiota, thus relieving metabolic syndrome²⁷⁴. Recent studies also suggest that BAs can participate in the liver-gut axis circulation and the improvement of HFD-initiated metabolic disorders by inhibiting the proliferation of pathogenic bacteria^{275,276}. By modulating the gut microbiota, BAs have also been reported to induce multiple beneficial effects on the intestinal lumen and intestinal walls such as the suppression of intestinal inflammatory responses^{277,278}, the resolution of endoplasmic reticulum (ER) stress in the intestinal epithelial cells underlying the pathology of inflammatory bowel disease²⁷⁹ and the improvement of gut barrier dysfunction²⁸⁰⁻²⁸². These findings suggest that there is a complex relationship between BAs, gut microbiota and metabolic syndrome. Tauroursodeoxycholic acid (TUDCA) is one of the chemical chaperones that constitute a group of low-molecular-weight compounds known to modulate ER function, stabilize protein conformation, improve the folding capacity of the ER, and facilitate the trafficking of mutant proteins²⁶². A recent study found that TUDCA could alleviate the increased ER stress seen in obesity and reverse insulin resistance and type 2 diabetes in experimental models²⁶⁷, suggesting TUDCA as a promising new regulator for mediating autophagy, ER stress, and insulin resistance via certain signaling pathways in the liver of obese mice. However, the intracellular events responsible for TUDCA-mediated effects in autophagy, ER stress, and insulin resistance remain elusive.

Previous studies have reported the association of BAs with oxidative stress, which has been shown to treat metabolic dysfunction by acting as an endogenous chemical chaperone to protect cells against ER stress²⁶². Intestinal microenvironment (including inflammation status, the function of the epithelial tight junction and gut microbiota) plays an essential role in the progression of obese-induced IR. The presence of gut microbiota and BAs in the intestine may be closely associated with intestinal metabolic state. Analyses from metagenomic sequencing and metabolomics show that fucoidan treatment increases the levels of the conjugated bile acid in the gut by decreasing the abundance and bile salt hydrolase (BSH) activity of *Bifidobacterium* species in the intestines of individuals with T2D²⁷⁷⁻²⁸⁰. BAs are signal molecules that control the dynamic balance between energy metabolism and liver protection. It has been reported that BAs change with obesity, IR and nonalcoholic steatohepatitis (NASH). However, the mechanism by which BAs alleviate HFD-induced IR and the underlying role played by the gut microbiota during this process are not clear.

Accumulating evidence has clearly indicated that oxidative stress plays a major role in the pathological process of IR⁴⁹⁻⁵². What's more, mitochondrial dysfunction, reactive oxygen species (ROS) over production, and lipid peroxidation have been found in the liver of Zucker rats with T2DM⁵². Increased oxidative stress seems to be a deleterious factor leading to insulin resistance and impaired glucose tolerance in T2DM⁵³. Nuclear factor-erythroid-2-related factor 2 (Nrf2), tightly interacts with kelch-like ECH-associated protein 1 (keap1), an important transcription factor responsible for inducing phase II detoxifying and antioxidant enzymes, is a key player in the antioxidant response and glucose metabolism^{54, 55}. Recent study has confirmed Keap1-Nrf2 system as a critical target for preventing the onset of IR⁵⁶, and bile acids have a great influence on the Nrf2/ARE antioxidant signal pathway^{57, 58}. This study investigated how fucoidan prevents the development of IR in HFD-induced obese mice by modulating the

dysbiosis of gut microbiota and alteration metabolites. Exploring the mechanism behind this improves our knowledge of gut microbiota and metabolic interactions underlying the anti-insulin resistance effects of fucoidan.

6.2. Materials and methods

6.2.1. Materials and reagents

Tauroursodeoxycholic acid (TUDCA, purity $\geq 99\%$) was purchased from Selleck (Houston, Texas, USA). Both the normal chow diet (NCD, containing 10% fat by energy) and high-fat diet (HFD, containing 60% fat by energy) were purchased from Beijing HFk Bio-Technology Co., Ltd. (Beijing, China). Antibodies against Akt, phospho-Akt (Ser473), IRS-1, phospho-IRS-1 (Ser307), Keap1, I κ B, phospho-I κ B (Ser32), p65, phospho-p65 (Ser536), GAPDH, Lamin B1 and β -tubulin were obtained from Cell Signaling Technology (Beverly, MA, USA). Nrf2, phospho-Nrf2 (Ser40), and 4-HNE were purchased from Abcam (Cambridge, UK). Horseradish peroxidase (HRP)-conjugated secondary antibody was obtained from Santa Cruz Biotechnology (Santa Cruz, USA).

6.2.2. Animal experiments

All male mice (ICR mice, 7 weeks old, body weight 20 ± 1 g; C57BL/6J mice, 7 weeks old, body weight 24.0 ± 1 g; *ob/ob* mice, 7 weeks old, body weight 41 ± 1 g) were housed in ventilated cages (three animals per cage) at the SPF facility of Wenzhou University under controlled environmental conditions (temperature $22 \pm 2^\circ\text{C}$; relative humidity 60–70%) with free access to standard laboratory chow and tap water. The mice were maintained on a regular 12/12 h light/dark cycle. All animal care and experimental procedures were approved by the Animal Care Ministry of Health and were performed in accordance with the guide for the Care and Use of Experimental Animals of Wenzhou University.

Mice were acclimatized to their environment for 1 week before the experiments. Mice

were randomly allocated into six groups ($n = 9$ for each group). A co-worker blinded to the experimental protocol randomized animals into these groups. For C57BL/6J mice experiment, all groups were fed with NCD, one group of *ob/ob* mice was administered TUDCA (300mg/kg body weight), whereas the other group was treated with an equal volume of saline for 8 weeks. For ICR mice experiment, three groups of animals were fed with HFD. One group mice was administered SFF (200mg/kg body weight), one group mice was administered SFF and water-feed the antibiotic mixture (the cocktail of antibiotics used consisted of 0.5 g/L vancomycin [Sigma-Aldrich, UK] and 1 g/L neomycin, metronidazole and ampicillin [Sigma-Aldrich, UK]) every three days for 24h, and one group of mice were treated with an equal volume of saline for 9 weeks. The whole study lasted 10 weeks, during which the body weight, water consumption and food intake were measured every week. At week 18, intraperitoneal glucose tolerance test (IPGTT) and intraperitoneal insulin tolerance test (IPITT) were performed as previously described⁴¹.

Fresh feces were collected and stored immediately at 80°C for subsequent analysis. At the end of the trial, after overnight fasting for 12 h, blood samples were collected, and serum was isolated by centrifugation at $1000 \times g$ for 15 min at 4°C, and stored at -80°C for further assay. Tissues, including the adipose tissue, liver and ileum, were weighed; one portion of the tissues was fixed with 10% formaldehyde for histological analysis, and the other portion was immediately frozen in liquid nitrogen for further analysis.

Total cholesterol (T-CHO), triacylglycerol (TG), fasting blood glucose (FBG), fasting serum insulin (FINS), catalase (CAT), malondialdehyde (MDA) were determined by biochemical kits purchased from Jiancheng Bioengineering Institute (Nanjing, China). The ratio of reduced glutathione (GSH) and oxidized glutathione (GSSG) were determined by a GSH:GSSG kit (Jiancheng Bioengineering Institute, Nanjing, China). Homeostasis model

assessment-estimated insulin resistance (HOMA-IR) was calculated using the following formula:

$$\text{HOMA-IR} = \text{FBG (mmol/L)} \times \text{FINS (mU)} / 22.5$$

6.2.3. Cell culture

Human liver hepatocellular carcinoma (HepG2) cells were cultured in MEM (Sigma, St. Louis, MO, USA) supplemented with 10% FBS (Gibco, South American), penicillin and streptomycin. Cells were maintained in 5% CO₂ at 37°C.

6.2.4. siRNA Transfection

Nrf2 was knocked-down by RNA interference (RNAi) using the following 19-bp (including a 2-deoxynucleotide overhang) siRNAs (Origene, Beijing, China): *Nrf2*, SR321100A-AUUGAUGUUUCUGAUCUAUCACUTT; SR321100B-GUCAGUAUGUUGAAUCAGUAGUUTC; SR321100C-CCAGUCUUCAUUGCUACUAAUCAGG. Stealth RNAi (Origene, Beijing, China) was used as a negative control (siCont). For transfection, cells were seeded on a six-well plate, grown to ~80% confluence and transfected with siRNA duplexes using Lipofectamine 3000 (Invitrogen, Camarillo, CA, USA) according to the manufacturer's recommendations. After incubation for 48 h, the expression level of Nrf2 protein was detected by western blot.

6.2.5. Glucose uptake assay

Cells were plated at 1 x 10⁴/well in 96-well plates and used at subconfluence after 24 h of preincubation. For experiments, all culture medium was removed from each well and replaced with 100 µM fluorescent 2-Deoxy-2-[(7-nitro-2,1,3-benzoxadiazol-4-yl) amino]-D-glucose (2-NBDG)⁴² in serum-free medium and incubated for 30 min. Subsequently, cells were washed thrice with PBS and then the fluorescence intensity was determined with a fluorescence microplate reader (Ex/Em, 488/520 nm). The glucose concentration in the medium supernatant

was determined by a glucose detection kit (Jiancheng Bioengineering Institute, Nanjing, China) following the manufacturer's instructions.

6.2.6. Flow cytometry assays

The reactive oxygen species (ROS) level was evaluated by flow cytometry (FACSCanto II, BD, USA) using the DCFDA cellular reactive oxygen species detection assay kit (Byotime, Shanghai, China) according to the manufacturer's protocol. Cells were briefly stained with 2',7'-dichlorofluorescein diacetate (DCFDA) at 37°C for 30 min, washed with 1× PBS buffer, and the signal was read at an excitation of 485 nm and an emission of 535 nm.

6.2.7. Quantitative RT-PCR

Total mRNA was isolated from tissue samples using TRIzol reagent (TAKARA, Tokyo, Japan) and was reverse-transcribed into cDNA using a high-capacity cDNA reverse transcription kit (TAKARA, Tokyo, Japan) according to the manufacturer's protocol. The mRNA levels were quantified with quantitative PCR (qPCR) using SYBR Green (Qiagen, Hilden, Germany). Amplification was performed on a LightCycler480 qRT-PCR system (Roche, Mannheim, Germany) under the following reactions: 95°C for 15 min, followed by 40 cycles at 95°C for 10 s, 60°C for 20 s, and 72°C for 20 s. The relative mRNA levels of target genes were normalized to the expression of β -actin calculated using $2^{-\Delta\Delta ct}$ method. The primer pairs used in this study are listed in **Table 6.1**.

Table 6.1. Designed primer sets for qRT-PCR

| <i>Gene</i> | Primer | 5'-3' | Size (bp) |
|------------------------------------|-----------|------------------------|-----------|
| Mus <i>Nrf2</i> | sense | AAGAATAAAGTCGCCGCCCA | 326 |
| | antisense | GAAAAGGCTCCATCCTCCCG | |
| Homo <i>Nrf2</i> | sense | GGTTGGGGTCTTCTGTGG | 247 |
| | antisense | GACATTGAGCAAGTTTGGGAGG | |
| Mus <i>Tnf-α</i> | sense | ACCCTCACACTCACAAACCA | 212 |
| | antisense | ATAGCAAATCGGCTGACGGT | |

| | | | |
|--------------------------------------|-----------|------------------------|-----|
| Homo <i>Tnf-α</i> | sense | CCCTCCAACCCCGTTTTCTC | 157 |
| | antisense | GCCCCTCAAAACCTATTGCC | |
| Mus <i>Il-1β</i> | sense | TGCCACCTTTTGACAGTGATG | 220 |
| | antisense | AAGGTCCACGGGAAAGACAC | |
| Homo <i>Il-1β</i> | sense | CTCTCAGCAGGTCCGATACC | 198 |
| | antisense | AACATGGCACCTCTGCAACT | |
| Mus <i>Il-6</i> | sense | CCCCAATTTCCAATGCTCTCC | 141 |
| | antisense | CGCACTAGGTTTGCCGAGTA | |
| Homo <i>Il-6</i> | sense | GGAGTCAGAGGAAACTCAGTT | 210 |
| | antisense | ACTCAGCACTTTGGCATGTCT | |
| Mus <i>Il-10</i> | sense | AGGGCACCCAGTCTGAGAACA | 225 |
| | antisense | CGGCCTTGCTCTTGTTTTTAC | |
| Mus <i>Ho-1</i> | sense | CACGCATATACCCGCTACCT | 175 |
| | antisense | CCAGAGTGTTTCATTGAGCA | |
| Homo <i>Ho-1</i> | sense | CCTTCTTACCTTCCCAAC | 124 |
| | antisense | GCCTCTTCTATCACCCCTCTG | |
| Mus <i>Nqo1</i> | sense | TCACCTGGGCAAGTCCATTC | 241 |
| | antisense | TGCCCTGAGGCTCCTAATCT | |
| Homo <i>Nqo1</i> | sense | CAGTTGGGATGGACTTGC | 101 |
| | antisense | CCAGGCAGGATTCTTAATG | |
| Mus <i>Keap1</i> | sense | TACACAGCGGGCGGTTACT | 244 |
| | antisense | TCATAGAGGCACAGGGCGA | |
| Homo <i>β-actin</i> | sense | CTCTTCCAGCCTTCCTTCT | 201 |
| | antisense | TCTTCATTGTGCTGGGTGCC | |
| Mus <i>β-actin</i> | sense | CGTGGGCCCGCCCTAGGCACCA | 214 |
| | antisense | TTGGCCTTAGGGTTCAGGGGGG | |

6.2.8. Western blot analysis

Samples were homogenized with ice-cold RIPA lysis buffer containing protease and phosphatase inhibitors (Beyotime, Shanghai, China). The homogenates were centrifuged at $10\,000 \times g$ for 20 min at 4°C to remove the insoluble tissue debris. The protein concentration in the supernatant was determined using a BCA protein assay kit (Beyotime, Shanghai, China) according to the manufacturer's protocol. Equal amount of protein for each group were denatured in boiling water for 5 min. Aliquots (40 μg) of protein samples were subjected to

10% SDS-PAGE and transferred to PVDF membranes (Millipore, Bedford, MA, USA). After blocking with 5% nonfat milk (dissolved in TBST) for 1 h, the membranes were incubated with the indicated antibodies at 4°C overnight, followed by incubation with the appropriate HRP-conjugated second antibodies for 1 h at room temperature. Chemiluminescent detection was performed using the ECL Plus Western blotting reagent (TransStart, Beijing, China). Semi-quantitative analysis for densitometry of each band was performed using ImageJ software.

6.2.9. Co-immunoprecipitation

For co-immunoprecipitation (Co-IP), the whole protein lysates prepared from HepG2 cells were extracted in a RIPA lysis buffer. Briefly, Nrf2 or Keap1 antibodies were first mixed with magnetic-beads (Thermo scientific, Rockford, USA) for at least 4 hours. Antibody-beads complexes were then mixed with the supernatants of protein lysates with a rotator overnight. The final antibody–protein immunocomplex was stripped by boiling with 5x loading sample buffer for WB incubated with Keap1, Nrf2, and GAPDH antibodies. Co-IP was repeated at least three times.

6.2.10. Determination of hepatic/serum TUDCA

The contents of TUDCA in tissues were determined by high-performance liquid chromatography (HPLC). Briefly, 200 mg of frozen tissue was homogenized with a TissueLyserII (Qiagen, Germantown, MD, USA) in 1 mL of PBS to prepare the tissue homogenates. The impurities were removed through a 0.22 µm filter, then the filtrate was precipitated by methanol and 10 µL of supernatant was analyzed using an Agilent 1290 HPLC system (Santa Clara, CA) equipped with a Hypersil ODS-2 column (5 µm, 4.6 × 250 mm; Waters, USA). The supernatant was detected at the wavelength of 210 nm, eluted with the mobile phase of 0.03 M phosphate buffer solution (pH 4.4) and methanol (32:68, v/v) at a flow rate of 1.0 mL/min.

6.2.11. Statistical analysis

Statistical comparisons among experimental groups were analyzed by one-way ANOVA and Duncan's multiple-comparison test using the SPSS software (Version 21.0. Armonk, NY: IBM Corp.). *P* values less than 0.05 were considered statistically significant.

6.3. Results

6.3.1. TUDCA improves obesity and insulin resistance in *ob/ob* mice

To assess the efficacy of TUDCA on the treatment of obese mice with IR, animals were divided into the wild type, *ob/ob* and *ob/ob*+TUDCA groups. Daily oral administration of TUDCA significantly alleviated diet-induced body weight increase from week 7 onwards (**Figure 6.1a**). At the end of TUDCA treatment, the weight gain was also significantly decreased (**Figure 6.1b**). TUDCA prevented fat deposition in the subcutaneous adipose, and the indexes of the pancreas and kidney were not affected by TUDCA administration. The liver index was significantly reduced in TUDCA-treated mice (**Figure 6.1c**). The diet-induced hepatic steatosis and dyslipidemia were effectively prevented by TUDCA treatment as indicated by the lower concentration of T-CHO and TG in both the liver and the serum of the *ob/ob*+TUDCA group compared with the *ob/ob* group (**Figure 6.2**). In addition, the expression of inflammatory factors in ileum tissue was reduced at the gene level with the addition of TUDCA (**Figure 6.3**).

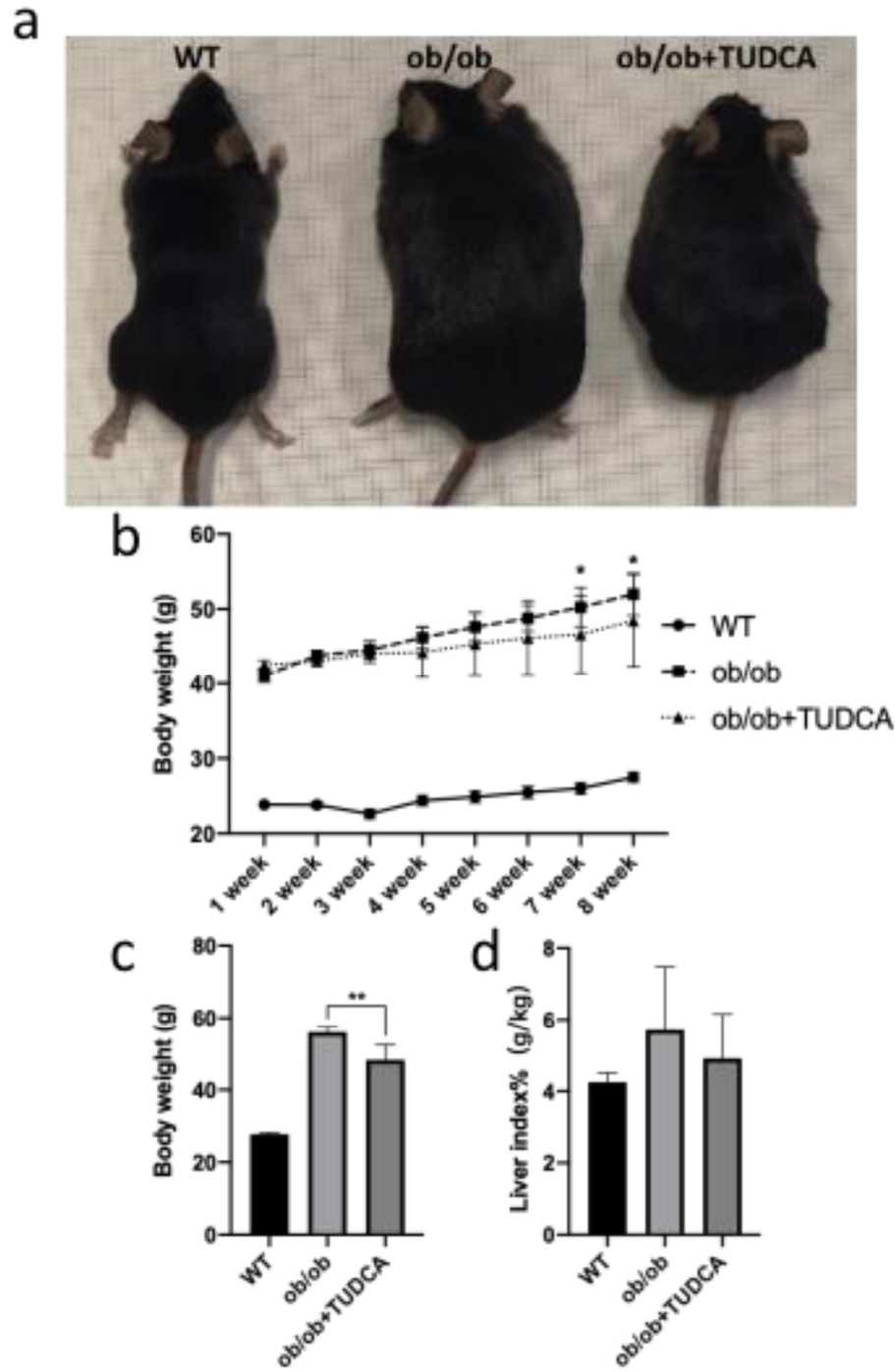


Figure 6.1. TUDCA improves obesity in *ob/ob* mice. Body size (a), body weight change(b), body weight (c) and liver index (d), data are expressed as mean \pm SD. * $P < 0.05$, ** $P < 0.01$ and *** $P < 0.001$.

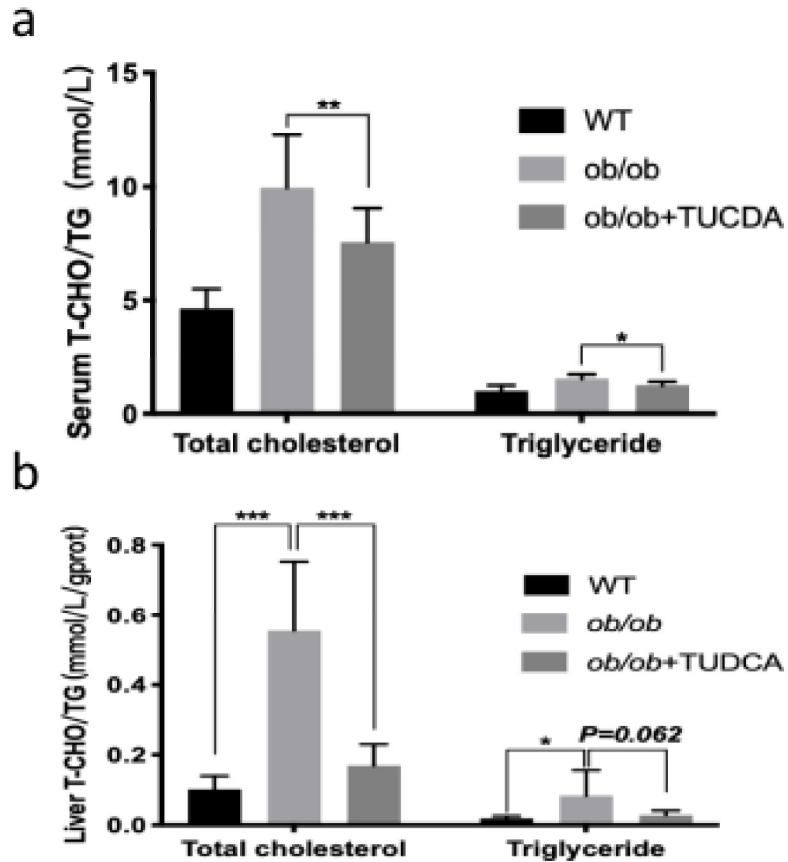


Figure 6.2. TUDCA relieves serum/liver lipid accumulation in *ob/ob* mice. levels of total cholesterol and triglycerides in liver (a) and serum (b). Data are expressed as the mean \pm SD. * $P < 0.05$, ** $P < 0.01$ and *** $P < 0.001$.

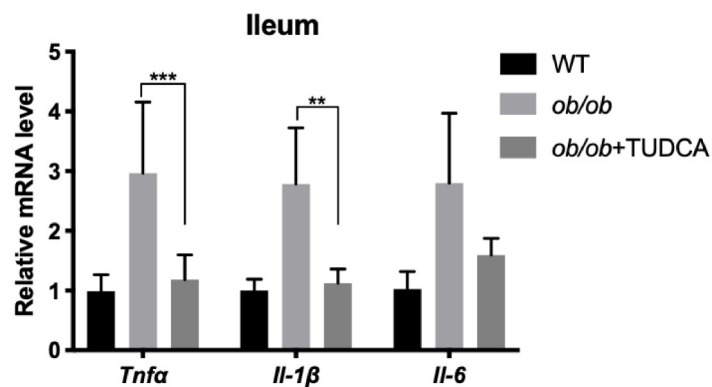


Figure 6.3. TUDCA relieves intestinal inflammation in *ob/ob* mice. The relative mRNA levels of *Tnf-α*, *Il-1β* and *Il-6* in ileum were determined by qPCR. Data are expressed as the mean \pm SD. * $P < 0.05$, ** $P < 0.01$ and *** $P < 0.001$.

Glycemic homeostasis was determined by IPGTT and IPITT. As shown in **Figure 6.4a**, the oral administration of glucose increased the blood glucose (BG) level within 30 min in mice, which remained high for the subsequent 90 min. This indicated that *ob/ob* markedly impaired glucose tolerance. In addition, the BG of the WT group peaked within 30 min but dropped to the normal level after 120 min. TUDCA significantly inhibited the rise of BG level and enhanced glucose clearance in the *ob/ob* mice after oral administration of glucose. The results of IPGTT were expressed as the area under the curve (AUC) of BG over 120 min. The AUC of the *ob/ob*+TUDCA group was significantly decreased compared with that of the *ob/ob* group (**Figure 6.4a and b**, $P < 0.05$). The improvement of insulin resistance (IR) was also supported by the results of IPITT. After intraperitoneally injected insulin at 0.75 U/kg, the BG levels at 30, 60, and 120 min revealed that the mice in the *ob/ob*+TUDCA group took more advantage of insulin compared with the mice in the *ob/ob* group (**Figure 6.4c**). The significant difference ($P < 0.05$) of the slope between the *ob/ob* group and the *ob/ob*+TUDCA group suggested that TUDCA increased the utilization of insulin and improved insulin sensitivity in the *ob/ob* mice (**Figure 6.4d**). Moreover, the FBG level in the *ob/ob* group was significantly higher compared to that in the WT group. Compared with the *ob/ob* group, the mice treated with TUDCA had a lower FBG level (**Figures 6.5a**). Marked elevation in fasting serum insulin (FINS) was observed in the *ob/ob* group compared with the WT group. Notably, TUDCA treatment tended to reverse the increase in FINS (**Figure 6.5b**). HOMA-IR is an indicator for evaluating the level of insulin resistance in an individual. Based on the HOMA-IR analysis, we found that the HOMA-IR of the *ob/ob*+TUDCA group was comparable to that of the WT group but significantly lower compared with that of the *ob/ob* group (**Figure 6.5c**).

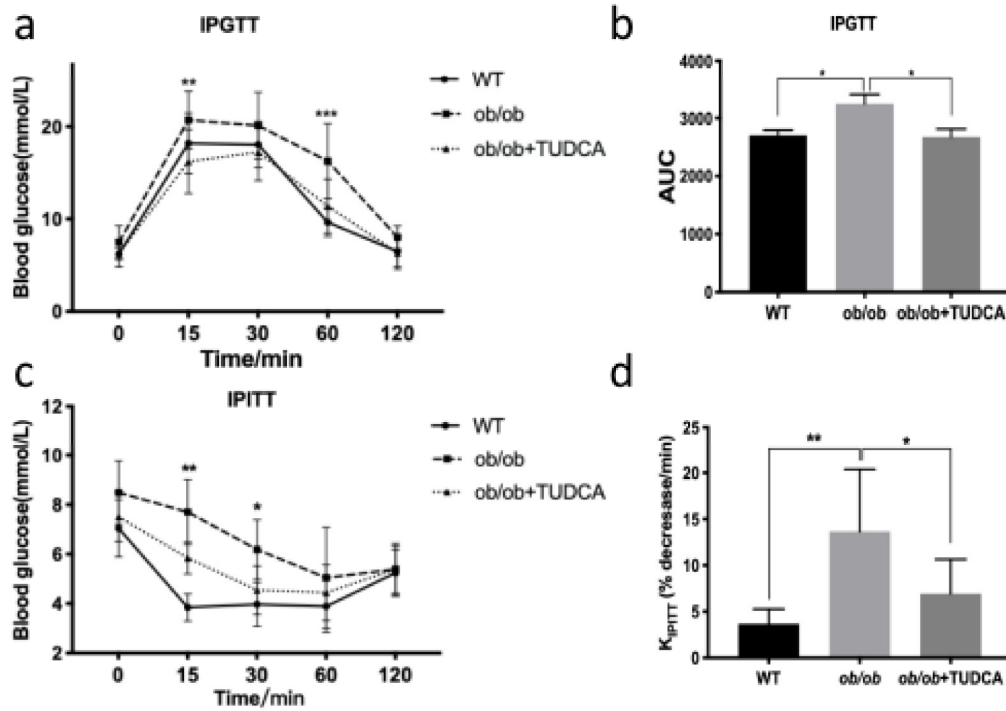


Figure 6.4. TUDCA improves glucose homeostasis and insulin sensitivity in *ob/ob* mice. IPGTT (a); AUC of IPGTT (b); IPITT (c); slope of IPITT (d) measured at the end of the experimental period. Data are expressed as mean \pm SD. * $P < 0.05$, ** $P < 0.01$ and *** $P < 0.001$.

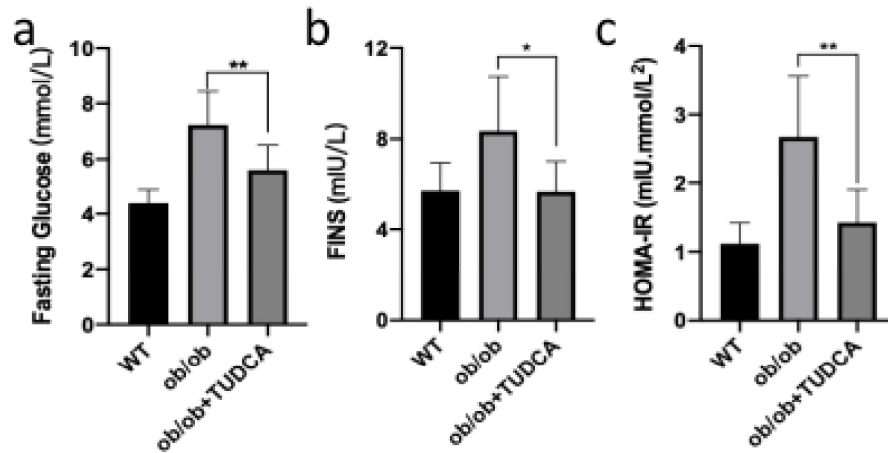


Figure 6.5. TUDCA improves insulin resistance in *ob/ob* mice. Serum level of FBG (a), FINS (b), and HOMA-IR (c) measured at the end of the experimental period. Data are expressed as mean \pm SD. * $P < 0.05$, ** $P < 0.01$ and *** $P < 0.001$.

PI3K/Akt and insulin receptor substrate-1 (IRS-1) are the main signaling molecules in the

signaling pathway of the insulin receptor. The level of phosphorylated Akt at Ser473 was significantly reduced in the liver of the *ob/ob* mice, but the level was restored in the *ob/ob*+TUDCA group (Figure 6.6). These results indicate that the preventive effect of TUDCA on obesity resulted in improved glucose homeostasis and insulin sensitivity.

6.3.2. TUDCA activates the Nrf2/ARE signaling pathway in *ob/ob* mice liver

Isolation of liver nuclear and cytoplasmic proteins revealed that Nrf2 was significantly up-regulated in the nucleus of TUDCA-treated mice, and its downstream antioxidant genes Nqo1 and Ho-1 were substantially increased at the transcriptional level, suggesting that the Nrf2/ARE signaling pathway was activated by TUDCA (Figure 6.6).

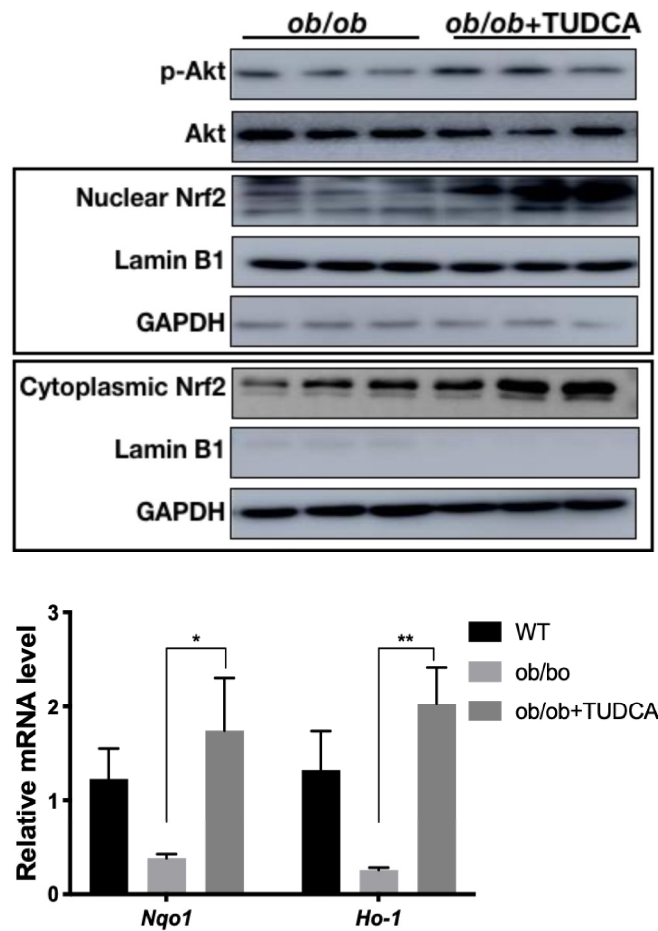
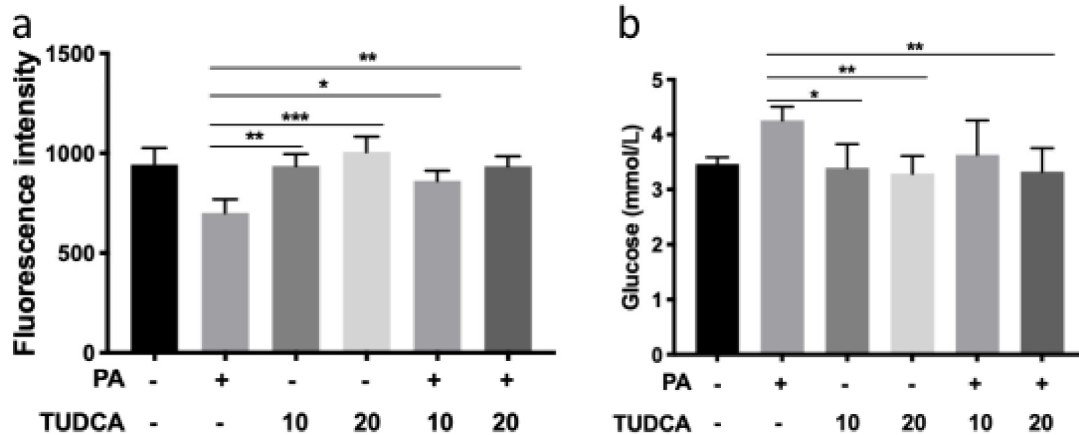


Figure 6.6. TUDCA improves obesity and insulin resistance in *ob/ob* mice by activating Nrf2/ARE signaling pathway. Protein expression of Akt, phosphorylated Akt, nuclear Nrf2, cytoplasmic Nrf2,

Lamin B1 and GAPDH. Quantitative RT-PCR analysis of representative downstream genes (*Nqo1* and *Ho-1*). Data are expressed as mean \pm SD. * $P < 0.05$, ** $P < 0.01$ and *** $P < 0.001$.

6.3.3. TUDCA improves PA-induced insulin resistance and lipid peroxidation

Further study was carried out to determine whether TUDCA could alleviate hepatic insulin resistance using a PA-treated HepG2 cell model. PA exposure (200 μ M) resulted in a decrease in glucose uptake of HepG2 cells, demonstrated by the reduction of fluorescence density in the cytoplasm (**Figure 6.7a**) and the high concentration of glucose in the medium (**Figure 6.7b**). In addition, PA decreased the level of phosphorylated Akt at Ser473 and increased phosphorylated IRS-1 at Ser307 (**Figure 6.7c**), thus, revealing a typical symptoms of insulin resistance. Moreover, the suppressed phosphorylation level of Akt in PA-treated HepG2 cells was elevated by TUDCA, while the phosphorylated IRS-1 at Ser307 was also significantly reduced (**Figure 6.7c**). These findings confirmed that TUDCA could improve hepatic glucose intolerance and enhance insulin sensitivity of PA-treated hepatocyte.



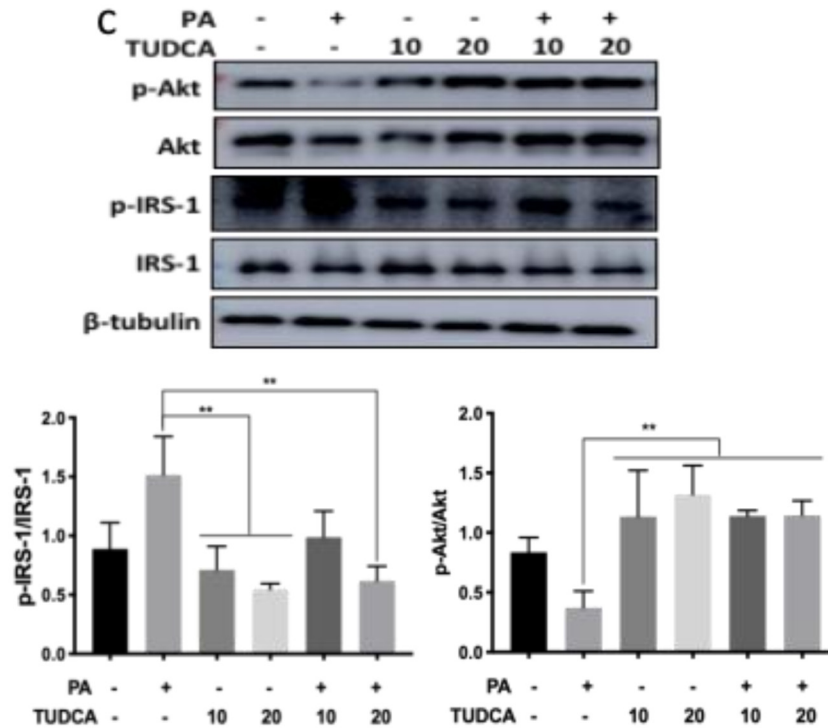


Figure 6.7. TUDCA alleviates insulin resistance caused by PA. Glucose uptake (a) and the blood glucose remaining in supernatant (b). Protein levels of p-Akt, Akt, pIRS-1 Ser307, IRS-1 were determined by western blot (c). Data are expressed as the mean \pm SD. * $P < 0.05$, ** $P < 0.01$ and *** $P < 0.001$.

Homeostasis imbalances on glucose metabolism often cause inflammation and oxidative stress damage in hepatic cells. Thus, we further investigated whether TUDCA could alleviate these pathological processes. As shown in **Figure 6.8a**, PA could increase ROS generation in HepG2 cells, while TUDCA significantly decreased PA-induced ROS production. On the other hand, the ratio of GSH/GSSG was significantly increased by TUDCA (**Figure 6.8b**). In addition, pro-inflammatory cytokines such as *Tnf- α* , *Il-1 β* and *Il-6* were also significantly reduced by TUDCA treatment at mRNA level (**Figure 6.9**).

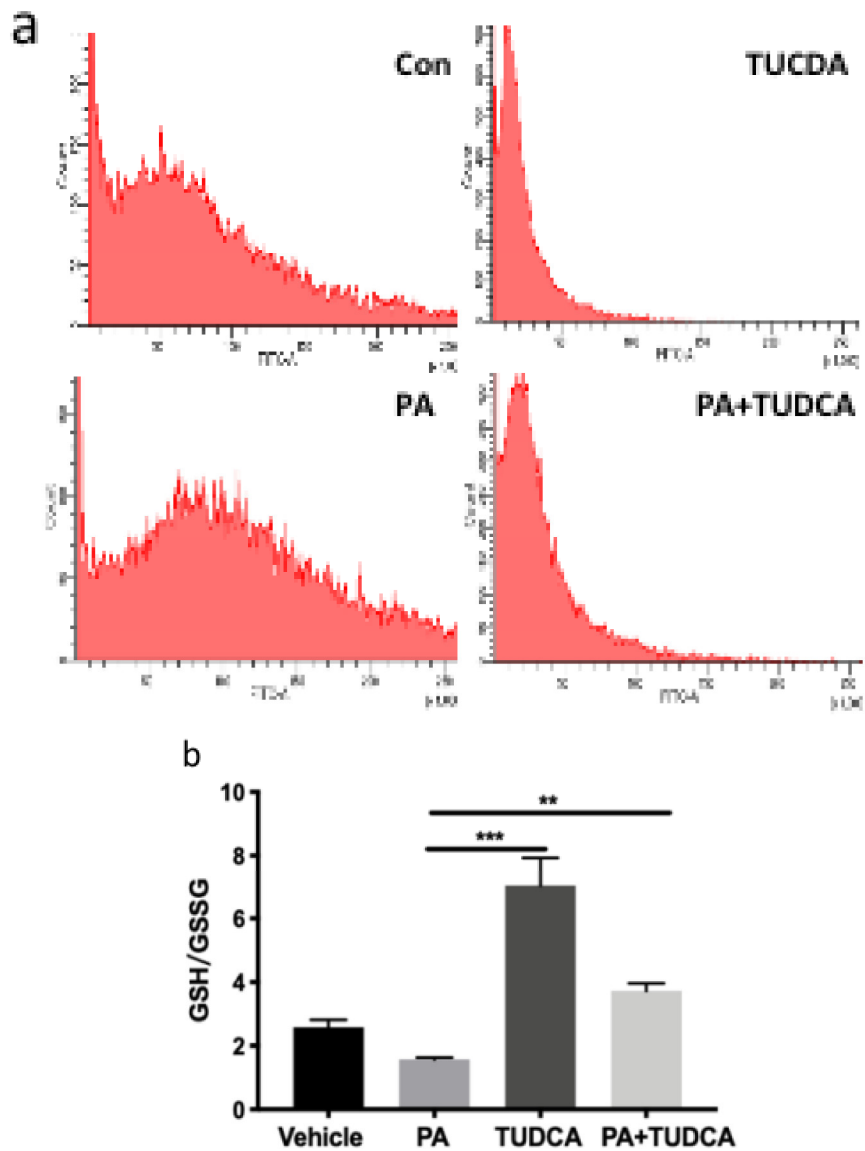


Figure 6.8. TUDCA relieves PA-induced ROS and oxidative stress. Intracellular ROS content (a) and the ratio of GSH/GSSG (b) are shown. Data are expressed as mean \pm SD. * $P < 0.05$, ** $P < 0.01$ and *** $P < 0.001$.

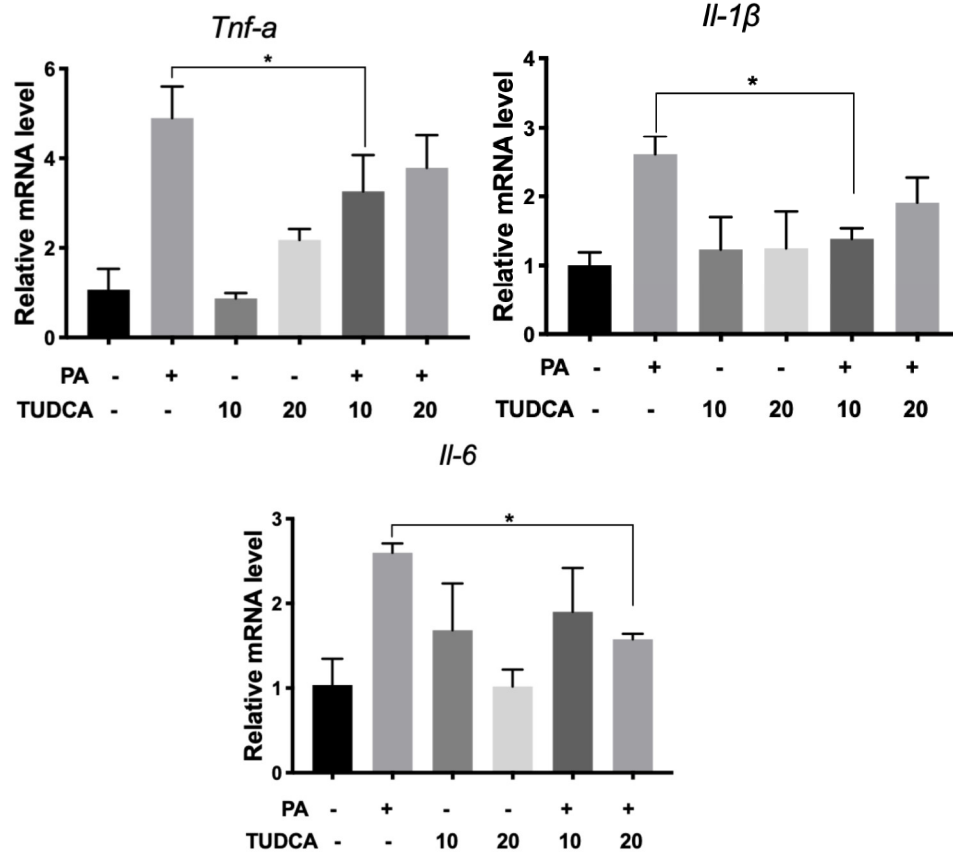


Figure 6.9. TUDCA reduces the secretion of pro-inflammatory cytokines. HepG2 cells were pre-treated with 200 μ M PA for 24 h and then incubated with TUDCA (10 or 20 μ M) for 12 h. The relative mRNA levels of *Tnf- α* , *Il-1 β* , and *Il-6* were determined by *q*PCR. Data are expressed as mean \pm SD, * P < 0.05.

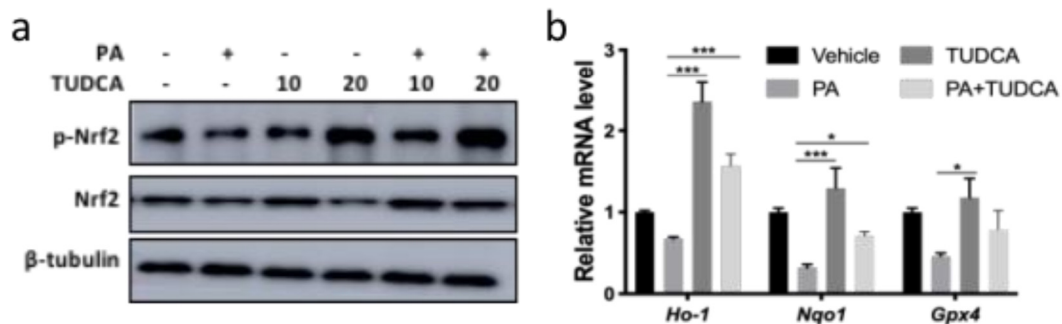


Figure 6.10. TUDCA activates Nrf2/ARE signaling pathway. Protein levels of p-Nrf2 and Nrf2 were determined by western blot (a); Quantitative RT-PCR analysis of *Nrf2*, representative Nrf2 downstream genes *Ho-1*, *Nqo1* and *Gpx4* (b). Data are expressed as mean \pm SD. * P < 0.05, ** P < 0.01 and *** P < 0.001.

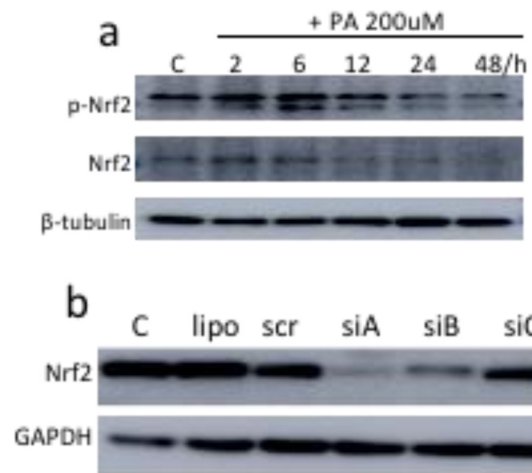


Figure 6.11. PA inhibits Nrf2 expression and activation. (a) PA (200 μM) was incubated with HepG2 cells, and then the protein expression of p-Nrf2 and total Nrf2 was detected by western blotting. (b) Silencing Nrf2 expression in HepG2 cells by siRNA. Protein levels of Nrf2 were determined by western blotting after 48 hours of transfection with siRNA.

We further investigated whether TUDCA alleviates PA-induced insulin resistance through the Nrf2/ARE signaling pathway. The transcriptional activity of Nrf2 was determined by measuring the mRNA levels of its representative downstream target genes. TUDCA significantly up-regulated the expression of Nrf2 as well as its phosphorylation level, suppressed by PA (**Figure 6.10 and 6.11**). It also up-regulated the expression of antioxidant genes, *Ho-1*, *Nqo1*, and *Gpx4*, downstream of the Nrf2/ARE signaling pathway (**Figure 6.10**). We found that TUDCA was unable to alleviate PA-impaired glucose uptake PA-induced insulin resistance in HepG2 cells that interfered with Nrf2 expression (**Figure 6.11 and 6.12**). The physical interaction between Nrf2 and Keap1 was reduced by TUDCA (**Figure 6.13**), suggesting that TUDCA antagonizes with Keap1 to keep Nrf2 from protein degradation by ubiquitination-proteasome. Together, the results suggest that TUDCA may significantly activate the Nrf2/ARE signaling, thereby enhancing antioxidant capacity and alleviating insulin resistance in PA-treated HepG2 cells.

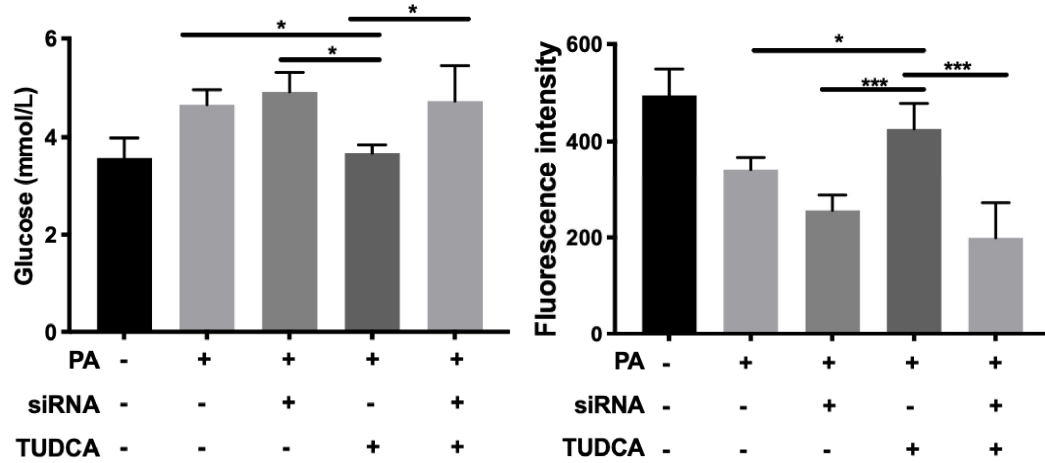
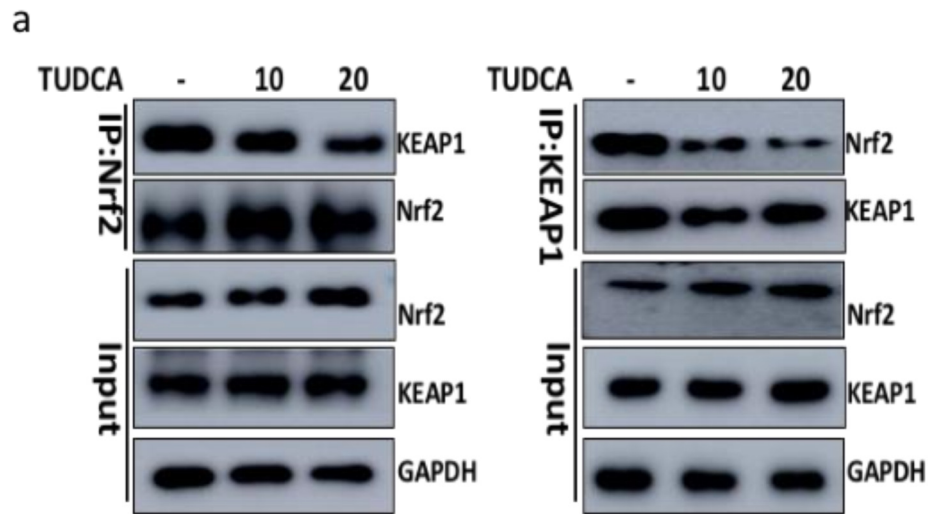


Figure 6.12. TUDCA relieves PA-induced insulin resistance by Nrf2/ARE signaling pathway activation. Under Nrf2 knock-down and glucose uptake are shown. Data are expressed as mean \pm SD. * $P < 0.05$, ** $P < 0.01$ and *** $P < 0.001$.



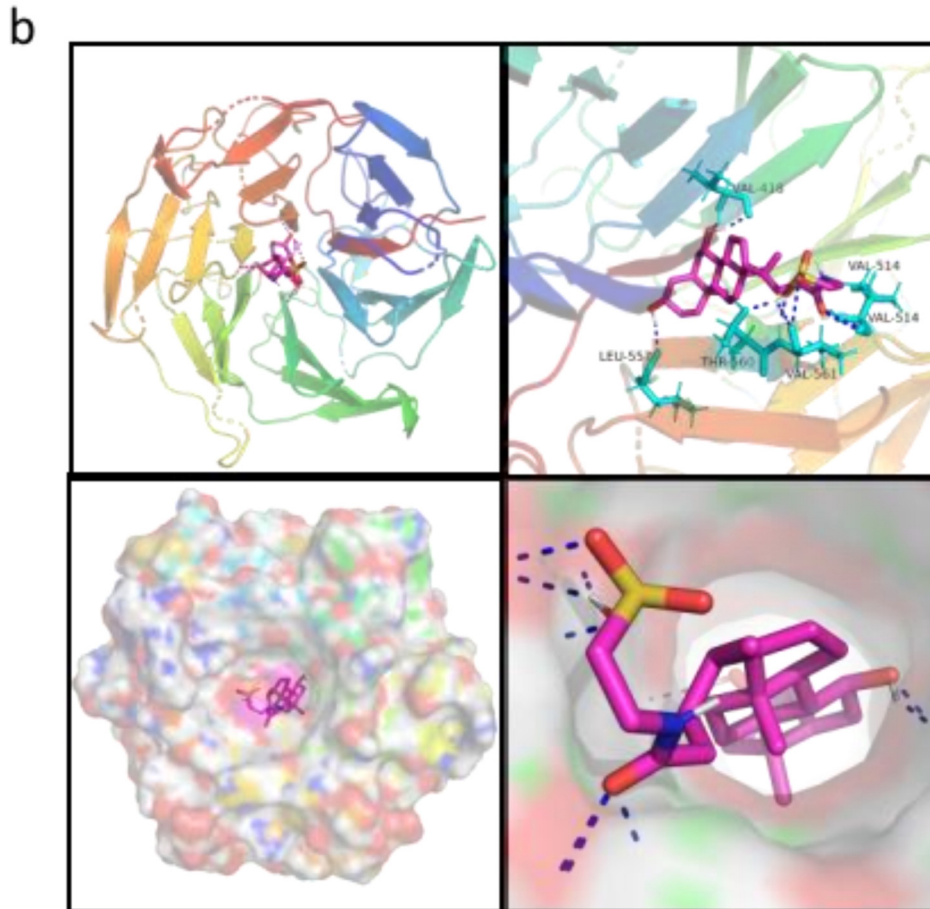


Figure 6.13. TUDCA relieves PA-induced insulin resistance via activating Nrf2/ARE signaling pathway. (a) HepG2 cells were treated with or without TUDCA, and then lysates were immunoprecipitated with the indicated antibodies, followed by western blotting. (b) Docking of TUDCA with Kelch domain of KEAP1. The residues of KEAP1 were represented using sticks or surface structures; TUDCA was shown in pink; the dashed lines (blue) represent hydrogen-bonding interactions. Data are expressed as mean \pm SD. * $P < 0.05$, ** $P < 0.01$ and *** $P < 0.001$. GSH, glutathione; GSSG, oxidized glutathione; PA, palmitic acid; TUDCA, tauroursodeoxycholic acid.

6.3.4. Effects of fucoidan to alleviate insulin resistance are mediated by gut microbiota

As assessed by 16S rRNA analysis, the gut microbiota of ICR mice was remodeled and metabolites altered after fucoidan administration. To investigate whether the fucoidan-induced remodeling of gut microbiota was causally related to the alleviation of insulin resistance, the ICR mice were divided into three groups: HFD, HFD+SFF and HFD+SFF+Abs. The three groups of mice were sequentially fed high-fat chow, high-fat chow with fucoidan in water, and

high-fat chow with fucoidan and antibiotic mixture in water. The mice treated with the antibiotic mixture were pseudo-germ-free mice, which were used to verify whether the alleviating effect of fucoidan on insulin resistance was mediated by the gut microbiota. The experiment lasted for 12 weeks, and it was found that obesity was induced in mice on a long-term high-fat diet, on the basis of which weight gain in fucoidan-treated mice leveled off at week nine. At the tenth week, there was a significant difference in body weight between the three groups of mice, with the HFD+SFF group having significantly lower body weight values than the HFD+SFF+Abs group. In serum and liver extracts, the HFD+SFF group significantly reduced triglyceride and cholesterol levels, whereas fucoidan failed to exert its lipid-lowering effect after treatment with the antibiotic mixture.

6.3.5. Correlation between gut microbiota abundance and mice TUDCA

In the initial lefSE analysis in mice experiments, SFF was found to significantly increase the dominant abundance of Bacteroidetes, Alistipes, Parabacteroides, Dubosiella, Faecalibacterium and Clostridium, while in HFD the dominant bacteria tended more towards Erysipelotrichia and Desulfovibrionaceae (**Figure 6.14**). Subsequently, TUDCA was added to the association analysis of flora and obesity parameters, and it was found that TUDCA was negatively correlated with fasting blood glucose, and when TUDCA increased, fasting blood glucose tended to decrease and was closely associated with Clostridiales bacteria. In Addition, Clostridium was also associated with a decrease in free fatty acid and liver weight. We hypothesize that SFF increases TUDCA content through remodeling of *Clostridium intestinalis* and thus exerts its effect on alleviating insulin resistance.

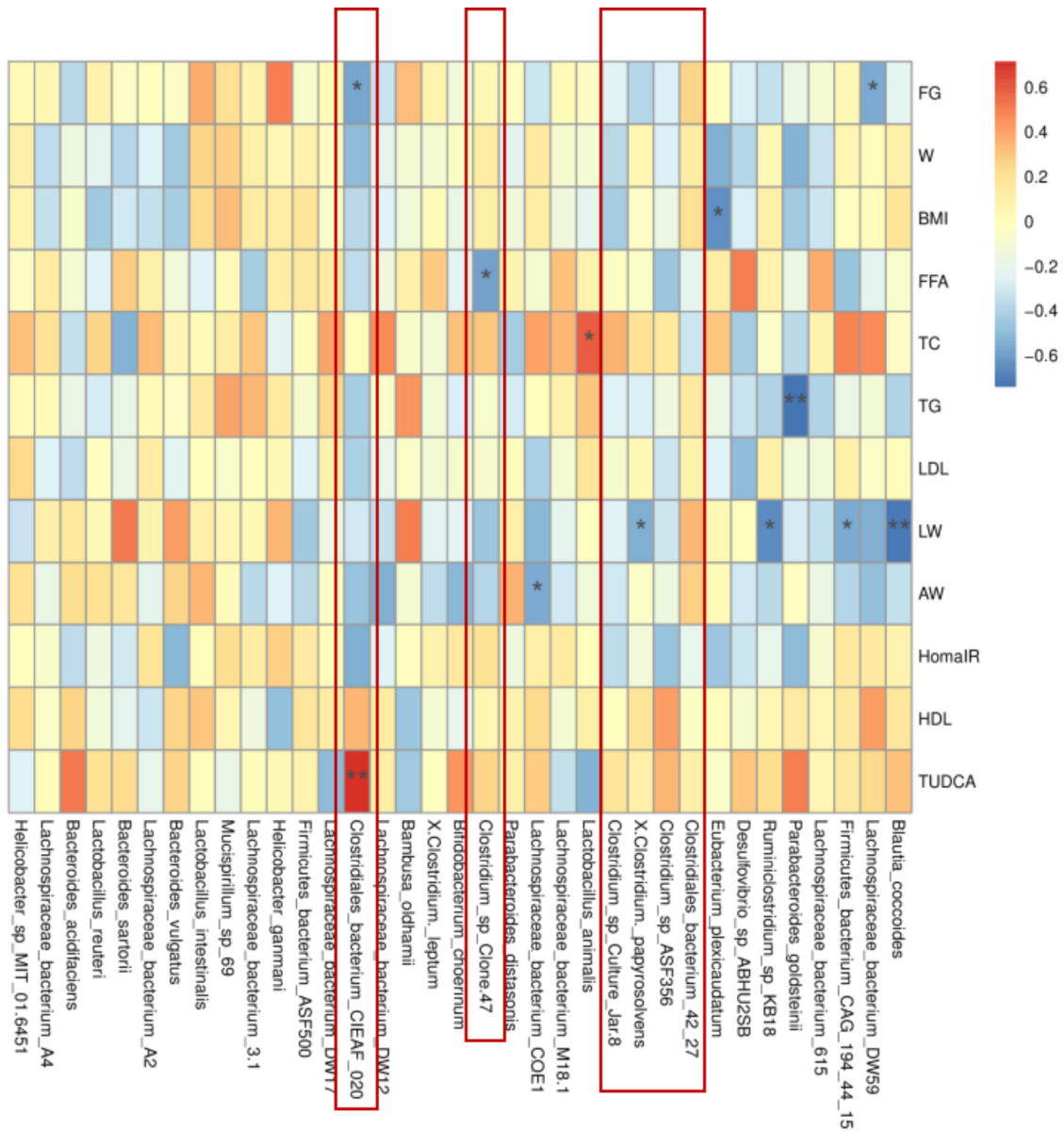


Figure 6.14. Spearman's correlation between gut microbiota, TUDCA and obesity-related indexes (species). Good's coverage and the genus with significant correlations are shown.

To verify the hypothesis, TUDCA levels in intestinal contents and serum were measured, and TUDCA levels in intestine and serum were significantly higher in the HFD+SFF group compared to the HFD group, while there was no significant difference between the HFD+SFF+Abs and HFD groups. In addition, SPH and ceramide were significantly higher in the feces and lower in the serum of the HFD+SFF group compared to the HFD group, whereas

in the germ-free mice, SPH and ceramide were heavily accumulated in the intestine and absorbed by the serum. This phenomenon is most likely due to the decrease of TUDCA in the intestine.

6.4. Discussion

Metabolic syndromes such as obesity, NAFLD and T2D are increasingly prevalent globally, especially in recent decades¹². Fucoidan, the most abundant active substance in brown polysaccharides, has been reported to favorably influence metabolic and cellular processes, alleviate insulin resistance⁶⁻⁸; however, the mechanism is still not clear. Recent studies have revealed that the development of metabolic disease strongly correlates to gut microbiota and metabolites. Multiple studies have investigated the impact of fucoidan on gut microbiota, metabolites and related host targets which regulate glucose metabolism⁴⁵⁻⁵⁰. We explored the potential mechanism involving the gut microbiota and intestinal metabolites to reveal how fucoidan improves diet-induced obesity and insulin resistance. We established that the daily administration of TUDCA strongly ameliorated the obesity-related interruption of gut microbiota. The bile acid TUDCA was maintained at a high level in the intestine, which in turn promoted the proliferation of *Clostridium*, improved the integrity of the intestinal wall and reduced intestinal inflammation. Furthermore, TUDCA was identified as an activator of Nrf2/ARE signaling in hepatocyte that decreased oxidative stress imbalance, while improving hepatic inflammation and insulin resistance.

T2D is both an inflammatory and a natural immune disease. There is a variety of microbiota in the human intestine, which is involved in body immunity, infection and nutrient metabolism, and they are closely associated with the occurrence of diabetes²¹. The gut microbiota imbalance in composition and diversity can result in the release of bacterial endotoxin. This could lead to chronic inflammation and destruction of the normal physiological

functions of tissues and organs. Several studies have confirmed that chronic inflammation can cause insulin resistance and subsequently diabetes. The decrease in Firmicutes/Bacteroidetes ratio is considered to be an indicator of improved metabolism by fucoidan therapy^{217, 218}. LDA analysis showed that the decreased abundance of Firmicutes by fucoidan could be due to the decrease in *Erysipelotrichia* species, which belongs to the Firmicutes phylum. The role of *Erysipelotrichia* species in human disease may be well established in studies investigating metabolic disorders²¹⁹. For instance, a previous study showed a bloom of species belonging to the *Erysipelotrichaceae* family (initially classified as *Mollicutes*) in diet-induced obese animals²²⁰. Within the host, *Erysipelotrichia* species appear to be highly immunogenic, however, in surplus, they induce intestinal inflammation. Studies have shown that species in *Erysipelotrichaceae* are positively correlated with TNF α and IL-6 in the intestine and the liver²¹⁹.

In contrast, most of the bacteria up-regulated by fucoidan were probiotics. For example, species in *Muribacaceae* are involved in the L-citrulline nitrogen metabolic cycle. They scavenge free radicals, improve immunity and maintain blood glucose. Fucoidan also up-regulates the abundance of *Parabacteroides*, including *P. distasonis* and *P. goldsteinii*. Study found that *P. distasonis* could transform bile acids, activate intestinal gluconeogenesis through succinic acid and improve the host metabolic disorders²⁸³. In another study, it is recorded that *P. goldsteinii* reduces systemic inflammation and increases insulin sensitivity by maintaining intestinal integrity²⁸⁴. The "dialogue" between the gut microbiota and the organism mainly depends on microbial metabolites. By producing various enzymes for biochemical metabolic pathways of the intestinal microbes, gut microbiota can perform diverse metabolic activities such as the metabolism of amino acids, carbohydrates and bile acids, as well as the formation of a co-metabolic relationship with the host. Bile acids produced by the gut microbiota are

essential in the regulation of glycolipids and energy. Studies have shown that in human primary hepatocytes, bile acids promote the β -oxidation of fatty acids by activating FXR and up-regulate the expression of apolipoprotein CII gene to reduce the triglyceride content in the liver^{285,286}.

In our present study, metabolomics data showed that TUDCA in the intestine of HFD+SFF group increased significantly. Previous studies revealed that fucoidan treatment increased the levels of conjugated bile acid in the gut by decreasing the abundance of *Bifidobacterium* and its bile salt hydrolase (BSH) activity in the intestines of individuals with T2D²⁶²⁻²⁶⁴. Bile salt hydrolase, secreted by intestinal bacteria, decomposes TUDCA in the intestine and metabolizes TUDCA to taurine and UDCA. However, data from the gut microbiota showed that fucoidan did not affect the abundance of *Bifidobacterium* and *Lactobacillus*, the major BSH-producing bacteria. In addition, we found that the content of taurine in the intestine increased significantly. *in vitro*, TCDCa can be transformed into TUDCA by $7\alpha/\beta$ -hydroxysteroid dehydrogenase ($7\alpha/\beta$ -HSDH)²⁶³. Data from the gut microbiota also revealed that fucoidan did not affect the abundance of *Eubacterium* and *Clostridium*, the major $7\alpha/\beta$ -HSDH-producing bacteria. Therefore, the increase in TUDCA in the intestine is purportedly not due to the inhibitory effect of fucoidan on BSH-producing bacteria. According to the biosynthesis of bile acids in liver, the conjugated bile acid TUDCA can be generated in the liver through a series of catalytic reactions and enzymes such as CYP7A1 and BAAT²⁶⁵.

TUDCA has been shown to treat NAFLD by acting as an endogenous chemical chaperone; to protect cells against ER stress²⁶ and to reduce liver steatosis²⁸⁷. Moreover, TUDCA can alleviate dextran sulfate sodium-induced colitis in mice^{288,289}. *in vitro*, we found that TUDCA antagonizes with KEAP1 to keep Nrf2 from protein degradation to activated Nrf2/ARE signaling pathway. This is reminiscent of the expression pattern of Nrf2, a crucial stress

regulator to reduce ROS, which is a key factor in sensitizing insulin signaling²⁹⁰. It has also been confirmed that up-regulation of the Nrf2 expression both by genetic manipulation and pharmacological interference, can significantly decrease the content of ROS and ameliorate IR and T2D. In the mice supplement with fucoidan, the significant up-regulation in the expression of *Nrf2* and its downstream target genes (*Gclc*, *Cat* and *Ho-1*) occurred, which further alleviated IR and over-oxidation. Conversely, the stress-resistant effect of TUDCA was dramatically repressed by the inhibition of the Nrf2/ARE signaling. We also found that TUDCA can effectively reduce the inflammation and oxidative stress as well as decreasing the accumulation of lipid peroxide *in vitro* and *in vivo*. This might be a novel mechanism for fucoidan in the treatment of insulin resistance and diabetes.

6.5. Summary

Overall, in our present study, fucoidan was found to increase TUDCA which antagonized the interaction between KEAP1 and Nrf2, prevented Nrf2 degradation and promoted its nuclear translocation. TUDCA activated Nrf2/ARE pathway and increased the gene transcription of antioxidant enzyme, further reduced oxidative stress and sensitized insulin signaling. The increase of TUDCA in the intestine corresponded to the increase in the abundance of *Clostridium*. Fucoidan remodeled the gut microbiota by promoting probiotics such as *Muribacaceae*, and *Parabacteroides*, and inhibiting pathogenic bacteria such as *Erysipelotrichia* and *Helicobacter*, which maintained intestinal integrity and reduced inflammation. However, for a better understanding of the crucial mechanisms involved in the long-term treatment with fucoidan in humans, the role of the intestine-liver axis should be explored. Since TUDCA is a novel effector molecule of fucoidan in the gut, plays an important role in alleviating metabolic syndrome.

Chapter 7

CONCLUSION AND RECOMMENDATIONS

7.1. Synthesis and conclusion

The polysaccharides were extracted and purified from *S. fusiforme*, and three components, alginate, aminaran and fucoidan, were obtained by further delipidation and decolorization, and their physicochemical properties were analyzed. The three components were evaluated by *in vitro* antioxidant assay and *in vivo Drosophila* anti-aging assay, and fucoidan was selected as the best antioxidant component. Fucoidan was established in a mouse model of obesity and insulin resistance induced by high-fat diet and orally administered for a long period of time to determine the effect of fucoidan on insulin resistance in this model. From the dual perspectives of gut microbiomics and metabolomics, the regulatory effects of fucoidan on insulin resistance in high-fat diet-fed mice and its mechanism of action were investigated in depth, and the main findings of this paper are as follows :

1. The crude polysaccharides were obtained by heat extraction and alcohol precipitation method, and further graded into alginate, aminaran and fucoidan by degreasing and decolorization. fucoidan with strong antioxidant properties was screened by total reducing power *in vitro*, DPPH scavenging ability, Fe²⁺ reducing ability and anti-aging effect in *Drosophila*.
2. The modulating effect of fucoidan on insulin resistance in high-fat diet-fed mice was investigated by adding 200 mg/kg of fucoidan to the diet. The results of the study showed that the addition of fucoidan significantly improved the insulin resistance induced by high-fat diet. The addition of fucoidan significantly reduced body weight, total weight gain, epididymal fat

weight and liver index compared to the HFD group. fucoidan addition significantly reduced fasting glucose, serum insulin and thus HOMA-IR index in mice compared to the NCD group. It was also confirmed by IPGTT and IPITT experiments that fucoidan could improve insulin sensitivity in high-fat mice. Compared with the HFD group, mice in the fucoidan group showed improved liver function and systemic hypo-inflammation, with significantly lower serum concentrations of pro-inflammatory factors and LPS. Preliminary investigation of the mechanism of action of fucoidan in regulating insulin resistance revealed that the addition of fucoidan could activate the hepatic Nrf2/ARE signaling pathway, increase the transcription of downstream antioxidant genes, increase the activity of antioxidant enzymes such as GSH and CAT, reduce the accumulation of lipid peroxides MDA and 4-HNE, and thus alleviate the inhibition of insulin signaling pathway by high-fat diet.

3. Based on 16S rRNA high-throughput sequencing technology, we investigated the mechanism of action of fucoidan in alleviating insulin resistance from the perspective of gut microbiomics. It was found that fucoidan has a modulating effect on intestinal microecological disorders induced by high-fat diet, and through the remodeling of gut microbiota, it reduces the F/B ratio and significantly increases the abundance and diversity of probiotics, which in turn maintains intestinal wall integrity and reduces intestinal inflammation.

4. Based on the analysis of intestinal metabolomics, it is known that fucoidan significantly increased the content of sphingosine and TUDCA in the intestine of mice. By HPLC and ELISA, fucoidan was found to increase TUDCA and decrease ceramide in serum. Caco-2 cells mimic intestinal epithelial cells and TUDCA was found to reduce ceramide-related synthase gene expression and thus intestine-derived ceramide biosynthesis by inhibiting the FXR/SHP signaling pathway.

5. Using *ob/ob* C57BL/6J mice as study subjects, TUDCA was found to significantly reduce body weight, fasting glucose and HOMA-IR and increase insulin sensitivity in *ob/ob* mice. The activation of hepatic Nrf2/ARE signaling pathway in mice treated with TUDCA increased the phosphorylation of Nrf2 and promoted its entry into the nucleus. A HepG2 insulin-resistant cell model was constructed by PA and TUDCA was found to reduce ROS content by activating the Nrf2/ARE signaling pathway. By the Co-IP method, TUDCA which antagonized the interaction between KEAP1 and Nrf2, prevented Nrf2 degradation and promoted its nuclear translocation.

6. The experimental results of the pseudo-sterile mouse model constructed based on the compound antibiotic treatment showed that the effect of adding fucoidan on the improvement of insulin resistance in high-fat diet-fed mice targeted the intestinal microecology. It was found that body weight, fasting glucose and insulin sensitivity were not significantly improved in the HFD+SFF+Abs group of mice. Antibiotic treatment disrupted the remodeling of intestinal microecology by fucoidan, and TUDCA levels in the intestine and serum did not change significantly. In contrast, sphingosine entered serum in large amounts and ceramide levels were elevated.

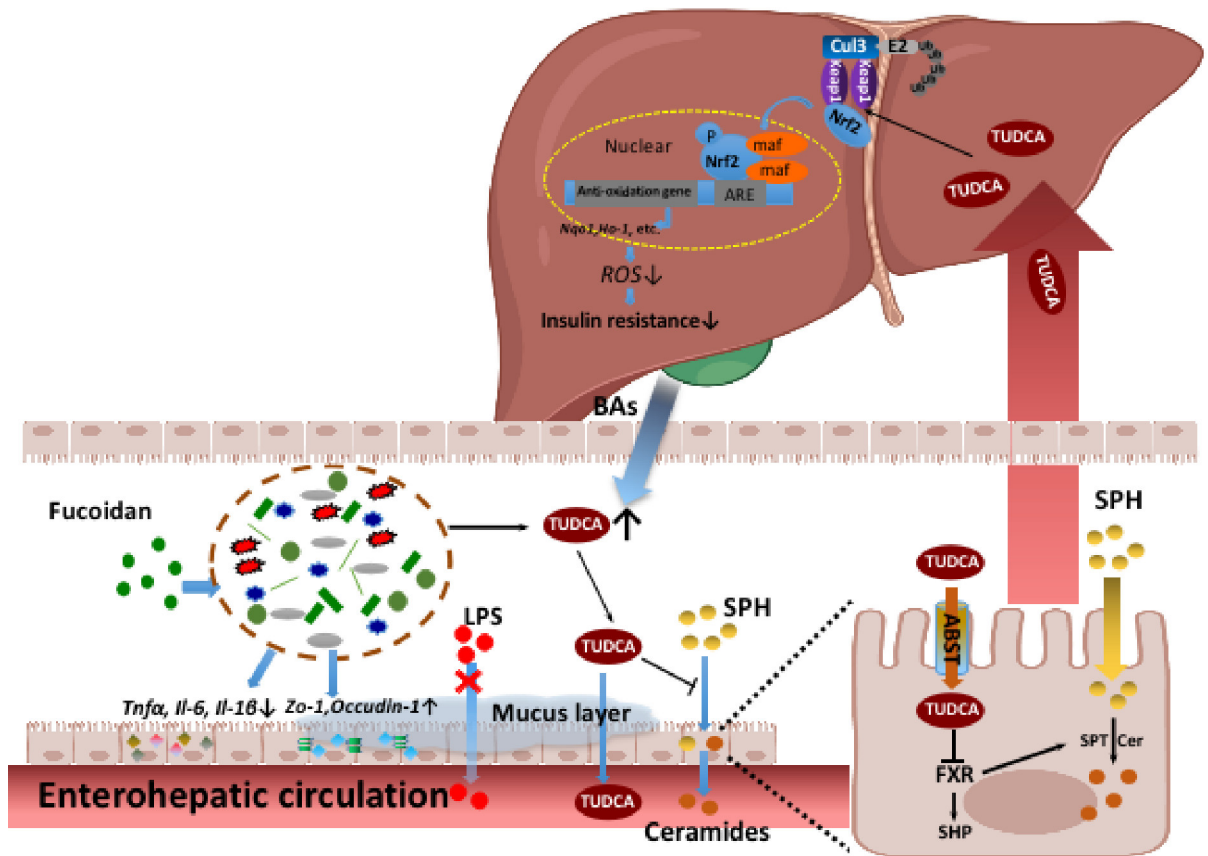


Figure 7.1. Total mechanism of insulin resistance improvement by *S. fusiforme* fucoidan

7.2. Limitations and future research

In this study, the effect of fucoidan on the improvement of insulin resistance and intestinal microecological imbalance in mice fed with high-fat diet was elucidated through insulin-resistant mice, and the mechanism of inhibition of insulin signaling pathway by fucoidan through increasing TUDCA entry into blood and activating Nrf2/ARE signaling to alleviate high-fat was investigated in depth by means of multi-omics analysis. However, due to the limitation of time and experimental conditions, there are still some shortcomings in this study, and there are still some problems that need to be studied and explored in depth, and the main directions of follow-up research are as follows:

1. The addition of fucoidan can improve insulin resistance based on the targeted regulation of

intestinal microecology. Clostridium, as the dominant bacterium of the corresponding fucoidan reshaping gut microbiota, its effect on the metabolic regulation of high-fat diet-fed mice is not yet clear, and its regulatory effect and mechanism of action can be studied by the targeted colonization experiment system of Clostridium subsequently.

2. After fucoidan treatment, TUDCA and Clostridium were positively correlated in the intestinal tract of mice, but their sequence is still unclear. Whether fucoidan inhibits the catabolism of clostridia by remodeling Clostridium abundance and then by Clostridium, or whether the accumulation of TUDCA in the intestine promotes the amplification of Clostridium remains to be investigated.

3. Current studies on the biological activity of TUDCA have been elaborated through the classical bile acid receptor pathway mechanism, and it is speculated that the activation of SPT and CerS by TUDCA is not direct, but may be accomplished through intermediate receptors such as PXR (pregnane X receptor) or TGR5 (Gprotein-coupled bile acid receptor 5) and other intermediate receptors to accomplish this. Therefore, the mechanism of action of TUDCA through increasing sphingosine efflux deserves further investigation.

4. During the molecular docking of TUDCA with Keap1, it was found that TUDCA was able to interact with the primary amino acid residues on the active site of KEAP1. TUDCA was positioned at the hydrophobic pocket, surrounded by the residues Val-418, Leu-557, Val-514, Val-561, and Thr-560, forming a stable using HepG2 cells as a model, point mutation of the Val-418, Leu-557, Val-514, Val-561, and Thr-560 sites on KEAP1 was necessary to verify the correctness of the results.

5. In the investigation of the biological activity of fucoidan, we have neglected the effect of fucoidan's own structure on the organism. Due to the complexity of fucoidan and the limitation of experimental time, the structural analysis of fucoidan is still at a superficial level

and the conformational relationship of fucoidan is still a major problem and deserves a lot of efforts to continue the research.

6. In addition to insulin resistance, other metabolic disturbances induced by a high-fat diet can be alleviated by SFF, such as reduced body weight, reduced TG and T-CHO in serum and liver, etc. In our preliminary investigation, we found that the lipolytic enzyme Cpt1 in the liver was significantly increased in the HFD+SFF group and the thermogenic gene Ucp1 was dramatically upregulated in white adipose tissue, which could be a key reason for the reduction of body weight and TG by SFF and deserves further investigation.

References

1. Chen Z, Liu J, Fu ZF, Ye C, Zhang RS, Song YY, et al. 24(S)-Saringosterol from edible marine seaweed *Sargassum fusiforme* is a novel selective LXR β agonist. *J. Agric. Food Chem.* 2014, 64: 6130-6137.
2. Mao WJ, Li BF, Gu QQ, Fang YC, Xing HT. Preliminary studies on the chemical characterization and antihyperlipidemic activity of polysaccharide from the brown alga *Sargassum fusiforme*. *Hydrobiologia.* 2004, 512: 263–266.
3. Huang XX, Zhou HQ, Zhang H. The effect of *Sargassum fusiforme* polysaccharide extracts on vibriosis resistance and immune activity of the shrimp, *Fenneropenaeus chinensis*. *Fish Shellfish Immunol.* 2006, 20: 750-757.
4. Hu ZM, Zhang J, Bautista JL, Duan DL. Asymmetric genetic exchange in the brown seaweed *Sargassum fusiforme* (Phaeophyceae) driven by oceanic currents. *Mar. Biol.* 2013, 160: 1407–1414.
5. Luthuli S, Wu SY, Cheng Y, Zheng XL, Wu MJ, Tong HB. Therapeutic effects of fucoidan: A review on recent studies. *Mar. Drugs.* 2019, 17: e487.
6. Wu XD, Jiang W, Lu JJ, Yu J, Wu B. Analysis of the monosaccharide composition of water-soluble polysaccharides from *Sargassum fusiforme* by high performance liquid chromatography/electrospray ionisation mass spectrometry. *Food Chem.* 2014, 145: 976-983.
7. Pomin VH, Mourão PA. Structure, biology, evolution, and medical importance of sulfated fucans and galactans. *Glycobiology.* 2008, 18: 1016–1027.
8. Morya VK, Kim J, Kim EK. Algal fucoidan: Structural and size-dependent bioactivities and their perspectives. *Appl. Microbiol. Biotechnol.* 2012, 93: 71–82.
9. Zhang R, Zhang X, Tang Y, Mao J. Composition, isolation, purification and biological activities of *Sargassum fusiforme* polysaccharides: A review. *Carbohydr. Polym.* 2020, 228: e115381.
10. Chen XM, Nie WJ, Yu GQ, Li YL, Hu YS, Lu JX. Antitumor and immunomodulatory activity of polysaccharides from *Sargassum fusiforme*. *Food Chem. Toxicol.* 2012, 50: 695–700.
11. Chen BJ, Shi MJ, Cui S, Hao SX, Hider RT, Zhou T. Improved antioxidant and anti-tyrosinase activity of polysaccharide from *Sargassum fusiforme* by degradation. *Int. J. Biol. Macromol.* 2016, 92: 715–722.

12. Milburn MV, Lawton KA. Application of metabolomics to diagnosis of insulin resistance. *Annual review of medicine*. 2013, 64: 291-305.
13. Wishart DS, Feunang YD, Marcu A. HMDB: the human metabolome database for 2018. *Nucleic acids research*. 2018, 46: 608-617.
14. Ma Q, Li Y, Wang M. Progress in metabonomics of type 2 diabetes mellitus. *Molecules*, 2018, 23(7): 1834.
15. Wu GJ. Improving effects of polysaccharide from adzuki bean on type 2 diabetes and its mechanism. Nanchang university. 2020.
16. Louis JS, Martirosyan D. Nutritionally attenuating the human gut microbiome to prevent and manage metabolic syndrome. *J. Agric. Food Chem*. 2019, 67: 125675-12684.
17. Shang QS, Jiang H, Cai C, Hao JJ, Li GY, Yu GL. Gut microbiota fermentation of marine polysaccharides and its effects on intestinal ecology: An overview. *Carbohydr. Polym*. 2018, 179: 173-185.
18. Shang QS, Shan XD, Cai C, Hao JJ, Li GY, Yu GL. Dietary fucoidan modulates the gut microbiota in mice by increasing the abundance of Lactobacillus and Ruminococcaceae. *Food Funct*. 2016, 7: 3224-3232.
19. Chang CJ, Lin CS, Lu CC, Martel J, Ko YF, Ojcius DM. Ganoderma lucidum reduces obesity in mice by modulating the composition of the gut microbiota. *Nat Commun*. 2015, 6: e7489.
20. Wu TR, Lin CS, Chang CJ, Lin TL, Martel J, Ko YF. Gut commensal Parabacteroides goldsteinii plays a predominant role in the anti-obesity effects of polysaccharides isolated from *Hirsutella sinensis*. *Gut*. 2018, 14: 1-13.
21. Biddinger SB, Kahn CR. From mice to men: Insights into the insulin resistance syndromes. *Annu. Rev. Physiol*. 2006, 68: 123-158.
22. Muoio DM, Newgard CB. Mechanisms of disease: Molecular and metabolic mechanisms of insulin resistance and beta-cell failure in type 2 diabetes. *Nat. Rev. Mol. Cell. Biol*. 2008, 9: 193-205.
23. Finck BN. Targeting metabolism, insulin resistance, and diabetes to treat nonalcoholic steatohepatitis. *Diabetes*. 2008, 67: 2485-2893.
24. Kahn SE, Hull RL, Utzschneider KM. Mechanisms linking obesity to insulin resistance and type 2 diabetes. *Nature*. 2006, 444: 840-886.
25. Rani V, Deep G, Singh RK, Palle K, Yadav UC. Oxidative stress and metabolic disorders:

- Pathogenesis and therapeutic strategies. *Life Sci.* 2016, 148: 183-193.
26. Savage DB, Petersen KF, Shulman GL. Disordered lipid metabolism and the pathogenesis of insulin resistance. *Physiol. Rev.* 2007, 87: 507-520.
 27. Jiménez-Osorio AS, González-Reyes S, Pedraza-Chaverri J. Natural Nrf2 activators in diabetes. *Clin. Chim. Acta.* 2015, 448: 182-192.
 28. Hu D, Bao T, Lu Y, Su H, Ke H, Chen W. Polysaccharide from mulberry fruit (*Morus alba* L.) protects against palmitic-acid-induced hepatocyte lipotoxicity by activating the Nrf2/ARE signaling pathway. *J. Agric, Food Chem.* 2019, e03335.
 29. David JA, Rifkin WJ, Rabbani PS, Ceradini DJ. The Nrf2/Keap1/ARE pathway and oxidative stress as a therapeutic target in type II diabetes mellitus. *J. Diabetes Res.* 2017, 17: e4826724.
 30. Eo H, Park JE, Jeon YJ, Lim Y. Ameliorative effect of *Ecklonia cava* polyphenol extract on renal inflammation associated with aberrant energy metabolism and oxidative stress in HFD-induced obese mice. *J. Agric, Food Chem.* 2017, 65: 3811-3818.
 31. Elmus GB. Insulin signaling and insulin resistance. *J Investig Med.* 2013, 61(1): 11-14.
 32. Michael PC. Insulin action and resistance in obesity and type 2 diabetes. *Nat Med.* 2017, 23(7): 804-814.
 33. Ryder JW, Gilbert M, Zierath JR. Skeletal muscle and insulin sensitivity: pathophysiological alterations. *Front Biosci.* 2001, 6: 154–163.
 34. DeFronzo RA. Insulin resistance, lipotoxicity, type 2 diabetes and atherosclerosis: the missing links. The Claude Bernard Lecture 2009. *Diabetologia.* 2010, 53: 1270–1287.
 35. Popkin BM, Adair LS, Ng SW. Global nutrition transition and the pandemic of obesity in developing countries. *Nutr Rev.* 2012, 70(1): 3–21.
 36. American Medical Association House of Delegates. *Resolution.* 2013, 420.
 37. Pataky Z, Bobbioni-Harsch E, Golay A. Open questions about metabolically normal obesity. *Int J Obes (Lond).* 2010, 34(2): 18-23.
 38. Alberti KG, Eckel RH, Grundy SM, Zimmet PZ, Cleeman JI, Donato KA, et al. Harmonizing the metabolic syndrome: a joint interim statement of the International Diabetes Federation Task Force on Epidemiology and Prevention; National Heart, Lung, and Blood Institute; American Heart Association; World Heart Federation; International Atherosclerosis Society; and International Association for the Study of Obesity. *Circulation.* 2010, 120(16): 1640–1645.

39. Barazzonil R, Cappellari GG, Ragni M, Nisoli E. Insulin resistance in obesity: an overview of fundamental alterations. *Eating and weight disorders-studies on Anorexia, Bulimia and Obesity*. 2018, 23: 149-157.
40. Pizzino G, Irrera N, Cucinotta M, Pallio G, Mannino F, Arcoraci V, et al. Oxidative Stress: Harms and Benefits for Human Health. *Oxid. Med. Cell Longev*. 2017, e8416763.
41. Di MS, Reed TT, Venditti P, Victor VM. Harmful and Beneficial Role of ROS. *Oxid. Med. Cell Longev*. 2016, e7909186.
42. Moloney JN, Cotter TG. ROS signalling in the biology of cancer. *Semin. Cell Dev. Biol*. 2018, 80: 50–64.
43. Savini I, Catani MV, Evangelista D, Gasperi V, Avigliano L. Obesity-associated oxidative stress: Strategies finalized to improve redox state. *Int. J. Mol. Sci*. 2013, 14: 10497–10538.
44. Serra D, Mera P, Malandrino MI, Mir JF, Herrero L. Mitochondrial fatty acid oxidation in obesity. *Antioxid. Redox Signal*. 2013, 19: 269–284.
45. Manna P, Jain SK. Obesity, oxidative stress, adipose tissue dysfunction, and the associated health risks: causes and therapeutic strategies. *Metab. Syndr. Relat. Disord*. 2015, 13: 423–444.
46. Furukawa S, Fujita T, Shimabukuro M, Iwaki M, Yamada Y, Nakajima Y, et al. Increased oxidative stress in obesity and its impact on metabolic syndrome. *J. Clin. Investig*. 2004, 114: 1752–1761.
47. Horvath TL, Andrews ZB, Diano S. Fuel utilization by hypothalamic neurons: Roles for ROS. *Trends Endocrinol. Metab*. 2009, 20: 78–87.
48. Reuter S, Gupta SC, Chaturvedi MM, Aggarwal BB. Oxidative stress, inflammation, and cancer: How are they linked? *Free Radic. Biol. Med*. 2010, 49: 1603–1616.
49. Chartoumpekis DV, Ziros PG, Psyrogiannis AI, Papavassiliou AG, Kyriazopoulou VE, Sykiotis GP, et al. Nrf2 represses FGF21 during long-term high-fat diet-induced obesity in mice. *Diabetes*, 2011, 60: 2465–2473.
50. Shin S, Wakabayashi J, Yates MS, Wakabayashi N, Dolan PM, Aja S, et al. Role of Nrf2 in prevention of high-fat diet-induced obesity by synthetic triterpenoid CDDO-imidazolide. *Eur. J. Pharmacol*. 2009, 620: 138–144.
51. Liu Z, Dou W, Ni Z, Wen Q, Zhang R, Qin M, et al. Deletion of Nrf2 leads to hepatic insulin resistance via the activation of NF-kappaB in mice fed a high-fat diet. *Mol. Med. Rep*. 2016, 14: 1323–1331.

52. Pi J, Leung L, Xue P, Wang W, Hou Y, Liu D, et al. Deficiency in the nuclear factor E2-related factor-2 transcription factor results in impaired adipogenesis and protects against diet-induced obesity. *J. Biol. Chem.* 2010, 285: 9292–9300.
53. Slocum SL, Skoko JJ, Wakabayashi N, Aja S, Yamamoto M, Kensler TW, et al. Keap1/Nrf2 pathway activation leads to a repressed hepatic gluconeogenic and lipogenic program in mice on a high-fat diet. *Arch. Biochem. Biophys.* 2016, 591: 57–65.
54. Xu J, Kulkarni SR, Donepudi AC, More VR, Slitt AL. Enhanced Nrf2 activity worsens insulin resistance, impairs lipid accumulation in adipose tissue, and increases hepatic steatosis in leptin-deficient mice. *Diabetes.* 2012, 61: 3208–3218.
55. Zhang YK, Wu KC, Liu J, Klaassen CD. Nrf2 deficiency improves glucose tolerance in mice fed a high-fat diet. *Toxicol. Appl. Pharmacol.* 2012, 264: 305–314.
56. Yu Z, Shao W, Chiang Y, Foltz W, Zhang Z, Ling W, et al. Oltipraz upregulates the nuclear factor (erythroid-derived 2)-like 2 [corrected](NRF2) antioxidant system and prevents insulin resistance and obesity induced by a high-fat diet in C57BL/6J mice. *Diabetologia.* 2011, 54: 922–934.
57. Sampath C, Rashid MR, Sang S, Ahmedna M. Green tea epigallocatechin 3-gallate alleviates hyperglycemia and reduces advanced glycation end products via nrf2 pathway in mice with high fat diet-induced obesity. *Biomed. Pharmacother.* 2017, 87: 73–81.
58. Kim CY, Kang B, Suh HJ, Choi HS. Parthenolide, a feverfew-derived phytochemical, ameliorates obesity and obesity-induced inflammatory responses via the Nrf2/Keap1 pathway. *Pharmacol. Res.* 2019, 145: 104259.
59. Meher AK, Sharma PR, Lira VA, Yamamoto M, Kensler TW, Yan Z, et al. Nrf2 deficiency in myeloid cells is not sufficient to protect mice from high-fat diet-induced adipose tissue inflammation and insulin resistance. *Free Radic. Biol. Med.* 2012, 52: 1708–1715.
60. Li S, Eguchi N, Lau H, Ichii H. The role of the Nrf2 signaling in obesity and insulin resistance. *Int J Mol Sci.* 2020, 21: 6973.
61. Yu M, Li H, Liu Q, Liu F, Tang L, Li C, et al. Nuclear factor p65 interacts with Keap1 to repress the Nrf2-ARE pathway. *Cell Signal.* 2011, 23: 883–892.
62. Kobayashi A, Kang MI, Watai Y, Tong KI, Shibata T, Uchida K, et al. Oxidative and electrophilic stresses activate Nrf2 through inhibition of ubiquitination activity of Keap1. *Mol. Cell. Biol.* 2006, 26: 221–229.

63. Ishii T, Itoh K, Takahashi S, Sato H, Yanagawa T, Katoh Y, et al. Transcription factor Nrf2 coordinately regulates a group of oxidative stress-inducible genes in macrophages. *J. Biol. Chem.* 2000, 275: 16023–16029.
64. Chartoumpekis DV, Palliyaguru DL, Wakabayashi N, Fazzari M, Khoo NKH, Schopfer FJ, et al. Nrf2 deletion from adipocytes, but not hepatocytes, potentiates systemic metabolic dysfunction after long-term high-fat diet-induced obesity in mice. *Am. J. Physiol. Endocrinol. Metab.* 2018, 315: 180–195.
65. Xue P, Hou Y, Chen Y, Yang B, Fu J, Zheng H, Yarborough K, et al. Adipose deficiency of Nrf2 in ob/ob mice results in severe metabolic syndrome. *Diabetes* 2013, 62: 845–854.
66. Uruno A, Yagishita Y, Katsuoka F, Kitajima Y, Nunomiya A, Nagatomi R, et al. Nrf2-Mediated Regulation of Skeletal Muscle Glycogen Metabolism. *Mol. Cell Biol.* 2016, 36: 1655–1672.
67. Chartoumpekis DV, Yagishita Y, Fazzari M, Palliyaguru DL, Rao UN, Zaravinos A, et al. Nrf2 prevents Notch-induced insulin resistance and tumorigenesis in mice. *JCI Insight.* 2018, 3: e97735.
68. Fernandez-Sanchez A, Madrigal-Santillan E, Bautista M, Esquivel-Soto J, Morales-Gonzalez A, Esquivel-Chirino C, et al. Inflammation, oxidative stress, and obesity. *Int. J. Mol. Sci.* 2011, 12: 3117–3132.
69. Ozata M, Mergen M, Oktenli C, Aydin A, Sanisoglu SY, Bolu E, et al. Increased oxidative stress and hypozincemia in male obesity. *Clin. Biochem.* 2002, 35: 627–631.
70. Capel ID, Dorrell HM. Abnormal antioxidant defence in some tissues of congenitally obese mice. *Biochem. J.* 1984, 219: 41–49.
71. Cheng AS, Cheng YH, Chiou CH, Chang TL. Resveratrol upregulates Nrf2 expression to attenuate methylglyoxal-induced insulin resistance in Hep G2 cells. *J. Agric. Food Chem.* 2012, 60: 9180–9187.
72. He HJ, Wang GY, Gao Y, Ling WH, Yu ZW, Jin TR. Curcumin attenuates Nrf2 signaling defect, oxidative stress in muscle and glucose intolerance in high fat diet-fed mice. *World J. Diabetes* 2012, 3: 94–104.
73. Zhai Y, Meng X, Luo Y, Wu Y, Ye T, Zhou P, et al. Notoginsenoside R1 ameliorates diabetic encephalopathy by activating the Nrf2 pathway and inhibiting NLRP3 inflammasome activation. *Oncotarget.* 2018, 9: 9344–9363.
74. Ng M, Fleming T, Robinson M, Thomson B, Graetz N, et al. Global, regional, and national

- prevalence of overweight and obesity in children and adults during 1980–2013: a systematic analysis for the Global Burden of Disease Study 2013. *Lancet*. 2014, 384(9945): 766–781.
75. Swinburn BA, Sacks G, Hall KD, McPherson K, Finegood DT, Moodie ML, et al. The global obesity pandemic: shaped by global drivers and local environments. *Lancet*. 2011, 378 (9793): 804–814.
 76. Hill JO. Understanding and addressing the epidemic of obesity: an energy balance perspective. *Endocr Rev*. 2006, 27(7):750–761.
 77. Clavel T, Desmarchelier C, Haller D, Gerard P, Rohn S, Lepage P, et al. Intestinal microbiota in metabolic diseases: from bacterial community structure and functions to species of pathophysiological relevance. *Gut Microbes*. 2014, 5(4): 544–551.
 78. Rosenbaum M, Knight R, Leibel RL. The gut microbiota in human energy homeostasis and obesity. *Trends Endocrinol Metab*. 2015, 26(9): 493–501.
 79. Aagaard K, Ma J, Antony KM, Ganu R, Petrosino J, Versalovic J. The placenta harbors a unique microbiome. *Sci Transl Med*. 2014, 6(237): 237-265.
 80. Palmer C, Bik EM, DiGiulio DB, Relman DA, Brown PO. Development of the human infant intestinal microbiota. *PLoS Biol*. 2007, 5(7): e177.
 81. Koenig JE, Spor A, Scalfone N, Fricker AD, Stombaugh J, Knight R, Angenent LT, Ley RE. Succession of microbial consortia in the developing infant gut microbiome. *Proc Natl Acad Sci USA*. 2011, 108(1): 4578–4585.
 82. Faith JJ, Guruge JL, Charbonneau M, Subramanian S, Seedorf H, Goodman AL, et al. The long-term stability of the human gut microbiota. *Science*. 2013, 341(6141): 1237439.
 83. Dethlefsen L, Huse S, Sogin ML, Relman DA. The pervasive effects of an antibiotic on the human gut microbiota, as revealed by deep 16S rRNA sequencing. *PLoS Biol*. 2008, 6(11): e280.
 84. Dethlefsen L, Relman DA. Incomplete recovery and individualized responses of the human distal gut microbiota to repeated antibiotic perturbation. *Proc Natl Acad Sci USA*. 2011, 108(1): 4554–4561.
 85. Zhang C, Zhang M, Wang S, Han R, Cao Y, Hua W, et al. Interactions between gut microbiota, host genetics and diet relevant to development of metabolic syndromes in mice. *ISME J*. 2010, 4(2): 232–241.
 86. Turnbaugh PJ, Hamady M, Yatsunenko T, Cantarel BL, Duncan A, Ley RE, et al. A core

- gut microbiome in obese and lean twins. *Nature*. 2009, 457(7228): 480–484
87. Lozupone CA, Stombaugh JI, Gordon JI, Jansson JK, Knight R. Diversity, stability and resilience of the human gut microbiota. *Nature*. 2012, 489(7415): 220–230.
 88. Franzosa EA, Huang K, Meadow JF, Gevers D, Lemon KP, Bohannan BJ, Huttenhower C. Identifying personal microbiomes using metagenomic codes. *Proc Natl Acad Sci USA*. 2015, 112(22): 2930–2938.
 89. Ley RE, Hamady M, Lozupone C, Turnbaugh PJ, Ramey RR, Bircher JS, Schlegel ML, Tucker TA, Schrenzel MD, Knight R, Gordon JI. Evolution of mammals and their gut microbes. *Science*. 2008, 320(5883): 1647–1651.
 90. O’Hara AM, Shanahan F. The gut flora as a forgotten organ. *EMBO Rep*. 2006, 7(7): 688–693.
 91. Olsen GJ, Lane DJ, Giovannoni SJ, Pace NR, Stahl DA. Microbial ecology and evolution: a ribosomal RNA approach. *Annu Rev Microbiol*. 1986, 40: 337–365.
 92. Ge´rard P. Le microbiote intestinal: composition et fonctions. *Phytothe’rapie*. 2011, 9(2): 72–75
 93. Eckburg PB, Bik EM, Bernstein CN, Purdom E, Dethlefsen L, Sargent M, et al. Diversity of the human intestinal microbial flora. *Science*. 2005, 308(5728): 1635–1638.
 94. Frank DN, St Amand AL, Feldman RA, Boedeker EC, Harpaz N, Pace NR. Molecular-phylogenetic characterization of microbial community imbalances in human inflammatory bowel diseases. *Proc Natl Acad Sci USA*. 2007, 104(34): 13780–13785.
 95. Hsiao WW, Fraser-Liggett CM. Human Microbiome Project—paving the way to a better understanding of ourselves and our microbes. *Drug Discov Today*. 2009, 14(7–8): 331–333.
 96. Turnbaugh PJ, Ley RE, Hamady M, Fraser-Liggett CM, Knight R, Gordon JI. The human microbiome project. *Nature*. 2007, 449(7164):804–810.
 97. Frank DN, Pace NR. Gastrointestinal microbiology enters the metagenomics era. *Curr Opin Gastroenterol*. 2008, 24(1):4–10.
 98. Gill SR, Pop M, Deboy RT, Eckburg PB, Turnbaugh PJ, Samuel BS, Gordon JI, Relman DA, Fraser-Liggett CM, Nelson KE. Metagenomic analysis of the human distal gut microbiome. *Science*. 2006, 312(5778):1355–1359.
 99. Li J, Jia H, Cai X, Zhong H, Feng Q, Sunagawa S, et al. An integrated catalog of reference genes in the human gut microbiome. *Nat Biotechnol*. 2014, 32(8):834–841.
 100. Dethlefsen L, McFall-Ngai M, Relman DA. An ecological and evolutionary perspective

- on human-microbe mutualism and disease. *Nature*. 2007, 449(7164):811–818.
101. Qin J, Li R, Raes J, Arumugam M, Burgdorf KS, Manichanh C, et al. A human gut microbial gene catalogue established by metagenomic sequencing. *Nature*. 2010, 464(7285):59–65.
 102. Arumugam M, Raes J, Pelletier E, Le Paslier D, Yamada T, Mende DR, et al. Enterotypes of the human gut microbiome. *Nature*. 2011, 473(7346):174–180.
 103. Wu GD, Chen J, Hoffmann C, Bittinger K, Chen YY, Keilbaugh SA, et al. Linking long-term dietary patterns with gut microbial enterotypes. *Science*. 2011, 334(6052):105–108.
 104. Knights D, Ward TL, McKinlay CE, Miller H, Gonzalez A, McDonald D, Knight R. Rethinking “enterotypes”. *Cell Host Microbe*. 2014, 16(4):433–437.
 105. Backhed F, Ley RE, Sonnenburg JL, Peterson DA, Gordon JI. Host-bacterial mutualism in the human intestine. *Science*. 2005, 307(5717):1915–1920.
 106. Hooper LV, Midtvedt T, Gordon JI. How host-microbial interactions shape the nutrient environment of the mammalian intestine. *Annu Rev Nutr*. 2002, 22:283–307.
 107. Ge´rard P, Bernalier-Donadille A. Les fonctions majeures du microbiote intestinal. *Cahiers de Nutrition et de Diete´tique*. 2007, 42:28–36.
 108. Backhed F, Fraser CM, Ringel Y, Sanders ME, Sartor RB, Sherman PM, et al. Defining a healthy human gut microbiome: current concepts, future directions, and clinical applications. *Cell Host Microbe*. 2012, 12(5):611–622.
 109. Cotillard A, Kennedy SP, Kong LC, Prifti E, Pons N, Le Chatelier E, et al. Dietary intervention impact on gut microbial gene richness. *Nature*. 2013, 500(7464):585–588.
 110. Mondot S, de Wouters T, Dore J, Lepage P. The human gut microbiome and its dysfunctions. *Dig Dis*. 2013, 31(3–4):278–285.
 111. Turnbaugh PJ, Backhed F, Fulton L, Gordon JI. Diet-induced obesity is linked to marked but reversible alterations in the mouse distal gut microbiome. *Cell Host Microbe*. 2008, 3(4):213–223.
 112. Turnbaugh PJ, Ridaura VK, Faith JJ, Rey FE, Knight R, Gordon JI. The effect of diet on the human gut microbiome: a metagenomic analysis in humanized gnotobiotic mice. *Sci Transl Med*. 2009, (6):6-14.
 113. Ridaura VK, Faith JJ, Rey FE, Cheng J, Duncan AE, Kau AL, et al. Gut microbiota from twins discordant for obesity modulate metabolism in mice. *Science*. 2013, 341(6150):1241214.

114. Vijay-Kumar M, Aitken JD, Carvalho FA, Cullender TC, Mwangi S, Srinivasan S, et al. Metabolic syndrome and altered gut microbiota in mice lacking Toll-like receptor 5. *Science*. 2010, 328(5975):228–231.
115. Di Luccia B, Crescenzo R, Mazzoli A, Cigliano L, Venditti P, Walser JC, et al. Rescue of fructose-induced metabolic syndrome by antibiotics or faecal transplantation in a rat model of obesity. *PLoS One*. 2015, 10(8):e0134893.
116. Blunt JW, Copp BR, Hu WP, Munro MHG, Northcote PT, Prinsep MR. Marine natural products. *Nat. Prod. Rep.* 2007, 24, 31–86.
117. Rajasulochana P, Dhamotharan R, Krishnamoorthy P, Murugesan S. Antibacterial activity of the extracts of marine red and brown algae. *J. Am. Sci.* 2009, 5, 20–25.
118. Liu X, Du P, Liu X, Cao S, Qin L, He M, et al. Anticoagulant properties of a green algal phanman-type sulfated polysaccharide and its low-molecular-weight fragments prepared by mild acid degradation. *Mar. Drugs*. 2018, 16: 445.
119. Chandini SK, Ganesan P, Bhaskar N. In vitro antioxidant activities of three selected brown seaweeds of India. *Food Chem.* 2008, 107, 707–713.
120. Gomes DL, Melo KRT, Queiroz MF, Batista LANC, Santos PC, Costa MSSP, et al. In vitro studies reveal antiurolithic effect of antioxidant sulfated polysaccharides from the green seaweed *Caulerpa cupressoides* var *flabellata*. *Mar. Drugs*. 2019, 17: 326.
121. Liu L, Heinrich M, Myres S, Dworjanyn SA. Towards a better understanding of medicinal uses of the brown seaweed *Sargassum* in traditional Chinese medicine: A phytochemical and pharmacological review. *J. Ethnopharmacol.* 2012, 142: 591–619.
122. Yoo HJ, You DJ, Lee KW. Characterization and immunomodulatory effects of high molecular weight fucoidan fraction from the Sporophyll of *Undaria pinnatifida* in cyclophosphamide-induced immunosuppressed mice. *Mar. Drugs*. 2019, 17: 447.
123. McDowell PE. In *Methods in Plant Biochemistry*, 1st ed, Elsevier: Amsterdam, The Netherlands. 1990, 2: 523–547.
124. Cui K, Tai W, Shan X, Hao J, Li G, Yu G. Structural characterization and anti-thrombotic properties of fucoidan from *Nemacystus decipiens*. *Int. J. Biol. Macromol.* 2018, 120: 1817–1822.
125. Yokota T, Nomura K, Nagashima M, Kamimura N. Fucoidan alleviates high-fat diet-induced dyslipidemia and atherosclerosis in ApoEshl mice deficient in apolipoprotein E expression. *J. Nutr. Biochem.* 2016, 32:46–54.

126. Koh HSA, Lu J, Zhou W. Structure characterization and antioxidant activity of fucoidan isolated from *Undaria pinnatifida* grown in New Zealand. *Carbohydr. Polym.* 2019, 212: 178–185.
127. Jin W, Wu W, Tang H, Wei B, Wang H, Sun J, et al. Structure analysis and anti-tumor and anti-angiogenic activities of sulfated galactofucan extracted from *Sargassum thunbergii*. *Mar. Drugs.* 2019, 17: 52.
128. Usoltseva RV, Anastyuk SD, Surits VV, Shevchenko NM, Thinh PD, Zadorozhny PA, Ermakova SP. Comparison of structure and in vitro anticancer activity of native and modified fucoidans from *Sargassum feldmannii* and *S. duplicatum*. *Int. J. Biol. Macromol.* 2019, 124: 220–228.
129. Usoltseva RV, Shevchenko NM, Malyarenko OS, Anastyuk SD, Kaspruk AE, Zvyagintsev NV, et al. Fucoidans from brown algae *Laminaria longipes* and *Saccharina cichorioides*: Structural characteristics, anticancer and radio-sensitizing activity in vitro. *Carbohydr. Polym.* 2019, 221: 157–165.
130. Lahrsen E, Liewert I, Alban S. Gradual degradation of fucoidan from *Fucus vesiculosus* and its effect on structure, antioxidant and antiproliferative activities. *Carbohydr. Polym.* 2018, 192: 208–216.
131. Zhang Z, Till S, Jiang C, Knappe S, Reutterer S, Scheiflinger F, et al. Structure-activity relationship of the pro- and anticoagulant effects of *Fucus vesiculosus* fucoidan. *Thromb. Haemost.* 2014, 111: 429–437.
132. Bilan MI, Grachev AA, Ustuzhanina NE, Shashkov AS, Nifantiev NE, Usov AI. A highly regular fraction of a fucoidan from the brown seaweed *Fucus distichus* L. *Carbohydr. Res.* 2004, 339: 511–517.
133. Descamps V, Colin S, Lahaye M, Jam M, Richard C, Potin P, et al. Isolation and culture of a marine bacterium degrading the sulfated fucans from marine brown algae. *Mar. Biotechnol.* 2006, 8: 27–39.
134. Jabbar Mian A, Percival E. Carbohydrates of the brown seaweeds *Himanthalia lorea* and *Bifurcaria bifurcata*: Part II. structural studies of the “fucans”. *Carbohydr. Res.* 1973, 26: 147–161.
135. Mak W, Hamid N, Liu T, Lu J, White WL. Fucoidan from New Zealand *Undaria pinnatifida*: Monthly variations and determination of antioxidant activities. *Carbohydr. Polym.* 2013, 95: 606–614.

136. Fletcher HR, Biller P, Ross AB, Adams JMM. The seasonal variation of fucoidan within three species of brown macroalgae. *Algal Res.* 2017, 22: 79–86.
137. Garcia-Vaquero M, Rajauria G, O’Doherty JV, Sweeney T. Polysaccharides from macroalgae: Recent advances, innovative technologies and challenges in extraction and purification. *Food Res. Int.* 2017, 99: 1011–1020.
138. Chevlot L, Foucault A, Chaubet F, Kervarec N, Siquin C, Fisher AM, et al. Further data on the structure of brown seaweed fucans: Relationships with anticoagulant activity. *Carbohydr. Res.* 1999, 319: 154–165.
139. Marais MF, Joseleau JP. A fucoidan fraction from *Ascophyllum nodosum*. *Carbohydr. Res.* 2001, 336: 155–159.
140. Ponce NMA, Pujol CA, Damonte EB, Flores ML, Stortz CA. Fucoidans from the brown seaweed *Adenocystis utricularis*: Extraction methods, antiviral activity and structural studies. *Carbohydr. Res.* 2003, 338: 153–165.
141. Shan XD, Liu X, Hao JJ, Cai C, Fan F, Dun YL, et al. In vitro and in vivo hypoglycemic effects of brown algal fucoidans. *Int. J. Biol. Macromol.* 2016, 82: 249–255.
142. Yang WZ, Yu XF, Zhang QB, Lu QJ, Wang J, Cui WT, et al. Attenuation of streptozotocin-induced diabetic retinopathy with low molecular weight fucoidan via inhibition of vascular endothelial growth factor. *Exp. Eye Res.* 2013, 115: 96–105.
143. Cui W, Zheng Y, Zhang Q, Wang J, Wang L, Yang W, et al. Low-molecular-weight fucoidan protects endothelial function and ameliorates basal hypertension in diabetic Goto-Kakizaki rats. *Lab. Investig.* 2014, 94: 382–393.
144. Jeong YT, Kim YD, Jung YM, Park DC, Lee DS, Ku SK, et al. Low molecular weight fucoidan improves endoplasmic reticulum stress-reduced insulin sensitivity through AMP-Activated protein kinase activation in L6 myotubes and restores lipid homeostasis in a mouse model of type 2 diabetes. *Mol. Pharmacol.* 2013, 84: 147–157.
145. Hu SW, Xia GH, Wang JF, Wang YM, Li ZJ, Xue CH. Fucoidan from sea cucumber protects against high-fat high-sucrose diet-induced hyperglycaemia and insulin resistance in mice. *J. Funct. Foods.* 2014, 10: 128–138.
146. Chen Q, Liu M, Zhang P, Fan S, Huang J, Yu S, Zhang C, Li H. Fucoidan and galacto-oligosaccharides ameliorate high-fat diet-induced dyslipidemia in rats by modulating the gut microbiota and bile acid metabolism. *Nutrition.* 2019, 65: 50–59.
147. Li S, Li J, Mao G, Wu T, Hu Y, Ye X, Tian D, et al. A fucoidan from sea cucumber

- Pearsonothuria graeffei with well-repeated structure alleviates gut microbiota dysbiosis and metabolic syndromes in HFD-fed mice. *Food Funct.* 2018, 9: 5371–5380.
148. Parnell JA, Reimer RA. Prebiotic fiber modulation of the gut microbiota improves risk factors for obesity and the metabolic syndrome. *Gut Microbes.* 2012, 3: 29–34.
 149. Cheng Y, Luthuli S, Hou LF, Jiang HJ, Chen PC, Zhang X, et al. *Sargassum fusiforme* fucoidan modifies the gut microbiota during alleviation of streptozotocin-induced hyperglycemia in mice. *Int. J. Biol. Macromol.* 2019, 131: 1162–1170.
 150. Sohal RS, Orr WC. The redox stress hypothesis of aging. *Free Radical Biology & Medicine.* 2012, 52(3): 539–555.
 151. Hernandez-Segura A, Nehme J, Demaria M. Hallmarks of cellular senescence. *Trends in Cell Biology.* 2018, 28(6) : 436–453.
 152. López-Otín C, Blasco MA, Partridge L, Serrano M, Kroemer G. The hallmarks of aging. *Cell.* 2013, 153(6): 1194–1217.
 153. Finkel T, Holbrook NJ. Oxidants, oxidative stress and the biology of ageing. *Nature.* 2000, 408(6809): 239–247.
 154. Harman D. Free radical theory of aging: an update: increasing the functional life span. *Annals of the New York Academy of Science.* 2006, 1067:10–21.
 155. Back P, de Vos WH, Depuydt GG, Matthijssens F, Vanfleteren JR, Braeckman BP. Exploring real-time in vivo redox biology of developing and aging *Caenorhabditis elegans*. *Free Radical Biology & Medicine.* 2012, 52(5): 850–859.
 156. Lustgarten M, Muller FL, Van Remmen H. An Objective Appraisal of the Free Radical Theory of Aging. in *Handbook of the Biology of Aging, E. J. Masoro and S. N. Austad, Eds.* 2011: 177–202
 157. Yang CS, Suh N, Kong ANT. Does vitamin E prevent or promote cancer. *Cancer Prevention Research.* 2012, 5(5): 701–705.
 158. Marantz PR, Kritchevsky D, Goldstein MR. Beta carotene, vitamin E, and lung cancer. *The New England Journal of Medicine.* 1994, 331(9): 611–614.
 159. Malhotra D, Portales-Casamar E, Singh A, et al. Global mapping of binding sites for Nrf2 identifies novel targets in cell survival response through ChIP-Seq profiling and network analysis. *Nucleic Acids Research.* 2010, 38(17): 5718– 5734.
 160. Lewis KN, Mele J, Hayes JD, Buffenstein R. Nrf2, a guardian of healthspan and gatekeeper of species longevity. *Integrative and Comparative Biology.* 2010, 50(5): 829–

- 843.
161. Sykiotis GP, Bohmann D. Keap1/Nrf2 signaling regulates oxidative stress tolerance and lifespan in *Drosophila*. *Developmental Cell*. 2008, 14: 76–85.
 162. Bruns DR, Drake JC, Biela LM, Peelor FF, Miller BF, Hamilton KL. Nrf2 signaling and the slowed aging phenotype: evidence from long-lived models. *Oxidative Medicine and Cellular Longevity*. 2015, 15: e732596.
 163. Miller CJ, Gounder SS, Kannan S. Disruption of Nrf2/ARE signaling impairs antioxidant mechanisms and promotes cell degradation pathways in aged skeletal muscle. *Biochimica et Biophysica Acta*. 2012, 1822(6): 1038–1050.
 164. Lewis KN, Wason E, Edrey YH, Kristan DM, Nevo E, Buffenstein R. Regulation of Nrf2 signaling and longevity in naturally long-lived rodents. *Proc Natl Acad Sci USA*. 2015, 112:3722–3727.
 165. Zamponi E, Zamponi N, Coskun P. Nrf2 stabilization prevents critical oxidative damage in Down syndrome cells. *Aging Cell*. 2018, 17(5):e12812.
 166. Zhang H, Davies KJA, Forman HJ. Oxidative stress response and Nrf2 signaling in aging. *Free Rad Bio Med*. 2015, 88:314–336.
 167. Fan S, Zhang J, Nie W, et al. Antitumor effects of polysaccharide from *Sargassum fusiforme* against human hepatocellular carcinoma HepG2 cells. *Food Chem Toxic*. 2017, 102: 53–62.
 168. Chen L, Chen P, Liu J, et al. *Sargassum Fusiforme* Polysaccharide SFP-F2 Activates the NF- κ B Signaling Pathway via CD14/IKK and P38 Axes in RAW264.7 Cells. *Mar Drugs*. 2018, 16(8):264.
 169. Chen P, He D, Zhang Y, et al. *Sargassum fusiforme* polysaccharides activate antioxidant defense by promoting Nrf2-dependent cytoprotection and ameliorate stress insult during aging. *Food Func*. 2016, 7(11): 4576–4588.
 170. Chen P, Yang S, Hu CX, et al. *Sargassum fusiforme* polysaccharide rejuvenates the small intestine in mice through altering its physiology and gut microbiota composition. *Curr Molecu Med*. 2017, 17(5): 350–358.
 171. Navarro-Cruz AR, Ramírez Ayala R, Ochoa-Velasco C, et al. Effect of chronic administration of resveratrol on cognitive performance during aging process in rats. *Oxida Med Cell Longe*. 2017, 8: 8510761.
 172. Cartwright M, Tchkonina T, Kirkland J. Aging in adipocytes: potential impact of inherent,

- depot-specific mechanisms. *Exper Geront.* 2007, 42(6): 463–471.
173. Silva-Palacios A, Ostolga-Chavarría M, Zazueta C, Königsberg M. Nrf2: molecular and epigenetic regulation during aging. *Age Res Revi.* 2018, 47:31–40.
174. De La Vega MR, Dodson M, Chapman E, Zhang DD. NRF2-targeted therapeutics: new targets and modes of NRF2 regulation. *Curr Opi Toxic.* 2016, 1: 62–70.
175. Ren D, Villeneuve NF, Jiang T, et al. Brusatol enhances the efficacy of chemotherapy by inhibiting the Nrf2-mediated defense mechanism. *Proc Nat Acad Sci USA.* 2011, 108(4): 1433–1438.
176. Guo D, Yu K, Sun XY, Ouyang JM. Structural characterization and repair mechanism of *Gracilaria lemaneiformis* sulfated polysaccharides of different molecular weights on damaged renal epithelial cells. *Oxida Med Cell Longe.* 2018, 15:e7410389.
177. Pomatto LCD, Davies KJA. Adaptive homeostasis and the free radical theory of ageing. *Free Rad Bio Med.* 2018, 124: 420–430.
178. Liu XF, Hao JL, Xie T, et al. Nrf2 as a target for prevention of age-related and diabetic cataracts by against oxidative stress. *Aging Cell.* 2017, 16(5): 934–942.
179. Wakabayashi N, Itoh K, Wakabayashi J, et al. Keap1-null mutation leads to postnatal lethality due to constitutive Nrf2 activation. *Nature Genetics.* 2003, 35(3): 238–245.
180. Yoon DS, Choi Y, Lee JW. Cellular localization of NRF2 determines the self-renewal and osteogenic differentiation potential of human MSCs via the P53-SIRT1 axis. *Cell Death Dis.* 2016, 7(2):e2093.
181. Wen ZS, Xue R, Du M, et al. Hemp seed polysaccharides protect intestinal epithelial cells from hydrogen peroxide-induced oxidative stress. *Inter J Bio Macro.* 2019, 135: 203–211.
182. Wen ZS, Tang Z, Ma L, et al. Protective effect of low molecular weight seleno-aminopolysaccharide on the intestinal mucosal oxidative damage. *Mar Drugs.* 2019, 17(1): 64.
183. Liao Z, Zhang J, Liu B, et al. Polysaccharide from okra (*Abelmoschus esculentus* (L.) Moench) improves antioxidant capacity via PI3K/AKT pathways and Nrf2 translocation in a type 2 diabetes model. *Molecules.* 2019, 24:1906.
184. Zhang L, Hao J, Zheng Y, et al. Fucoidan protects dopaminergic neurons by enhancing the mitochondrial function in a rotenone-induced rat model of Parkinson's disease. *Aging Dis.* 2018, 9(4): 590–604.
185. Wang YQ, Wei JG, Tu MJ, Gu JG, Zhang W. Fucoidan alleviates acetaminophen-induced

- hepatotoxicity via oxidative stress inhibition and Nrf2 translocation. *Inter J Molecu Sci.* 2018, 19(12): 4050.
186. Ma MX, Sun XY, Yu K, Gui BS, Gui Q, Ouyang JM. Effect of content of sulfate groups in seaweed polysaccharides on antioxidant activity and repair effect of subcellular organelles in injured HK-2 cells. *Oxida Med Cell Longe.* 2017, 13: e2542950.
187. Shang Q, Shan X, Cai C, Hao J, Li G, Yu G. Dietary fucoidan modulates the gut microbiota in mice by increasing the abundance of Lactobacillus and Ruminococcaceae. *Food Func.* 2016, 7(7): 3224–3232.
188. Huang X, Nie S, Xie M. Interaction between gut immunity and polysaccharides. *Crit Rev Food Sci Nutr.* 2017, 57(14): 2943–2955.
189. Shang Q, Song G, Zhang M, et al. Dietary fucoidan improves metabolic syndrome in association with increased Akkermansia population in the gut microbiota of high-fat diet-fed mice. *J Func Food.* 2017, 28: 138–146.
190. Cheng Y, Sibusiso L, Hou LF, Jiang HJ, Chen PC, Zhang X, et al. *Sargassum fusiforme* fucoidan modifies the gut microbiota during alleviation of streptozotocin-induced hyperglycemia in mice. *Int. J. Biol. Macromol.* 2019, 131: 1162-1170.
191. Cani PD, Bibiloni R, Knauf C, Waget A, Neyrinck AM, Delzenne DN. Changes in gut microbiota control metabolic endotoxemia-induced inflammation in high-fat diet-induced obesity and diabetes in mice. *Diabetes.* 2008, 57: 1470-1481.
192. Heeba GH, Morsy MA. Fucoidan ameliorates steatohepatitis and insulin resistance by suppressing oxidative stress and inflammatory cytokines in experimental non-alcoholic fatty liver disease. *Environ. Toxicol. Pharmacol.* 2015, 40: 907-914.
193. Shang QS, Song GR, Zhang MF, Shi JJ, Xu CY, Hao JJ, et al. Dietary fucoidan improves metabolic syndrome in association with increased Akkermansia population in the gut microbiota of high-fat diet-fed mice. *J. Func. Foods.* 2017, 28: 138-146.
194. Wang J, Jin W, Zhang W, Hou Y, Zhang H, Zhang Q. Hypoglycemic property of acidic polysaccharide extracted from *Saccharina japonica* and its potential mechanism. *Carbohydr. Polym.* 2013, 95: 143-147.
195. Sim SY, Shin YE, Kim HK. Fucoidan from *Undaria pinnatifida* has anti-diabetic effects by stimulation of glucose uptake and reduction of basal lipolysis in 3T3-L1 adipocytes. *Nutr. Res.* 2019, 65: 54-62.
196. Rains JL, Jain SK. Oxidative stress, insulin signaling, and diabetes. *Free Radic. Biol. Med.*

- 2011, 50: 567-575.
197. Bloch-Damti A, Bashan N. Proposed mechanisms for the induction of insulin resistance by oxidative stress. *Antioxid. Redox Sign.* 2005, 7: 1553–1567.
198. Morino K, Petersen KF, Shulman GI. Molecular mechanisms of insulin resistance in humans and their potential links with mitochondrial dysfunction. *Diabetes.* 2006, 55: 9–15.
199. Schönfeld P, Wojtczak L. Fatty acids as modulators of the cellular production of reactive oxygen species. *Free Radic. Biol. Med.* 2008, 45: 231-241.
200. Boden, G. Obesity, insulin resistance and free fatty acids. *Curr. Opin. Endocrinol. Diabetes Obes.* 2011, 18: 139-143.
201. Evans JL, Goldfine ID, Maddux BA, Grodsky GM. Are oxidative stress-activated signaling pathways mediators of insulin resistance and beta-cell dysfunction? *Diabetes.* 2003, 52: 1-8.
202. Evans JL, Goldfine ID, Maddux BA, Grodsky GM. Oxidative stress and stress-activated signaling pathways: A unifying hypothesis of type 2 diabetes. *Endocr. Rev.* 2002, 23: 599-622.
203. Jones DP. Redox potential of GSH/GSSG couple: assay and biological significance. *Methods Enzymol.* 2002, 348: 93-112.
204. Vazquez-Prieto MA, González RE, Renna NF, Galmarini CR, Miatello RM. Aqueous garlic extracts prevent oxidative stress and vascular remodeling in an experimental model of metabolic syndrome. *J. Agric. Food Chem.* 2010, 58: 6630-6635.
205. Shuya K, Sunao S, Yota T, Junsei M, Ken I. Regulation of Nrf2 by Mitochondrial Reactive Oxygen Species in Physiology and Pathology. *Biomolecules.* 2020 Feb; 10(2): 320.
206. Dalleau S, Baradat M, Guéraud F, Huc L. Cell death and diseases related to oxidative stress: 4-hydroxynonenal (HNE) in the balance. *Cell Death Differ.* 2013, 20: 1615-1630.
207. Ahn JH, Shin MC, Kim DW, Kim H, Song M, Lee TK, et al. Antioxidant properties of fucoidan alleviate acceleration and exacerbation of hippocampal neuronal death following transient global cerebral ischemia in high-fat diet-induced obese gerbils. *Int. J. Mol. Sci.* 2019, 20: e554.
208. Uruno A, Yagishita Y, Yamamoto M. The Keap1-Nrf2 system and diabetes mellitus. *Arch. Biochem. Biophys.* 2015, 566: 76-84.
209. Uruno A, Furusawa Y, Yagishita Y, Fukutomi T, Muramatsu H, Negishi T. The Keap1-

- Nrf2 system prevents onset of diabetes mellitus. *Mol. Cell Biol.* 2013, 33: 2996-3010.
210. Heiss EH, Schachner D, Zimmermann K, Dirsch VM. Glucose availability is a decisive factor for Nrf2-mediated gene expression. *Redox Biol.* 2013, 21: 359-365.
211. Yang Y, Li W, Li Y, Wang Q, Zhao JJ. Dietary *Lycium barbarum* polysaccharide induces Nrf2/ARE pathway and ameliorates insulin resistance induced by high-fat via activation of PI3K/AKT signaling. *Oxid. Med. Cell Longev.* 2014, e145641.
212. Zhang L, Hao JW, Zheng Y, Su RJ, Liao YL, Gong XL. Fucoidan protects dopaminergic neurons by enhancing the mitochondrial function in a rotenone-induced rat model of Parkinson's disease. *Aging Dis.* 2018, 9: 590-604.
213. Zhou J, Ho CT, Long P, Meng Q, Zhang L, Wan X. Preventive efficiency of green tea and its components on nonalcoholic fatty liver disease. *J. Agric. Food. Chem.* 2019, 67: 5306-5317.
214. Wang YQ, Wei JG, Tu MJ, Gu JG, Zhang W. Fucoidan alleviates acetaminophen-induced hepatotoxicity via oxidative stress inhibition and Nrf2 translocation. *Int. J. Mol. Sci.* 2018, 19: e4050.
215. Hijova E. Gut bacterial metabolites of indigestible polysaccharides in intestinal fermentation as mediators of public health. *Bratisl. Lek. Listy.* 2019, 120: 807-812.
216. Solden LM, Hoyt DW, Collins WB, Plank JE, Daly RA, Hildebrand E. New roles in hemicellulosic sugar fermentation for the uncultivated Bacteroidetes family BS11. *ISME J.* 2017, 11: 691-703.
217. Xue M, Ji X, Liang H, Liu Y, Wang B, Sun L. The effect of fucoidan on intestinal flora and intestinal barrier function in rats with breast cancer. *Food Funct.* 2018, 9: 1214-1223.
218. Chen QC, Liu M, Zhang PY, Fan SJ, Huang JL, Yu SY. Fucoidan and galactooligosaccharides ameliorate high-fat diet-induced dyslipidemia in rats by modulating the gut microbiota and bile acid metabolism. *Nutrition.* 2019, 65: e50.
219. Thingholm LB, Rühlemann MC, Koch M, Fuqua B, Laucke G. Obese individuals with and without type 2 diabetes show different gut microbial functional capacity and composition. *Cell Host Microbe.* 2019, 26: 252-264.
220. Liu J, Hao W, He Z, Kwek E, Zhao Y, Zhu H. Beneficial effects of tea water extracts on the body weight and gut microbiota in C57BL/6J mice fed with a high-fat diet. *Food Funct.* 2019, 10: 2847-2860.
221. Long SL, Gahan GCM, Joyce SA. Interactions between gut bacteria and bile in health and

- disease. *Mol. Aspects Med.* 2017, 56: 54-65.
222. Martinez-Guryn K, Hubert N, Frazier K, Urlass S, Musch MW, Ojeda P. Small intestine microbiota regulate host digestive and absorptive adaptive responses to dietary lipids. *Cell Host Microbe.* 2018, 23: 458-469.
223. Jung Y, Kim I, Manna M, Kim J, Wang S, Park I. Effect of Kombucha on gut-microbiota in mouse having non-alcoholic fatty liver disease. *Food Sci. Biotechnol.* 2018, 28: 261-267.
224. Le J, Zhang X, Jia W, Zhang Y, Luo J, Sun Y. Regulation of microbiota-GLP1 axis by senoside A in diet-induced obese mice. *Acta. Pharm. Sin. B.* 2019, 9: 758-768.
225. Wu TR, Lin CS, Chang CJ, Lin TL, Martel J, Ko YF. Gut commensal *Parabacteroides goldsteinii* plays a predominant role in the anti-obesity effects of polysaccharides isolated from *Hirsutella sinensis*. *Gut.* 2018, 14: 1-13.
226. Biddinger SB, Kahn CR. From mice to men: insights into the insulin resistance syndromes. *Annu Rev Physiol.* 2006, 68: 123-158.
227. Muoio DM, Newgard CB. Mechanisms of disease: Molecular and metabolic mechanisms of insulin resistance and beta-cell failure in type 2 diabetes. *Nat Rev Mol Cell Biol.* 2008, 9: 193-205.
228. Finck BN. Targeting Metabolism, Insulin Resistance, and Diabetes to Treat Nonalcoholic Steatohepatitis. *Diabetes.* 2008, 67: 2485-2493.
229. Kahn SE, Hull RL, Utzschneider KM. Mechanisms linking obesity to insulin resistance and type 2 diabetes. *Nature.* 2006, 444: 840-886.
230. Rani V, Deep G, Singh RK, Palle K, Yadav UD. Oxidative stress and metabolic disorders: Pathogenesis and therapeutic strategies. *Life Sci.* 2016, 148: 183-193.
231. Summers SA, Nelson DH. A role for sphingolipids in producing the common features of type 2 diabetes, metabolic syndrome X, and Cushing's syndrome. *Diabetes.* 2005, 54: 591-602.
232. Argraves KM, Obeid LM, Hannun YA. Sphingolipids in vascular biology. *Adv Exp Med Biol.* 2002, 507: 439-444.
233. Blachnio-Zabielska AU, Hady HR, Markowski AR, Kurianiuk A, Karwowska A, Górski J, Zabielski P. Inhibition of Ceramide *De Novo* Synthesis Affects Adipocytokine Secretion and Improves Systemic and Adipose Tissue Insulin Sensitivity. *Int J Mol Sci.* 2018, 19: e3995.
234. Jia W, Xie G, Jia W. Bile acid-microbiota crosstalk in gastrointestinal inflammation and

- carcinogenesis. *Nat Rev Gastroenterol Hepatol*. 2018, 15(2):111-128.
235. Schroeder BO, Backhed F. Signals from the gut microbiota to distant organs in physiology and disease. *Nat. Med.* 2016, 22: 1079–1089.
236. Martinez MP, Romero CI, Requena P, Hernandez CC, Aranda CJ, Gonzalez R, et al. Dose-dependent antiinflammatory effect of ursodeoxycholic acid in experimental colitis. *Int Immunopharmacol*. 2013, 15: 372–380.
237. Renga B, Mencarelli A, Cipriani S, D’Amore C, Carino A, Bruno A, et al. The bile acid sensor FXR is required for immune-regulatory activities of TLR-9 in intestinal inflammation. *PLoS One*. 2013, 8: e54472.
238. Berger E, Haller D. Structure-function analysis of the tertiary bile acid TUDCA for the resolution of endoplasmic reticulum stress in intestinal epithelial cells. *Biochem Biophys Res Commun*. 2011, 409: 610–615.
239. Stenman LK, Holma R, Gylling H, Korpela R. Genetically obese mice do not show increased gut permeability or faecal bile acid hydrophobicity. *Br J Nutr*. 2013, 110: 1157–1164.
240. Arab JP, Karpen SJ, Dawson PA, Arrese M, Trauner M. Bile acids and nonalcoholic fatty liver disease: Molecular insights and therapeutic perspectives. *Hepatology*. 2017, 65: 350–362.
241. Wang WJ , Zhao JF, Gui WF, Sun D, Dai HJ, Xiao L, Chu HK, Fan D, et al. Tauroursodeoxycholic acid inhibits intestinal inflammation and barrier disruption in mice with non-alcoholic fatty liver disease. *British Journal of Pharmacology*. 2018, 175: 469–484.
242. Choi YJ, Shin HS, Choi HS, Park JW, Jo I, Oh ES, et al. Uric acid induces fat accumulation via generation of endoplasmic reticulum stress and SREBP-1c activation in hepatocytes. *Lab Invest*. 2014, 94: 1114–1125.
243. Legry V, Van Rooyen DM, Lambert B, Sempoux C, Poekes L, Español-Suñer R, et al. Endoplasmic reticulum stress does not contribute to steatohepatitis in obese and insulin-resistant high-fat-diet-fed foz/foz mice. *Clin Sci (Lond)*. 2014, 127(7):507-518.
244. Chen QC, Liu M, Zhang PY, Fan SJ, Huang JL, Yu SY, et al. Fucoidan and galactooligosaccharides ameliorate high-fat diet-induced dyslipidemia in rats by modulating the gut microbiota and bile acid metabolism. *Nutrition*. 2019, 65: 50-59.
245. Jiang CT, Xie C, Lv Y, Li J, Krausz KW, Shi JM, Brocker CN, et al. Intestine-selective

- farnesoid X receptor inhibition improves obesity-related metabolic dysfunction. *Nat Comm.* 2015, 6: 10166.
246. Long HR, Gu XY, Zhou N, Zhu ZJ, Wang CH, Liu XL, Zhao MM. Physicochemical characterization and bile acid-binding capacity of water-extract polysaccharides fractionated by stepwise ethanol precipitation from *Caulerpa lentillifera*. *Int J Biol Macromol.* 2020, 150: 654-661.
247. Park J, Choi JU, Kim K, Byun Y. Bile acid transporter mediated endocytosis of oral bile acid conjugated nanocomplex. *Biomaterials.* 2017, 147: 145-154.
248. Wahlström A, Sayin SI, Marschall HU, et al. Intestinal Crosstalk between Bile Acids and Microbiota and Its Impact on Host Metabolism. *Cell Metabolism.* 2016, 24: 41-50.
249. Q. de Aguiar VT, Tarling E, Edwards P. Pleiotropic Roles of Bile Acids in Metabolism. *Cell Metabolism.* 2013, 17: 657-669.
250. Liu J, Luthuli S, Yang Y, Cheng Y, Zhang Y, Wu MJ, et al. Therapeutic and nutraceutical potentials of a brown seaweed *Sargassum fusiforme*. *Food Sci Nutri.* 2020, 8: 5195-5205.
251. Liu J, Wu SY, Chen L, Li QJ, Shen YZ, Jin L, et al. Different extraction methods bring about distinct physicochemical properties and antioxidant activities of *Sargassum fusiforme* fucoidans. *Int J Biol Macromol.* 2020, 155: 1385–1392.
252. Luthuli S, Wu SY, Cheng Y, Zheng XL, Wu MJ, Tong HB. Therapeutic effects of fucoidan: A review on recent studies. *Mar Drugs.* 2019, 17: e487.
253. Zhang Y, Zuo JH, Yan LP, Cheng Y, Li QJ, Wu SY, et al. *Sargassum fusiforme* fucoidan alleviates high-fat diet-induced obesity and insulin resistance associated with the improvement of hepatic oxidative stress and gut microbiota profile. *J Agri Food Chem.* 2020, 68: 10626–10638.
254. Cheng Y, Sibusiso L, Hou LF, Jiang HJ, Chen PC, Zhang X, et al. *Sargassum fusiforme* fucoidan modifies the gut microbiota during alleviation of streptozotocin-induced hyperglycemia in mice. *Int J Biol Macromol.* 2019, 131: 1162-1170.
255. Zhang Y, Xu M, Hu CX, Liu AM, Chen JJ, Gu CF, et al. *Sargassum fusiforme* Fucoidan SP2 Extends the Lifespan of *Drosophila melanogaster* by Upregulating the Nrf2-Mediated Antioxidant Signaling Pathway. *Oxid Med Cell Longev.* 2019, 2019: e8918914.
256. Mao WJ, Li BF, Gu QQ, Fang YC, Xing HT. Preliminary studies on the chemical characterization and antihyperlipidemic activity of polysaccharide from the brown alga *Sargassum fusiforme*. *Hydrobiologia.* 2004, 512: 263–266.

257. Cani PD, Bibiloni R, Knauf C, Waget A, Neyrinck AM, Delzenne NM, Burcelin R. Changes in gut microbiota control metabolic endotoxemia-induced inflammation in high-fat diet-induced obesity and diabetes in mice. *Diabetes*. 2008, 57: 1470-1481.
258. Heeba GH, Morsy MA. Fucoïdan ameliorates steatohepatitis and insulin resistance by suppressing oxidative stress and inflammatory cytokines in experimental non-alcoholic fatty liver disease. *Environ Toxicol Pharmacol*. 2015, 40: 907-914.
259. Shang Q, Shan X, Cai C, Hao J, Li G, Yu G. Dietary fucoïdan modulates the gut microbiota in mice by increasing the abundance of *Lactobacillus* and Ruminococcaceae. *Food Funct*. 2016, 7: 3224-3232.
260. Wu TR, Lin CS, Chang CJ, Lin TL, Martel J, Ko YF, et al. Gut commensal *Parabacteroides goldsteinii* plays a predominant role in the anti-obesity effects of polysaccharides isolated from *Hirsutella sinensis*. *Gut*. 2019, 68: 248-262.
261. Huebbe P, Nikolai P, Schloesser A, Herebian D, Campbell G, Glüer CC, et al. An extract from the Atlantic brown algae *Saccorhiza polyschides* counteracts diet-induced obesity in mice via a gut related multi-factorial mechanisms. *Oncotarget*. 2017, 8(43):73501-73515.
262. Sun LL, Xie C. Gut microbiota and intestinal FXR mediate the clinical benefits of metformin. *Nat Med*. 2018, 24(12): 1919-1929.
263. Jia W, Xie G, Jia W. Bile acid-microbiota crosstalk in gastrointestinal inflammation and carcinogenesis. *Nat Rev Gastroenterol Hepatol*. 2018, 15(2):111-28.
264. Jones BV, Begley M. Functional and comparative metagenomic analysis of bile salt hydrolase activity in the human gut microbiome. *Proc Nat Acad Sci USA*. 2008, 105: 13580-13585.
265. Lien F. Metformin interferes with bile acid homeostasis through AMPK-FXR crosstalk. *J Clin Invest*. 2014, 124: 1037-51.
266. Wang K, Liao MF, Zhou N, Bao L, Ma K, Zheng ZY, et al. *Parabacteroides distasonis* alleviates obesity and metabolic dysfunctions via production of succinate and secondary bile acids. *Cell Rep*. 2019, 26: 222-235.
267. Liu LL, Liu ZL, Li H, Cao ZW, Li W, Song ZQ, et al. Naturally Occurring TPE-CA Maintains Gut Microbiota and Bile Acids Homeostasis via FXR Signaling Modulation of the Liver-Gut Axis. *Front Pharmacol*. 2020, 11:12.
268. Si X, Tian JL, Shu C, Wang YH, Gong E, Zhang Y, et al. Serum ceramide reduction by blueberry anthocyanin-rich extract alleviates insulin resistance in hyperlipidemia mice. *J*

- Agric Food Chem.* 2020, 68: 8185-8194.
269. Hui SC, Liu Y, Chen MT, Wang XL, Lang HD, Zhou M, et al. Capsaicin improves glucose tolerance and insulin sensitivity through modulation of the gut microbiota-bile acid-FXR axis in type 2 diabetic db/db Mice. *Mol. Nutr. Food Res.* 2019, 63: e1900608.
270. Shmueli E, Alberti KGMM, Record CO. Diacylglycerol/protein kinase C signalling: A mechanism for insulin resistance. *J. Intern. Med.* 1993, 234 (4): 397–400.
271. Kurz J, Parnham MJ, Geisslinger G, Schiffmann S. Ceramides as novel disease biomarkers. *Trends Mol. Med.* 2019, 25 (1): 20–32.
272. Wigger L, Cruciani-Guglielmacci C, Nicolas A, Denom J, Fernandez N, Fumeron F, et al. Plasma dihydroceramides are diabetes susceptibility biomarker candidates in mice and humans. *Cell Rep.* 2017, 18 (9): 2269–2279.
273. Schroeder BO, Backhed F. Signals from the gut microbiota to distant organs in physiology and disease. *Nat. Med.* 2016, 22: 1079-1089.
274. Guo JL, Han X, Tan HY, Huang WD, You YL, Zhan JC. Blueberry extract improves obesity through regulation of the gut microbiota and bile acids via pathways involving FXR and TGR5. *iScience.* 2019, 19:676-690.
275. Sun LL , Xie C, Wang G, Wu Y, Wu Q, Wang XM, Liu J, et al. Gut microbiota and intestinal FXR mediate the clinical benefits of metformin. *Nat Med.* 2018, 24(12): 1919-1929.
276. Lee H, Lee Y, Kim J, An J, Lee S, Kong H, et al. Modulation of the gut microbiota by metformin improves metabolic profiles in aged obese mice. *Gut Microbes.* 2018, 9(2): 155-165.
277. Martínez-Moya P, Romero-Calvo I, Requena P, Hernández-Chirlaque C, Aranda CJ, González R, et al. Dose-dependent antiinflammatory effect of ursodeoxycholic acid in experimental colitis. *Int Immunopharmacol.* 2013, 15(2): 372–380.
278. Renga B, Mencarelli A, Cipriani S, D'Amore C, Carino A, Bruno A, et al. The bile acid sensor FXR is required for immune-regulatory activities of TLR-9 in intestinal inflammation. *PLoS One.* 2013, 8(1): e54472.
279. Berger E, Haller D. Structure-function analysis of the tertiary bile acid TUDCA for the resolution of endoplasmic reticulum stress in intestinal epithelial cells. *Biochem Biophys Res Commun.* 2011; 409: 610–615.
280. Stenman LK, Holma R, Gylling H, Korpela R. Genetically obese mice do not show

- increased gut permeability or faecal bile acid hydrophobicity. *Br J Nutr.* 2013, 110: 1157–1164.
281. Arab JP, Karpen SJ, Dawson PA, Arrese M, Trauner M. Bile acids and nonalcoholic fatty liver disease: Molecular insights and therapeutic perspectives. *Hepatology.* 2017, 65: 350–362.
282. Wang WJ , Zhao JF, Gui WF, Sun D, Dai HJ, Xiao L, et al. Tauroursodeoxycholic acid inhibits intestinal inflammation and barrier disruption in mice with non-alcoholic fatty liver disease. *British J of Pharmaco.* 2018, 175: 469–484.
283. Wu TR, Lin CS, Chang CJ, Lin TL, Martel J, Ko YF, et al. Gut commensal *Parabacteroides goldsteinii* plays a predominant role in the anti-obesity effects of polysaccharides isolated from *Hirsutella sinensis*. *Gut* 2018:1–14.
284. Manley S, Ding WX. Role of farnesoid X receptor and bile acids in alcoholic liver disease. *Acta Pharmaceutica Sinica B.* 2015, 5(2):158–167.
285. Turnbaugh PJ, Backhed F, Fulton L, Gordon JI. Marked alterations in the distal gut microbiome linked to diet-induced obesity. *Cell Host Microbe.* 2008, 3(4): 213–223.
286. Renga B, Mencarelli A, Cipriani S, D’Amore C, Carino A, Bruno A, et al. The bile acid sensor FXR is required for immune-regulatory activities of TLR-9 in intestinal inflammation. *PLoS One.* 2013, 8(1): e54472.
287. Fazakerley DJ, Chaudhuri R, Yang PY, Maghzal GJ, Thomas KC, Krycer JR, et al. Mitochondrial CoQ deficiency is a common driver of mitochondrial oxidants and insulin resistance. *eLife* . 2018, 7:e32111.
288. Hancock M, Hafstad AD, Nabeebaccus AA, Catibog N, Logan A, Smyrniak L, et al. Myocardial NADPH oxidase-4 regulates the physiological response to acute exercise. *eLife.* 2018, 7:e41044.
289. Hu H, Fan X, Guo Q, Wei X, Yang D, Zhang B, et al. Silicon dioxide nanoparticles induce insulin resistance through endoplasmic reticulum stress and generation of reactive oxygen species. *Part Fibre Toxicol.* 2019, 16(1):41.
290. You L, Yang C, Du Y, Liu Y, Chen G, Sai N, et al. Matrine exerts hepatotoxic effects via the ROS-dependent mitochondrial apoptosis pathway and inhibition of Nrf2-mediated antioxidant response. *Oxid Med Cell Longev.* 2019, 2019:e1045345.

APPENDIX A

Optimization of conditions for establishing a model of insulin resistance in HepG2 hepatocytes using palmitic acid

Cell culture

HepG2 cells were placed in DMEM low-glucose medium containing 10% fetal bovine serum (FBS), and cultured in an incubator at 37 ° C and 5% CO₂. When the cells are adherent, the medium is decanted, digested with 0.25% trypsin, and passaged at a ratio of 1: 3 every 3 days. Cells in logarithmic growth phase are taken for experiments. The subcultured cells were seeded into a 6-well plate, and after 24 hours of culture, the following experiments were performed.

Determination of optimal concentration and time of insulin resistance in HepG2 cells

1. Determination of the optimal concentration of PA

After the cells in the logarithmic growth phase were digested, the concentration of the cell suspension was adjusted, and transferred to a 96-well cell culture plate to continue the culture. Each plate was divided into a control group and a model group. Add 100ul to each well, set 5 duplicate wells, and then plate to adjust the density of the cells to be tested to 1000-10000 wells (the marginal wells are filled with sterile PBS). Incubate at 5% CO₂, 37 ° C, until the cell monolayer covers the bottom of the well (96-well flat bottom plate). Discard the medium and add DMEM high-sugar medium containing palmitic acid at different concentrations (10, 25, 50, 10, 200, 400, 800 uM), and continue to culture for 24 to 72 hours. Observe the cell growth under an inverted microscope. After the reaction time is completed, the medium is discarded, washed once with PBS, and then incubated with 2% FBS in RPMI1640 medium for 20 minutes.

Repeat the above process once. After washing with PBS, replace with serum-free medium. After 24 hours of incubation, add 20ul MTT solution (5mg / ml in PBS, pH = 7.4) to each well. After 4 hours of incubation, carefully discard the culture supernatant in the well. For suspended cells, centrifuge and then discard the culture supernatant in the well. Add 150ul of dimethyl sulfoxide (DMSO) to each well and shake for 10min on a shaker to fully melt the crystals. The absorbance of each well was measured at OD 490 nm on a microplate reader. The concentration of PA was selected to have a significant effect on cells but less effect on cell proliferation.

2. Determination of the optimal time of PA

Method 1: Detect the glucose content in the culture supernatant

After the cells in the logarithmic growth phase were digested, the cell density was adjusted to 2×10^4 / mL, and transferred to a 96-well cell culture plate to continue the culture. Each plate was divided into a control group and a model group. After the cells adhered to the monolayer, the control group was added with normal medium, and the model group was added with newly prepared medium containing 200 μ m PA, and incubated in a 5% CO₂ in a 37 ° C incubator for 36 h. After determining the concentration (200 μ mol / L) in 2.2.1, select 2, 4, 6, 12, 24, 36, 48, 72 h as the eight candidate times. The glucose content of the cell culture supernatant was measured by a glucose measurement kit, and the optimal palmitic acid action time with significantly reduced glucose consumption and the shortest time was selected as the optimal insulin action time.

Method 2: 2-NBDG uptake test to detect glucose uptake in cells

After treating and culturing HepG2 cells with the optimal concentration of palmitic acid (200 μ mol / L) in 2.2.1, the cells were incubated in a 37 ° C incubator. After the cells in the logarithmic growth phase were digested, the MEM basal medium was adjusted to a cell density of 2×10^4 / mL, and transferred into a 6-well cell culture plate. One well was used as a control

group, and the remaining five wells were used as a model group. Model groups were set up according to the incubation time: 2, 6, 12, 24, 48 h respective groups. The PA solution with the optimal concentration (200 $\mu\text{mol} / \text{L}$) was added to the corresponding wells in order according to time, and the same amount of medium and cell suspension was added to the blank control group. After the treatment, the cells were washed 2 to 5 times with PBS solution, and the cells were treated with 2-NBDG at the same concentration for 1 hour, and then the cells were washed 2 to 5 times with PBS. After a certain period of time, read with a fluorescence microplate reader (Ex / Em, 488 / 520 nm) to detect changes in fluorescence intensity in the cells; finally, add 10 μL of CCK-8 to each group of cells and incubate for 4 h, then read with a microplate reader. CCK-8 was used to correct the error of the fluorescence intensity of each group due to the difference in the number of cells. Each time group was repeated 3 times.

Results

Effect of PA solution at different concentrations on the survival rate of HepG2 cells

In order to select a suitable PA solution treatment concentration, the effect of PA on the activity and value-added of HepG2 was first detected by MTT method in this experiment. According to step 2.2, HepG2 cells were treated with 10 μM , 25 μM , 50 μM , 100 μM , 200 μM , 400 μM , and 800 μM sodium palmitate in MEM medium for 24 h. The results are shown in **Figure A1**. It was found that under the treatment of the PA solution, the MTT reading continued to decrease, which was inversely proportional to the PA concentration. Above 400 μM , the absorbance of OD 490 decreased significantly, indicating that high concentration PA solution was toxic to HepG2 cells. Combined with references, a 200 μM sodium palmitate solution was selected to continue the next experiment.

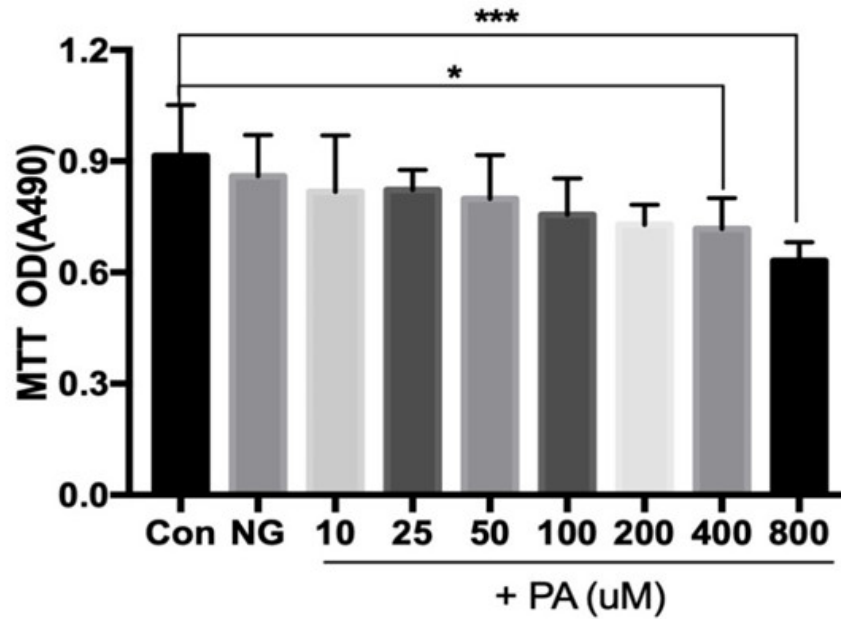


Figure A1. Determination of the optimal concentration of PA

Effect of 200uM PA on HepG2 cell survival after different time

Method 1: In order to determine a reasonable treatment time for sodium palmitate solution, different times were tried for comparison in this experiment. After referencing the literature, 0, 2, 4, 6, 12, 24, 36, 48, and 72 h were selected as the candidate times in this experiment. MEM medium containing 200 uM sodium palmitate solution was sequentially added for processing. Then 50nM of insulin solution was added for pretreatment 30min in advance, and then the glucose uptake of HepG2 cells was detected. As shown in **Figure A2**, the cell supernatant was collected for glucose content determination. It was found that the glucose content of the cell supernatant gradually increased after 200 uM PA solution treatment, indicating that the glucose uptake by the cells began to decline, and the difference was significant after 24 hours.

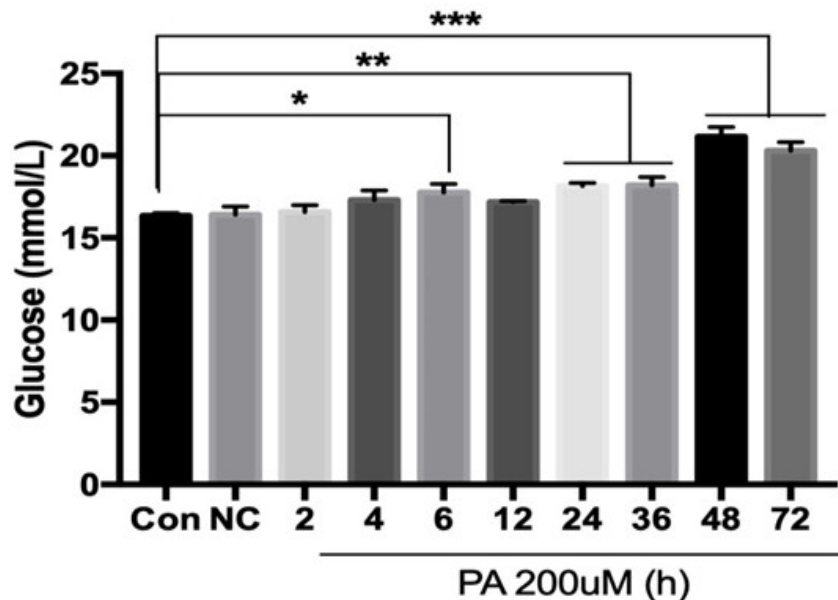


Figure A2. Determination of the optimal action time of PA

Method 2: In view of the high glucose content in the culture supernatant, errors may occur, and the more accurate 2-NBDG fluorescent glucose probe method is used for further judgment. As shown in **Figure A3**, after different time treatments (200 uM PA solution), the glucose absorption gradually decreases, and the fluorescence intensity decreases sequentially. Compared with the Control group, there was a significant decrease at 12h, and an extremely significant decrease at 24h and 48h. Considering the above, 24h is selected as a reasonable PA processing time.

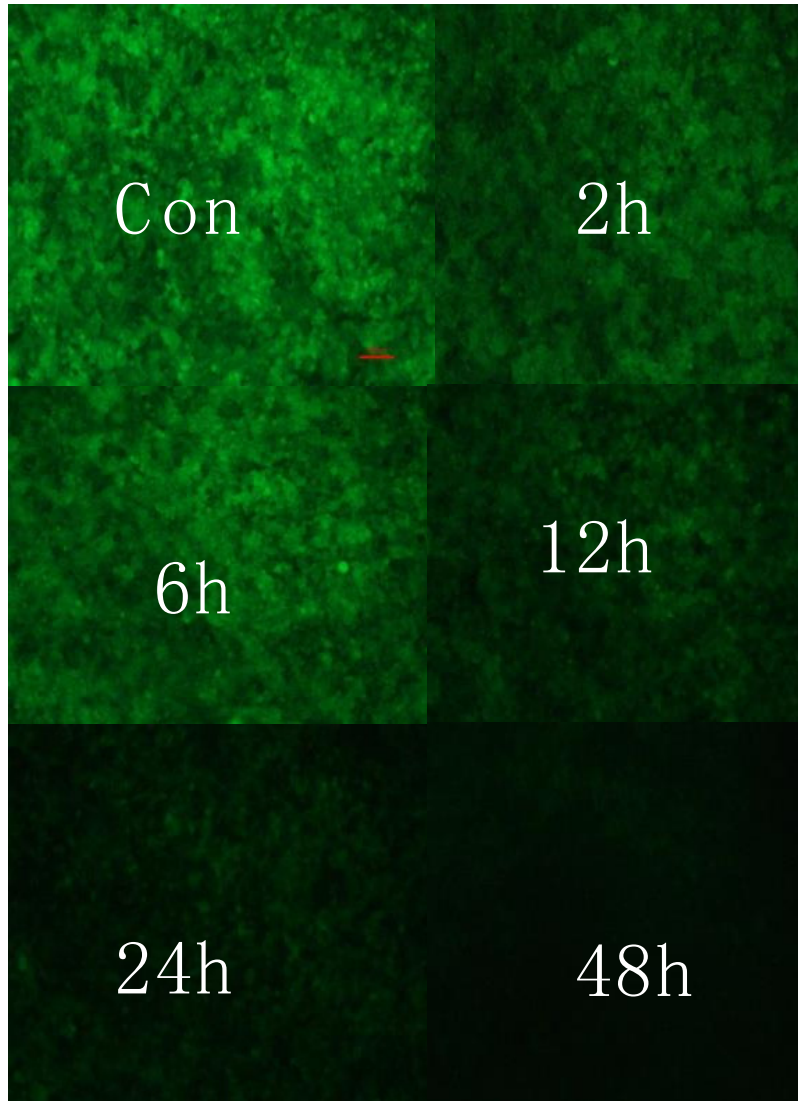


Figure A3. Changes in glucose uptake caused by different periods of PA

PA inhibits insulin signaling pathway in HepG2 cells

In order to further verify the success of the model, the protein level was used to detect whether the insulin signaling pathway was inhibited. The insulin signaling pathway plays an important role in glucose uptake and is inhibited when insulin resistance occurs. It can be seen from **Figure A4** that at the protein level, after 200 uM PA solution treatment at different times, IRS-1 does not change significantly, but p-IRS-1 gradually increases with time, reaching a significant difference at 24h. This indicates that IRS-1 has been activated incorrectly. In

addition, p-Akt protein also decreased over time, indicating that PA can reduce the phosphorylation of Akt. The above shows that the insulin signal pathway in HepG2 cells was inhibited under 200 uM PA solution.

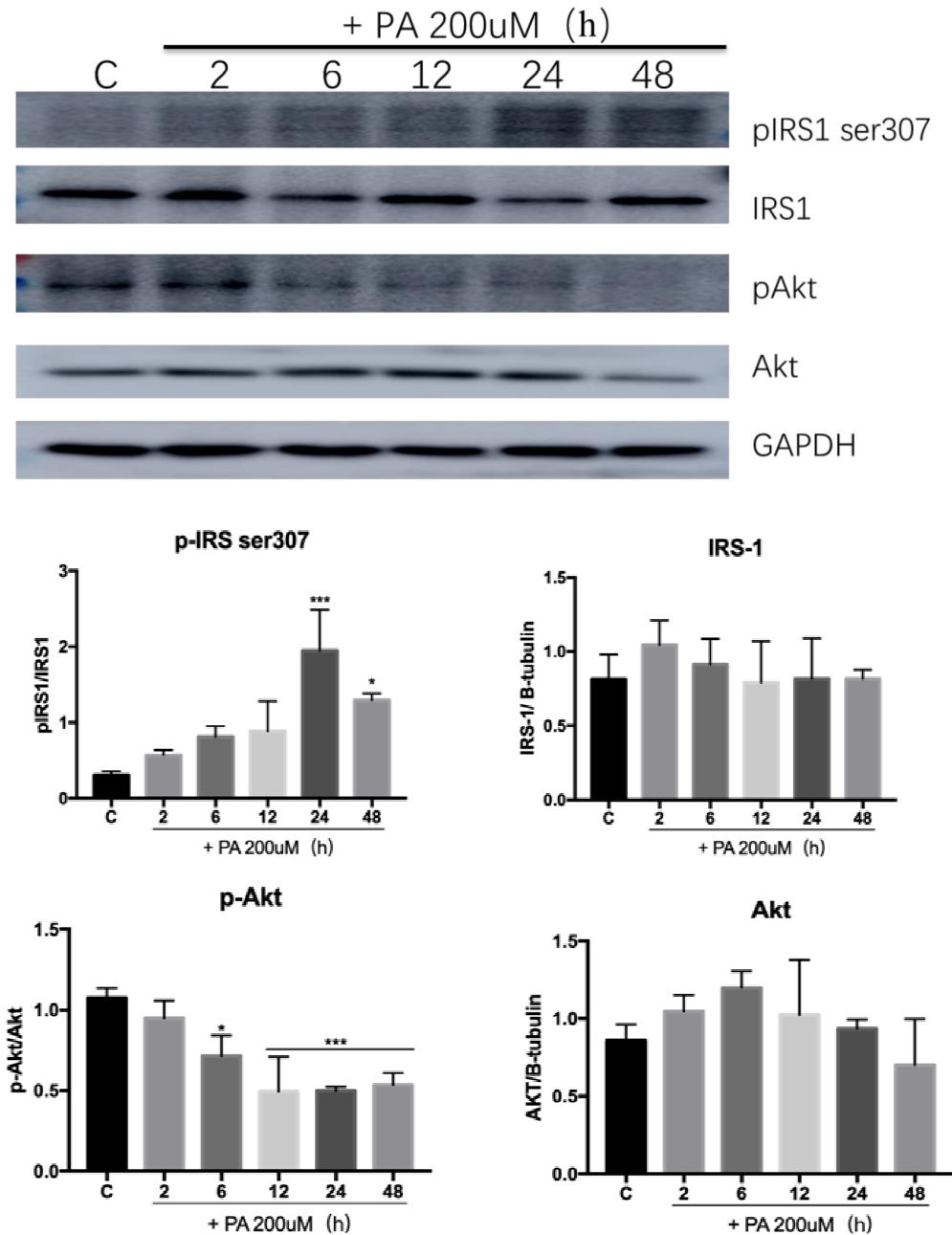


Figure A4. PA inhibits insulin signaling pathway in HepG2 cells

PA causes oxidative stress in cells and causes lipid peroxide accumulation

Oxidative stress is a common symptom accompanied by insulin resistance. It has been

reported that PA can cause oxidative stress in HepG2 cells. The Nrf2 / ARE signal pathway is a classic oxidative stress signal pathway. It was found through experiments that during the early stage of PA treatment, the level of Nrf2 protein briefly increased, and the level of phosphorylation was also the same. However, with the extension of PA treatment time, a significant decrease in Nrf2 was found. Here we believe that short-term oxidative stress caused the up-regulation of Nrf2 to reduce the content of reactive oxygen species such as ROS. Similarly, it was found that 4-HNE also accumulated over time, indicating that the lipids in the cells are continuously oxidized and accumulated, and may damage the cells. See **Figure A5**.

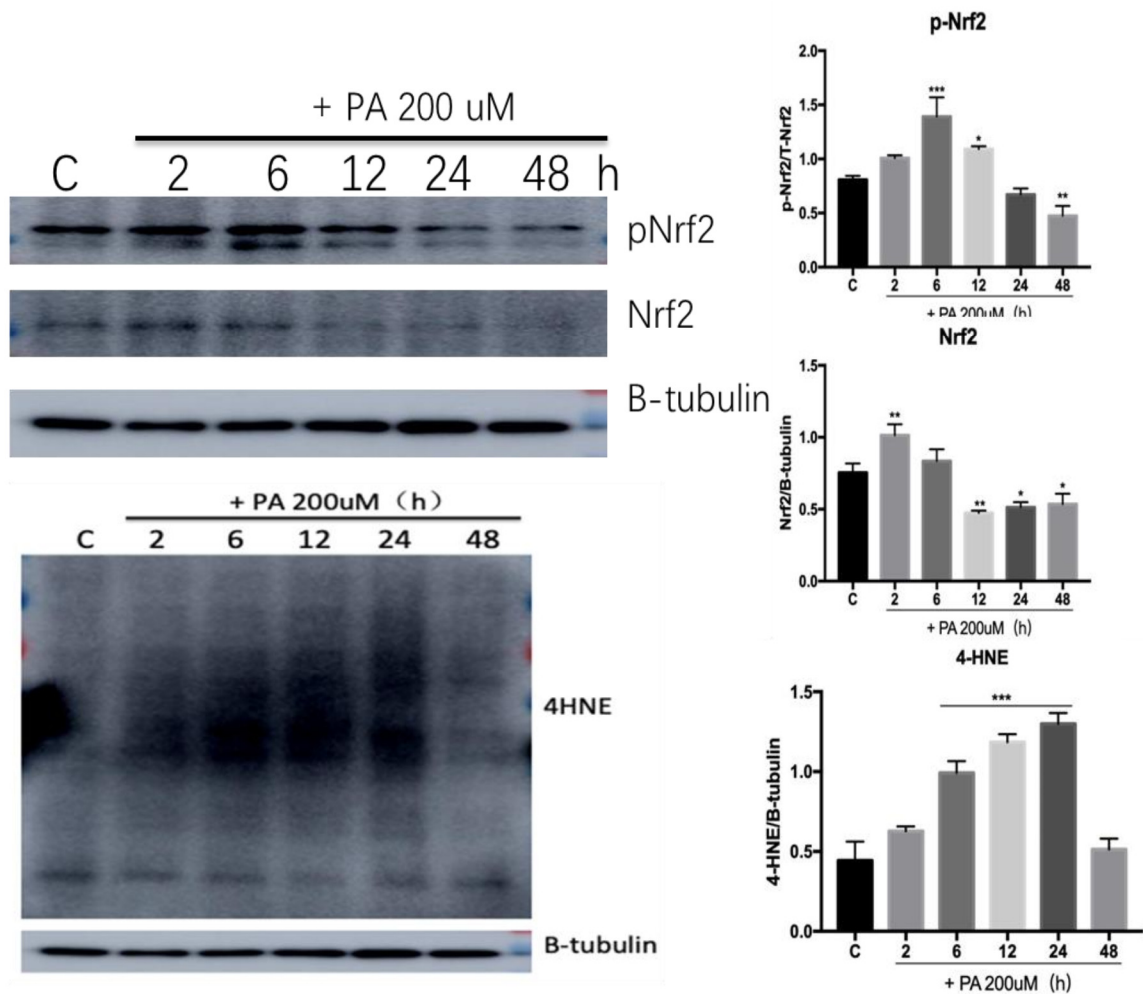


Figure A5. PA inhibits Nrf2/ARE signaling pathway in HepG2 cells

Discussions

Insulin has many functions in the body, such as promoting the synthesis of glycogen, fat and protein; promoting the use of glucose and energy production; inhibiting the breakdown of fat; increasing cell proliferation, differentiation, and protecting cells. Insulin resistance is a phenomenon in which biological effects above insulin are weakened, making the biological response of human tissues to a certain amount of insulin lower than expected normal levels. Insulin resistance is closely related to the pathogenesis of T2DM and metabolic syndrome, and is one of its main pathogenesis.

In this experiment, we determined the optimal time and concentration of insulin resistance in HepG2 cells by *in vitro* induction method of PA, and established an insulin resistance model. The experimental results showed that the glucose consumption of cells after 24 h of 200 μ M insulin was significantly reduced and significantly reduced. The cell kill rate remains low. Therefore, we chose a PA concentration of 200 μ M as the optimal concentration for insulin resistance. Then it was found that after treatment with 200 μ M of PA solution, the glucose content of the cell supernatant gradually increased, indicating that the cell's glucose uptake began to decrease. There was a significant increase at 24h and 36h, and the increase increased at 48h and 72h. It shows that insulin resistance has appeared in the experiment at 24h. However, in order to make the experiment time reasonable, choose 24h to shorten the experiment time. In order to further verify whether the optimal time is the most reasonable with 24h, the experiment adopts a more accurate 2-NBDG fluorescent glucose probe method for further judgment. After treatment at different times (200 μ M PA solution), glucose absorption gradually decreased, and the fluorescence intensity decreased in turn. Compared with the Control group, there was a significant decrease at 12h, and extremely significant drops at 24h and 48h. Comprehensively

considering the above, 24h is selected as a more reasonable PA processing time node.

According to the determined optimal concentration and optimal time, an insulin resistance model is established, and the establishment of the model is verified by the enzyme-linked immunoassay method to further detect whether the insulin signaling pathway is inhibited from the protein level. The insulin signaling pathway plays an important role in glucose uptake, which is inhibited when insulin resistance occurs. The results showed that IRS-1 was activated incorrectly, the lysine that should be activated was changed to serine 307, and the p-Akt protein also declined over time, indicating that PA can cause the phosphorylation of Akt to decrease. It can be seen that the IRS / Akt signaling pathway is suppressed. In addition, as the time of PA treatment prolonged, it was found that Nrf2 showed a significant decline. Here we believe that transient oxidative stress caused the upregulation of Nrf2 to reduce the content of reactive oxygen species such as ROS, but long-term PA treatment destroyed the cell Exciting mode. Similarly, it was found that 4-HNE also accumulates with time, indicating that the lipids in the cell continue to oxidize and accumulate and may damage the cell. It can be seen that the Nrf2 / ARE signaling pathway is suppressed. As explained above, under 200uM PA solution treatment, the insulin signaling pathway in HepG2 cells is inhibited.

The experimental results suggest that 200uM of insulin acting on HepG2 cells for 24 h can establish a stable and successful HepG2 cell insulin resistance model. Compared with animal models, this model has a short experimental period and low cost. It provides a stable *in vitro* insulin resistance model for studying the mechanism of insulin resistance, screening drugs for treating insulin resistance *in vitro*, and studying the mechanism of drug treatment for insulin resistance.

APPENDIX B

Table B1. Raw data for Figure 4.13

| Taxonomy | Firmicutes | Bacteroidetes | unidentified | Proteobacteria | Deferribacteres | Actinobacteria | Oxyphotobacteria | Melainabacteres | Tenericutes | Gemmatimonadetes | Others | ratio |
|----------|------------|---------------|--------------|----------------|-----------------|----------------|------------------|-----------------|-------------|------------------|---------|---------|
| Con1 | 0.26217 | 0.71425 | 0.00875 | 0.01328 | 0.00065 | 0.00046 | 0.00000 | 0.00025 | 0.00000 | 0.00000 | 0.00019 | 0.36705 |
| Con3 | 0.30288 | 0.62990 | 0.03487 | 0.01864 | 0.00029 | 0.00632 | 0.00031 | 0.00333 | 0.00017 | 0.00010 | 0.00318 | 0.48083 |
| Con6 | 0.47665 | 0.50308 | 0.00521 | 0.00861 | 0.00013 | 0.00312 | 0.00000 | 0.00027 | 0.00247 | 0.00000 | 0.00046 | 0.94747 |
| Con7 | 0.61028 | 0.31253 | 0.05836 | 0.01221 | 0.00144 | 0.00205 | 0.00013 | 0.00258 | 0.00034 | 0.00002 | 0.00006 | 1.95269 |
| Con8 | 0.53790 | 0.42727 | 0.01200 | 0.01665 | 0.00063 | 0.00444 | 0.00057 | 0.00017 | 0.00023 | 0.00000 | 0.00015 | 1.25893 |
| Con9 | 0.24856 | 0.73540 | 0.00873 | 0.00515 | 0.00017 | 0.00144 | 0.00004 | 0.00008 | 0.00040 | 0.00000 | 0.00002 | 0.33798 |
| Con10 | 0.44046 | 0.54264 | 0.00752 | 0.00505 | 0.00027 | 0.00268 | 0.00008 | 0.00008 | 0.00121 | 0.00000 | 0.00000 | 0.81171 |
| HFD1 | 0.52603 | 0.10984 | 0.15375 | 0.08764 | 0.10898 | 0.01361 | 0.00008 | 0.00000 | 0.00004 | 0.00000 | 0.00002 | 4.78913 |
| HFD2 | 0.44195 | 0.40451 | 0.00827 | 0.13526 | 0.00040 | 0.00549 | 0.00046 | 0.00002 | 0.00000 | 0.00151 | 0.00214 | 1.09257 |
| HFD3 | 0.54477 | 0.42438 | 0.00431 | 0.01321 | 0.00019 | 0.01164 | 0.00000 | 0.00000 | 0.00000 | 0.00000 | 0.00149 | 1.28369 |
| HFD4 | 0.87540 | 0.06521 | 0.00431 | 0.04745 | 0.00153 | 0.00597 | 0.00000 | 0.00010 | 0.00000 | 0.00000 | 0.00002 | 13.4238 |
| HFD5 | 0.59803 | 0.35867 | 0.00103 | 0.03508 | 0.00027 | 0.00689 | 0.00000 | 0.00000 | 0.00004 | 0.00000 | 0.00000 | 1.66737 |
| HFD6 | 0.61690 | 0.35018 | 0.00119 | 0.01003 | 0.00040 | 0.02092 | 0.00002 | 0.00002 | 0.00034 | 0.00000 | 0.00000 | 1.76163 |
| HFD7 | 0.71802 | 0.06236 | 0.05011 | 0.06963 | 0.06781 | 0.03200 | 0.00000 | 0.00000 | 0.00006 | 0.00000 | 0.00000 | 11.5134 |
| SFF4 | 0.50297 | 0.47508 | 0.00337 | 0.01158 | 0.00008 | 0.00674 | 0.00000 | 0.00000 | 0.00017 | 0.00000 | 0.00000 | 1.05871 |
| SFF5 | 0.75840 | 0.13702 | 0.00417 | 0.09801 | 0.00010 | 0.00163 | 0.00000 | 0.00002 | 0.00065 | 0.00000 | 0.00000 | 5.53492 |
| SFF6 | 0.59128 | 0.31988 | 0.00224 | 0.04578 | 0.00010 | 0.02997 | 0.01049 | 0.00013 | 0.00013 | 0.00000 | 0.00000 | 1.84845 |
| SFF8 | 0.54624 | 0.35088 | 0.00279 | 0.07319 | 0.00004 | 0.02590 | 0.00000 | 0.00008 | 0.00063 | 0.00000 | 0.00025 | 1.55679 |
| SFF7 | 0.67823 | 0.20726 | 0.00756 | 0.08852 | 0.00394 | 0.01418 | 0.00000 | 0.00008 | 0.00004 | 0.00000 | 0.00019 | 3.27241 |
| SFF9 | 0.37703 | 0.41862 | 0.03275 | 0.09455 | 0.07239 | 0.00423 | 0.00002 | 0.00040 | 0.00000 | 0.00000 | 0.00000 | 0.90065 |

SFF10 0.34882 0.62165 0.00044 0.02255 0.00021 0.00620 0.00006 0.00000 0.00000 0.00000 0.56113

Table B2. Raw data for Figure 4.15. and 4.16.

| | Clostridia | Bacteroidia | Bacilli | Erysipelotrichia | Bacteria | Deltaproteobacteria | Deferribacteres |
|------|----------------|----------------------|------------------|------------------|---------------------|---------------------|-----------------|
| FG | 0.24665 | 0.04852 | 0.92637 | 0.00616 | 0.13934 | 0.13550 | 0.83361 |
| W | 0.23247 | 0.03253 | 0.63096 | 0.00021 | 0.10109 | 0.03476 | 0.83672 |
| BMI | 0.19465 | 0.06242 | 0.65811 | 0.00211 | 0.26476 | 0.02214 | 0.67980 |
| IN | 0.38051 | 0.17752 | 0.66522 | 0.42517 | 0.52394 | 0.31313 | 0.88677 |
| FFA | 0.48369 | 0.60963 | 0.32715 | 0.07620 | 0.28412 | 0.54752 | 0.54633 |
| CAT | 0.72650 | 0.06233 | 0.66166 | 0.07761 | 0.22773 | 0.54920 | 0.89569 |
| MDA | 0.68280 | 0.60508 | 0.63717 | 0.54637 | 0.82268 | 0.73520 | 0.84411 |
| TC | 0.05774 | 0.02889 | 0.35479 | 0.00142 | 0.01558 | 0.03994 | 0.62362 |
| TG | 0.63076 | 0.70015 | 0.08426 | 0.95820 | 0.70007 | 0.85928 | 0.47910 |
| LDL | 0.46018 | 0.18374 | 0.33100 | 0.00162 | 0.14091 | 0.02263 | 0.96117 |
| LW | 0.21748 | 0.79711 | 0.26155 | 0.49018 | 0.31577 | 0.46808 | 0.54225 |
| AW | 0.48382 | 0.23990 | 0.68374 | 0.00004 | 0.02192 | 0.15556 | 0.89078 |
| Homa | 0.17520 | 0.02978 | 0.54595 | 0.03116 | 0.20194 | 0.17864 | 0.77769 |
| | Actinobacteria | Gammaaproteobacteria | Oxyphotobacteria | Coriobacteria | Alphaproteobacteria | Mollicutes | Gemmatimonades |
| FG | 0.01039 | 0.26532 | 0.47326 | 0.05053 | 0.48843 | 0.03982 | 0.20980 |
| W | 0.00056 | 0.04947 | 0.05009 | 0.41206 | 0.25899 | 0.02347 | 0.23260 |
| BMI | 0.00669 | 0.04987 | 0.10028 | 0.67271 | 0.38212 | 0.07471 | 0.38086 |
| IN | 0.11175 | 0.47252 | 0.00207 | 0.25356 | 0.14832 | 0.01137 | 0.92609 |

| | | | | | | | |
|---|----------------|----------------|----------------|----------------|----------------|----------------|----------------|
| FFA | 0.02945 | 0.80092 | 0.47790 | 0.65984 | 0.41015 | 0.18075 | 0.13568 |
| CAT | 0.27083 | 0.81060 | 0.70336 | 0.01654 | 0.29698 | 0.30860 | 0.30108 |
| MDA | 0.56411 | 0.45734 | 0.91938 | 0.90837 | 0.96265 | 0.83488 | 0.28107 |
| TC | 0.00223 | 0.57316 | 0.17912 | 0.11840 | 0.21287 | 0.03707 | 0.01317 |
| TG | 0.45902 | 0.79694 | 0.30100 | 0.25560 | 0.93157 | 0.27698 | 0.86585 |
| LDL | 0.00257 | 0.22131 | 0.23551 | 0.35868 | 0.86467 | 0.12652 | 0.07574 |
| LW | 0.92844 | 0.85548 | 0.13158 | 0.48700 | 0.80259 | 0.24813 | 0.08598 |
| AW | 0.01640 | 0.07629 | 0.15407 | 0.23572 | 0.46278 | 0.03816 | 0.16785 |
| Homa | 0.00617 | 0.31591 | 0.01068 | 0.78940 | 0.08115 | 0.00454 | 0.51408 |
| Verrucomicrobiae Fusobacteriia Acidimicrobiia Acidobacteria Acidobacteriia Negativicutes Thermoleophilia | | | | | | | |
| FG | 0.13899 | 0.88925 | 0.92424 | 0.92424 | 0.92424 | 0.13715 | 0.13715 |
| W | 0.79904 | 0.45571 | 0.94420 | 0.88075 | 0.88075 | 0.49147 | 0.59348 |
| BMI | 0.96197 | 0.24903 | 0.95218 | 0.87290 | 0.87290 | 0.39913 | 0.49159 |
| IN | 0.62773 | 0.36823 | 0.66276 | 0.65547 | 0.65547 | 0.70342 | 0.81953 |
| FFA | 0.38245 | 0.92533 | 0.60539 | 0.71470 | 0.71470 | 0.39899 | 0.13762 |
| CAT | 0.38603 | 0.55993 | 0.87681 | 0.77546 | 0.77546 | 0.24627 | 0.39899 |
| MDA | 0.87328 | 0.77312 | 0.41711 | 0.39101 | 0.39101 | 0.35528 | 0.81907 |
| TC | 0.35807 | 0.19138 | 0.19281 | 0.16186 | 0.16186 | 0.09866 | 0.81963 |
| TG | 0.18942 | 0.55971 | 0.59639 | 0.64268 | 0.64268 | 0.87912 | 0.39872 |
| LDL | 0.79412 | 0.11822 | 0.78701 | 0.69603 | 0.69603 | 0.24627 | 0.49147 |
| LW | 0.15298 | 0.65825 | 0.29170 | 0.34186 | 0.34186 | 0.93945 | 0.13773 |
| AW | 0.79172 | 0.29600 | 0.70729 | 0.61256 | 0.61256 | 0.18672 | 0.49159 |
| Homa | 0.36498 | 0.47469 | 0.62680 | 0.69240 | 0.69240 | 0.70358 | 0.31723 |
| Fimbrimonadia Dehalococcoidia Melanobacteria Elusimicrobia Nitrospira Rhodothermia Ignavibacteria | | | | | | | |
| FG | 0.13715 | 0.99201 | 0.13715 | 0.13715 | 0.13715 | 0.13715 | 0.13715 |
| W | 0.49147 | 0.86105 | 0.49147 | 0.49147 | 0.59348 | 0.59348 | 0.59348 |
| BMI | 0.39913 | 0.88079 | 0.39913 | 0.39913 | 0.49159 | 0.49159 | 0.49159 |
| IN | 0.70342 | 0.92827 | 0.70342 | 0.70342 | 0.81953 | 0.81953 | 0.81953 |
| FFA | 0.39899 | 0.04830 | 0.39899 | 0.39899 | 0.13762 | 0.13762 | 0.13762 |

| | | | | | | | |
|-------------|----------------|----------------|----------------|----------------|----------------|----------------|----------------|
| CAT | 0.24627 | 0.79087 | 0.24627 | 0.24627 | 0.39899 | 0.39899 | 0.39899 |
| MDA | 0.35528 | 0.88636 | 0.35528 | 0.35528 | 0.81907 | 0.81907 | 0.81907 |
| TC | 0.09866 | 0.33144 | 0.09866 | 0.09866 | 0.81963 | 0.81963 | 0.81963 |
| TG | 0.87912 | 0.71079 | 0.87912 | 0.87912 | 0.39872 | 0.39872 | 0.39872 |
| LDL | 0.24627 | 0.63028 | 0.24627 | 0.24627 | 0.49147 | 0.49147 | 0.49147 |
| LW | 0.93945 | 0.13314 | 0.93945 | 0.93945 | 0.13773 | 0.13773 | 0.13773 |
| AW | 0.18672 | 0.86896 | 0.18672 | 0.18672 | 0.49159 | 0.49159 | 0.49159 |
| Homa | 0.70358 | 0.80253 | 0.70358 | 0.70358 | 0.31723 | 0.31723 | 0.31723 |

Note: FG, fasting glucose; W, weight; BMI, body mass index; IN, insulin; FFA, free fatty acid; CAT, catalase; MDA, Malondialdehyde; TC, serum total cholesterol; TG, triglyceride; LDL, low density lipoprotein; LW, liver weight; AW, adipose weight; HOMA-IR, homeostasis model assessment of insulin resistance.

Table B3. Raw data for Figure 4.15., 4.16. and 6.15.

| Sample | FG | W | BMI | FFA | TC | TG | LDL | LW | AW | HomaIR | HDL | TUDCA |
|---------------|-----------|----------|------------|------------|-----------|-----------|------------|-----------|-----------|---------------|------------|--------------|
| Con1 | 4.2 | 39 | 5.40 | 2.506 | 4.54 | 2.20 | 0.532 | 52.76 | 4.31 | 1.71 | 5.44 | 0.29 |
| Con3 | 3.8 | 43.6 | 6.03 | 1.843 | 3.27 | 2.13 | 0.497 | 50.47 | 5.62 | 1.28 | 2.82 | 0.34 |
| Con6 | 4.8 | 45.5 | 6.77 | 2.988 | 3.46 | 2.24 | 0.451 | 45.33 | 11.41 | 1.27 | 4.09 | 0.28 |
| Con7 | 4.7 | 37.7 | 5.75 | 2.783 | 3.43 | 1.75 | 0.416 | 54.23 | 5.73 | 1.12 | 2.61 | 0.27 |
| Con8 | 5.8 | 35.6 | 5.29 | 2.904 | 4.82 | 2.47 | 0.555 | 50.21 | 4.35 | 1.04 | 2.40 | 0.26 |
| Con9 | 4.8 | 38 | 5.26 | 2.434 | 4.57 | 2.90 | 0.647 | 49.38 | 8.68 | 0.95 | 2.75 | 0.39 |
| Con10 | 4.7 | 39.6 | 6.19 | 2.410 | 5.11 | 1.69 | 0.832 | 46.83 | 8.94 | 0.70 | 3.39 | 0.23 |
| HFD1 | 6.8 | 57.8 | 8.39 | 2.241 | 8.31 | 2.73 | 1.942 | 55.61 | 31.21 | 1.38 | 2.33 | 0.22 |
| HFD2 | 7.2 | 52.7 | 7.84 | 2.928 | 7.23 | 2.58 | 1.225 | 56.62 | 26.57 | 2.29 | 2.15 | 0.29 |

| | | | | | | | | | | | | |
|-------|------|------|------|-------|-------|------|-------|-------|-------|------|------|------|
| HFD3 | 6.7 | 66.9 | 8.84 | 2.337 | 9.42 | 3.30 | 1.063 | 57.09 | 56.89 | 2.46 | 3.02 | 0.58 |
| HFD4 | 5.4 | 65.3 | 8.63 | 1.807 | 11.48 | 2.71 | 1.086 | 43.19 | 22.13 | 2.95 | 3.53 | 0.53 |
| HFD5 | 5.4 | 55.4 | 7.32 | 2.422 | 10.63 | 2.20 | 1.110 | 50.23 | 41.90 | 1.95 | 2.93 | 0.35 |
| HFD6 | 10.5 | 60.5 | 8.18 | 1.566 | 12.02 | 2.71 | 1.445 | 50.76 | 36.76 | 3.31 | 2.82 | 0.29 |
| HFD7 | 6.4 | 50 | 6.76 | 2.325 | 10.94 | 1.94 | 1.711 | 52.07 | 22.14 | 2.25 | 2.40 | 0.71 |
| SFF4 | 5.7 | 48.6 | 6.89 | 1.759 | 6.60 | 1.02 | 1.722 | 53.17 | 22.90 | 1.34 | 2.05 | 2.84 |
| SFF6 | 5.2 | 46.2 | 6.39 | 2.193 | 10.09 | 2.56 | 0.949 | 53.65 | 16.02 | 1.07 | 2.58 | 1.13 |
| SFF7 | 6.9 | 52.5 | 7.27 | 1.819 | 9.33 | 1.60 | 1.029 | 49.45 | 22.48 | 1.83 | 2.65 | 2.22 |
| SFF8 | 5.1 | 60 | 8.50 | 2.639 | 7.83 | 1.62 | 1.479 | 42.25 | 20.83 | 2.08 | 2.65 | 0.93 |
| SFF9 | 5.2 | 55.4 | 8.24 | 1.771 | 10.02 | 2.13 | 1.098 | 43.27 | 29.29 | 1.90 | 4.80 | 1.81 |
| SFF10 | 5.6 | 45.6 | 6.31 | 2.060 | 10.56 | 1.94 | 1.445 | 50.96 | 32.24 | 0.93 | 4.48 | 0.48 |

Table B4. Raw data for Figure 5.1.

| ID | HFD1 | HFD2 | HFD3 | HFD4 | HFD5 |
|----------------------|---------|---------|---------|---------|---------|
| L-Proline | 6.38172 | 2.94443 | 5.40654 | 6.04668 | 6.11006 |
| L-Valine | 0.40425 | 0.35843 | 0.62376 | 0.37401 | 0.43100 |
| L-Ornithine | 1.62779 | 2.39100 | 2.21501 | 2.40622 | 2.26469 |
| Spermidine | 2.00535 | 1.89161 | 1.44658 | 1.86818 | 1.77049 |
| L-Lysine | 0.78396 | 0.31061 | 0.58670 | 0.25057 | 0.46042 |
| 3-Dehydroshinganine | 0.15936 | 0.12375 | 0.10260 | 0.17748 | 0.07003 |
| Sphingosine | 0.06771 | 0.15892 | 0.03234 | 0.16012 | 0.05710 |
| 7-Dehydrocholesterol | 0.28453 | 0.00241 | 0.31090 | 0.27658 | 0.36109 |
| 1,2-Dioleoyl PC | 0.22086 | 0.12732 | 0.39990 | 0.16341 | 0.19483 |

| | 0.58715 | 0.68126 | 0.53801 | 0.71190 | 0.39841 |
|---------------------------|---------|---------|---------|---------|---------|
| Tauroursodeoxycholic acid | SFF1 | SFF2 | SFF3 | SFF4 | SFF5 |
| L-Proline | 6.28226 | 7.92646 | 7.76136 | 6.20722 | 6.99457 |
| L-Valine | 0.40633 | 0.27455 | 0.23408 | 0.38861 | 0.29828 |
| L-Ornithine | 1.91022 | 2.40339 | 0.87337 | 1.30106 | 0.97577 |
| Spermidine | 0.41869 | 0.31968 | 1.13939 | 0.93769 | 1.76428 |
| L-Lysine | 0.02321 | 0.12786 | 0.42240 | 0.24730 | 0.20667 |
| 3-Dehydrospinganine | 0.90164 | 0.41095 | 0.35847 | 0.57750 | 0.45918 |
| Sphingosine | 0.66794 | 0.30568 | 0.08021 | 0.19843 | 0.53735 |
| 7-Dehydrocholesterol | 1.14159 | 0.38270 | 0.86524 | 0.71781 | 0.62094 |
| 1,2-Dioleoyl PC | 0.54372 | 0.68776 | 0.51893 | 0.16694 | 0.53477 |
| Tauroursodeoxycholic acid | 2.84575 | 2.22426 | 1.13490 | 1.81334 | 0.90262 |

APPENDIX C

Analysis of molecular docking

Molecular docking analysis

To investigate the probable binding of TUDCA to Keap1 as the potential inhibitor, the automated docking studies were carried out using AutoDock vina 1.1.2 package. The X-ray crystal structure of the human KEAP1 (PDB ID: 6LRZ) was downloaded from RCSB Protein Data Bank. The 3D structure of TUDCA (ZINC ID: 3914813) was downloaded from ZINC. The AutoDockTools 1.5.6 package was employed to generate the docking input files. The molecular docking simulation protein of Keap1 was prepared by removing water molecules and bound ligands. The binding site of the KEAP1 was identified as centre_x: -9.944, centre_y: -38.993, and centre_z: 3.869 with dimensions size_x: 85, size_y: 85, and size_z: 85. The best-scoring (i.e., with the lowest docking energy) pose as judged by the Vina docking score was chosen and further analysed using PyMoL 2.4.0 software.

Theoretical binding mode of TUDCA and KEAP1

Binding to the KEAP1 kelch domain to achieve the inhibition of KEAP1-NRF2 interaction is a well-documented mechanism for NRF2 activation (From: Discovery of direct inhibitors of Keap1-Nrf2 protein-protein interaction as potential therapeutic and preventive agents). We performed molecular docking analysis to explore the interaction between TUDCA and Keap1 Kelch domain.

The theoretical three-dimensional binding mode of the complex with the lowest docking energy is illustrated in **Figure. C**. The simulation results revealed TUDCA actually interacted with the primary amino acid residues on the active site of Keap1. The TUDCA was positioned at the hydrophobic pocket, surrounded by the residues Val-418, Leu-557, Val-514, Val-561, and Thr-560, forming a stable hydrophobic binding. All those interactions help TUDCA to

anchor in the binding site of Keap1. In addition, the estimated the binding energy of Keap1-TUDCA complex was found to be -10.21 kcal/mol, suggesting that TUDCA is an inhibitor of KEAP1. The docking simulation provided supportive data for this compound induced inhibition by allowing us to predict the binding site in the active site pocket.

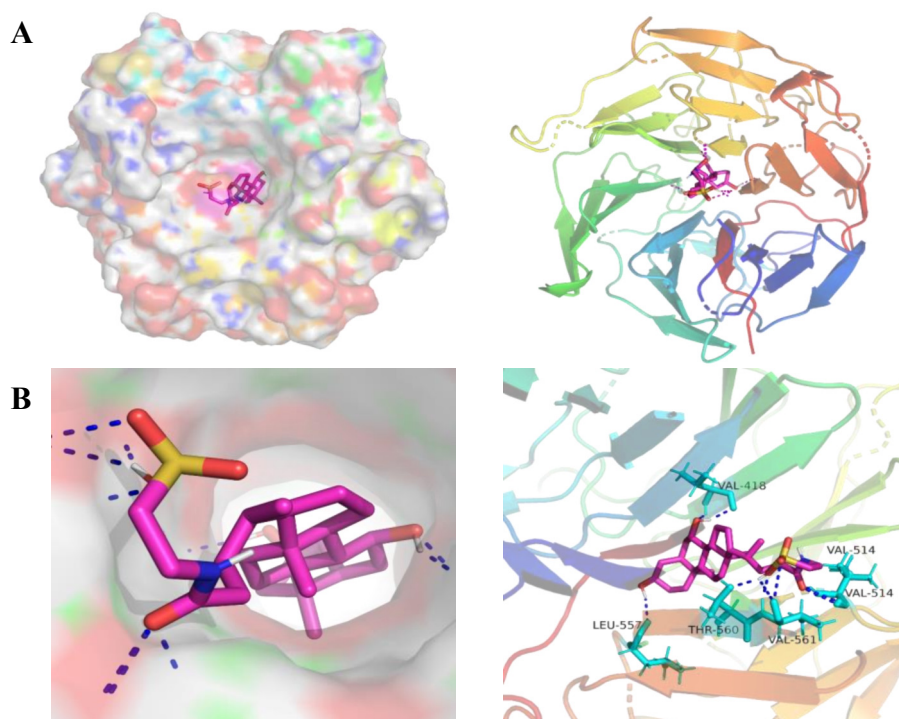


Figure. C. Docking of TUDCA into Keap1 protein Kelch domain. (A) Predicted binding mode of TUDCA docked with Keap1 Kelch domain molecular surface. TUDCA is shown in pink; (B) The interaction between TUDCA and Keap1 protein. The residues of KEAP1 were represented using sticks or surface structures. The dashed lines (blue) represent hydrogen-bonding interactions.